UNIVERSITY OF CALIFORNIA SAN DIEGO

The Impact of Seasonal Environmental Variables on Phytoplankton Ecology at the Antarctic Ice-Ocean Boundary

Studies through field work, numerical models, data science, and machine learning

A dissertation submitted in partial satisfaction of the
requirements for the degree Doctor of Philosophy

in

Oceanography

by

B. Jack Pan

Committee in charge:

Maria Vernet, Chair
Katherine A. Barbeau
Andrew D. Barton
B. Greg Mitchell
Rick A. Reynolds
Jonathan Shurin
Fiammetta Straneo

2020

The Dissertation of B. Jack Pan is approved, and it is acceptable in quality and form for publication on microfilm and electronically:

_____

_____

_____

_____

_____

_____

_____
Chair

University of California San Diego

2020

DEDICATION

To Family, friends, and everyone who supported me over the years.

EPIGRAPH

People don't understand the earth, but they want to,
so they build a model,
and then
they have two things they don't understand.

Gerard Roe in *Modeling Methods for Marine Science*

TABLE OF CONTENTS

LIST OF FIGURES

LIST OF TABLES

ACKNOWLEDGEMENTS

This work was made possible by all who has supported me over the years.

First, I would like to thank my advisor, Maria Vernet. I am very grateful for her guidance in scientific research and her confidence in me. Through working with her, I was able to freely pursue my academic interests. Moreover, she gave me the unprecedented opportunity to conduct field work in Antarctica multiple times – a truly unforgettable experience which I will always cherish.

I would also like to thank my dissertation committee for supporting this endeavor -- Kathy Barbeau, Andrew Barton, Greg Mitchell, Rick Reynolds, Jon Shurin, and Fiamma Straneo. Thank you for the thoughtful advice and invaluable discussions over the years. A special thanks to everyone at the Stramski Lab and Barbeau Lab for our collaborations. I hope more will come for the advancement of oceanography.

The staff at SIO and UCSD have been very helpful and they enriched my graduate school experience. Thank you to Gilbert Bretado, Hanna Choe, Denise Darling, Brittany Hook, Chase Martin, Robert Monroe, Maureen McGreevy, Gwen Nero, Dejan Ristic, Josh Reeves, Vanessa Scott, Chris Toombs, Adrielle Wai, Shelley Weisel, Laruen Wood and everyone else at SIO IOD, the Graduate Department, SIO Communications Office, SIO Office of Corporate Alliance, and UCSD Facility.

Thank you to the many organizations and individuals that have supported my research: NSF, NASA, UCSD, the SIO Department, and the generous donors who made this work possible.

My friends in the SIO community have been a source of support and comfort and my graduate school experience would have not been the same without them. Thank you to my curricular group cohort and the broader 2014 cohort, as well as the many friends who came to SIO before and after us. *Per ardua ad astra*.

And finally, I am thankful for my family. They have always supported my academic pursuits and motivated me to do more in life and be a better person. I am truly grateful for all the sacrifices

they have made for me. I also want to thank all my previous science teachers in school. You taught me well.

Thank you so much everyone, for everything you have done for me. IWFBOM.

=====

Chapter 2, in full, is a manuscript of the material as it appears in Pan, B.J., Vernet, M., Reynolds, R.A., and Mitchell, B.G. (2019) The optical and biological properties of glacial meltwater in an Antarctic fjord. *PLoS ONE* 14(2): e0211107. The dissertation author was the primary investigator and first author of this paper.

Chapter 3, in full, is a manuscript of the material as it appears in Pan, B.J., Vernet, M., Manck, L., Forsch, K., Ekern, L., Mascioni, M., Barbeau, K, Almandoz, G., and Orona, A.J. (2020) Environmental Drivers of Phytoplankton Taxonomic Composition in an Antarctic Fjord. *Progress in Oceanography* 183: 102295. The dissertation author was the primary investigator and first author of this paper.

Chapter 4 is currently being prepared for publication as: Pan, B.J., Vernet, M., Barton, A.D. and Orona, A.J. Environmental Drivers Modulate Phytoplankton Community Seasonal Succession in the Western Antarctic Peninsula. The dissertation author was the primary investigator and first author of this paper.

VITA

2009-2014	Research Assistant Department of Earth System Science, University of California Irvine
2013	Participant, NASA DEVELOP Program at the Jet Propulsion Laboratory
2013	B.S. in Earth & Environmental Sciences School of Physical Sciences, University of California Irvine
2014	Team Lead, NASA DEVELOP Program at the Jet Propulsion Laboratory
2016	M.S. in Marine Biology Scripps Institution of Oceanography, University of California San Diego
2020	Ph.D. in Oceanography Scripps Institution of Oceanography University of California San Diego

PUBLICATIONS

1. Pan, B.J., Vernet, M., Manck, L., Forsch, K., Ekern, L., Mascioni, M., Barbeau, K, Almandoz, G., and Orona, A.J. (2020) “Environmental Drivers of Phytoplankton Taxonomic Composition in an Antarctic Fjord.” Progress in Oceanography 183: 102295.

2. Pan, B.J., Vernet, M., Reynolds, R.A., and Mitchell, B.G. (2019) “The optical and biological properties of glacial meltwater in an Antarctic fjord.” PLoS ONE 14(2): e0211107.

3. Gierach, M., Holt, B., Trinh R., Pan, B., and Rains, C. (2016) “Satellite Detection of Wastewater Diversion Plumes in Southern California.” *Estuarine, Coastal and Shelf Science* 186:171-82.

ABSTRACT OF THE DISSERTATION

The Impact of Seasonal Environmental Variables on Phytoplankton Ecology at the Antarctic Ice-Ocean Boundary

Studies through field work, numerical models, data science, and machine learning

by

B. Jack Pan

Doctor of Philosophy in Oceanography

University of California San Diego, 2020

Maria Vernet, Chair

The Western Antarctic Peninsula (WAP) is rapidly changing due to climate forcing in recent decades. These changes manifest as an overall increase in ocean and air temperatures (with some regional cooling), retreating glaciers, and increases in precipitation associated with shifts in atmospheric circulation. As these changes continue and intensify, meteoric water input to the coastal ocean is expected to increase. Continued monitoring of these changes can help us

better understand their impacts. The physical effects of glacial melting on sea level has been extensively studied in the past. However, the impact of glacial meltwater on phytoplankton community composition remains largely elusive. Due to the critical role of primary producers in the Antarctic food web and their significance to local biogeochemical cycle and ecosystem dynamics, the immediate ramification of meltwater input on these communities need to be better understood.

This dissertation contains three main chapters. In Chapter 2, I aim to understand the spatial and temporal distribution of glacial meltwater in Andvord Bay and characterize their optical features in order to develop a method for quantifying meltwater fraction based on water column optics. The fjord severs as an end-member and thus an extreme in various environmental and biological gradients. Hence, the ecological connectivity between the fjord and the shelf has significant implications to the entire Antarctic ecosystem. In Chapter 3, I investigate the phytoplankton community composition within Andvord Bay and understand how environmental conditions, particularly meltwater, impact this community. Data from this chapter are utilized to train a machine learning model to predict phytoplankton abundance and community composition. The techniques developed in this chapter is applied to the broader ecosystem over the WAP continental shelf in Chapter 4. I hope this dissertation can improve our understanding of how environmental variables influence phytoplankton community in the WAP, as well as contextualize the physical impacts of climate forcing in the perspective of Antarctic ecosystems.

Chapter 1: Introduction

The Western Antarctic Peninsula (WAP) is experiencing a rapid climate change. The WAP is the fastest warming region in the Southern Hemisphere, and this warming rate is only comparable with two other locations on Earth (northwestern North America and the Siberian Plateau) (Meredith et al., 2010) (Trenberth et al., 2007). These significant environmental changes lead to retreating of glaciers. Most glaciers on the WAP are retreating at an accelerated rate (Cook et al., 2016) (Cook et al., 2005) (Vaughan et al., 2003). In addition, the annual melting period is also increasing in the WAP at a rate of ~1/2 day annually (Torinesi et al., 2003). Consequently, glacial meltwater input to the ocean is expected to increase in the 21st century (Meredith et al., 2010). A substantial amount of glacial meltwater into the marine environment would have profound implications for the local, as well as distant marine systems (Henley et al., 2019) (Ducklow et al., 2007) (Dierssen et al., 2002). For instance, seawater's freezing point is directly related to salinity and hence glacial meltwater will impact sea ice formation (Schwerdtfecer, 1963). This, in turn, can influence local heat flux (Lytle & Ackley, 1996). On a broader spatial and temporal scale, freshwater input from the WAP over time can cause changes in temperature, salinity, and density in the tropical Atlantic (Meredith et al., 2010) (Hickey & Weaver, 2004).

Glacial input is important to the Antarctic marine ecosystem (Henley et al., 2020) (Henley et al., 2019) (Ducklow et al., 2007) (Dierssen et al., 2002). Glacial meltwater can be enriched in iron and serve as a trace nutrient source in the glaciers' vicinities and in offshore waters (Forsch et al., 2018) (Arrigo et al., 2017). As a High-Nutrient Low-Chlorophyll (HNLC) region, iron addition by meltwater can impact phytoplankton growth and hence primary production over the WAP shelf (Dierssen et al., 2002). The presence of glacial meltwater can also enhance water column stratification (Pan et al., 2020) (Höfer et al., 2019) (Dierssen et al., 2002) (Mitchell & Holm-Hansen, 1991). This will create favorable light conditions to support phytoplankton growth.

Stabilizing water column and shallow mixed layer depth are important for developing phytoplankton blooms in the WAP (Holm-Hansen & Mitchell, 1991). The seasonal variability of glacial meltwater will undoubtedly change following the WAP's rapid environmental warming, and this increases the uncertainty in predicting local productivity and its influence on biogeochemical cycle and ecological dynamics.

Many glaciers in the WAP are situated in fjords (Howe et al., 2010) (Powell & Domack, 1995) (Domack & Ishman, 1993). This geographic advantage offers an unprecedented site for studying meltwater and its impact on phytoplankton ecology. Polar fjords are semi-enclosed systems, and often have a glacial terminus in contact with the ocean establishing a gradient in meltwater from the terminus to coastal ocean through the mouth of the fjord (Pan et al., 2019) (Meire et al., 2015) (Murray et al., 2015). This pattern provides a unique opportunity to study meltwater properties and understand its impact on primary producers. Conventionally, an effective method to study and track meltwater would be using in-situ temperature and salinity (Cape et al., 2019b) (Motyka et al., 2003). However, field methods are often limited in space and time. Satellite remote sensing can greatly alleviate these limitations by providing a cost-effective sampling solution that can cover broad geographic regions over an extended temporal scale (Babin et al., 2015). However, currently, there are very few remote sensing and optical methods for monitoring and tracking meltwater over in the ocean (Pan et al., 2019) (Mascarenhas et al., 2017) (Murray et al., 2015). Existing algorithms are predominately for the high-latitude regions in the Northern Hemisphere, a region with very different characteristics than Antarctic waters at the ice-ocean boundary (Murray et al., 2015) (Hudson et al., 2014) (Lund-Hansen et al., 2010).

In order to achieve a better understanding of the changes in Antarctic coastal ecosystem, it is important to develop additional means to monitor glacial meltwater discharge and other ice-ocean interactions. These methods will allow a better assessment of meltwater's dispersion and its impact on primary producers in the water column – which are vital to the rest of the Antarctic food web. In this dissertation, I aim to understand the influence of ice-ocean interaction on coastal

phytoplankton ecology. The studies presented here were conducted in an Antarctic fjord and over the continental shelf of the WAP. The results from these studies provide a comprehensive perspective of glacial-marine processes and their ecological consequences in nearshore waters. The rest of this chapter establishes the context for the following three studies presented in Chapter 2, 3 and 4.

1.1. Phytoplankton Community

There are typically six distinct groups of phytoplankton in nearshore waters and over the continental shelf of the WAP. These groups are **diatom, cryptophyte, mixed flagellate, dinoflagellate, haptophyte** comprised of mostly ***Phaeocystis spp.*****,** and **prasinophyte**. The main group that is generally abundant and drives primary production is diatom (Vernet et al., 2008) (Ducklow et al., 2007) (Garibotti et al., 2003). Diatom cells are usually between 2 and 200 µm in size. Centric diatoms have concentric or radial symmetry around a point or points, while pennate diatoms have a symmetry around a longitudinal axis (Scott & Marchant, 2005). These subtle differences within the diatom group result in different diatom assemblages which are important to community seasonal succession (described in more detail in Chapter 4). Cryptophytes are also common in the WAP (Pan et al., 2020) (Schofield et al., 2017). They are comparatively small between 3 and 50 µm in length (including flagellum) and << 20 µm wide; while heterotrophic cryptophytes have been found in other parts of the world, they have not yet been recorded in the WAP (Scott & Marchant, 2005). Mixed flagellates presented in this work represent a group of unidentified small flagellates beyond the optical limitation of microscopy; this group is likely comprised of small single-cell *Phaeocystis spp.*, very small dinoflagellates, and very small cryptophytes (Garibotti et al., 2005) (Kozlowski et al., 2011). Dinoflagellates are motile single cells generally < 100 µm; they can be autotrophic, heterotrophic, or mixotrophic (Scott & Marchant, 2005). Dinoflagellates identified in this work are mainly based on their distinct pigment peridinin and the common photosynthetic pigment chlorophyll-a (chl-a), so they are pigmented and non-heterotrophic (Wright et al., 2010). However, non-pigmented heterotrophic

dinoflagellates can also become abundant in WAP fjords (Mascioni et al., 2019). Haptophytes are mostly represented by *Phaeocystis spp.* in the WAP. *Phaeocystis* are between 5 and 8 μm in diameter. Their two common life stages are biflagellate motile single cells and palmelloid colonial cells; in the latter stage, cells lose their flagella and form a gelatinous aggregation (Scott & Marchant, 2005). Prasinophytes are small cell and their motile form possesses 2 or 4 (occasionally 6 or 8) anteriorly inserted flagella; each cell has a single-cup-shaped or lobed chloroplast (Scott & Marchant, 2005). They are commonly a minor component of the WAP phytoplankton community (Pan et al., 2020) (Petrou et al., 2016) (Kozlowski et al., 2011). However, rare massive blooms of prasinophyte in the inner channels of the WAP have been documented in the past (Bird & Karl, 1991) (Vernet et al., 1991).

In this dissertation, a key variable to assess and quantify phytoplankton community is chlorophyll-a (chl-a) concentration – which is a major photosynthetic pigment of phytoplankton and plants in general (Falkowski & Raven, 2013). This variable is based on fluorescence measurement, according to Smith et al., and it serves as a proxy for phytoplankton biomass in the water (Smith et al., 1996) (Smith et al., 1981). However, in fjords and shelf regions of the Western Antarctic Peninsula, the relationship between chl-a concentration and biomass has been found to differ among phytoplankton groups. In Andvord Bay, microscopy analysis of phytoplankton has found diatoms have a higher C:Chl-a ratio than other groups – hence, while cryptophytes were more numerous during our study periods, diatoms still represented the bulk of the phytoplankton carbon in the community (Mascioni et al., 2020).

1.2. Fjord System

1.2.1. Geographic Boundary

Fjord provides a linkage between the cryosphere and the marine environment by forming a land-ice-ocean interface. Fjords are commonly characterized as deep estuaries in the high latitudes that often contain one or multiple sills that separate various basins; these basins are formed by prehistoric movement of glaciers. Fjords with tidewater glaciers (also known as glacio-

marine fjords) are relatively ephemeral features on a geological scale. They were formed as results of the ice retreat after the Last Glacial Maximum (LGM) (Syvitski et al., 1987b). In the past, WAP fjords have been studied due to their crucial role in glacial ice transport to the coastal ocean in their vicinity; fjords also have an intrinsic connection to past deglaciation, ice sheet mass balance, and sea level rise (Syvitski et al., 1987a) (Freeland, 1979). For these reasons, many previous studies were primarily focused on the perspectives of glaciology (Pritchard et al., 2009) (Pritchard & Vaughan, 2007) (Cook et al., 2005) (Thomas et al., 2004) and geology (Lu et al., 2010) (Powell & Domack, 1995) (Domack & Ishman, 1993) (Domack, 1990) (Griffith & Anderson, 1989). However, ecosystem within these fjords, particularly the impact of environmental change on phytoplankton community composition, is often overlooked.

1.2.2. Physical Oceanography of Fjords

In the last decade, numerous studies were conducted in the Arctic and Greenlandic fjords to improve our understanding on their physical oceanography. Initially, a two-layer model developed based on data from LeConte Bay in Alaska was proposed as a general schematic for fjord circulation (Motyka et al., 2003); this model was also adapted by Rignot et al. (2010) for understanding circulation in Greenland fjords: Eqip Sermia, Kangilerngata Sermia, and Sermeq Kujatdleq and Avangnardleq (Rignot et al., 2010). In this particular model, subglacial discharge drives convection and draws deep, warm saline water (2-10 ^{o}C, originating from subtropical Atlantic waters) towards the nearly vertical glacial terminus, where the two components mix by turbulence. These plumes continue to mix as they rise along the ice face at the fjord's head and melt ice which further contributes to convection. These subglacial meltwater plume often surface >1 km from the glaciers (Rignot et al., 2010) (Motyka et al., 2003). More detailed studies in recent years reveal that the circulation in fjords are far more complex than previously proposed. For instance, in the Sermilik Fjord where Helheim Glacier is situated, the "layering" of dense, warm Atlantic water and light, cold Arctic water masses can strongly influence glacial melting (Straneo et al., 2011). Both field measurements and model studies have indicated that the circulation

consists of a “double-cell” circulation: there is a buoyant plume rising along the ice edge and an inflow of oceanic water at depth (Straneo et al., 2011). The outflow of a mixture of glacial meltwater and oceanic water occurs both at surface as well as along an interface between the layered water masses (Sciascia et al., 2013) (Straneo et al., 2011). The outflow plumes also have a strong seasonality, where substantial subglacial discharge occur during summer and early fall which enhance submarine melt rate along the glacial front (Straneo & Cenedese, 2015). Summer plumes are typically more buoyant, more turbulent, and serves as a significant heat transport towards the glacier, while winter plumes are slower and less buoyant (Sciascia et al., 2013). These results demonstrate an evolved understanding of fjord circulation in the Arctic where, in addition to the influence of Atlantic shelf water inflow (Jackson et al., 2014), the buoyancy-driven flows due to summer glacier basal melting are also recognized as an important physical driver for circulation (Straneo & Cenedese, 2015).

In comparison, circulation in Antarctic fjords is less understood. Recent studies indicate a distinct schematic that significantly differs from those found in fjords located in Greenland and the broader Arctic latitudes (Lundesgaard et al., 2019). Andvord Bay is dynamically quiet in comparison to currents in Gerlache Strait connected with the mouth of Andvord Bay. Low frequency density fluctuations at the fjord mouth provide exchange between the fjord and Gerlache Strait; rotational effects may also impact exchange with the shelf but it largely depends on the geomorphology and stratification of the fjord (Lundesgaard, 2018). Wind forcing serves as an additional driver (Ekern, 2017); there is supporting evidence for prominent wind forcing events and their impact on surface outflow and mixing, but these wind events are sporadic and are ephemeral meteorological features in Andvord Bay (Lundesgaard et al., 2019) (Ekern, 2017). Meltwater processes were also found to be very weak and inadequate for driving overall circulation in Andvord Bay (Lundesgaard et al., 2019). This mostly due to the cold deep water entering the WAP fjords from the WAP shelf (0—2 ^{o}C); water temperature is often below 0 ^{o}C in the Bransfield Strait, originating from the Weddell Sea (Lundesgaard et al., 2019) (Lundesgaard,

2018) (Martinson et al., 2008). In this way, during spring and fall in Andvord Bay, meltwater plumes near the glaciers were nearly indistinguishable by conventional physical oceanography measurements alone, such as temperature and salinity. However, the mere presence of major glaciers at the head of Andvord Bay beckons a new method for detecting glacial meltwater and understanding its spatial and temporal distribution. This is an important question to pursue, because unlike solid ice flux, meltwater can be directly entrained into the fjord's water column and hence it has a significant impact on phytoplankton ecology.

1.2.3. Iron in Fjords

Glacial meltwater is known to be a source of trace nutrient (Hawkings et al., 2014) (Raiswell et al., 2006), of particular importance to Antarctic waters is the availability of iron (Blain et al., 2007) (Boyd et al., 2000). Greenland and Antarctic ice sheets cover ~10% of the Earth's surface, and the bioavailable iron flux attributed to these glaciers is significant. Glacial runoff in Greenland is 0.40—2.54 Tg/yr and 0.06—0.17 Tg/yr in Antarctica. These estimates of labile iron fluxes in meltwater are comparable with aerosol dust flux to the marine environment in the high latitudes (Hawkings et al., 2014) (Raiswell et al., 2006). The iron fluxes are dominated by highly reactive and potentially bioavailable nanoparticulate suspended sediments, which are similar to those found in Antarctic icebergs (Hawkings et al., 2014) (Raiswell et al., 2006). While the amount and seasonality of iron delivery from the cryosphere to the marine environment may vary by location, the mechanism of which the delivery is carried out by suspended fine sediments that contain iron nanoparticles is generally ubiquitous. High-resolution microscopy has revealed that suspended sediments from glacial meltwater, supraglacial/proglacial sediments, and sediments in basal ice, from study sites in the Arctic, Alpine, and Antarctica, all contain iron (oxyhydr)oxide nanoparticles. These particles are typically ~5 nm in diameter and occur as single grains or aggregates (Raiswell et al., 2006). The presence of glaciers has a disproportionate impact on nutrient availability in fjords. For an instance, marine-terminating glaciers subject to warmer deep Atlantic water (such as that in Godthabsfjord) induce upwelling which bring up nutrient-rich deep

water to the surface (Cape et al. 2020) – this mechanism can sustain high primary productivity during summer. In this way, spring bloom dynamics in Godthabsfjord, SW Greenland appears to be primarily driven by a combination of wind and upwelling due to glacial meltwater, which control the timing, location and intensity of the bloom (Meire et al., 2017). This iron fertilization effect, due to ice-ocean interaction, is directly linked to the glacier's geomorphology, which is also significant to primary producers. In contrast, Young Sound (in the vicinity of Godthabsfjord) has a land-terminating glacier, no deep nutrient input, and the productivity is significantly lower. The lower productivity in Young Sound is also due to its land-terminating glaciers' sediment discharge in meltwater (Meire et al., 2017). While the impact of glacial meltwater on nutrient availability to phytoplankton biomass has been investigated, the entire community was often observed as a "bulk quantity."

1.2.4. Phytoplankton Ecology in Fjords

Most studies of fjords thus far were conducted in the northern hemisphere (Cape et al., 2019a) (Halbach et al., 2019) (Meire et al., 2017) (Straneo & Cenedese, 2015) (Rignot et al., 2013) (Syvitski et al., 1987a), indicating changes in ambient environment, particularly those associated with ice-ocean interaction, can have a direct and significant impact on phytoplankton abundance and community composition. In most Arctic fjords (such as those in Greenland, Svalbard Archipelago and Baffin Island), the water column is often heavily impacted by ice melting processes and turbid plumes (Syvitski et al., 1987a) (Freeland, 1979). The inner and middle areas of these fjords typically sustain high sedimentation rates which limit primary production and cause significant burial disturbance in the benthic environment (Hop et al., 2002) (Syvitski, 1989) (Węsławski et al., 2010). For example, a significant shift in phytoplankton community composition is observed in two Spitsbergen fjords in relation to turbidity. Kongsfjorden and the colder Hornsund are impacted by Atlantic-derived inflow during summer and diatoms remain the dominant taxa, the second most abundant taxa are significantly different – autotrophic dinoflagellates in Kongsfjorden and nanoflagellates in Hornsund (Piwosz et al., 2009). Total

phytoplankton biomass and chl-a concentration are higher in Hornsund, and primary production rates are also one order of magnitude higher there than those of Kongsfjorden. In both fjords, phytoplankton biomass is lower in the inner basin which is likely due to sediment loading and the associated turbidity in the inner basins. These gradients are likely attributed to differences in advected water masses and freshwater runoff, which affect the timing of bloom (Piwosz et al., 2009). In fjords with low turbidity, such as the Scotland lochs, other factors become important drivers for phytoplankton composition and abundance (e.g. in Loch Linnhe). There is a significant freshwater outflow from the head of the fjord which causes stratification of the water column. This feature leads to flagellastes thriving in this environment (cryptophytes and dinoflagellates, in absence of diatoms). Results from the Arctic illustrate the impact of ice-ocean interaction on phytoplankton community composition.

In contrast, there have been fewer studies on the impact of ice-ocean interaction on phytoplankton community in Antarctic fjords. Particularly, we need to understand how environmental variables impact different phytoplankton groups. Phytoplankton community composition is important in the WAP region. For example, diatoms are preferred diet to Antarctic krill (*Euphausia superba*) in comparison to cryptophytes (Cleary et al., 2018) (Knox, 2006). There are fewer trophic levels between primary producers and megafauna – for instance, krill are directly consumed by baleen whales, seals, and penguins (Ducklow et al., 2007) (Knox, 2006). WAP fjords are of particular interest in this context because they have high primary productivity (Pan et al., 2020) (Höfer et al., 2019) (Mascioni et al., 2019) leading to krill aggregation (Espinasse et al., 2012) (Nowacek et al., 2011); this makes the WAP fjords “biological hotspots” with abundant and diverse megafaunal communities (Grange & Smith, 2013) (Nowacek et al., 2011) and productive benthic ecosystems (Ziegler et al., 2020). Hence, any environment-induced changes in phytoplankton community composition will significantly impact the broader ecosystem in the WAP. Given the rapid environmental change and ecological importance of the Antarctic coastal ocean

(Henley et al., 2020) (Henley et al., 2019) (Vernet et al., 2019), the studies presented in this dissertation can fill some of the knowledge gaps in this area.

1.3. The Western Antarctic Peninsula Continental Shelf

In the vicinity of Andvord Bay is the continental shelf of the Western Antarctic Peninsula. Any advected materials from WAP fjords would most certainly arrive in this region due to geographic constraints. The water column of WAP is strongly impacted by the Antarctic Circumpolar Current (ACC), a zonal current around the Antarctic continent (Moffat & Meredith, 2018). The WAP encompasses an area from the Bellingshausen Sea to the northern tip of the peninsula, and from the continental margin to the shelf break (Henley et al., 2019) (Ducklow et al., 2007), with the ACC always present along the shelf break. In this area, the water masses are spatially separated into three categories coinciding with bathymetry and topographically controlled features – slope, shelf, and coastal waters (Martinson et al., 2008). However, unmodified upper Circumpolar Deep Water on the shelf is restricted to the deep canyons and only occasionally appear on the shelf floor in the middle of the shelf, as sampled by the Palmer Long-Term Ecological Research (LTER) program (Henley et al., 2019) (Hendry et al., 2018) (Martinson et al., 2008). Anomalous summer sea surface temperature (SST) reflect wind strength such that stronger wind mixing induces subsurface cold (winter) water to surface and decreases SST (Martinson et al., 2008). Moreover, average annual ocean heat flux to the atmosphere decreased between 1993 and 2004, while ocean heat content over the shelf linearly increased, most is attributed to upwelling of warm Upper Circumpolar Deep Water (Martinson et al., 2008). The heat delivered by the ACC drives the ocean temperature 0.6 ^{o}C higher which warms the upper shelf water (<300 m), combined with a 2 ^{o}C increase in annual mean temperature, and a 6 ^{o}C increase in mean winter temperature, making the WAP one of the most rapidly warming regions on Earth (Smith et al., 2003a) (Smith et al., 2003b) (Vaughan et al., 2003). Ecosystem is responding to this regional warming. There are local declines in Adelie penguins which are ice-dependent, while an increase in Gentoo and Chinstrap penguins which are ice-tolerant species. Organisms at lower

trophic levels are also changing. There are alternations in phytoplankton and zooplankton community composition, particularly as changes in krill recruitment, abundance, and availability to predators. These changes are expected to profoundly transform the “classic” diatom-krill-whale/seal/penguin food chain in this habitat, and have profound effects on the rest of the ecosystem (Ducklow et al., 2007).

Phytoplankton community composition in the WAP has been evaluated in the past. One of the driving factors for seasonal community shift is attributed to sea ice. The annual recurrent assemblages in the WAP are closely related to sea ice retreat. After early sea ice retreat, sea ice edge diatom assemblage is spatially limited; however, after late sea ice retreat, the diatoms at ice edge extend over larger areas (Garibotti et al., 2005). Moreover, this study, along with size structure analysis of phytoplankton in the WAP, indicates that phytoplankton community response to long-term environmental variation is not merely expressed as a trend to small cell size (Montes-Hugo et al., 2008), but rather likely a significant shift in ecological functional type manifested as changes in taxa. Near Averse Island in the WAP, the dominant group is diatom and cryptophyte remains the second most abundant, while mixed flagellates also contribute a significant fraction to the total chl-a concentration but show less interannual variability than diatoms and cryptophytes (Schofield et al., 2017). These existing studies beckon further investigation pertaining to future phytoplankton community shift as more meltwater becomes available in the WAP.

As the WAP continues to warm, glacial meltwater input may become a prominent feature in the local ecosystem (Henley et al., 2019) (Meredith et al., 2010) (Clarke et al., 2007). The presence of meltwater leads to stratification and nearshore turbidity, and it is also correlated with phytoplankton blooms – these meltwater plumes often extend beyond 100 km offshore from the WAP (Dierssen et al., 2002). The contribution of meltwater is significant enough that Antarctic coastal waters is optically classified as “Case II waters” – especially at times when phytoplankton blooms are absent (Dierssen et al., 2002) (Dierssen & Smith, 2000). This is when relatively higher

optical reflectance is observed in all wavelengths due to high backscattering coefficient attributed to the presence of the surface meltwater layer (Dierssen & Smith, 2000).

Material and water mass transport from fjords to the WAP continental shelf is expected, however glaciers' contribution from fjords to shelf waters are less understood (Lundesgaard et al., 2019) (Forsch et al., 2018) (Syvitski et al., 1987a). In comparison, Greenland fjords are known to export fjord-derived products and materials to the open ocean (Cape et al., 2019a) (Beaird et al., 2018) (Arrigo et al., 2017) (Straneo & Cenedese, 2015). This export is directly linked to melting at glacier's face (Straneo et al., 2011). Large-scale summer phytoplankton blooms in the Labrador Sea around Greenland extend >300 km from the coast are usually timed with the arrival of freshwater discharge from outlet glaciers (Arrigo et al., 2017). These summer blooms in the Arctic typically develop about one week after the arrival of glacial meltwater in early July and persists until August/September with slowing meltwater delivery. These blooms account for ~40% of annual net primary production in this area (Arrigo et al., 2017), indicating its importance to overall regional productivity. In the WAP, Annett et al. have found the interannual distribution of iron was closely related to glacial meltwater and precipitation (Annett et al., 2017). These results suggest an export of glacial meltwater, which can bring both dissolved iron and low salinity waters, from the fjords to the shelf in the WAP (Forsch et al., 2018) (Annett et al., 2017). Such spatial pattern of glacial meltwater has been observed over multiple years in the past where a "meltwater lens" extended from the coastline to beyond >100 km over the shelf region (Dierssen et al., 2002). As the WAP region continues to warm in the future, the impacts of glacial meltwater on the physical environment and phytoplankton community requires further investigation and more frequent monitoring. A comprehensive perspective of the entire WAP coastal region, from the glacial terminus to the open ocean, is necessary to better understand how present and future environmental changes will impact the phytoplankton community and regional ecosystem dynamics.

1.4 References

Annett, A.L., Fitzsimmons, J.N., Séguret, M.J., Lagerström, M., Meredith, M.P., Schofield, O., Sherrell, R.M., 2017. Controls on dissolved and particulate iron distributions in surface waters of the Western Antarctic Peninsula shelf. *Marine Chemistry*, 196, 81-97.

Arrigo, K.R., Dijken, G.L., Castelao, R.M., Luo, H., Rennermalm, Å.K., Tedesco, M., Mote, T.L., Oliver, H., Yager, P.L., 2017. Melting glaciers stimulate large summer phytoplankton blooms in southwest Greenland waters. *Geophysical Research Letters*.

Babin, M., Arrigo, K., Bélanger, S., Forget, M.-H., 2015. Ocean Colour Remote Sensing in Polar Seas.

Beaird, N.L., Straneo, F., Jenkins, W., 2018. Export of strongly diluted Greenland meltwater from a major glacial fjord. *Geophysical Research Letters*, 45, 4163-4170.

Bird, D., Karl, D., 1991. Massive prasinophyte bloom in northern Gerlache Strait. *Antarct J US*, 26, 152-154.

Blain, S., Quéguiner, B., Armand, L., Belviso, S., Bombled, B., Bopp, L., Bowie, A., Brunet, C., Brussaard, C., Carlotti, F., 2007. Effect of natural iron fertilization on carbon sequestration in the Southern Ocean. *Nature*, 446, 1070-1074.

Boyd, P.W., Watson, A.J., Law, C.S., Abraham, E.R., Trull, T., Murdoch, R., Bakker, D.C., Bowie, A.R., Buesseler, K., Chang, H., 2000. A mesoscale phytoplankton bloom in the polar Southern Ocean stimulated by iron fertilization. *Nature*, 407, 695-702.

Cape, M.R., Straneo, F., Beaird, N., Bundy, R.M., Charette, M.A., 2019a. Nutrient release to oceans from buoyancy-driven upwelling at Greenland tidewater glaciers. *Nature Geoscience*, 12, 34.

Cape, M.R., Vernet, M., Pettit, E.C., Wellner, J.S., Truffer, M., Akie, G., Domack, E., Leventer, A., Smith, C.R., Huber, B.A., 2019b. Circumpolar Deep Water impacts glacial meltwater export and coastal biogeochemical cycling along the west Antarctic Peninsula. *Frontiers in Marine Science*, 6, 144.

Clarke, A., Murphy, E.J., Meredith, M.P., King, J.C., Peck, L.S., Barnes, D.K., Smith, R.C., 2007. Climate change and the marine ecosystem of the western Antarctic Peninsula. *Philosophical Transactions of the Royal Society B: Biological Sciences*, 362, 149-166.

Cleary, A.C., Durbin, E.G., Casas, M.C., 2018. Feeding by Antarctic krill Euphausia superba in the West Antarctic Peninsula: differences between fjords and open waters. *Marine Ecology Progress Series*, 595, 39-54.

Cook, A., Fox, A., Vaughan, D., Ferrigno, J., 2005. Retreating glacier fronts on the Antarctic Peninsula over the past half-century. *Science*, 308, 541-544.

Cook, A.J., Holland, P., Meredith, M., Murray, T., Luckman, A., Vaughan, D.G., 2016. Ocean forcing of glacier retreat in the western Antarctic Peninsula. *Science*, 353, 283-286.

Dierssen, H.M., Smith, R.C., 2000. Bio-optical properties and remote sensing ocean color algorithms for Antarctic Peninsula waters. *Journal of Geophysical Research: Oceans*, 105, 26301-26312.

Dierssen, H.M., Smith, R.C., Vernet, M., 2002. Glacial meltwater dynamics in coastal waters west of the Antarctic peninsula. *Proceedings of the National Academy of Sciences*, 99, 1790-1795.

Domack, E.W., 1990. Laminated terrigenous sediments from the Antarctic Peninsula: the role of subglacial and marine processes. *Geological Society, London, Special Publications*, 53, 91-103.

Domack, E.W., Ishman, S., 1993. Oceanographic and physiographic controls on modern sedimentation within Antarctic fjords. *Geological Society of America Bulletin*, 105, 1175-1189.

Ducklow, H.W., Baker, K., Martinson, D.G., Quetin, L.B., Ross, R.M., Smith, R.C., Stammerjohn, S.E., Vernet, M., Fraser, W., 2007. Marine pelagic ecosystems: the west Antarctic Peninsula. *Philosophical Transactions of the Royal Society B: Biological Sciences*, 362, 67-94.

Ekern, L., 2017. Assessing Primary Production via nutrient deficits in Andvord Bay, Antarctica 2015-2016. *Scripps Institution of Oceanography*, Vol. Master's University of California, San Diego.

Espinasse, B., Zhou, M., Zhu, Y., Hazen, E.L., Friedlaender, A.S., Nowacek, D.P., Chu, D., Carlotti, F., 2012. Austral fall− winter transition of mesozooplankton assemblages and krill aggregations in an embayment west of the Antarctic Peninsula. *Marine Ecology Progress Series*, 452, 63-80.

Falkowski, P.G., Raven, J.A., 2013. *Aquatic photosynthesis*: Princeton University Press.

Forsch, K., Manck, L., Ekern, L., Pan, B.J., Vernet, M., Barbeau, K., 2018. Links Between Sources of Iron and Organic Iron-binding Ligands to the Supply of Cryospheric Iron to Coastal West Antarctic Peninsula. *Ocean Sciences Meeting*. Portland, Oregon.

Freeland, H., 1979. *Fjord oceanography*: Springer Science & Business Media.

Garibotti, I.A., Vernet, M., Ferrario, M.E., 2005. Annually recurrent phytoplanktonic assemblages during summer in the seasonal ice zone west of the Antarctic Peninsula (Southern Ocean). *Deep Sea Research Part I: Oceanographic Research Papers*, 52, 1823-1841.

Garibotti, I.A., Vernet, M., Kozlowski, W.A., Ferrario, M.E., 2003. Composition and biomass of phytoplankton assemblages in coastal Antarctic waters: a comparison of chemotaxonomic and microscopic analyses. *Marine Ecology Progress Series*, 247, 27-42.

Grange, L.J., Smith, C.R., 2013. Megafaunal communities in rapidly warming fjords along the West Antarctic Peninsula: hotspots of abundance and beta diversity. *Plos One*, 8, e77917.

Griffith, T.W., Anderson, J.B., 1989. Climatic control of sedimentation in bays and fjords of the northern Antarctic Peninsula. *Marine Geology*, 85, 181-204.

Halbach, L., Vihtakari, M., Duarte, P., Everett, A., Granskog, M.A., Hop, H., Kauko, H.M., Kristiansen, S., Myhre, P.I., Pavlov, A.K., 2019. Tidewater glaciers and bedrock characteristics

control the phytoplankton growth environment in a fjord in the arctic. *Frontiers in Marine Science*, 6, 254.

Hawkings, J.R., Wadham, J.L., Tranter, M., Raiswell, R., Benning, L.G., Statham, P.J., Tedstone, A., Nienow, P., Lee, K., Telling, J., 2014. Ice sheets as a significant source of highly reactive nanoparticulate iron to the oceans. *Nature Communications*, 5, 1-8.

Hendry, K.R., Meredith, M.P., Ducklow, H.W., 2018. The marine system of the West Antarctic Peninsula: status and strategy for progress. The Royal Society Publishing.

Henley, S.F., Cavan, E.L., Fawcett, S.E., Kerr, R., Monteiro, T., Sherrell, R.M., Bowie, A.R., Boyd, P.W., Barnes, D.K., Schloss, I.R., 2020. Changing biogeochemistry of the Southern Ocean and its ecosystem implications. *Frontiers in Marine Science*.

Henley, S.F., Schofield, O.M., Hendry, K.R., Schloss, I.R., Steinberg, D.K., Moffat, C., Peck, L.S., Costa, D.P., Bakker, D.C., Hughes, C., 2019. Variability and change in the west Antarctic Peninsula marine system: research priorities and opportunities. *Progress in Oceanography*.

Hickey, H., Weaver, A.J., 2004. The Southern Ocean as a source region for tropical Atlantic variability. *Journal of Climate*, 17, 3960-3972.

Höfer, J., Giesecke, R., Hopwood, M.J., Carrera, V., Alarcón, E., González, H.E., 2019. The role of water column stability and wind mixing in the production/export dynamics of two bays in the Western Antarctic Peninsula. *Progress in Oceanography*.

Holm-Hansen, O., Mitchell, B.G., 1991. Spatial and temporal distribution of phytoplankton and primary production in the western Bransfield Strait region. *Deep Sea Research Part A. Oceanographic Research Papers*, 38, 961-980.

Hop, H., Pearson, T., Hegseth, E.N., Kovacs, K.M., Wiencke, C., Kwasniewski, S., Eiane, K., Mehlum, F., Gulliksen, B., Wlodarska-Kowalczuk, M., Lydersen, C., Weslawski, J.M., Cochrane, S., Gabrielsen, G.W., Leakey, R.J.G., Lønne, O.J., Zajaczkowski, M., Falk-Petersen, S., Kendall, M., Wängberg, S.-Å., Bischof, K., Voronkov, A.Y., Kovaltchouk, N.A., Wiktor, J., Poltermann, M., Prisco, G., Papucci, C., Gerland, S., 2002. The marine ecosystem of Kongsfjorden, Svalbard. *Polar Research*, 21, 167-208.

Howe, J.A., Austin, W.E., Forwick, M., Paetzel, M., Harland, R., Cage, A.G., 2010. Fjord systems and archives: a review. *Geological Society, London, Special Publications*, 344, 5-15.

Hudson, B., Overeem, I., McGrath, D., Syvitski, J., Mikkelsen, A., Hasholt, B., 2014. MODIS observed increase in duration and spatial extent of sediment plumes in Greenland fjords. *The Cryosphere*, 8, 1161-1176.

Jackson, R.H., Straneo, F., Sutherland, D.A., 2014. Externally forced fluctuations in ocean temperature at Greenland glaciers in non-summer months. *Nature Geoscience*, 7, 503.

Knox, G.A., 2006. *Biology of the southern ocean*: CRC Press.

Kozlowski, W.A., Deutschman, D., Garibotti, I., Trees, C., Vernet, M., 2011. An evaluation of the application of CHEMTAX to Antarctic coastal pigment data. *Deep Sea Research Part I: Oceanographic Research Papers*, 58, 350-364.

Lu, Z., Rickaby, R.E., Wellner, J., Georg, B., Charnley, N., Anderson, J.B., Hensen, C., 2010. Pore fluid modeling approach to identify recent meltwater signals on the west Antarctic Peninsula. *Geochemistry, Geophysics, Geosystems*, 11.

Lund-Hansen, L.C., Andersen, T.J., Nielsen, M.H., Pejrup, M., 2010. Suspended matter, Chl-a, CDOM, grain sizes, and optical properties in the Arctic fjord-type estuary, Kangerlussuaq, West Greenland during summer. *Estuaries and Coasts*, 33, 1442-1451.

Lundesgaard, Ø., 2018. Physical Processes in a Western Antarctic Peninsula Fjord. University of Hawai'i at Manoa.

Lundesgaard, Ø., Winsor, P., Truffer, M., Merrifield, M., Powell, B., Statscewich, H., Eidam, E., Smith, C., 2019. Hydrography and energetics of a cold subpolar fjord: Andvord Bay, western Antarctic Peninsula. *Progress in Oceanography*, In review.

Lytle, V., Ackley, S., 1996. Heat flux through sea ice in the western Weddell Sea: Convective and conductive transfer processes. *Journal of Geophysical Research: Oceans*, 101, 8853-8868.

Martinson, D.G., Stammerjohn, S.E., Iannuzzi, R.A., Smith, R.C., Vernet, M., 2008. Western Antarctic Peninsula physical oceanography and spatio–temporal variability. *Deep Sea Research Part II: Topical Studies in Oceanography*, 55, 1964-1987.

Mascarenhas, V.J., Voß, D., Wollschlaeger, J., Zielinski, O., 2017. Fjord light regime: Bio-optical variability, absorption budget, and hyperspectral light availability in Sognefjord and Trondheimsfjord, Norway. *Journal of Geophysical Research: Oceans*, 3828-3847.

Mascioni, M., Almandoz, G.O., Cefarelli, A.O., Cusick, A., Ferrario, M.E., Vernet, M., 2019. Phytoplankton composition and bloom formation in unexplored nearshore waters of the western Antarctic Peninsula. *Polar Biology*, 42, 1859-1872.

Mascioni, M., Almandoz, G.O., Ekern, L., Pan, B.J., Vernet, M., 2020. Microplanktonic diatom assemblages dominated the primary production in an Antarctic fjord. *in prep.*

Meire, L., Mortensen, J., Meire, P., Juul-Pedersen, T., Sejr, M.K., Rysgaard, S., Nygaard, R., Huybrechts, P., Meysman, F.J., 2017. Marine-terminating glaciers sustain high productivity in Greenland fjords. *Global Change Biology*, 23, 5344-5357.

Meire, L., Søgaard, D., Mortensen, J., Meysman, F., Soetaert, K., Arendt, K., Juul-Pedersen, T., Blicher, M., Rysgaard, S., 2015. Glacial meltwater and primary production are drivers of strong CO2 uptake in fjord and coastal waters adjacent to the Greenland Ice Sheet. *Biogeosciences*, 12, 2347-2363.

Meredith, M.P., Wallace, M.I., Stammerjohn, S.E., Renfrew, I.A., Clarke, A., Venables, H.J., Shoosmith, D.R., Souster, T., Leng, M.J., 2010. Changes in the freshwater composition of the

upper ocean west of the Antarctic Peninsula during the first decade of the 21st century. *Progress in Oceanography*, 87, 127-143.

Moffat, C., Meredith, M., 2018. Shelf–ocean exchange and hydrography west of the Antarctic Peninsula: a review. *Philosophical Transactions of the Royal Society A: Mathematical, Physical and Engineering Sciences*, 376, 20170164.

Montes-Hugo, M., Vernet, M., Martinson, D., Smith, R., Iannuzzi, R., 2008. Variability on phytoplankton size structure in the western Antarctic Peninsula (1997–2006). *Deep Sea Research Part II: Topical Studies in Oceanography*, 55, 2106-2117.

Motyka, R.J., Hunter, L., Echelmeyer, K.A., Connor, C., 2003. Submarine melting at the terminus of a temperate tidewater glacier, LeConte Glacier, Alaska, USA. *Annals of Glaciology*, 36, 57-65.

Murray, C., Markager, S., Stedmon, C.A., Juul-Pedersen, T., Sejr, M.K., Bruhn, A., 2015. The influence of glacial melt water on bio-optical properties in two contrasting Greenlandic fjords. *Estuarine, Coastal and Shelf Science*, 163, 72-83.

Nowacek, D.P., Friedlaender, A.S., Halpin, P.N., Hazen, E.L., Johnston, D.W., Read, A.J., Espinasse, B., Zhou, M., Zhu, Y., 2011. Super-aggregations of krill and humpback whales in Wilhelmina Bay, Antarctic Peninsula. *Plos One*, 6, e19173.

Pan, B.J., Vernet, M., Manck, L., Forsch, K., Ekern, L., Mascioni, M., Barbeau, K.A., Almandoz, G.O., Orona, A.J., 2020. Environmental drivers of phytoplankton taxonomic composition in an Antarctic fjord. *Progress in Oceanography*, 183, 102295.

Pan, B.J., Vernet, M., Reynolds, R.A., Mitchell, B.G., 2019. The optical and biological properties of glacial meltwater in an Antarctic fjord. *Plos One*, 14, e0211107.

Petrou, K., Kranz, S.A., Trimborn, S., Hassler, C.S., Ameijeiras, S.B., Sackett, O., Ralph, P.J., Davidson, A.T., 2016. Southern Ocean phytoplankton physiology in a changing climate. *Journal of Plant Physiology*, 203, 135-150.

Piwosz, K., Walkusz, W., Hapter, R., Wieczorek, P., Hop, H., Wiktor, J., 2009. Comparison of productivity and phytoplankton in a warm (Kongsfjorden) and a cold (Hornsund) Spitsbergen fjord in mid-summer 2002. *Polar Biology*, 32, 549-559.

Powell, R., Domack, E., 1995. Modern glaciomarine environments. *Glacial environments*, 1, 445-486.

Pritchard, H.D., Arthern, R.J., Vaughan, D.G., Edwards, L.A., 2009. Extensive dynamic thinning on the margins of the Greenland and Antarctic ice sheets. *Nature*, 461, 971.

Pritchard, H.D., Vaughan, D.G., 2007. Widespread acceleration of tidewater glaciers on the Antarctic Peninsula. *Journal of Geophysical Research: Earth Surface*, 112.

Raiswell, R., Tranter, M., Benning, L.G., Siegert, M., De'ath, R., Huybrechts, P., Payne, T., 2006. Contributions from glacially derived sediment to the global iron (oxyhydr)oxide cycle: Implications for iron delivery to the oceans. *Geochimica Et Cosmochimica Acta*, 70, 2765-2780.

Rignot, E., Jacobs, S., Mouginot, J., Scheuchl, B., 2013. Ice-shelf melting around Antarctica. *Science*, 341, 266-270.

Rignot, E., Koppes, M., Velicogna, I., 2010. Rapid submarine melting of the calving faces of West Greenland glaciers. *Nature Geoscience*, 3, 187.

Schofield, O., Saba, G., Coleman, K., Carvalho, F., Couto, N., Ducklow, H., Finkel, Z., Irwin, A., Kahl, A., Miles, T., 2017. Decadal variability in coastal phytoplankton community composition in a changing West Antarctic Peninsula. *Deep Sea Research Part I: Oceanographic Research Papers*, 124, 42-54.

Schwerdtfecer, P., 1963. The thermal properties of sea ice. *Journal of Glaciology*, 4, 789-807.

Sciascia, R., Straneo, F., Cenedese, C., Heimbach, P., 2013. Seasonal variability of submarine melt rate and circulation in an East Greenland fjord. *Journal of Geophysical Research: Oceans*, 118, 2492-2506.

Scott, F.J., Marchant, H.J., 2005. *Antarctic marine protists*: Australian Biological Resources Study Canberra.

Smith, R.C., Baker, K.S., Dustan, P., 1981. Fluorometric Techniques For The Measurement Of Oceanic Chlorophyll In The Support Of Remote Sensing. *SIO Refence*, 81, 1-14.

Smith, R.C., Dierssen, H.M., Vernet, M., 1996. Phytoplankton biomass and productivity in the western Antarctic Peninsula region. *Antarctic Research Series*, 70, 333-356.

Smith, R.C., Fraser, W.R., Stammerjohn, S.E., 2003a. *Climate variability and ecological response of the marine ecosystem in the western Antarctic Peninsula (WAP) region*: Oxford University Press, New York.

Smith, R.C., Fraser, W.R., Stammerjohn, S.E., Vernet, M., 2003b. Palmer Long-Term Ecological Research on the Antarctic Marine Ecosystem. *Antarctic Peninsula Climate Variability: Historical and Paleoenvironmental Perspectives*, 131-144.

Straneo, F., Cenedese, C., 2015. The dynamics of Greenland's glacial fjords and their role in climate. *Annual review of marine science*, 7, 89-112.

Straneo, F., Curry, R.G., Sutherland, D.A., Hamilton, G.S., Cenedese, C., Våge, K., Stearns, L.A., 2011. Impact of fjord dynamics and glacial runoff on the circulation near Helheim Glacier. *Nature Geoscience*, 4, 322.

Syvitski, J., 1989. On the deposition of sediment within glacier-influenced fjords: oceanographic controls. *Marine Geology*, 85, 301-329.

Syvitski, J., Burrell, D., Skei, J., 1987a. *Fjords: Processes and Products*: Springer-Verlag.

Syvitski, J.P., Burrell, D.C., Skei, J.M., 1987b. Fjords and Their Study. *Fjords* (pp. 3-17): Springer.

Thomas, R., Rignot, E., Casassa, G., Kanagaratnam, P., Acuña, C., Akins, T., Brecher, H., Frederick, E., Gogineni, P., Krabill, W., 2004. Accelerated sea-level rise from West Antarctica. *Science*, 306, 255-258.

Torinesi, O., Fily, M., Genthon, C., 2003. Variability and trends of the summer melt period of Antarctic ice margins since 1980 from microwave sensors. *Journal of Climate*, 16, 1047-1060.

Trenberth, K.E., Jones, P.D., Ambenje, P., Bojariu, R., Easterling, D., Tank, A.K., Parker, D., Rahimzadeh, F., Renwick, J.A., Rusticucci, M., Soden, B., Zhai, P., 2007. Observations: surface and atmospheric climate change. *In: Solomon, D.Q.S., Manning, M., Chen, Z., Marquis, M., Averyt, K.B., Tignor, M., Miller, H.L. (Eds.), Climate Change 2007: The Physical Science Basis. Contributions of Working Group 1 to the Fourth Assessment Report of the Intergovernmental Panel on Climate Change*.

Vaughan, D.G., Marshall, G.J., Connolley, W.M., Parkinson, C., Mulvaney, R., Hodgson, D.A., King, J.C., Pudsey, C.J., Turner, J., 2003. Recent rapid regional climate warming on the Antarctic Peninsula. *Climatic change*, 60, 243-274.

Vernet, M., Geibert, W., Hoppema, M., Brown, P.J., Haas, C., Hellmer, H., Jokat, W., Jullion, L., Mazloff, M., Bakker, D., 2019. The Weddell Gyre, Southern Ocean: present knowledge and future challenges. *Reviews of Geophysics*, 57, 623-708.

Vernet, M., Letelier, R., Karl, D.M., 1991. RACER: Phytoplankton growth rates in the northern Gerlache Strait during the spring bloom of 1989. *Antarctic Journal of the United States*, 26, 154.

Vernet, M., Martinson, D., Iannuzzi, R., Stammerjohn, S., Kozlowski, W., Sines, K., Smith, R., Garibotti, I., 2008. Primary production within the sea-ice zone west of the Antarctic Peninsula: I—Sea ice, summer mixed layer, and irradiance. *Deep Sea Research Part II: Topical Studies in Oceanography*, 55, 2068-2085.

Węsławski, J.M., Kendall, M.A., Włodarska-Kowalczuk, M., Iken, K., Kędra, M., Legezynska, J., Sejr, M.K., 2010. Climate change effects on Arctic fjord and coastal macrobenthic diversity—observations and predictions. *Marine Biodiversity*, 41, 71-85.

Wright, S.W., van den Enden, R.L., Pearce, I., Davidson, A.T., Scott, F.J., Westwood, K.J., 2010. Phytoplankton community structure and stocks in the Southern Ocean (30–80 E) determined by CHEMTAX analysis of HPLC pigment signatures. *Deep Sea Research Part II: Topical Studies in Oceanography*, 57, 758-778.

Ziegler, A., Cape, M., Lundesgaard, Ø., Smith, C., 2020. Intense deposition and rapid processing of seafloor phytodetritus in a glaciomarine fjord, Andvord Bay (Antarctica). *Progress in Oceanography*, 102413.

Chapter 2. The Optical and Biological Properties of Glacial Meltwater in an Antarctic Fjord

2.1. Abstract

As the Western Antarctic Peninsula (WAP) region responds to a warmer climate, the impacts of glacial meltwater on the Southern Ocean are expected to intensify. The Antarctic Peninsula fjord system offers an ideal system to understand meltwater's properties, providing an extreme in the meltwater's spatial gradient from the glacio-marine boundary to the WAP continental shelf. Glacial meltwater discharge in Arctic and Greenland fjords is typically characterized as relatively lower temperature, fresh and with high turbidity. During two cruises conducted in December 2015 and April 2016 in Andvord Bay, we found a water lens of low salinity and low temperature along the glacio-marine interface. Oxygen isotope ratios identified this water lens as a mixture of glacial ice and deep water in Gerlache Strait suggesting this is glacial meltwater. Conventional hydrographic measurements were combined with optical properties to effectively quantify its spatial extent. Fine suspended sediments associated with meltwater (nanoparticles of ~ 5nm) had a significant impact on the underwater light field and enabled the detection of meltwater characteristics and spatial distribution. In this study, we illustrate that glacial meltwater in Andvord Bay alters the inherent and apparent optical properties of the water column, and develop statistical models to predict the meltwater content from hydrographic and optical measurements. The predicted meltwater fraction is in good agreement with *in-situ* values. These models offer a potential for remote sensing and high-resolution detection of glacial meltwater in Antarctic waters. Furthermore, the possible influence of meltwater on phytoplankton abundance in the surface is highlighted; a significant correlation is found between meltwater fraction and chlorophyll concentration.

2.2. Introduction

The physical impact of Antarctic glacial melting on sea level variability is being extensively studied (Rignot et al., 2013) (Vaughan, 2006) (DeConto & Pollard, 2016) (Nerem et al., 2018). The effects of glacial meltwater on Antarctic coastal hydrography and regional marine ecosystem are also expected to be critical to future marine productivity, but understanding of these processes is limited. Meltwater is undoubtedly a significant feature as a consequence of atmospheric and oceanic warming in climate-sensitive polar regions (Keigwin et al., 1991). In addition to sea level rise, the melting of both glacial and sea ice also induces water column stratification (particularly in shallow coastal regions), where the meltwater is likely to impact light availability, as well as the function and structure of food webs (Vernet et al., 2008a) (Vernet et al., 2008b) (Dierssen et al., 2002). The Western Antarctic Peninsula (WAP) is a region experiencing rapid climate change (Vaughan et al., 2003). Mean air temperatures along the WAP have increased significantly (1–2 °C) over the last 50 years (Steig et al., 2009), which has profound consequences on sea ice, ice shelves, and glacial melting (Dierssen et al., 2002) (Smith & Stammerjohn, 2001). This change had already triggered the collapse of Larsen ice shelf A and B east of the Peninsula (Cook, 2017) (Cape et al., 2015) (Cape et al., 2014).

Fjord systems provide a unique opportunity for studying meltwater effect on coastal ecosystems. Fjords are submerged valleys established by erosion of glacial ice and sea level rise since the last glaciation, and they typically contain one or more sills and sediment-laden basins (Syvitski, 1989) (Syvitski et al., 1987). Fjords with glaciers connected with the ocean, or tidewater glaciers, are common geographic features at mid- and high latitudes and they form an important glacio-marine boundary (Powell & Domack, 1995). In polar regions, the physical transport in these semi-enclosed fjord systems serves as a major mechanism for moving glacial ice to the sea, hence they are sensitive to climatic warming and changes in ice-ocean dynamics (Syvitski, 1989) (Węsławski et al., 2010) (Pritchard & Vaughan, 2007). These characteristics can result in a spatial gradient of meltwater from the glacial terminus to coastal ocean through the mouth of the fjord.

Initially, the transport and spatial distribution of meltwater in sub-Arctic fjords was considered to be consistent with a simple two-layer circulation – where warm oceanic water intrusion enters at depth, and then mixes with subglacial (i.e. at the glacier base) and submarine meltwater (i.e. generated at the glacier front) as it rises to the surface along the glacial terminus. The modified discharge water is transported out of the fjord and into the coastal ocean at the surface (Motyka et al., 2003). These processes broadly resemble those of an estuarine circulation. However, recent studies in Greenland fjords reveal that the physical oceanography and meltwater transport in glacial fjords are far more complex (Mankoff et al., 2016) (Straneo et al., 2011); for example, the subglacial discharge plume found in Saqqarliup Fjord (located near central western Greenland) is ~20m in diameter at surface of the glacial ice edge, but it spreads to a 200m by 300 m plume pool as it reaches the surface, before descending to its equilibrium depth (Mankoff et al., 2016).

Significant sediment plumes are associated with meltwater discharge; when the sediment plumes are prominent, they are detectable by ocean color sensors (Hudson et al., 2014) and can be used as a proxy for estimating ice sheet runoff in Greenland (McGrath et al., 2010). Meltwater-induced turbid plumes can sometimes emerge at the surface near the glaciers (Straneo & Cenedese, 2015) (Chu et al., 2009). Suspended sediments from glacial meltwater ubiquitously contain iron (oxyhydr)oxide nanoparticles, typically ~5nm in diameter, and they can occur as single grains or aggregates that may be isolated or attached to sediment grains (Raiswell et al., 2006). These discharged meltwater plumes not only have a significant impact on the coastal ocean in a fjord's vicinity (Beaird et al., 2015), but also on the global climate (Straneo & Cenedese, 2015).

The meltwater plumes carrying inorganic particles, or "glacial flour", have certain bio-optical characteristics. In western Greenland, Uummannaq Fjord and Vaigat–Disko Bay, freshwater influx from glacial terminus increases the diffuse attenuation coefficient of photosynthetically available radiation (K_d(PAR)) and the optical backscattering coefficient within

the water column (Holinde & Zielinski, 2015). The impact of a meltwater plume on underwater light field is so significant that PAR can be robustly modeled based on inorganic particle properties and chlorophyll-a (chl-a) concentrations alone (Holinde & Zielinski, 2016). Antarctic glacial meltwater can extend offshore >100m over the WAP shelf (Dierssen et al., 2002), but the plumes usually lack significant sediment load, due to lack of major sources of terrestrial runoff such as permafrost or riverine input, with the exception of penguin colonies (Park et al., 2007). In WAP fjords, including Andvord Bay, the cause of elevated beam attenuation coefficients along the glacial-marine interface have been identified as fine suspended sediment originating from the glaciers [17].

$\delta^{18}O$-salinity relationship has been used to study the evolution of water masses near ice shelves and to calculate the mean isotope ratio of melting ice by extrapolation of the mixing line to zero salinity (Jacobs et al., 1985) (Potter et al., 1984). Once the meltwater has been identified, an effective method to track meltwater is by *in-situ* temperature and salinity distribution (Jenkins, 1999). However, field methods are often limited in space and time. Therefore, it is important to develop additional means to monitor and track meltwater and assess its impact on regional scales. This beckons the utilization of non-conventional measurements to characterize meltwater and its spatial distribution. Optically derived relationships can allow *in-situ* data to be directly linked to remotely detectable variables, hence greatly expand the spatiotemporal range. Currently, the optical characteristics of Antarctic glacial meltwater are not well understood, in particular their inherent optical properties (IOPs) and how they are associated with other environmental variables. In this study, we aim to understand the spatial distribution of glacial meltwater throughout an Antarctic fjord, to characterize optical features associated with this meltwater in the water column, to quantify meltwater hydrography based on optical and physical measurements and finally, its impact on phytoplankton abundance.

2.3. Material and Methods

2.3.1. Study Area & Field Program

No specific permissions were required for these locations/activities presented in this manuscript. The field studies did not involve endangered or protected species. Sampling and data presented in this study were primarily collected in Andvord Bay, a fjord system in the WAP that is adjacent to Anvers Island and connected to Gerlache Strait (Fig 2.1). Andvord Bay is located on the WAP's Danco Coast and is significantly glaciated, thus it is a distinct glacial ice drainage system (Williams et al., 1989). The bay is historically free of sea ice during the summer months (Domack & Williams, 1990). However, physical forcing, such as wind and currents, can temporarily cover the inner fjord with brash ice and icebergs. The geometry of Andvord Bay follows a typical fjord-type embayment. It is approximately 20 km in length, and has two inner basins (Inner Basin West at ~64.8918 ^{o} S, 62.5973 ^{o} W, and Inner Basin East at ~64.8731^{o} S, 62.4476^{o} W). There are several partial and full sills throughout this fjord which contribute to variability in its bathymetry. At the head of the fjord (at ~64.8959 ^{o} S, 62.5397 ^{o} W), there are five glaciers in direct contact with oceanic water; Grubb Glacier and Bagshawe Glacier drain into Inner Basin West, while Arago Glacier, Moser Glacier, and Rudolph Glaicer drain into Inner Basin East. These glaciers form an important interface where glacio-marine interactions occur. The distance from these glaciers is calculated as the shortest displacement from a single glacial boundary line that encompasses all five glaciers in both inner basins. Ice-modified water masses are in contact with Gerlache Strait water at the mouth of the fjord situated at ~64.7697 ^{o} S, 62.7717 ^{o} W, approximately 20 km away from the glaciers.

The field program in Andvord Bay was conducted onboard *R/V Gould* (LMG1510) and *RVIB Palmer* (NBP1603) within the FjordEco Program. Sampling on LMG1510 occurred between November 27th – December 20th, 2015, and then between April 4th—April 26th, 2016 on NBP1603, which coincided with late Austral spring and fall respectively. Daily station sampling and various meridional and zonal transects were conducted in Andvord Bay, Gerlache Strait, as well as at an open ocean station on the WAP shelf (Station B at ~ 64.7732 ^{o} S, 65.3177 ^{o} W, which overlaps

with a shelf station on Line 600 in the Palmer LTER Program (Smith et al., 2006)). At each daily station and during transects, water samples and temperature-salinity-depth data were collected using a CTD rosette sampler with twenty-four 10-L bottles (Seabird SBE, Sea-Bird Electronics Inc., USA). Concurrently, light transmittance was measured by a CTD-mounted WebLabs C-Star transmissometer which was used to derive particulate beam attenuation coefficient (c_p(660)); the transmissometer has a path length of 25 cm and operates at 660 nm. The CTD sampler was also equipped with a WetLabs FLRTD fluorometer to detect phytoplankton fluorescence and a Biospherical Instrument QSP-200L4S to measure photosynthetic active radiation (PAR) irradiance in the water column. Bio-optical samples were primarily collected within the euphotic layer, generally at depths of 50%, 10%, 1% of surface PAR irradiance; other water samples were collected at various 12 depths throughout the water column in order to opportunistically target certain hydrographic features of interest, as well as to follow pre-determined depths based on surface PAR attenuation.

Other instrument casts were conducted daily immediately before and after a CTD cast. A Profiling Reflectance Radiometer (PRR-800, Biospherical Inc., USA) and a Hydroscat-6 (HS-6, HOBI Labs, USA) were deployed to measure water column radiometric quantities and to estimate the spectral backscattering coefficient, b_b(λ) (Table 2.1).

2.3.2. Radiometry and Apparent Optical Properties (AOPs)

PRR is a hand-deployed free-falling instrument that measures 16 spectral bands from 320nm – 670nm. It measures downwelling plane irradiance ($E_d(\lambda)$, where λ is defined as light wavelength in vacuum), upwelling radiance from the nadir direction ($L_u(\lambda)$), two PAR channels, as well as ancillary measurements such as depth, temperature and tilt/pitch angles of the instrument. A separate surface radiometer of this PRR package was setup on deck to record concurrent reference downwelling plane irradiance at surface ($E_s(\lambda)$) during each deployment. Depending on weather and ice conditions, the instrument was deployed off the vessel's stern, which was maneuvered to Sun-facing direction to avoid shadows of the research vessel. The instrument was

allowed to drift more than 50m away from the ship before surface measurements were recorded, followed by the freefall cast to profile the water column. Each cast was performed by lowering the profiler until the maximum depth was obtained. One cast was recorded for each daily station.

Upwelling radiance reflectance normalized to downwelling irradiance (hereafter referred to as reflectance and symbolized as $R(\lambda)$) was calculated as the ratio between $L_u(\lambda)$ and $E_d(\lambda)$ at each respective wavelength and concurrent depths (z):

$$R(\lambda, z) = \frac{L_u(\lambda, z)}{E_d(\lambda, z)} \quad (1)$$

where discrete $L_u(\lambda, z)$ is measured in unit of μW (sr cm^2 nm)$^{-1}$, $E_d(\lambda, z)$ is in unit of μW (cm^2 nm)$^{-1}$, and hence $R(\lambda, z)$ has units of sr^{-1}. Remote sensing reflectance ($R_{rs}(\lambda)$) was calculated as:

$$R_{rs}(\lambda) = 0.54 \frac{L_u(\lambda, 0-)}{E_s(\lambda)} \quad (2)$$

where $L_u(\lambda, 0-)$ indicates the value extrapolated to a depth just below the sea surface, and E_s is the above surface plane irradiance measured by the reference radiometer on deck. The advantage of this $R_{rs}(\lambda)$ calculation is that $E_s(\lambda)$ is not impacted by physical fluctuations which are common in underwater $E_d(\lambda)$ measurements (eg. wave focusing and vertical tilt); however, this method requires two instruments that are spatially separated, which may introduce bias due to moving clouds and ship's shadows. Nevertheless, the radiometric sampling was conducted with a rigorous protocol and precise coordination with vessel operation to reduce these biases. This calculation is also consistent with the NASA protocol which has been implemented in the past; a detailed description of data processing has been described by Mitchell and Kahru (Mitchell & Kahru, 1998).

2.3.3. Bio-optical measurements and Inherent Optical Properties (IOPs)

Backscattering ($b_b(\lambda)$)

The spectral backscattering coefficient, $b_b(\lambda)$, was obtained from the commercially available HS-6 developed by HOBI Labs (Maffione & Dana, 1997). HS-6 was winch-deployed on the starboard side of the research vessel. The instrument measures the volume scattering function (β) in six spectral bands (420, 442, 470, 510, 590, and 700 nm) at a scattering angle of 140°, which was then used to estimate $b_b(\lambda)$. The backscattering coefficient is defined as the integral of β over the backwards hemisphere relative to the direction of light propagation (Mobley, 1994),

$$b_b(\lambda) = 2\pi \int_{\pi/2}^{\pi} \beta(\psi,\lambda)\ \sin(\psi)\, d\psi \quad (3)$$

where ψ is the scattering angle. The values of $b_b(\lambda)$ were estimated from the measurements of $\beta(140^o, \lambda)$ following the method by Doxaran *et al.* (Doxaran et al., 2016) and assuming a χ value of 1.13. Preliminary data processing was conducted in Hydrosoft 2.95. Because there is a finite distance between the instance of scattering and the detector, this measurement is also corrected for attenuation of the signal along the measurement's path length, also known as "σ correction." The σ correction procedure follows that described by Reynolds *et al.* (Reynolds et al., 2016).

To derive particulate backscattering coefficient ($b_{bp}(\lambda)$), the effect of seawater backscattering needs to be excluded. Seawater backscattering ($b_{b,sw}(\lambda)$) was calculated based on temperature and salinity measured by CTD at corresponding depths of each HS-6 cast (Zhang et al., 2009). $b_{bp}(\lambda)$ was then calculated as:

$$b_{bp}(\lambda) = b_b(\lambda) - b_{b,SW}(\lambda) \quad (4)$$

Absorption ($a(\lambda)$)

Total particulate absorption (a_p) was derived from laboratory measurements onboard each cruise. Optical density of filtered sample (OD_f) was obtained by filtering water samples onto 25mm glass fiber filters (GF/Fs, ~0.8 μm pore size, Whatman) and scanning them in a spectrophotometer (UV/VIS PerkinElmer Lambda 18) from 200nm to 800nm with 1nm interval. An integrating sphere (Labsphere, Perkin−Elmer RSA−PE−18) was installed and each sample was measured in the transmittance port. Optical density of suspended sample (OD_s) was derived and a_p was calculated from OD_s according to Stramski *et al.* (Stramski et al., 2015) with moistened blank GF/Fs used as reference:

$$OD_s = 0.679\, OD_f^{1.2804} \tag{5}$$

$$a_p = \ln(10)\, OD_S\, \frac{A}{V} \tag{6}$$

where A is the sample-strained area on each GF/F, and V is the filtered volume of each water sample. The measured a_p was also partitioned into the absorption of non-algal particles (a_{NAP}) and phytoplankton (a_{ph}) through the use of methanol extraction according to Kishino *et al.* (Kishino et al., 1985).

Absorption of CDOM (a_{CDOM}) was measured by pressure-assisted filtration directly from the rosette bottles. Water samples were filtered through pre-combusted 47mm GF/Fs; each filter was heated to 450°C for 5 hours prior to the cruise. The sample filtrates were captured and stored in glass amber bottles that were cleaned with 10% HCl and then combusted before use. CDOM samples were measured in a 10cm cuvette by scanning in a dual-beam spectrophotometer (Cary 300 Agilent). Prior to each sample analysis, cuvette was rinsed with purified water (MilliQ) and then conditioned with sample water; MilliQ was used as the reference material. a_{CDOM} is derived from OD_s based on Mitchell *et al.* (Mitchell et al., 2002):

$$a_{CDOM} = \frac{2.303\, OD_{S,CDOM}}{0.1}$$

(7)

2.3.4. Chlorophyll-a

Phytoplankton abundance is estimated by the analysis of Chl-a concentrations. Water samples were filtered through Whatman GF/Fs under low vacuum, and immediately frozen at -80^{o}C. This was followed by extraction of the pigments using 90% acetone solution, and measuring the fluorescence of each sample's supernatant with a calibrated fluorometer (10AU Benchtop and Field Fluorometer, Turner Designs, USA). The calculation of Chl-a concentration from fluorescence was made according to Smith *et al.* (Smith et al., 1981).

2.3.5. Suspended Particulate Mass

For suspended particulate mass concentrations (SPM), water samples were filtered under low vacuum through rinsed, combusted, and pre-weighed 25mm GF/Fs. Following filtration, filters and their edges were carefully rinsed with deionized water to remove residual sea salt and transferred to clean glass containers. Sample filters were dried at 60^{o}C and stored in sealed containment until weighing. After determining SPM, the filters were combusted again in order to quantify the inorganic (SPM_i) and organic (SPM_o) fractions of each sample's total SPM content.

2.3.6. Meltwater Fraction

Oxygen isotopic ratio ($\delta^{18}O$) samples were collected from discrete depths and are used to estimate the meteoric water fraction in Andvord Bay. Utilizing $\delta^{18}O$ as a tracer to determine the source of water is based on the fractionation of the oxygen isotopes. Light water molecules, ^{16}O, evaporate more readily than ^{18}O, hence precipitation from this evaporation is enriched in ^{16}O and depleted in ^{18}O relative to the seawater standard. The $\delta^{18}O$ of water samples are measured in the Stable Isotope Laboratory at Oregon State University. The sample is measured using the water-CO_2 equilibration method modified from Epstein and Mayeda (Epstein & Mayeda, 1953). Standards are selected so that the range of expected sample $\delta^{18}O$ values is bracketed. Sample vials are connected to the equilibration line and placed in a water bath (18°C), and allowed to

temperature equilibrate for 15 minutes. After temperature equilibration, the headspace of the vials is pumped out for ~10 minutes, and then refilled with CO_2 gas. Samples are then allowed to isotopically equilibrate for 12 hours. During the entire analysis, samples are slowly shaken to aid isotopic equilibration. The water samples are analyzed by dual inlet mass spectrometry using the DeltaPlus XL.

Results of discrete oxygen isotopic samples are reported in units of the standard per mil notation (‰) relative to the Vienna Standard Mean Ocean Water (VSMOW) (Coplen, 1995):

$$\delta^{18}O = \left(\frac{\left(\frac{18_O}{16_O}\right)_{sample}}{\left(\frac{18_O}{16_O}\right)_{standard}} - 1 \right) \times 1000\ ‰ \quad (8)$$

The analysis on the component sources of each water sample is based on the method from Jenkins and Jacobs (Jenkins, 1999; Jenkins & Jacobs, 2008). In this study, we are using $\delta^{18}O$ as a one-dimensional domain to derive meteoric water fraction (Q_i):

$$Q_i = \frac{(\delta^{18}O_i - \delta^{18}O_{GD})}{(\delta^{18}O_{glacier} - \delta^{18}O_{GD})} \quad (9)$$

where $\delta^{18}O_i$ is the $\delta^{18}O$ value of each discrete sample, $\delta^{18}O_{glacier}$ is the $\delta^{18}O$ value of one end-member obtained from glacial ice, and $\delta^{18}O_{GD}$ is the averaged $\delta^{18}O$ values from mid-depths sampled in Gerlache Strait as the other end-member (Table 2.2). If water column properties are a result of the mixing of glacial ice with an oceanic source, then the isotope composition of the mixture is given approximately by Equation 9. In general, it is assumed the mixing occurs between deep oceanic water of $\delta^{18}O$ of ~0‰ with high salinity and a meteoric source of 0 PSU with low $\delta^{18}O$ of (known as the Gade line, after Gade 1979 (Gade, 1979)). From Andvord Bay we measured glacial ice with $\delta^{18}O$ of -12‰ in December and -15‰ in April (Table 2.2), similar to other WAP $\delta^{18}O$ estimates of -16‰ (Meredith et al., 2017) and -20‰ (Meredith et al., 2008). In

order to increase the spatial resolution of meltwater fraction, each Q_i value was correlated with its corresponding salinity value in order to interpolate Q_i according to *in-situ* salinity for the entire Andvord Bay. In this study Q_i is reported in decimal fraction units instead of percentages.

2.4. Results

2.4.1. Hydrography

A cold surface layer, a relatively warmer sub-surface layer, and a cold deep water are present in Andvord Bay, and this feature is more prominent during April (Figs 2.2a and 2.2b). Overall, the average potential temperature of these 3 layers ≤ 20 km from the glaciers is -0.17 ± 0.01 ^{o}C (0-25 m), -0.54 ± 0.01 ^{o}C (25-200 m), -0.95 ± 0.004 ^{o}C (>200 m) for December and , -0.52 ± 0.01 ^{o}C (0-25 m), -0.17 ± 0.01 ^{o}C (25-200 m), -0.52 ± 0.01 ^{o}C (>200 m) for April, respectively, Within the Bay, the maximum and minimum potential temperature values are both observed in the Inner Basin West; the maximum and minimum of 0.19 ^{o}C and -1.22 ^{o}C were near the surface at 3.5--3.9 km from the termini. The average salinity of the surface, intermediate and deep layers was 34.05 ± 0.01 PSU (0-25 m), 34.41 ± 0.004 PSU (25-200 m), 34.53 ± 0.004 PSU (>200 m) for December, and 33.72 ± 0.007 PSU (0-25 m), 34.26 ± 0.007 PSU (25 – 200 m), 34.50 ± 0.007 PSU (>200 m) for April respectively, with a minimum of 33.47 PSU at 1.8 m depth, 12 km away from the glacial termini. The low salinity surface water is generally constrained to the fjord (Figs 2.2c and 2.2d). The surface layer also exhibits depletion in $\delta^{18}O$ (z <25 m, -0.42 ± 0.009 ‰ for December and -0.51 ± 0.010 ‰ for April) while the rest of the water column presents relatively more enriched values (Figs 2.2e and 2.2f). The most depleted $\delta^{18}O$ value of -0.66 ‰ was found at the surface (1.3 m depth) at mid-fjord (12 km away from the glaciers), and the most enriched value (-0.12 ‰) was found 33 km away. Higher dissolved oxygen concentrations are found at the surface, while relatively lower values and oxygen minimum are found at depth (Figs 2.2g and 2h). The maximum value of 370 µmol/L was observed at 2m depth in a middle basin. In summary, there is a warming and freshening with depleted $\delta^{18}O$ from December to April, with the mean potential temperature increasing from -0.54 ± 0.01 ^{o}C to -0.36 ± 0.01 ^{o}C by April, the mean salinity

decreasing from 34.34 ± 0.008 PSU to 34.11 ± 0.007 PSU (Figs A1a and A1b). The distinct surface fresh layer in December also deepens in April from 30 m to 60 m (Figs 2.2c and 2.2d). The mean $\delta^{18}O$ value is -0.32 ± 0.006 ‰ in December and -0.36 ± 0.008 ‰ in April (Figs A1c and A1d).

2.4.2. Phytoplankton

Highest chl-a concentrations occurred at the surface layer in Andvord Bay, mostly constrained to the fjord's middle basins (Fig 2.3). Above 60 m depth, the average concentration was 1.211 ± 0.086 µg/l. The maximum value of 7.100 µg/L was found at 10 m depth and 12 km away from the glaciers coinciding with the minimum in salinity (Fig 2.2). Deep chl-a concentration (>300 m) followed a similar pattern, where high chl-a content was found in the middle and inner basins. Below 300 m depth, the overall concentrations varied from 0.002 µg/L to 0.061 µg/L. In contrast, surface maximum phaeo-pigment concentration occurred outside the fjord, in the Gerlache Strait (Fig 2.3). Above 60 m depth, the average phaeo-pigment concentration was 0.109 ± 0.003, ranging between 0.006 µg/L and 0.667 µg/L. The phaeo-pigment concentrations at depth (60 m to 300 m) generally occurred in the middle and inner basins. Below 300 m depth, the phaeo-pigment concentration varied from 0.005 µg/L to 0.265 µg/L.

There is a strong temporal variability pertaining to phytoplankton abundance in Andvord Bay. In December 2015, the mean chl-a concentration in the surface layer (0-60m) was 2.159 ± 0.144 µg/L (upper panel, Fig 2.3a), declining to 0.227 ± 0.009 µg/L in April (upper panel, Fig 2.3b). The overall mean chl-a concentration of the entire fjord was 1.063 µg/L in December decreasing to 0.122 µg/L in April (middle panels of Figs 2.3a and 2.3b). However, deep chl-a concentration (300 m — 500 m) depicts a different temporal variability: there is an overall increase from 0.019 ± 0.001 µg/L in December to 0.029 ± 0.001 µg/L by April (lower panels of Figs 2.3a and 2.3b). In the case of phaeo-pigments, concentrations increased from December to April in the whole water column, from a mean of 0.087 ± 0.005 µg/L to 0.124 ± 0.002 µg/L by April. At depth (300 m – 500

m), mean phaeo-concentration increased 3-fold from 0.040 ± 0.002 µg/L (lower panel, Fig 2.3c) to 0.161 ± 0.006 µg/L (lower panel, Fig 2.3d).

2.4.3. Optical Properties of Andvord Bay

Distinct features are observed in profiles of particulate backscattering coefficient at 442nm (b_{bp}(442)) as well as particulate beam attenuation coefficient at 660 nm ($c_p(660)$); these features are primarily found at subsurface in the inner basins (Fig 2.4). For instance, the maximum b_{bp}(442) value during the entire study period is 0.015 m^{-1}, found in Inner Basin West at 100 m depth, 3.9 km away from the glacier termini (Fig 2.4b). Similarly, c_p(660) presented a maximum of 2.213 m^{-1} in the Inner Basin West at 350 m depth and 3.09 km away from the glaciers (Fig 2.4c). On average, the b_{bp}(442) and c_p(660) decreased with distance from the glacier termini. In addition to the sub-surface features, there were also distinct surface optical signals (Figs 2.4a and 2.4b). Above 35 m depth, the maximum b_{bp}(442) of 0.013 m^{-1} was found 0.8 km away from the glaciers, while most high c_p(660) values aggregate at the surface and subsurface layers near the glacial front (Figs 2.4c and 2.4d). K_d(PAR) was also higher near the glaciers (Figs 2.4e and 2.4f), however, its highest values coincided with an accumulation of chl-a near the fjord's mouth (Fig 2.3b).

In contrast to b_{bp}(420) and c_p(660) upward trend towards the glaciers (Figs 2.5a—2.5d, Table 2.3), inorganic suspended particulate mass concentration (SPM_i) showed no statistically significant trend (Figs 2.5e and 2.5f; Table 2.3). However, $\delta^{18}O$ was more negative towards the glaciers in both December and April (Figs 2.5g and 2.5h; Table 2.3). Potential temperature and salinity changed their trend towards the glacier front between December and April, from relatively warmer and higher salinity values near the termini (Figs 2.5i and 2.5k; Table 2.3) to fresher and colder (Fig 2.5j; Table 2.3).

When comparing phytoplankton abundance with optical properties, chl-a correlates with the downwelling diffuse attenuation coefficient at 443 nm (K_d(443), p-value < 0.0001 for both December and April) but not with the backscattering coefficient, b_{bp}(442) (p-value = 0.24 and p =

0.65, December and April respectively). However, chl-a is inversely correlated with water leaving radiance, or reflectance, R(443 nm, p-value < 0.001 for both cruises) while b_{bp}(442) is positively correlated with R(443) (p-value < 0.001 in December and <0.0001 in April).

There is an overall higher particulate absorption coefficient at 442 nm (a_p(442)) in December and April in the upper 100 m; the mean in December is 0.100 m^{-1} varying from 0.001 m^{-1} to 0.393 m^{-1}. By April, mean a_p(442) has decreased an order of magnitude to 0.015 m^{-1} (0.007 m^{-1} - 0.220 m^{-1}) (Figs A2a and A2b). Non-algal particle absorption coefficient at 442nm (a_{NAP}(442)) also exhibits an overall decline from 0.008 m^{-1} (0.001 m^{-1} -- 0.023 m^{-1} in December) to 0.003 m^{-1} (0.001 m^{-1} -- 0.006 m^{-1} during April) (Figs A2c and A2d). Conversely, CDOM absorption coefficient at 442nm (a_{CDOM}(442)) increases from December to April (Figs A2e and A2f).

In this way, a_p(442) correlates with c_p(660) during December (r = 0.93, p-value < 0.0001), while only b_{bp}(442) correlates with c_p(660) in April (r = 0.87, p-value < 0.0001). The change in particle assemblage from December to April is also illustrated in the spectral surface reflectance (R_{rs}(λ)) (Fig 2.6). In December, a primary peak around 380 nm and a secondary peak around 490 nm were observed; these peaks are typical of certain phytoplankton pigments absorption in the blue spectral range (Mobley, 1994). However, the 380 nm peaks were absent in April and the primary peaks observed were at ~500 nm, indicating a coastal environment with sediment load (Kong et al., 2015).

2.4.4. Meltwater Fraction

Meltwater fraction for the entire bay was calculated based on the correlation between Q_i and salinity, First, meltwater fraction is calculated based on Jenkin's method (Jenkins, 1999); in this case, we utilized a two-component mixing model to estimate meltwater fraction based on $\delta^{18}O$ (Eq. 9). Then, in order to increase the spatial resolution of meltwater fraction, Q_i, each value was correlated with its corresponding salinity value in order to generate a correlation to interpolate Q_i according to *in-situ* salinity. Due to a strong temporal difference between the two periods, two equations are derived for interpolating Q_i for December (Eq. 10) and April (Eq. 11) respectively.

$$Q_i = -0.016\,S + 0.544 \quad (10)$$

$$Q_i = -0.021\,S + 0.740 \quad (11)$$

Eq. 10's correlation coefficient is r = 0.82 with a p-value < 0.0001, while Eq. 11's is r = 0.95 with a p-value < 0.0001. Finally, based on these equations, Q_i data range is expanded by interpolation based on the salinity dataset.

Meltwater fraction derived from $\delta^{18}O$ values illustrates the fraction of glacial meltwater present in the water column of Andvord Bay (Fig 2.2 and Fig 2.7). Overall, higher concentration of meltwater was found near the surface in the inner basins, within 100 m of the surface, with a mean of 0.012 ± 0.0001 in December and 0.015 ± 0.0003 in April. A maximum value of 0.024 was found at the surface in Inner Basin East during April, 2.3 km from the glacier. High meltwater was also found over the middle basins. Low meltwater fraction was typically found at depth. Tthe surface lens is persistent, increasing from December to April (Fig 2.7). Q_i integrated over 60 m within the fjord indicates that meltwater occupied 0.06 ± 0.003 m of the water column during December and 0.13 ± 0.017 m during April.

2.4.5. Modeling of Meltwater Fraction

A multiple-regression models was created in RStudio for predicting meltwater hydrographic features based on their IOPs. The IOP model (Model 1) is set as:

$$\mathrm{Q_{i,iop}} = \beta_1 + \alpha_1\, b_{bp}(442) + \alpha_2\, a_{NAP}(442) + \alpha_3\, \mathrm{Temp} \quad (12)$$

where $Q_{i,iop}$ is the predicted meltwater fraction, $b_{bp}(442)$ and $a_{NAP}(442)$ are utilized to encompass both backscattering and absorption of inorganic sediment particles known to be associated with glacial meltwater. Temp is in-situ temperature at the same depths (Fig 2.8). Various skill metrics were used to quantify model-data fits. The Pearson correlation coefficient (r) gives a measure of

linear correlation between the measured and predicated variables. The root-mean-square deviation (RMSD) quantifies the scale of the difference between the model and *in-situ* data for any given point. Standard errors (SE) were also used as a measure of the statistical accuracy of the estimate. Prediction interval estimates a range in which a future observation will fall, with 95% certainty. For December, the model has a p-value of 3.52 E-05 with a RMSD of 0.002 (Table 2.4). In comparison, the April model has a p-value of 1.62 E-04 and a RSMD of 0.003. Model 1 predicts Q_i in December with an adjusted correlation coefficient of 0.66 and 0.60 in April (Table 2.4).

Model 2 is based on AOPs and it is a modified algorithm from Sravanthi *et al.* (Sravanthi et al., 2013) for retrieving suspended sediment concentration in the Indian coastal ocean from remote sensing reflectance. Sravanthi *et al.*'s algorithm is based on a global algorithm originally published by Tassan (Tassan, 1994):

$$\mathrm{X_s} = \left[R(\lambda_\mathrm{i}) + R(\lambda_\mathrm{j})\right]\left[\frac{R(\lambda_\mathrm{m})}{R(\lambda_\mathrm{n})}\right]^\mathrm{b} \tag{13}$$

where X_s is the suspended sediment concentration, $R(\lambda)$ is remote sensing reflectance. λ's are defined as spectral regions (rather than particular wavelengths) for the general purpose of future algorithm development. λ_i and λ_j are zones of low phytoplankton and CDOM absorption, respectively. λ_m and λ_n are choosen in the slope zone of phytoplankton absorption spectrum (where the slope is the steepest). However, Sravanthi *et al.* found that this global algorithm cannot produce results with high statistical significance, so they modified it to fit regional conditions:

$$Y = \beta + \alpha\left([R(555) + R(620)] + \left[\frac{R(620)}{R(490)}\right]^2\right) \tag{14}$$

Where Y is suspended sediment concentration, λ_i and λ_j from Eq. 14 are 555nm and 620nm; these wavelengths are chosen because they represent low phytoplankton and CDOM absorptions

in the Indian Ocean. λ_m and λ_n are 620nm and 490nm, to normalize any effect of phytoplankton particles on the overall reflectance signal.

In this study, further modifications were made on λ_j and λ_m in Eq. 14 due the in-situ radiometer's optical band configuration which only provided L_u and E_d at 625nm (used in the R(625) calculation, see Materials and Methods section b). The final model is:

$$Q_{i,aop} = \beta_2 + \alpha_4 (R(555) + R(625)) + \alpha_5 \left(\frac{R(625)}{R(490)}\right)^2 \quad (15)$$

Model 2 (Eq. 15) predicts meltwater fraction based on a multivariate linear correlation, where $Q_{i,aop}$ is the predicted meltwater fraction based on AOPs, and β_2 is the intercept while α_4 and α_5 are the slopes for band addition and ratio respectively. Model 2 for April has a p-value of < 2.2 E-16 and RMSD of 0.003, predicting Q_i values, with an adjusted correlation coefficient of 0.844 while the December model has a correlation coefficient at 0.817 and a p-value < 2.2E-16 and RMDS of 0.002 (Table 2.4).

In summary, these two models, based on physical and optical parameters, are able to reproduce the variability in meltwater fraction from December to April as well as its spatial variability away from the glacier front (Figs 2.8 and 2.9).

2.5. Discussion

2.5.1. Meltwater Properties

The low salinity surface layer in Andvord Bay, persistent from December to April, in combination with lower $\delta^{18}O$ and higher $b_{bp}(442)$ suggests this surface lens might have a glacial origin. Its specific origin is uncertain, it could originate from surface glacial or subglacial meltwater, that is from glacier processes, and/or from melting of brash ice and icebergs in the bay which originate from glacier calving. The fresher and cooler surface lens has been identified in the WAP as "meteoric" water, based only on salinity and $\delta^{18}O$ properties [57, 58]. The optical properties of this freshwater lens, included in this study, and the proximity of this lens to the Bagshawe glacier

provide additional support to identify it as glacial meltwater, with the caveat that precipitation, mainly as snow, directly over the ocean or as input from the fjord's edges, could have contributed to the meltwater signal.

Meltwater fraction calculation was based on a two-component mixing model by Jenkins [1999] (Table 2.2). This model assumes all water within the fjord is a result of mixing between these two sources (Jenkins, 1999). The meltwater fraction derived from $\delta^{18}O$ samples is then linearly related to salinity profiles; this is based on the "Gade Line" method which assumes that salinity is largely influenced by two defined sources (Gade, 1979). A closer examination of the correlation between $\delta^{18}O$ and salinity reveals that the two properties are significantly more correlated in April 2016 than in December 2015, which are likely due to melting during the austral summer. The general linearity of all data points along the Gade Line for April (Fig 2.7) indicates a two end-member mixing with little influence from a third source (i.e. slight deviation in Gade Line during December). Moreover, temperature-salinity diagrams of Andvord Bay indicate the water mass found in the inner basins are different from that found in Gerlache Strait during December (Fig 2.2, right panels). However, the water masses in the two locations become more similar in April; this change in T-S and the similarity between the two locations further illustrate the mixing of glacial meltwater during summer. Mortensen *et al.* has observed a water mass' T-S signal in Kangersuneq, SW Greenland during summer that is similar to Andvord Bay in April (Mortensen et al., 2013).

Meltwater in Andvord Bay shares similar physical characteristics with properties found in other fjords, mainly those in the Arctic and Greenland; however, the magnitude of these characteristics as well as their impact on the water column optics and the spatial distribution of phytoplankton abundance differ significantly. Pure meltwater of glacier origin is known to have characteristics of colder temperature, lower salinity, and higher turbidity in comparison to ambient oceanic water masses (Dierssen et al., 2002) (Straneo & Cenedese, 2015) (Mortensen et al., 2013). In contrast, upwelling processes at the glacier front could bring up to the surface warmer,

more saline waters, depending on the properties of the deep water entering the fjord (Straneo et al., 2011). In Andvord Bay, we observed a consistent freshening at the surface layer (Figs 2.2c, 2d), associated with a decrease in temperature. However, the gradient of salinity along the fjord is not prominent (Fig 2.5l) in comparison to fjords with significant freshwater influx (Straneo & Cenedese, 2015). In Andvord Bay, there is an estimated 2--4 $x10^6$ m^3/day of solid ice flux from Bagshawe Glacier into Inner Basin West, but a low meltwater flux is expected (pers. comm. Truffer, M., University of Alaska, Fairbanks). The meltwater fraction in Andvord Bay (an average of 1.85% ± 0.29% in April) also suggests a weaker melting process than that observed in western Greenland fjords, in line with Marguerite Bay estimates where the percentage of meteoric water at 15m depth ranges from 2% to 4% (Meredith et al., 2008). In contrast, near Disko Bay in western Greenland, glacial sources comprise up to 5% of the glacially modified water in the fjord (Beaird et al., 2015).

The meltwater fraction observed in Andvord Bay within the 100-m surface layer is comparable to other estimates in WAP shelf waters. Low salinity surface waters (<33.5 PSU) are consistently observed off Anvers Island (Martinson et al., 2008). $\delta^{18}O$ values are approximately -0.50‰ (Meredith et al., 2017) resulting in a meteoric fraction of 2.5% to 3% meltwater in January.

Glacial meltwater is expected to contain sedimentary iron nanoparticles, which are ubiquitous in glacial ice (Raiswell et al., 2006). The impact of these particles on water column turbidity in Andvord Bay and the concentration of suspended sediments were lower than those in Arctic fjords (Hudson et al., 2014) where meltwater input, particularly associated with subglacial melting, can result in a substantial sediment loading. For instance, in Godthåbsfjord system situated in western Greenland, SPM concentration can reach >50 mg L^{-1} (Arendt et al., 2011), while in Andvord Bay, maximum values did not exceed 10 mg L^{-1}. While the optical signal from sedimentary particles in meltwater is relatively small in Andvord Bay, optical measurements such as particulate backscattering coefficient (b_{bp}(442) and particulate beam attenuation coefficient

(c_p(660)) are sensitive enough to detect the presence of all sedimentary particles and facilitate the mapping of their distribution in the water column, and hence meltwater.

There is a discrepancy between spatial distribution of particulate backscattering coefficient and SPM measurements, where b_{bp}(442) increases towards the glacier front and SPM does not (Figs 2.5a—2.5f). The difference between these two results suggests a large fraction of the glacial particles are smaller than the 0.7 μm nominal size of GF/F filters. This is consistent with the observation of the ubiquitous nature of iron nanoparticles in glacial meltwater (Raiswell et al., 2006).

Sea ice melting could also be contributing to the freshwater lens in Andvord Bay. However, sediment nanoparticles are known to be associated with glacial entrainment processes but not sea ice formation (Alley et al., 1997) (Thomas, 2011). In particular, in the surface and subsurface b_{bp}(443) signal close to the glacial front (Fig 2.4, Fig A3) suggests that the surface freshwater lens has similar origin. Sea ice melt also has a significantly higher $\delta^{18}O$ signal when compared with that of glacial meltwater (Meredith et al., 2008). In Marguerite Bay, sea ice melt contributes ~0% meltwater during Austral summer, within the error (RMSD) for glacial meltwater fraction by $\delta^{18}O$ (Table 2.2) and prediction by optical measurements (Table 2.4).

2.5.2. Fjord Phytoplankton

Meltwater in the fjord forms a surface layer (i.e., lens) where phytoplankton is retained, allowing for growth. Co-location of both variables, as seen in Fig 2.7 and Figs 2.3a--2.3b, defines a relationship between phytoplankton abundance and meltwater fraction (Fig 2.10). An exponential regression between the two variables, established based on measurements above 40 m depth suggests a role of meltwater in facilitating phytoplankton growth (Fig 2.10). The correlation coefficient between the two variables is 0.66, p-value <0.0001 in December (Fig 2.10a) and 0.82, p-value <0.0001 in April (Fig 2.10b).

The influence of meltwater on phytoplankton abundance has also been found over the WAP shelf; between 1991 and 1999, chlorophyll concentration significantly increased with a

decline in salinity attributed to glacial melt (Dierssen et al., 2002). When freshwater input in a fjord does not contain significant sediment loading, it is expected to increasewater column stratification without significantly affecting underwater light field (Meire et al., 2017) (Hernando et al., 2015). While K_d(PAR) significantly increased towards the glacial front in Andvord Bay, these values are incapable of hindering phytoplankton growth like the meltwater conditions in Greenland fjords (such as Godthåbsfjord in SW Greenland) (Murray et al., 2015). In addition, meltwater can bring macro-nutrients and iron, both from glacial melt and/or upwelling of deep water, as observed in east Greenland fjords (Meire et al., 2017) (Hernando et al., 2015) (Ekern, 2017) (pers. comm. Forsch, K., Scripps Institution of Oceanography), resulting in well illuminated surface waters, rich in nutrients. These conditions are known to give rise to phytoplankton growth with small and fast-growing species like cryptohytes (Brito et al., 2015). These clear, rich waters also sustain grazers resulting in an active marine food web (Hylander et al., 2011). In contrast, sub-Arctic Greenland fjords with high suspended sediment loading from meltwater, have high K_d(PAR), are found to interfere with copepods' feeding rates (Arendt et al., 2011). Thus, the low concentration of meltwater in Andvord Bay is sufficient to stabilize surface waters, without additional negative effects from high sediment loading (Schloss et al., 1997) (Schloss et al., 2012). These waters are transparent, potentially enriched in nutrients from the glacial ice and nanoparticles, providing an ideal environment for phytoplankton growth (Arrigo et al., 2017).

Very low salinity is known to affect negatively phytoplankton growth. At Potter Cove (a fjord-like embayment on King George Island, northern Antarctic Peninsula), Hernando *et al.* [2015] experimented with two different salinity treatments: one with natural ambient salinity (34 PSU), and one with low salinity (30 PSU) (Hernando et al., 2015). They found that hypo-osmotic conditions favor water influx into the cells and cause an increase in turgor pressure and oxidative stress, resulting in instantaneous inhibition of phytoplankton growth rate and biomass accumulation, and reduced chl-a concentrations. Notably, these changes coincide with a gradual replacement of big centric diatoms by small pennate diatoms (Hernando et al., 2015). We did not

observe this negative effect on phytoplankton in Andvord Bay (Fig 2.10). We interpret the salinities > 33.8 PSU are too high to affect phytoplankton or the dominant species were adapted to low salinity.

Phytoplankton abundance in Andvord Bay had a strong temporal variability, indicated by an order of magnitude decrease in chl-a concentration from December to April (Fig 2.3) This variability is likely due to the decrease in daylength from 18 h to 12 h and an increase in sun angle as the winter approaches (Knox, 2006). Within the bay, the influence of meltwater on phytoplankton is likely expressed through a combined effect of water column stratification and nutrient addition induced by meltwater. In contrast, it is unlikely the presence of sedimentary nanoparticles significantly impacted underwater light field.

Chl-a and phaeo-pigment concentrations in Andvord Bay at z > 300 m are notable. Chl-a is the active pigment in algae, present only in live cells. Phaeo-pigments are products of chl-a degradation such that the combination of both variables represents carbon originating from algal biomass. Phytoplankton, and thus chl-a, are expected to concentrate in surface waters where PAR is available to support photosynthesis. Below the photic zone, phytoplankton decreases to negligible values, usually <1% of surface concentrations. In this way, the deep pigment concentrations are attributed to derived matter from phytoplankton production at the surface. This observation is consistent with motion picture data collected by a benthic camera system situated in the middle basin in 2015-2016. Footage revealed marine snow particles falling between Mid-January and early March (austral summer). The marine snow had a visually distinct dark green coloration, likely a result of sedimentation of a phytoplankton summer bloom between December and April (pers. comm. Smith, C.R., University of Hawai'i). The distribution of deep chl-a and phaeo-pigment concentrations in April also coincided with lower oxygen concentration at depth (Fig 2.2h), presumably indicating oxygen consumption by microbes during decomposition of the sinking organic particles.

2.5.3. Fjord Optical Properties

Underwater Light Field

The underwater light field was largely influenced by phytoplankton in December, and by sedimentary particles in April. When particulate absorption and backscattering coefficients are compared with particulate beam attenuation coefficient, $c_p(660)$ is better correlated with $a_p(442)$ in December and with $b_{bp}(442)$ in autumn. Inorganic particles (such as glacial sediments) are generally more effective at scattering light than organic particles (such as phytoplankton) due to the sediments' minerology and geometric shapes (Bohren & Huffman, 2008), while the presence of phytoplankton's pigment make these organic particles more effective for light absorption (Kirk, 1994). In Andvord Bay, both types of particles existed concurrently but had different relative contribution to the particle assemblage in December and April. A clear $b_{bp}(442)$ signal near the glaciers was consistent through time suggesting the contribution from nanoparticles was constant. In contrast, $a_p(442)$, $a_{NAP}(442)$, and $a_{ph}(442)$ decreased in April, consistent with the one order of magnitude decrease in chl-a concentration (Fig 2.3).

The overall bio-optical profiles and their spatial distribution in Andvord Bay are comparable to those observed in northern Antarctic Peninsula and in Arctic fjords, with some distinct differences. Particulate backscattering and beam attenuation of light increase near the glaciers in Andvord Bay (Figs 2.4a—2.4d, 2.5a—2.5d). Mascarenhas *et al.* (Mascarenhas et al., 2017) also observed an increase in optical signal towards the head of fjords in central Norway, where they found an increase in $b_b(470)$ near the glacial fronts. This spatial pattern is also observed in Uummannaq Fjord and Vaigat-Disko Bay in western Greenland. These systems are strongly influenced by glacial meltwater runoff, which produces strong turbidity signals as a result of sediment plume discharge (Holinde & Zielinski, 2016).

Particulate backscattering coefficients in Andvord Bay (0.001 m^{-1} to 0.015 m^{-1}), are comparable to $b_{bp}(442)$ of 0.0004 m^{-1} to 0.0067 in northern Antarctic Peninsula (Ferreira et al., 2018) and are higher than $b_{bp}(488)$ over the shelf of 0.0015 m^{-1} to 0.006 m^{-1} (Dierssen & Smith,

2000b) (Dierssen & Smith, 2000a). Our results in Antarctic fjords are in the range of values observed in the southeastern Beaufort Sea, as well as in the Chukchi Sea and western Beaufort (Reynolds et al., 2016). In both the Arctic and Andvord Bay, $b_{bp}(\lambda)$ generally decrease with increasing wavelength for each sample. The high $b_{bp}(\lambda)$ values are associated with waters (Ferreira et al., 2018) near the glaciers in Andvord Bay, while the low values are found 170 km away, over the continental shelf adjacent to Anvers Island (Fig A3). December $b_{bp}(\lambda)$ values have a larger range in comparison to those of April across all wavelengths. For comparison, $b_{bp}(\lambda)$ values in Beaufort Sea and Chukchi Sea varied six orders of magnitude (Reynolds et al., 2016). The values ranged from the clearest offshore waters in the Beaufort sea where $b_{bp}(\lambda)$ was <0.005 m^{-1} to the highest $b_{bp}(\lambda)$ values, >0.1 m^{-1} from the Mackenzie River (Reynolds et al., 2016).

The difference between IOP values near and away from the glaciers in Andvord Bay is also reflected in AOP values. The largely absent spectral peaks in $R_{rs}(\lambda)$ between 360nm and 390nm in April 2016 indicate the significant shift from biotic to abiotic particles and CDOM absorption in comparison with December. The presence of nanoparticles also explains why while the range of $R_{rs}(\lambda)$ values in Andvord Bay are comparable to those found over the WAP shelf (Dierssen & Smith, 2000a), the spectral shapes are different.

Sediments in meltwater

Near the glaciers, the shift in particle assemblage is attributed to the sedimentary particles from glacial meltwater (Figs 2.4a—2.4d and 2.5a—2.5d, Fig A3). While surveys in Antarctic fjords have been scarce, limited studies from the past indicate the existence of “meltwater fingers” along the glacio-marine interface, including in Andvord Bay. Domack and Williams [1990] found a layered structure in the beam attenuation profile measured in this fjord, and speculated that these optical features are related to sediment loading as a result of glacial meltwater plumes (Domack & Williams, 1990). In 2010, these persistent plumes near the glaciers were observed also in $c_p(660)$ profiles (Cape et al., 2010). In this study, there was significantly higher $c_p(660)$ and $b_{bp}(442)$, in the inner basins near the glacier fronts (Table 2.3), with higher values found in April,

confirming the persistence of these subsurface features. At Brialmont Cove in Hughes Bay, central Antarctic Peninsula, Domack and Williams (1990) observed quartz silt grains originating from basal, sediment-rich meltwater from the submerged glacier. Buoyant meltwater carries these particles to mid-water column, while turbulent mixing at depth also facilitates the transport and breaking of these floccules. These processes produce a midwater feature and turbidity at different depths near the glacier front and they can account for 87% of the total sediment load (Domack et al., 1994).

The absorption and backscattering of light by sediments is also attributed to their size distribution. At Brialmont Cove in Hughes Bay, 0.1 – 2 mm floccules were composed of individual grains between 5 and 50 μm (Domack et al., 1994) and captured by $c_p(660)$. Smaller grain sizes are often un-detected and therefore overlooked. It is likely that a substantial portion of the sediment particle assemblage are not effectively captured by the SPM measurement, which retains suspended sediment onto a GF/F filter that has a nominal pore size of 0.7 μm. This is consistent with our observations in Andvord Bay, where inorganic SPM did not exhibit a significant increase towards the glaciers in the surface layer (Figs 2.5e and 2.5f; Table 2.3), while several optical variables, expected to be affected by fine sediment load, presented significant response (Figs 2.5a—2.5d; Table 2.3). Bio-optical modeling indicates that particles <0.1 μm contribute significantly to light backscattering in the ocean (Stramski et al., 2004). Other studies have predicted also that 50% of particulate backscattering are due to particles < 0.2 μm (Morel & Ahn, 1991). These theoretical studies have demonstrated that realistic concentrations of sub-micrometer particles in the size range of 0.4 – 1 μm (Isao et al., 1990) can indeed produce significant backscattering signal (Stramski & Kiefer, 1991). In the context of Andvord Bay, suspended nanoparticles entrained in glacial meltwater in meltwater are expected to contribute to the $b_{bp}(442)$ and $c_p(660)$ signal.

2.5.4. Optical Modeling of Meltwater Fraction

$\delta^{18}O$ measurement is a robust and accurate method for assessing meltwater fraction in the water column. This study shows that optical measurements can greatly complement conventional hydrographic tools to understand the spatial distribution of glacial meltwater (Figs 2.8 and 2.9, Table 2.4). More specifically, particulate backscattering and beam attenuation coefficients were sensitive to the low meltwater concentrations observed in Andvord Bay. The predicted meltwater fraction based on optical methods demonstrated good agreements with *in-situ* estimates based on $\delta^{18}O$ values (Figs 2.8 and 2.9), and the observed and predicted meltwater fractions in this study are comparable to the range of values previously found in this region (Meredith et al., 2017) (Meredith et al., 2008).

The predicted meltwater fraction based on specific IOPs ($Q_{i,iop}$), $b_{bp}(442)$, $a_{NAP}(442)$, and temperature, allow Model 1 to encompass both backscattering and absorption of inorganic sediment particles from glacial meltwater. $b_{bp}(\lambda)$ is expected to be associated with the sediment loading (Stramski et al., 2004) (Boss et al., 2018). Concurrently, the presence of small particles (<0.7 um) is likely linked to large particles retained by the GF/F filter (>0.7 um), hence $a_{NAP}(442)$ in Model 1 contributed to the overall statistical significance. Despite this, GF/F-based measurements of large particles alone cannot predict the concentration of small particle assemblage (Table 2.3). This leads to the speculation that the small particles are disproportionately linked to large particle concentrations (eg. as an exponential function), thus higher concentrations of small particles can be masked by the presence of large particles.

Modeling with reflectance ratio of suspended sediments modified from Tassan (1994) (Tassan, 1994) and Sravanthi *et al.* (Sravanthi et al., 2013) provided a significant prediction of meltwater fraction and distribution in the water column (Model 2, Table 2.4, Fig 2.9). This further confirms that the AOP variables are responding to the IOP sensitivity to the sediment loading in meltwater (See Figs 2.5a and 2.5b). Same as the algorithm by Sravanthi *et al.*, the model needed further adaptation to local conditions, attributed to a difference in Antarctic water properties with

respect to the global ocean average (Tassan, 1994) or the Indian Ocean (Sravanthi et al., 2013), where the algorithms (Eq. 13, 14) were developed and applied. While Sravanthi *et al.* (Sravanthi et al., 2013) added 2 coefficients to the original formulation predicting sediment loading based on one cumulative AOP variable, creating a non-zero intercept (α) and adjusting the slope (β), our adaptation of the method created variables in a multivariate linear model, $\boldsymbol{\alpha_4}\,(\mathbf{R}(\mathbf{555}) + \mathbf{R}(\mathbf{625})) + \boldsymbol{\alpha_5}\left(\frac{\boldsymbol{R(625)}}{\boldsymbol{R(490)}}\right)^{\mathbf{2}}$, that produced statistical significance for our study region with high correlation coefficients (r = 0.81 and 0.84 in December and April, respectively, Table 2.4). The first term is sensitive to sediment loading at the wavelengths of low phytoplankton and CDOM absorption. In Andvord Bay, $R_{rs}(\lambda)$ shows a maximum between 475 nm and 555 nm, and a minimum around 625 nm (Fig 2.6). The band ratio represents the correction by phytoplankton absorption at the wavelength of maximum steepness, similar to results derived from algorithms developed for the Indian Ocean and global ocean average.

There are certain limitations to this approach of estimating glacial meltwater fraction based on optical measurements. First, the determination of meltwater by $\delta^{18}O$ based on the two end-member mixing assumption does not account for sources from sea ice melt (see Discussion section a). As mentioned before, sea ice melt could have had a small signal in December, but did not seem present in April. In addition, this approach does not differentiate between meltwater from glaciers and from bergy bits as both originate from glacial ice and have similar $\delta^{18}O$ signal (Jenkins & Jacobs, 2008) (Meredith et al., 2017) (Silvano et al., 2018) (Aoki et al., 2017).

The multivariate linear regression approach has certain assumptions which require further diagnostics for verification. The standard linear model assumptions are linearity of the relationship, normality of residual errors, homogeneity of residuals' variance, and presence of influential values. The linear relationships between optical variables and meltwater fraction are indicated by their high r values (Table 2.4); there are also no outstanding outliers to significantly influence the models (Figs 2.8 and 2.9). The QQ plot of residuals were used to check the normality

assumption. The residuals follow the reference line (Figs A4a, A4b, A4e, A4f) indicating normal distribution. Homoscedasticity is verified by the scale-location plots to check the homogeneity of the residuals' variance. The predicted values spread along a horizontal line indicating homoscedasticity of our data used for developing Model 1 and Model 2 (Figs A4c, A4d, A4g, A4h). In this way, the error of the statistics applied in modeling are minimal and the models are robust (Table 2.4).

2.6. Conclusions

Glacial meltwater input in fjords and other coastal Antarctic regions has been associated with the regional warming [9]. The meltwater discharge can impact surface stratification and increase nearshore turbidity which influences underwater light field as shown in this study. Meltwater can also have secondary effects on Antarctic coastal ecosystems by influencing the timing of sea ice formation and promoting phytoplankton growth (Vernet et al., 2008b). In Andvord Bay, we observed a relatively weak meltwater process near the glacio-marine interface with Bagshawe glacier. Concurrent *in-situ* optical measurements, especially particulate backscattering coefficient and particulate beam attenuation coefficient, were found to detect the presence of fine sediment loading. The presence of sedimentary nanoparticles, in combination with more negative $\delta^{18}O$ and lower salinity, were attributed to the presence of meltwater. These nanoparticles were likely missed by sampling with standard GF/F (0.7 μm) filters. These optical features were utilized to model the spatial distribution of meltwater fraction in Andvord Bay (Model 1). Model 2 better correlates with *in-situ* meltwater measurements than Model 1 due to the integrative effect of the AOP variables. The models developed in this study can potentially be applied to remote sensing datasets to detect meltwater presence at the sea surface. In addition to the optical properties of glacial meltwater, we also documented a significant temporal variability in phytoplankton concentration, where surface chl-a decreased one-order of magnitude from December to April. Phytoplankton sedimentation was observed as deep chl-a and phaeo-pigments ($z > 300m$), increasing towards the end of the austral growing season.

2.7. Acknowledgements

The authors would like to thank all participating principle investigators and their affiliates during the NSF FjordEco project (PLR -1443705), Dr. Craig Smith (University of Hawai'i at Manoa), Dr. Mark Merrifield (University of Hawai'i at Manoa), Dr. Brian Powell (University of Hawai'i at Manoa), Dr. Martin Truffer (University of Alaska at Fairbanks), and Dr. Peter Winsor (University of Alaska at Fairbanks). The optical measurements were made possible by instrumentation and tutorials from Dr. Dariusz Stramski's Lab and Dr. Greg Mitchell's Photobiology Group; post-cruise analyses of optical data were supported by technical assistance and input from Dr. Linhai Li and Brian Schieber (Scripps Institution of Oceanography, UCSD). Lindsey Ekern from Dr. Maria Vernet's Lab, and Kiefer Forsch and Lauren Manck from Dr. Katherine Barbeau's Lab (Scripps Institution of Oceanography, UCSD) also participated in the Plankton Ecology team during this project. Our sampling efforts also received crucial help from Diana Gutierrez, Angela Klemmedson, and Dr. Lars Thoresen. Invaluable discussions with Dr. Mattias Cape (School of Oceanography, University of Washington) are acknowledged. The authors would also like to thank the captain and crew of R/V Lawrence M. Gould and RVIB Nathaniel B. Palmer and United States Antarctic Program contractors. Four anonymous reviewers' comments are greatly appreciated for improving this manuscript.

Chapter 2, in full, is a manuscript of the material as it appears in Pan, B.J., Vernet, M., Reynolds, R.A., and Mitchell, B.G. (2019) The optical and biological properties of glacial meltwater in an Antarctic fjord. *PLoS ONE* 14(2): e0211107. The dissertation author was the primary investigator and first author of this paper.

2.8. Figures and Tables

Table 2.1. Hydrological, biological, and bio-optical variables utilized in this study.

Variable	Definition	Unit
λ	Wavelength in vacuum	nm
	Inherent Optical Properties (IOPs)	
$a_p(\lambda)$	Particulate absorption coefficient	m^{-1}
$a_{NAP}(\lambda)$	Detritus/Non-algal particulate absorption coefficient	m^{-1}
$a_{ph}(\lambda)$	Phytoplankton absorption coefficient	m^{-1}
$a_{CDOM}(\lambda)$	Colored dissolved organic matter absorption coefficient	m^{-1}
$b_b(\lambda)$	Backscattering coefficient	m^{-1}
$b_{b,sw}(\lambda)$	Seawater backscattering coefficient	m^{-1}
$b_{bp}(\lambda)$	Particulate backscattering coefficient	m^{-1}
$c_p(660)$	Particulate beam attenuation at 660nm	m^{-1}
	Apparent Optical Properties (AOPs)	
$L_u(\lambda)$	Upwelling Radiance	μW / (cm^2 sr nm)
$E_d(\lambda)$	Downwelling Planar Irradiance	μW/(cm^2 nm)
$R(\lambda)$	Reflectance, ratio between $L_u(\lambda)$ and $E_d(\lambda)$ at discrete depths	sr^{-1}
$R_{rs}(\lambda)$	Remote sensing reflectance above surface	sr^{-1}
$K_d(PAR)$	Diffuse attenuation coefficient of PAR	m^{-1}
	In-situ Measurements	
SPM_t	Total suspended particulate mass concentration	mg/l
SPM_i	Inorganic fraction of suspended particulate mass concentration	mg/l
SPM_o	Organic fraction of suspended particulate mass concentration	mg/l
Chl-a	Chlorophyll-a pigment concentration	μg/l
Phaeo	Phaeo-pigment concentration	μg/l
$\delta\ ^{18}O$	Oxygen-18 isotope ratio	‰
Q_i	Meltwater fraction	Decimal

Table 2.2. Variables and their sample sizes (n) and standard errors (SE) utilized in the two-component mixing model for estimating meltwater fraction; the two components are averaged values from glacial samples, and averaged mid-depth values from Gerlache Strait.

December 2016	$\delta^{18}O$ (‰)	n	SE	Salinity (PSU)	n	SE
Gerlache	-0.17	7	0.01	34.508	7	0.013
Glacial melt	-12	5	1.16	0.000	--	--
April 2017						
Gerlache	-0.30	6	0.01	34.396	6	0.021
Glacial melt	-15	8	0.16	0.000	--	--

Table 2.3. Statistical results derived from Fig 2.5, based on general linear regressions between physical/optical variables (at 0 m—35 m depth) and their corresponding locations relative to the glaciers at the head of Andvord Bay. For each regression, correlation coefficient (r), the slope, and p-value are calculated to indicate the statistical significance of each slope, as well as to facilitate inter-comparisons among these variables.

	December 2015			**April 2016**		
	r	slope	p-value	r	slope	p-value
$b_{bp}(420)$	0.3797	-7.84E-05	<0.0001	0.6675	-7.58E-05	<0.0001
$c_p(660)$	0.2007	-0.008	<0.001	0.5980	-0.005	<0.0001
$\delta^{18}O$	0.3579	0.027	<0.05	0.0927	0.002	<0.05
SPM_i	0.0469	-0.011	0.7480	0.0141	-0.003	0.9388
Pot. Temp.	0.4982	-0.013	<0.0001	0.5144	0.015	<0.0001
Salinity	0.3351	-0.008	<0.0001	0.0510	0.001	0.3350
$R(490)$	0.3620	-0.0002	<0.01	0.5702	-0.0001	<0.0001
$K_d(PAR)$	0.2420	-0.0057	<0.001	0.3149	-0.0025	<0.001

Table 2.4. Statistical results of predicted meltwater fraction when compared to *in-situ* observations. Derived $Q_{i,IOP}$ from Model 1 is based on inherent optical properties, backscattering and non-algal particle absorption coefficients at 442nm, and temperature; while derived $Q_{i,AOP}$ from Model 2 is based on reflectance band addition of 555 nm and 625 nm, and band ratio between 625 nm and 490 nm (a variation based on Sravanthi *et al.* (Sravanthi et al., 2013)).

	December 2015	**April 2016**
Model 1: Derived Q_i from IOPs		
$\mathbf{Q_{i,iop} = \beta_1 + \alpha_1 b_{bp}(442) + \alpha_2 a_{NAP}(442) + \alpha_3 Temp}$		
p-value	3.52E-05	1.62E-04
RMSD	0.002	0.003
Multiple r	0.698	0.638
Adjusted r	0.661	0.600
β_1	0.012	0.012
α_1	-0.310	-1.054
α_2	0.267	1.530
α_3	-0.006	-0.005
β_1 SE	0.001	0.002
α_1 b_{bp}(442) SE	0.171	0.520
α_2 a_{NAP}(442) SE	0.071	0.373
α_3 Temp SE	0.001	0.002
Model 2: Derived Q_i from AOPs		
$\mathbf{Q_{i,aop} = \beta_2 + \alpha_4 (R(555) + R(625)) + \alpha_5 \left(\frac{R(625)}{R(490)}\right)^2}$		
p-value	< 2.2E-16	<2.2E-16
RMSD	0.002	0.003
Multiple r	0.821	0.849
Adjusted r	0.817	0.844
β_2	1.428e-02	1.774e-02
α_4	-3.077e-02	-6.599e-02
α_5	7.532e-06	2.245e-06
β_2 SE	2.168e-04	4.348e-04
$\alpha_4 (R(555) + R(625))$ SE	3.045e-03	6.915e-03
$\alpha_5 \left(\frac{R(625)}{R(490)}\right)^2$ SE	3.014e-06	1.929e-06

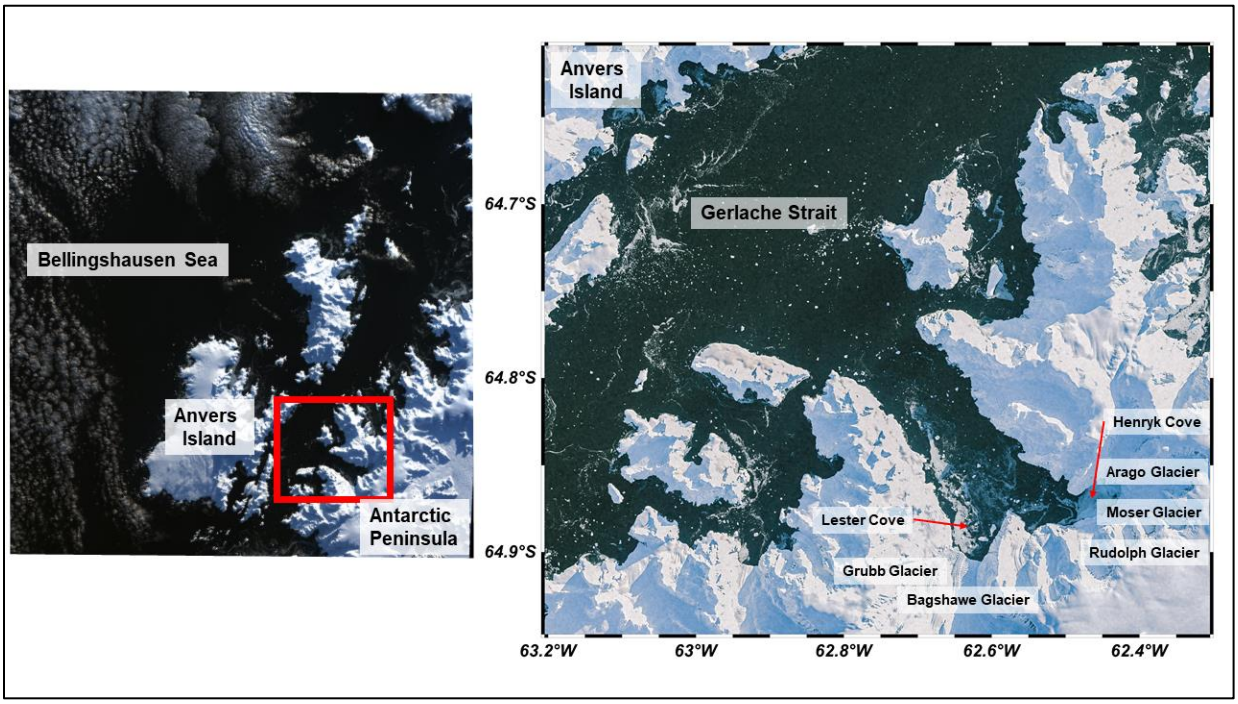

Figure 2.1. Map of the study region, Andvord Bay located on the Western Antarctic Peninsula. Map of Andvord Bay with colored contours depicting the fjord's bathymetry. The distance from these glaciers in this study is calculated as the shortest displacement from a single glacial boundary line that encompasses all five glaciers in both Inner Basins. Satellite imagery retrieved from NASA/USGS Landsat 8 Scene ID LC82191052016109LGN00.

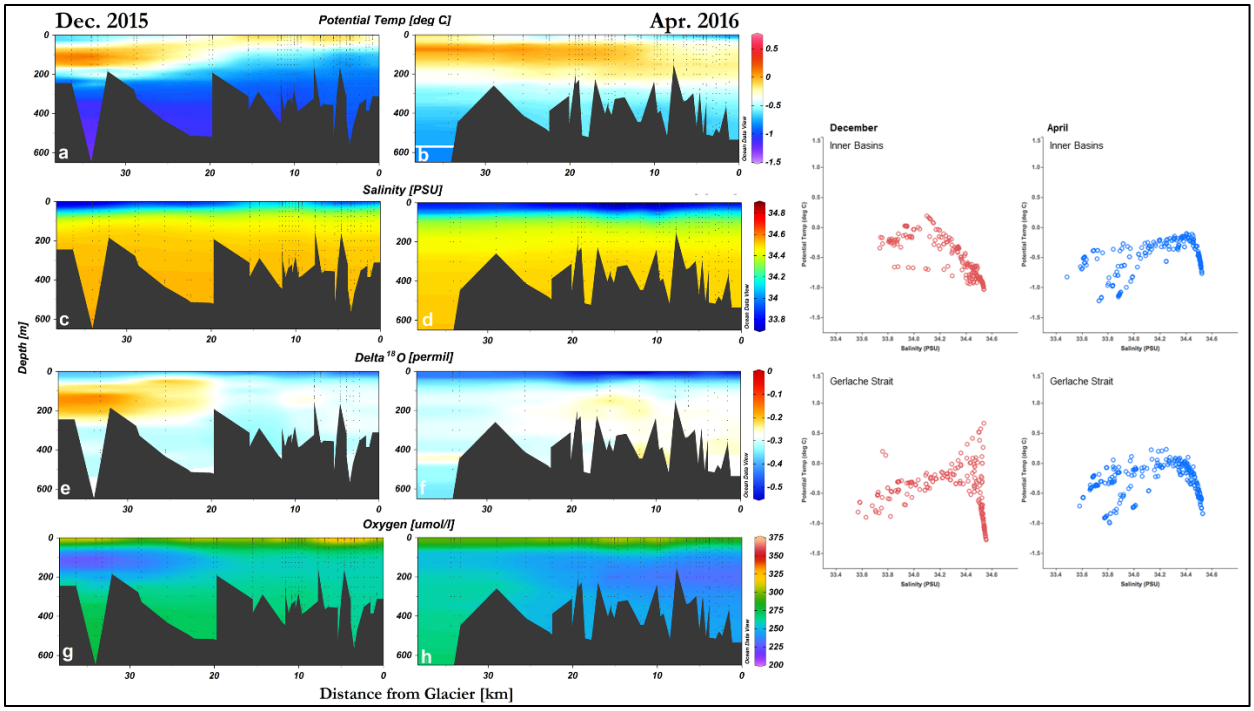

Figure 2.2. Overall hydrography profiles of Andvord Bay in December 2015, and April 2016. Left panels: Cross section plots of Andvord Bay depicting (a, b) potential temperature, (c, d) salinity, (e, f) oxygen isotope ratio, and (g, h) dissolved oxygen concentration, and as a function of their distance relative to the main glaciers situated in Andvord Bay. The differentiation between bottom topography is due to the slight differences in transect and sampling locations between the two study periods. Right panels: Temperature-salinity profiles of water masses within the inner basins and Gerlache Strait.

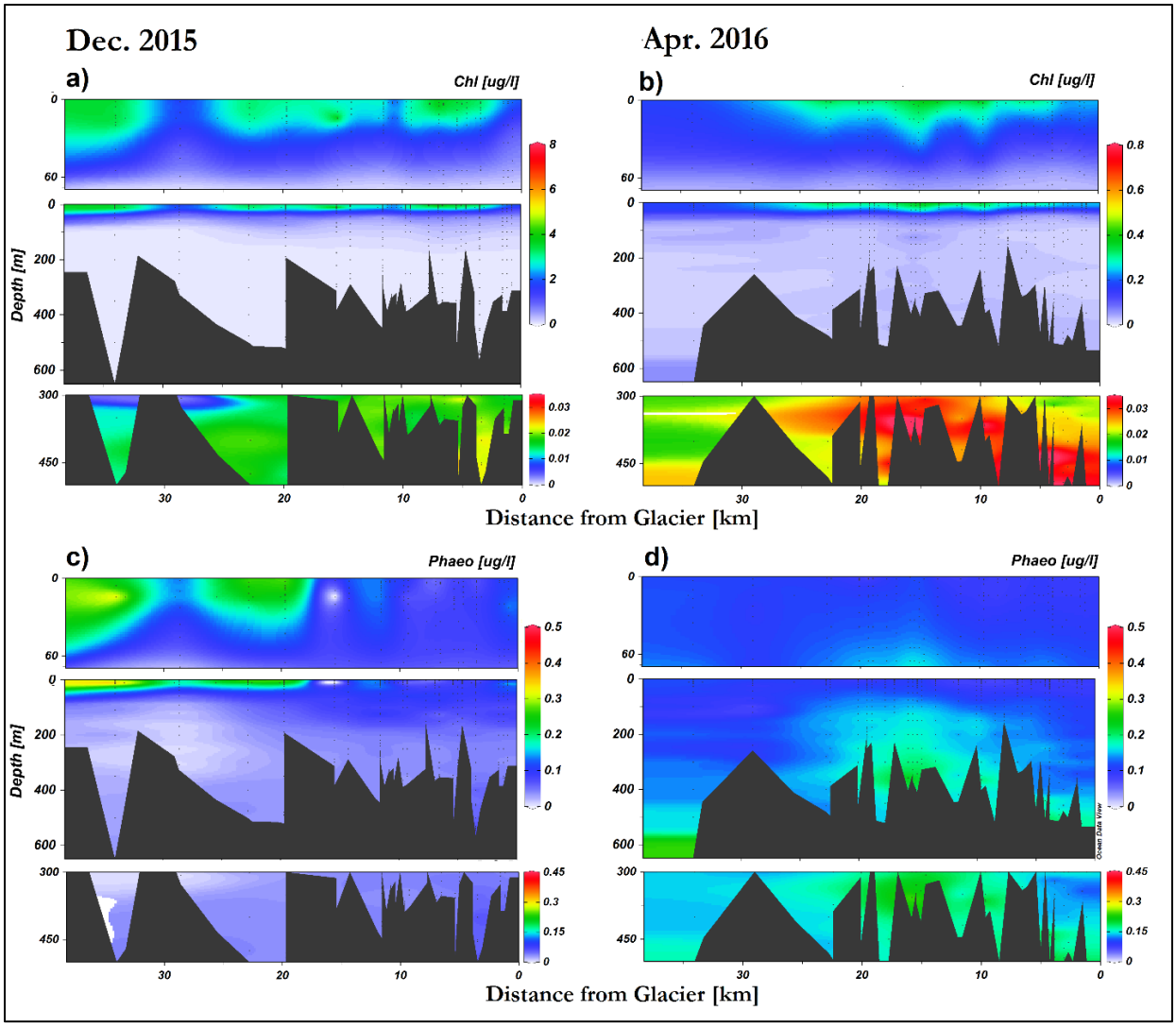

Figure 2.3. Chlorophyll-a concentration and phaeo-pigment concentration of Andvord Bay. (a, b) Chlorophyll-a concentration. (c, d) Phaeo-pigment concentration. Upper panel depicts surface profiles (0m – 100m), middle panel depicts the entire water column, and lower panel depicts deep profiles (300m – 500m). Depth axes in the surface plots are stretched to emphasize the euphotic layer. Appropriate scales are applied to certain color ramps to display data properly.

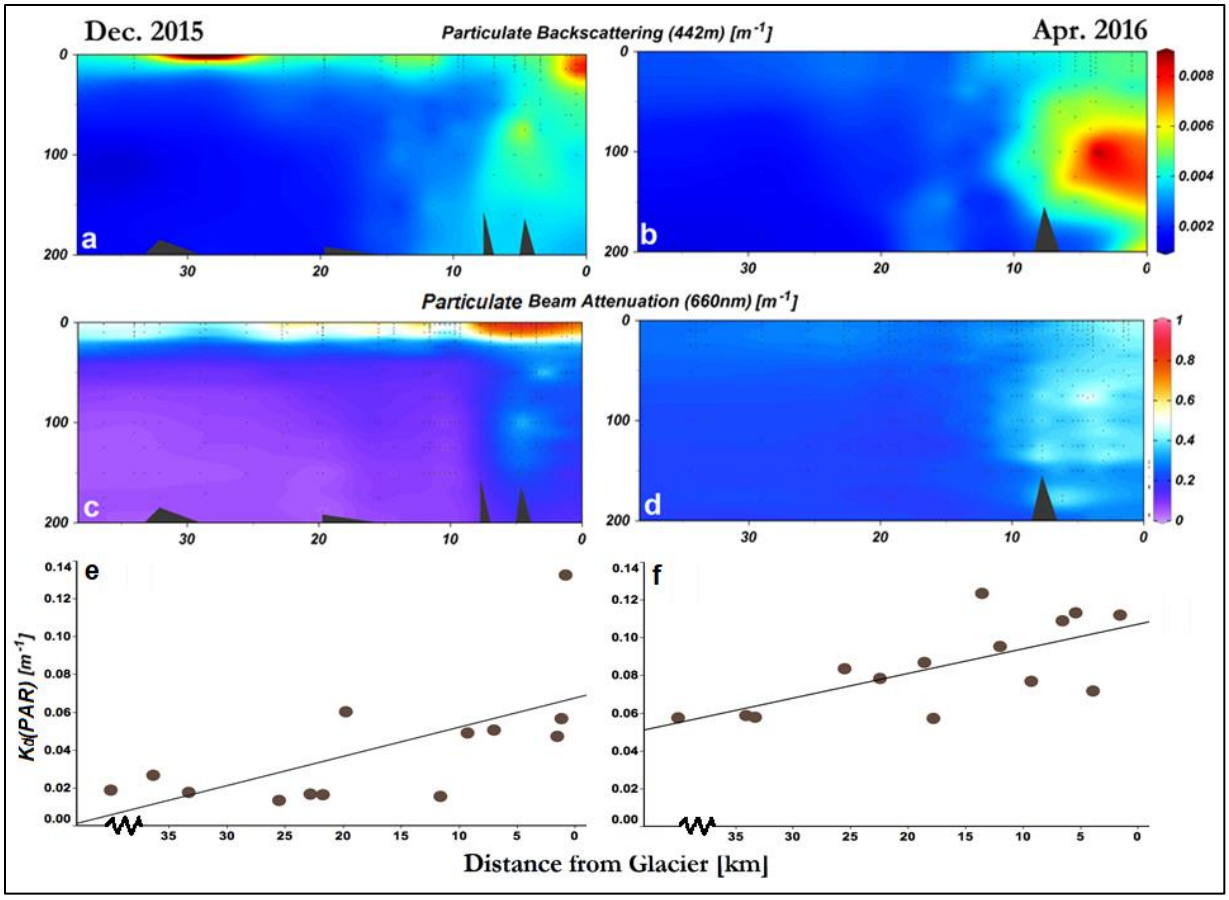

Figure 2.4. Spatial distribution of optical features in Andvord Bay. Profiles of particulate backscattering coefficient at 442nm and particulate beam attenuation coefficient at 660nm (a – d) in comparison to their corresponding diffuse attenuation coefficient of photosynthetically active radiation within the euphotic layer (e, f) in Andvord Bay during December 2015 and April 2016.

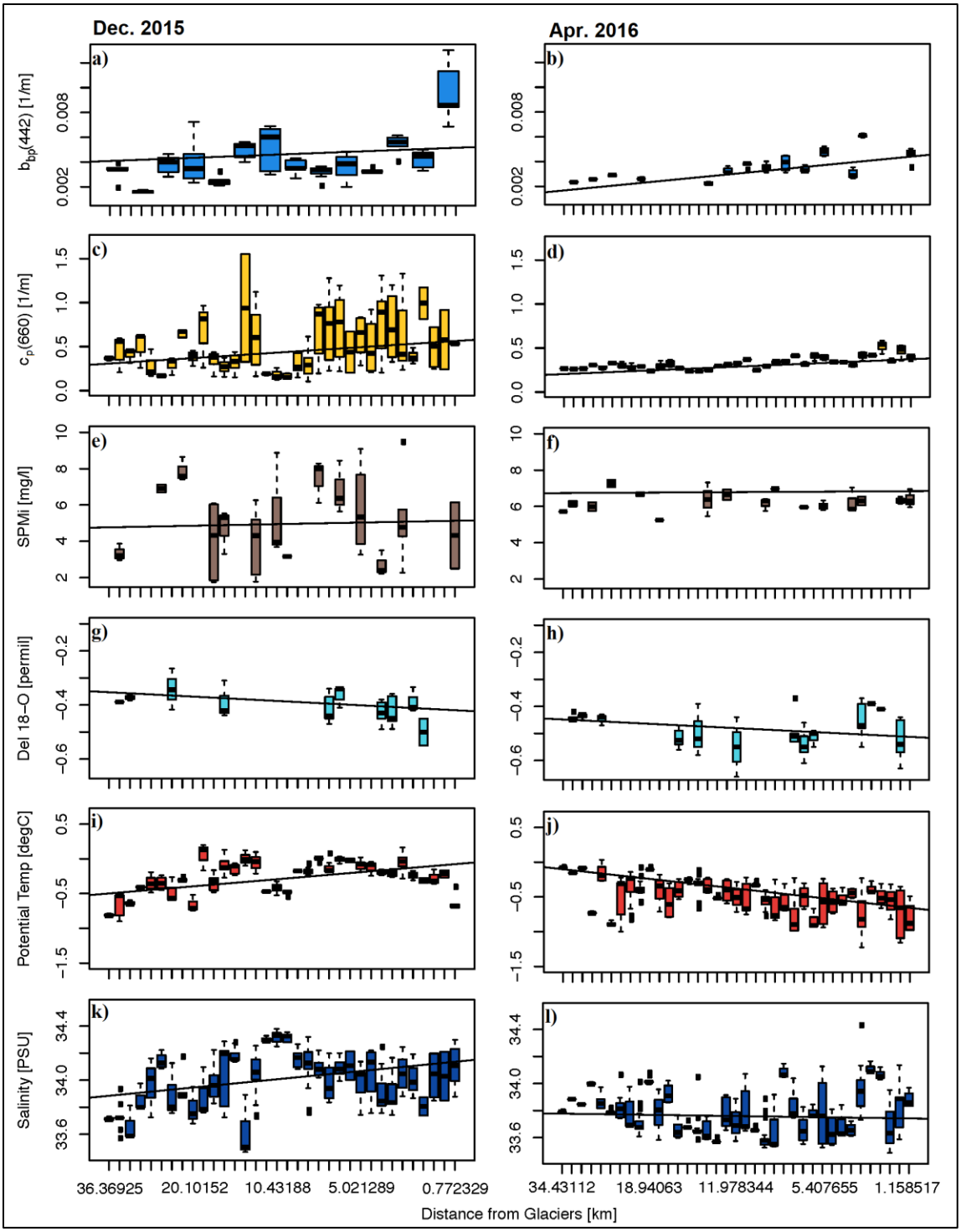

Figure 2.5. Profiles of optical and hydrographic variables. The box-whisker plots illustrate each variable's range, variability at the sampling station, the overall trend towards the glaciers, and an overview of optical measurements and their coherence, or lack thereof, with physical variables. Each box represents a CTD profile along the fjord, and the bars on each box represent local maximum and minimum while the marker within each box represents local mean. Depth is between 0 m – 35 m and statistics pertaining to this figure are in Table 3.

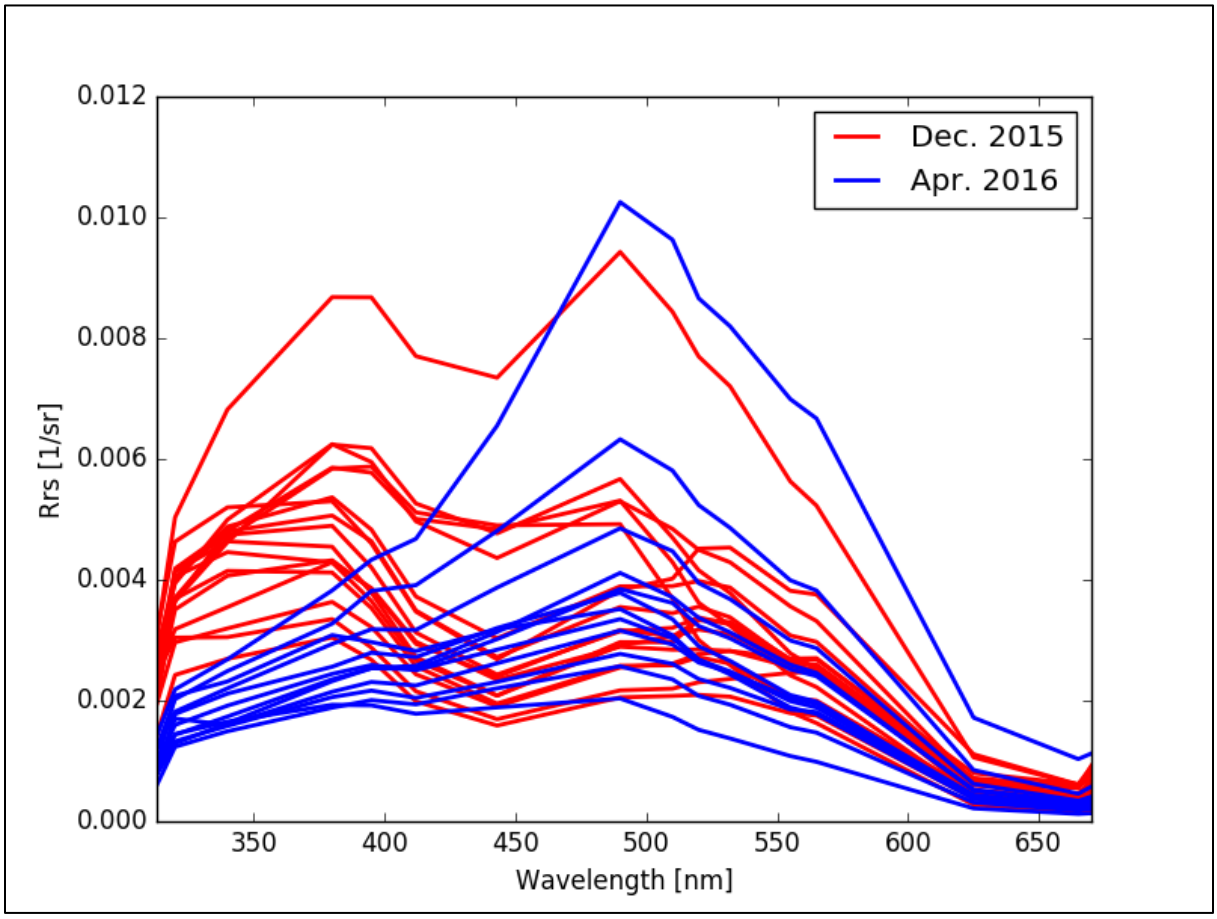

Figure 2.6. Remote sensing reflectance at the surface demonstrates a shift in spectral shape between December 2015 and April 2016.

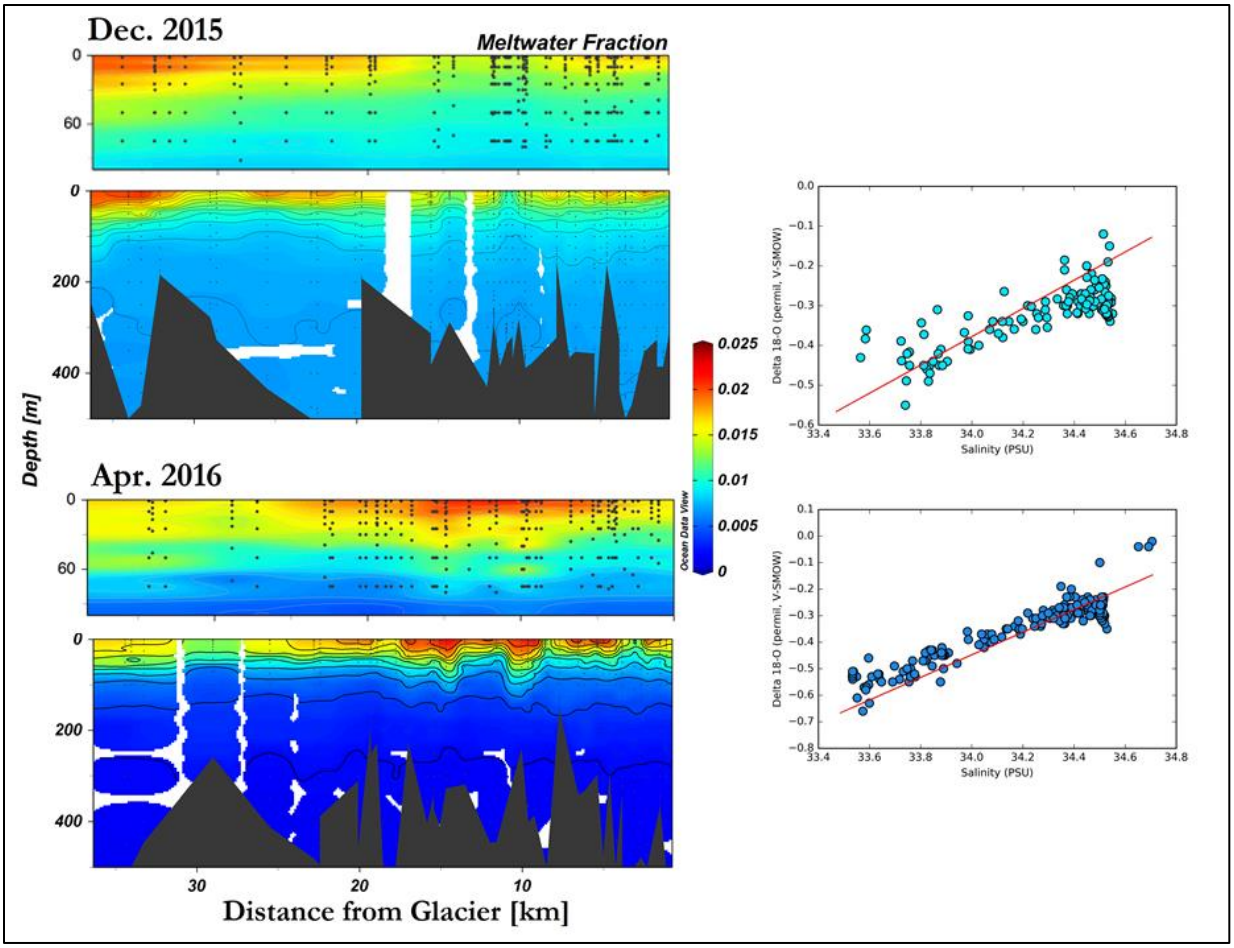

Figure 2.7. Meltwater fraction (Q_i) of Andvord Bay in December 2015, and April 2016. Left panels: Q_i is calculated based on oxygen-18 isotope ratio data, and then interpolated according to salinity profile to extend data spatial resolution (upper panel: 0—100m, lower panel: entire water column). Right panels: Gade Line indicates two-component mixing. Detected by correlation between $\delta^{18}O$ and salinity based on pure glacial meltwater and deep water of Gerlache Strait (Table 2); values sampled over the shelf are excluded in this calculation.

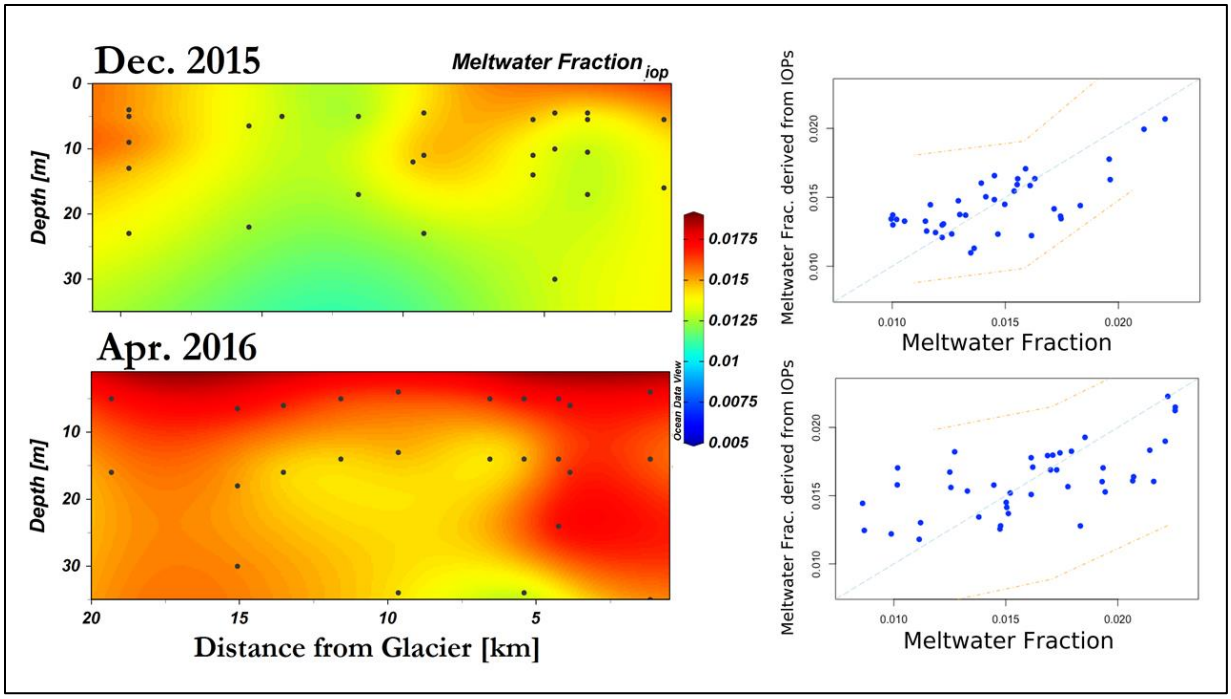

Figure 2.8. Section plots of meltwater fraction predicted based on Model 1 results. Left panels depict cross section plots of derived meltwater fraction from Model 1, which utilizes inherent optical properties – particulate backscattering coefficient at 442nm, non-algal particle absorption coefficient at 442nm, as well as temperature. Right panels depict their correlation with measured meltwater fraction based on oxygen-18 isotope ratios; orange dash lines indicate prediction intervals at 95% confidence.

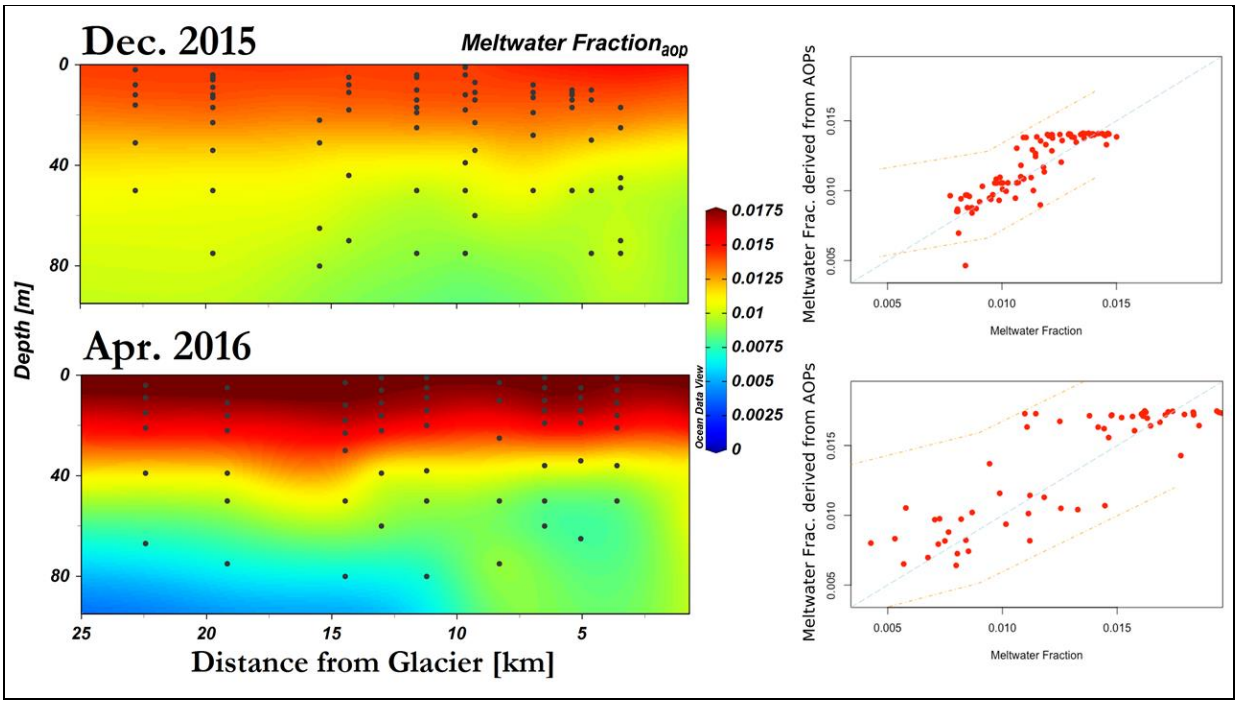

Figure 2.9. Section plots of meltwater fraction predicted based on Model 2 results. Left panels depict cross section plots of derived meltwater fraction from Model 1, which utilizes reflectance signal band ratio and addition. Right panels depict their correlation with measured meltwater fraction based on oxygen-18 isotope ratios; orange dash lines indicate predication intervals at 95% confidence.

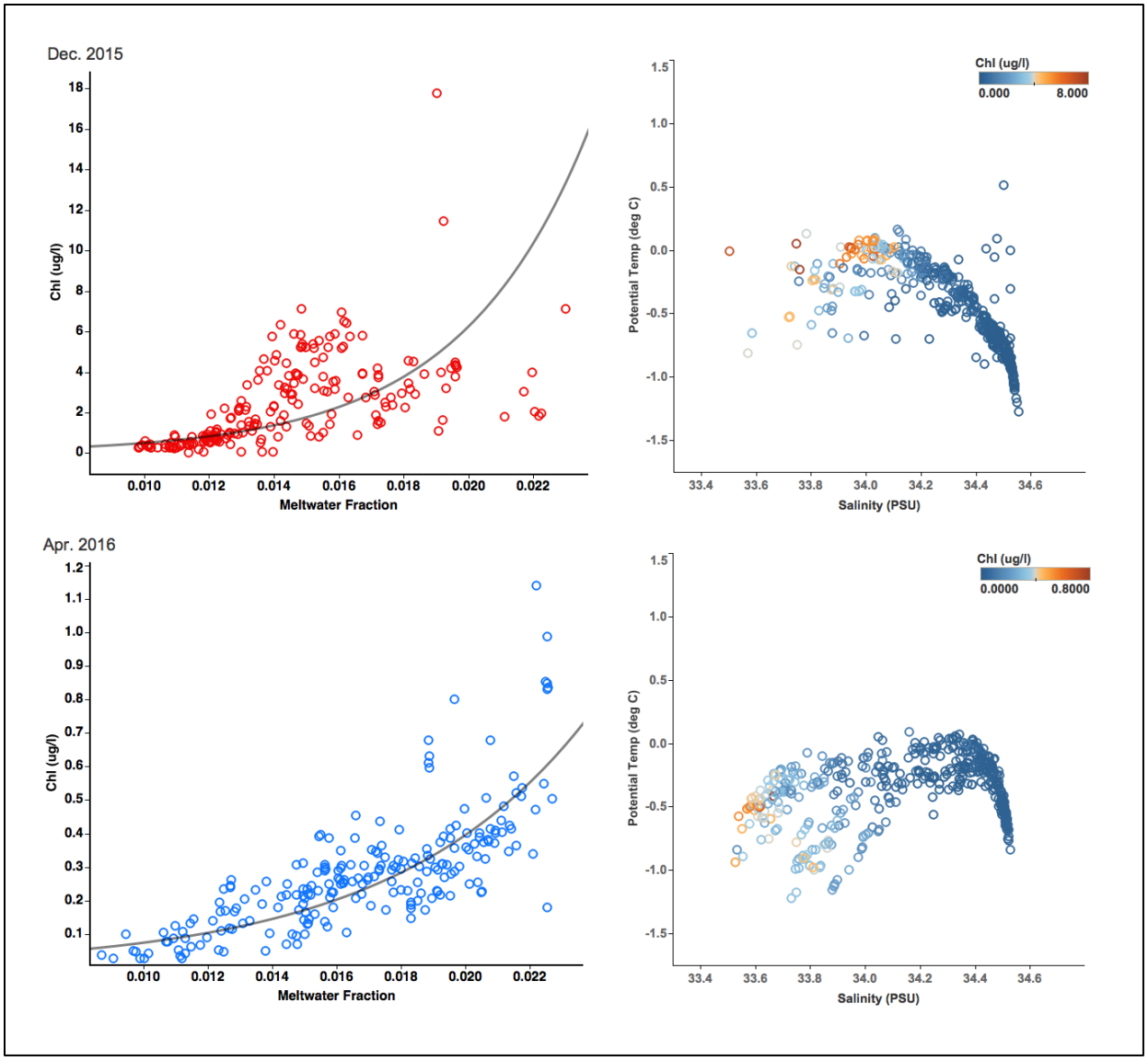

Figure 2.10. The relationship between meltwater fraction and chlorophyll-a concentration. Left panels: In the surface layer between 0 m and 40 m depth in Andvord Bay, the exponential regression between the two variables has a correlation coefficient of 0.66 and p-value of <0.0001 in December 2015, while the correlation coefficient is 0.82 and p-value is <0.0001 in April 2016. Right panels: T-S diagrams of Andvord Bay during December and April with color indicating chl-a concentration.

2.9. Appendix

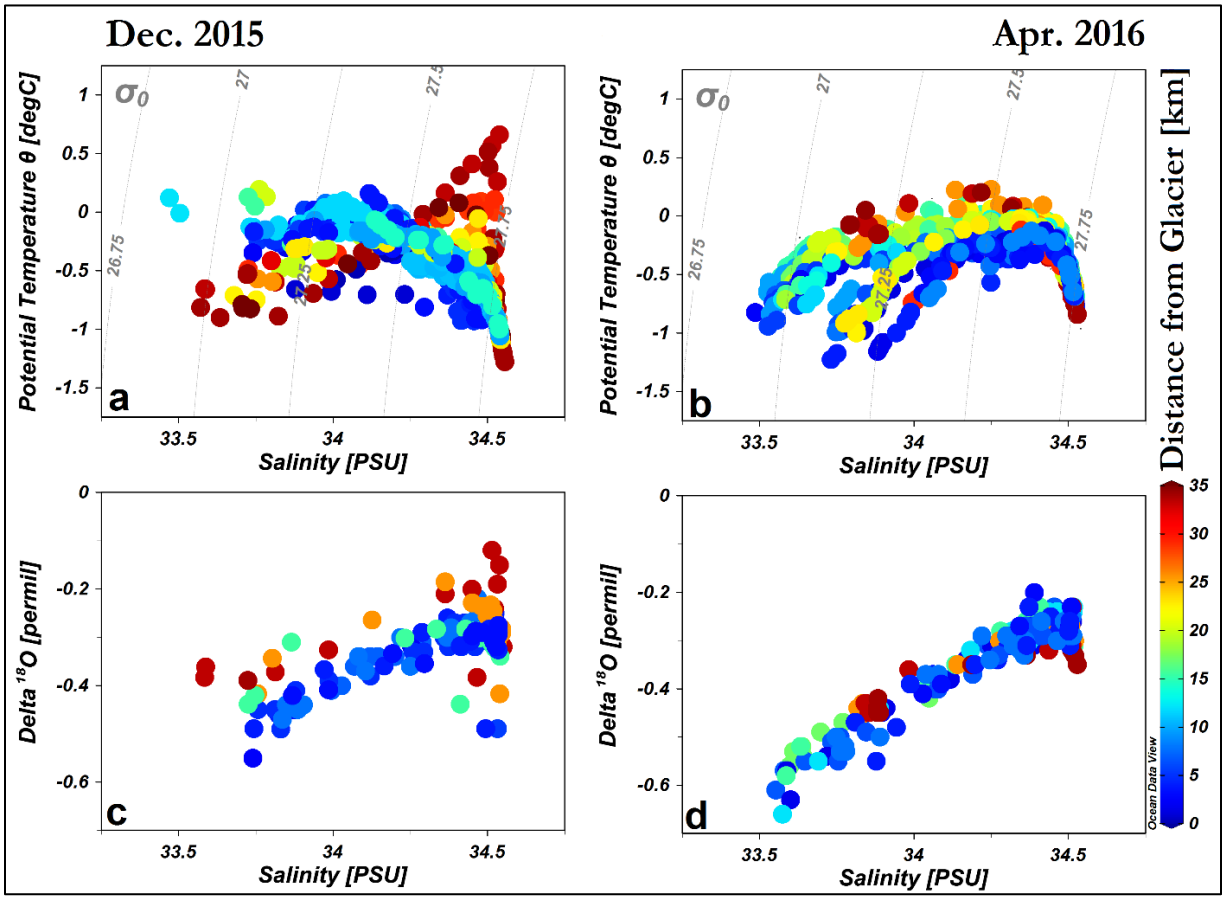

Figure A1. Temperature-salinity diagram and "Gade Line" between oxygen isotope ratio and salinity. T-S Diagram of cruise data in (a) December 2015 and (b) April 2016, and (c, d) $\delta^{18}O$ values along salinity gradient from each season. Each data point is a discrete water column sample, and the color of the point indicates its sampling station's distance from the glaciers, which are situated in the inner basins at the head of Andvord Bay.

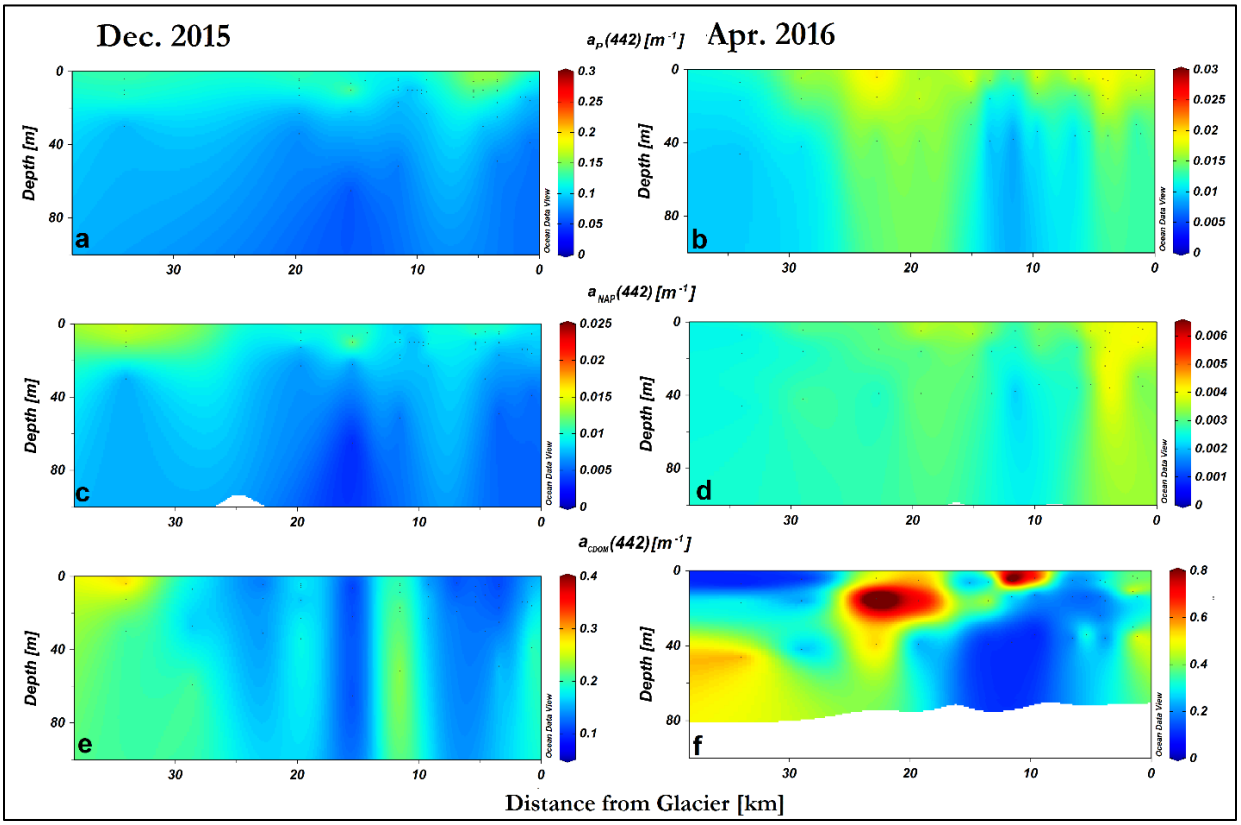

Figure A2. Cross section plots of particulate absorption, non-algal absorption, and CDOM absorption coefficients at 442 nm. (a, b) Particulate absorption coefficient at 442 nm. (c,d) Non-algal particle absorption coefficient at 442 nm. (e, f) CDOM absorption coefficient at 442 nm.

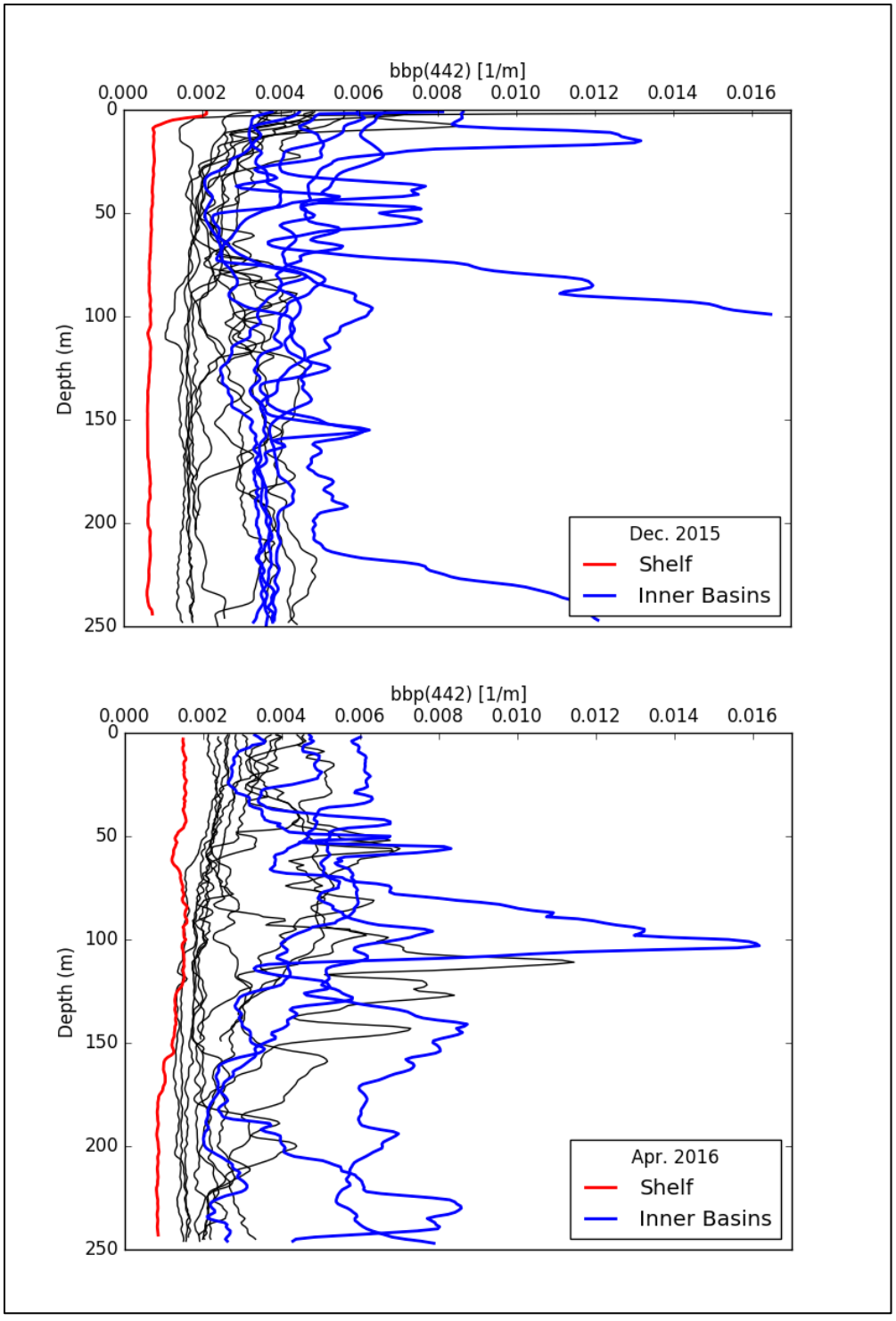

Figure A3. Profiles of particulate backscattering coefficient at 442 nm. December 2015 (above) and April 2016 (below), where high backscattering signals are observed in the inner basins (blue) in comparison to the significantly lower values found on the shelf (red); the profiles in black are the rest of the sampling stations between inner fjord and the shelf.

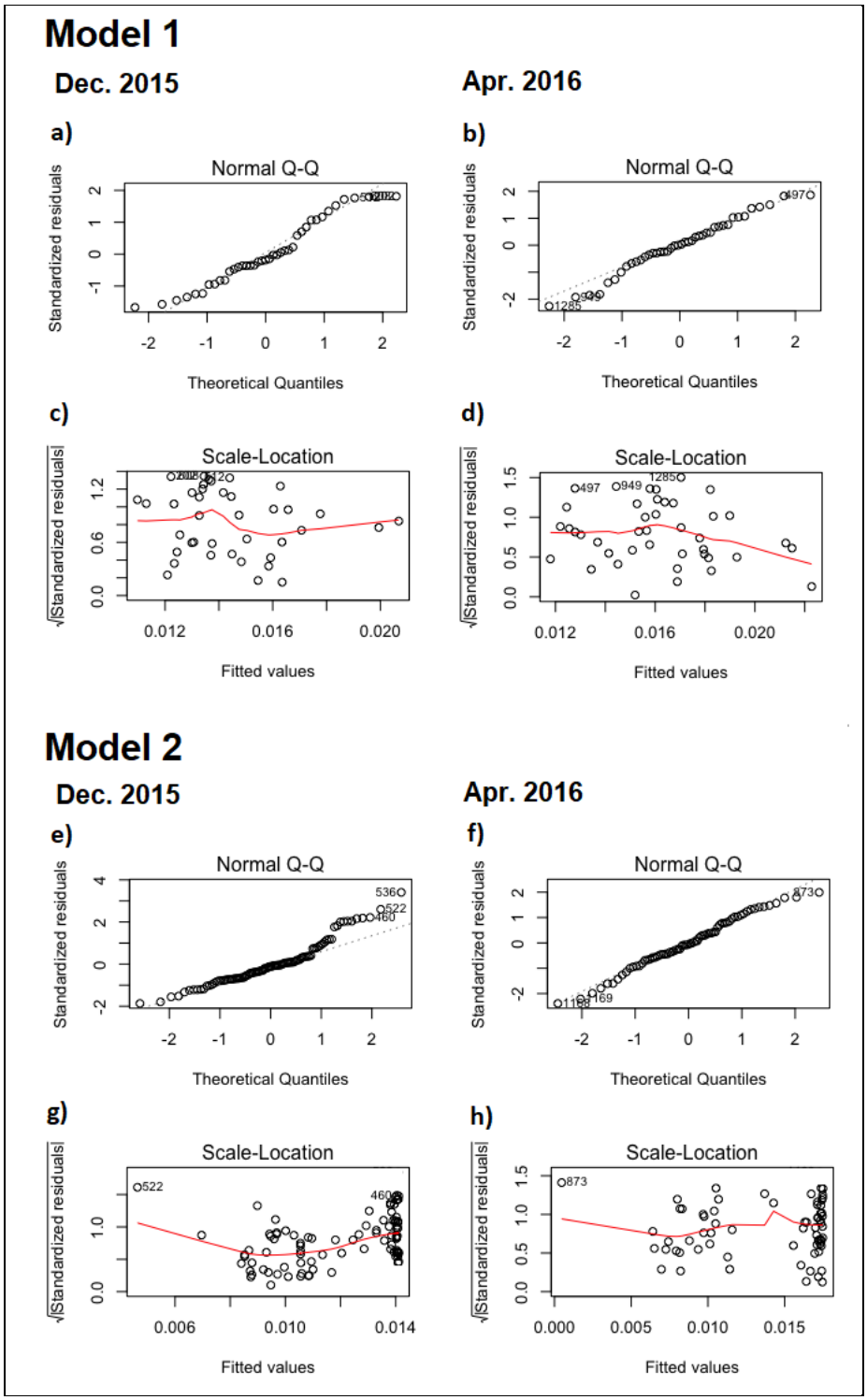

Figure A4. Multivariate linear regression model assumption diagnostics. Diagnostic plots for Models 1 and 2 which results are presented in Figs 2.8 and 2.9. Normality of residuals presented in normal Q-Q plots (upper panels) and homogeneity of residuals variance presented in location-scale plots (lower panels).

2.10. References

Alley, R., Cuffey, K., Evenson, E., Strasser, J., Lawson, D., Larson, G., 1997. How glaciers entrain and transport basal sediment: physical constraints. *Quaternary Science Reviews*, 16, 1017-1038.

Aoki, S., Kobayashi, R., Rintoul, S., Tamura, T., Kusahara, K., 2017. Changes in water properties and flow regime on the continental shelf off the Adélie/George VLand coast, East Antarctica, after glacier tongue calving. *Journal of Geophysical Research: Oceans*, 122, 6277-6294.

Arendt, K.E., Dutz, J., Jonasdottir, S.H., Jung-Madsen, S., Mortensen, J., Moller, E.F., Nielsen, T.G., 2011. Effects of suspended sediments on copepods feeding in a glacial influenced sub-Arctic fjord. *Journal of Plankton Research*, 33, 1526-1537.

Arrigo, K.R., Dijken, G.L., Castelao, R.M., Luo, H., Rennermalm, Å.K., Tedesco, M., Mote, T.L., Oliver, H., Yager, P.L., 2017. Melting glaciers stimulate large summer phytoplankton blooms in southwest Greenland waters. *Geophysical Research Letters*.

Beaird, N., Straneo, F., Jenkins, W., 2015. Spreading of Greenland meltwaters in the ocean revealed by noble gases. *Geophysical Research Letters*, 42, 7705-7713.

Bohren, C.F., Huffman, D.R., 2008. *Absorption and scattering of light by small particles*: John Wiley & Sons.

Boss, E., Sherwood, C., Hill, P., Milligan, T., 2018. Advantages and Limitations to the Use of Optical Measurements to Study Sediment Dynamics.

Brito, A.C., Sá, C., Mendes, C.R., Brand, T., Dias, A.M., Brotas, V., Davidson, K., 2015. Structure of late summer phytoplankton community in the Firth of Lorn (Scotland) using microscopy and HPLC-CHEMTAX. *Estuarine, Coastal and Shelf Science*, 167, 86-101.

Cape, Vernet, M., Smith, C., Grange, L., Leventer, A., Domack, E., 2010. Dynamic Patterns of Paleoproductivity in the Fjords and Coastal Bays of the Antarctic Peninsula. *SCAR Conference*.

Cape, M., Vernet, M., Kahru, M., Spreen, G., 2014. Polynya dynamics drive primary production in the Larsen A and B embayments following ice shelf collapse. *Journal of Geophysical Research: Oceans*, 119, 572-594.

Cape, M., Vernet, M., Skvarca, P., Marinsek, S., Scambos, T., Domack, E., 2015. Foehn winds link climate-driven warming to ice shelf evolution in Antarctica. *Journal of Geophysical Research: Atmospheres*, 120.

Chu, V.W., Smith, L.C., Rennermalm, A.K., Forster, R.R., Box, J.E., Reehy, N., 2009. Sediment plume response to surface melting and supraglacial lake drainages on the Greenland ice sheet. *Journal of Glaciology*, 55, 1072-1082.

Cook, S., 2017. Larsen C ice shelf sheds a trillion-tonne ice berg. In T. Wire (Ed.), *Community Broadcasting Association of Australia*: University of Tasmania, Australia.

Coplen, T.B., 1995. Reporting of stable hydrogen, carbon, and oxygen isotopic abundances. *Geothermics*, 24, 707-712.

DeConto, R.M., Pollard, D., 2016. Contribution of Antarctica to past and future sea-level rise. *Nature*, 531, 591.

Dierssen, H.M., Smith, R.C., 2000a. Bio-optical properties and remote sensing ocean color algorithms for Antarctic Peninsula waters. *Journal of Geophysical Research: Oceans*, 105, 26301-26312.

Dierssen, H.M., Smith, R.C., 2000b. Case 2 Antarctic coastal waters: The bio-optical properties of surface meltwater. *Proceedings Ocean Optics XV [CD-ROM], edited by S. Ackleson and J. Marra, Off. of Nav. Res., Kailua-Kona, Hawaii*.

Dierssen, H.M., Smith, R.C., Vernet, M., 2002. Glacial meltwater dynamics in coastal waters west of the Antarctic peninsula. *Proc Natl Acad Sci U S A*, 99, 1790-1795.

Domack, E.W., Foss, D.J.P., Syvitski, J.P.M., McClennen, C.E., 1994. Transport of suspended particulate matter in an Antarctic fjord. *Marine Geology*, 121, 161-170.

Domack, E.W., Williams, C.R., 1990. Fine structure and suspended sediment transport in three Antarctic fjords. *Contributions to Antarctic Research I*, 50, 71-89.

Doxaran, D., Leymarie, E., Nechad, B., Dogliotti, A., Ruddick, K., Gernez, P., Knaeps, E., 2016. Improved correction methods for field measurements of particulate light backscattering in turbid waters. *Optics Express*, 24, 3615-3637.

Ekern, L., 2017. Assessing Primary Production via nutrient deficits in Andvord Bay, Antarctica 2015-2016. *Scripps Institution of Oceanography*, Vol. Master's University of California, San Diego.

Epstein, S., Mayeda, T., 1953. Variation of O18 content of waters from natural sources. *Geochimica Et Cosmochimica Acta*, 4, 213-224.

Ferreira, A., Ciotti, Á.M., Garcia, C.A., 2018. Bio-optical characterization of the northern Antarctic Peninsula waters: Absorption budget and insights on particulate backscattering. *Deep Sea Research Part II: Topical Studies in Oceanography*, 149, 138-149.

Gade, H.G., 1979. Melting of ice in sea water: A primitive model with application to the Antarctic ice shelf and icebergs. *Journal of Physical Oceanography*, 9, 189-198.

Hernando, M., Schloss, I., Malanga, G., Almandoz, G., Ferreyra, G., Aguiar, M., Puntarulo, S., 2015. Effects of salinity changes on coastal Antarctic phytoplankton physiology and assemblage composition. *Journal of Experimental Marine Biology and Ecology*, 466, 110-119.

Holinde, L., Zielinski, O., 2015. Bio-optical characterization and light availability parametrization in two glacial melt water influenced estuary systems (West-Greenland). *Ocean Science Discussions*, 12, 1537-1566.

Holinde, L., Zielinski, O., 2016. Bio-optical characterization and light availability parameterization in Uummannaq Fjord and Vaigat–Disko Bay (West Greenland). *Ocean Science*, 12, 117-128.

Hudson, B., Overeem, I., McGrath, D., Syvitski, J., Mikkelsen, A., Hasholt, B., 2014. MODIS observed increase in duration and spatial extent of sediment plumes in Greenland fjords. *The Cryosphere*, 8, 1161-1176.

Hylander, S., Jephson, T., Lebret, K., Von Einem, J., Fagerberg, T., Balseiro, E., Modenutti, B., Souza, M.S., Laspoumaderes, C., Jönsson, M., 2011. Climate-induced input of turbid glacial meltwater affects vertical distribution and community composition of phyto-and zooplankton. *Journal of Plankton Research*, 33, 1239-1248.

Isao, K., Hara, S., Terauchi, K., Kogure, K., 1990. Role of sub-micrometre particles in the ocean. *Nature*, 345, 242-244.

Jacobs, S.S., Fairbanks, R.G., Horibe, Y., 1985. Origin and evolution of water masses near the Antarctic continental margin: Evidence from H218O/H216O ratios in seawater. *Oceanology of the Antarctic Continental Shelf*, 43, 59-85.

Jenkins, A., 1999. The Impact of Melting Ice on Ocean Waters. *Journal of Physical Oceanography*, 29, 2370-2381.

Jenkins, A., Jacobs, S., 2008. Circulation and melting beneath George VI Ice Shelf, Antarctica. *Journal of Geophysical Research*, 113.

Keigwin, L., Jones, G., Lehman, S., Boyle, E., 1991. Deglacial meltwater discharge, North Atlantic deep circulation, and abrupt climate change. *Journal of Geophysical Research: Oceans*, 96, 16811-16826.

Kirk, J.T., 1994. *Light and photosynthesis in aquatic ecosystems*: Cambridge university press.

Kishino, M., Takahashi, M., Okami, N., Ichimura, S., 1985. Estimation of the spectral absorption coefficients of phytoplankton in the sea. *Bulletin of Marine Science*, 37, 634-642.

Knox, G.A., 2006. *Biology of the southern ocean*: CRC Press.

Kong, J.-L., Sun, X.-M., Wong, D., Chen, Y., Yang, J., Yan, Y., Wang, L.-X., 2015. A semi-analytical model for remote sensing retrieval of suspended sediment concentration in the gulf of Bohai, China. *Remote Sensing*, 7, 5373-5397.

Maffione, R.A., Dana, D.R., 1997. Instruments and methods for measuring the backward-scattering coefficient of ocean waters. *Applied Optics*, 36, 6057.

Mankoff, K.D., Straneo, F., Cenedese, C., Das, S.B., Richards, C.G., Singh, H., 2016. Structure and dynamics of a subglacial discharge plume in a Greenlandic fjord. *Journal of Geophysical Research: Oceans*, 121, 8670-8688.

Martinson, D.G., Stammerjohn, S.E., Iannuzzi, R.A., Smith, R.C., Vernet, M., 2008. Western Antarctic Peninsula physical oceanography and spatio–temporal variability. *Deep Sea Research Part II: Topical Studies in Oceanography*, 55, 1964-1987.

Mascarenhas, V.J., Voß, D., Wollschlaeger, J., Zielinski, O., 2017. Fjord light regime: Bio-optical variability, absorption budget, and hyperspectral light availability in Sognefjord and Trondheimsfjord, Norway. *Journal of Geophysical Research: Oceans*, 3828-3847.

McGrath, D., Steffen, K., Overeem, I., Mernild, S.H., Hasholt, B., van den Broeke, M., 2010. Sediment plumes as a proxy for local ice-sheet runoff in Kangerlussuaq Fjord, West Greenland. *Journal of Glaciology*, 56, 813-821.

Meire, L., Mortensen, J., Meire, P., Juul-Pedersen, T., Sejr, M.K., Rysgaard, S., Nygaard, R., Huybrechts, P., Meysman, F.J., 2017. Marine-terminating glaciers sustain high productivity in Greenland fjords. *Global Change Biology*, 23, 5344-5357.

Meredith, M.P., Brandon, M.A., Wallace, M.I., Clarke, A., Leng, M.J., Renfrew, I.A., van Lipzig, N.P.M., King, J.C., 2008. Variability in the freshwater balance of northern Marguerite Bay, Antarctic Peninsula: Results from δ18O. *Deep Sea Research Part II: Topical Studies in Oceanography*, 55, 309-322.

Meredith, M.P., Stammerjohn, S.E., Venables, H.J., Ducklow, H.W., Martinson, D.G., Iannuzzi, R.A., Leng, M.J., van Wessem, J.M., Reijmer, C.H., Barrand, N.E., 2017. Changing distributions of sea ice melt and meteoric water west of the Antarctic Peninsula. *Deep Sea Research Part II: Topical Studies in Oceanography*, 139, 40-57.

Mitchell, B.G., Kahru, M., 1998. Algorithms for SeaWiFS standard products developed with the CalCOFI bio-optical data set. *CALCOFI Reports*, 133-147.

Mitchell, B.G., Kahru, M., Wieland, J., Stramska, M., 2002. Determination of spectral absorption coefficients of particles, dissolved material and phytoplankton for discrete water samples. *Ocean Optics Protocols for Satellite Ocean Color Sensor Validation, Revision 3*, 2, 231.

Mobley, C.D., 1994. *Light and water: radiative transfer in natural waters*: Academic press.

Morel, A., Ahn, Y.-H., 1991. Optics of heterotrophic nanoflagellates and ciliates: A tentative assessment of their scattering role in oceanic waters compared to those of bacterial and algal cells. *Journal of Marine Research*, 49, 177-202.

Mortensen, J., Bendtsen, J., Motyka, R.J., Lennert, K., Truffer, M., Fahnestock, M., Rysgaard, S., 2013. On the seasonal freshwater stratification in the proximity of fast-flowing tidewater outlet glaciers in a sub-Arctic sill fjord. *Journal of Geophysical Research: Oceans*, 118, 1382-1395.

Motyka, R.J., Hunter, L., Echelmeyer, K.A., Connor, C., 2003. Submarine melting at the terminus of a temperate tidewater glacier, LeConte Glacier, Alaska, U.S.A. *Annals of Glaciology*, 36, 57-65.

Murray, C., Markager, S., Stedmon, C.A., Juul-Pedersen, T., Sejr, M.K., Bruhn, A., 2015. The influence of glacial melt water on bio-optical properties in two contrasting Greenlandic fjords. *Estuarine, Coastal and Shelf Science*, 163, 72-83.

Nerem, R., Beckley, B., Fasullo, J., Hamlington, B., Masters, D., Mitchum, G., 2018. Climate-change–driven accelerated sea-level rise detected in the altimeter era. *Proceedings of the National Academy of Sciences*, 201717312.

Park, J.-H., Day, T.A., Strauss, S., Ruhland, C.T., 2007. Biogeochemical pools and fluxes of carbon and nitrogen in a maritime tundra near penguin colonies along the Antarctic Peninsula. *Polar Biology*, 30, 199-207.

Potter, J., Paren, J., Loynes, J., 1984. Glaciological and oceanographic calculations of the mass balance and oxygen isotope ratio of a melting ice shelf. *Journal of Glaciology*, 30, 161-170.

Powell, R., Domack, E., 1995. *Modern glaciomarine environments*.

Pritchard, H.D., Vaughan, D.G., 2007. Widespread acceleration of tidewater glaciers on the Antarctic Peninsula. *Journal of Geophysical Research*, 112.

Raiswell, R., Tranter, M., Benning, L.G., Siegert, M., De'ath, R., Huybrechts, P., Payne, T., 2006. Contributions from glacially derived sediment to the global iron (oxyhydr)oxide cycle: Implications for iron delivery to the oceans. *Geochimica Et Cosmochimica Acta*, 70, 2765-2780.

Reynolds, R.A., Stramski, D., Neukermans, G., 2016. Optical backscattering by particles in Arctic seawater and relationships to particle mass concentration, size distribution, and bulk composition. *Limnology and Oceanography*, 61, 1869-1890.

Rignot, E., Jacobs, S., Mouginot, J., Scheuchl, B., 2013. Ice-shelf melting around Antarctica. *Science*, 341, 266-270.

Schloss, I., Klöser, H., Ferreyra, G., Mercuri, G., Pinola, E., 1997. Factors governing phytoplankton and particulate matter variation in Potter Cove, King George island, Antarctica. *Antarctic communities*, 135-141.

Schloss, I.R., Abele, D., Moreau, S., Demers, S., Bers, A.V., González, O., Ferreyra, G.A., 2012. Response of phytoplankton dynamics to 19-year (1991–2009) climate trends in Potter Cove (Antarctica). *Journal of Marine Systems*, 92, 53-66.

Silvano, A., Rintoul, S.R., Peña-Molino, B., Hobbs, W.R., van Wijk, E., Aoki, S., Tamura, T., Williams, G.D., 2018. Freshening by glacial meltwater enhances melting of ice shelves and reduces formation of Antarctic Bottom Water. *Science Advances*, 4, eaap9467.

Smith, C.R., Mincks, S., DeMaster, D.J., 2006. A synthesis of bentho-pelagic coupling on the Antarctic shelf: food banks, ecosystem inertia and global climate change. *Deep Sea Research Part II: Topical Studies in Oceanography*, 53, 875-894.

Smith, R., Stammerjohn, S., 2001. Variations of surface air temperature and sea-ice extent in the western Antarctic Peninsula region. *Annals of Glaciology*, 33, 493-500.

Smith, R.C., Baker, K.S., Dustan, P., 1981. Fluorometric Techniques For The Measurement Of Oceanic Chlorophyll In The Support Of Remote Sensing.

Sravanthi, N., Ramana, I., Yunus Ali, P., Ashraf, M., Ali, M., Narayana, A., 2013. An algorithm for estimating suspended sediment concentrations in the coastal waters of India using remotely sensed reflectance and its application to coastal environments. *International Journal of Environmental Research*, 7, 841-850.

Steig, E.J., Schneider, D., Rutherford, S., Mann, M., Comiso, J., Shindell, D., 2009. Warming of the Antarctic ice-sheet surface since the 1957 International Geophysical Year. *Nature*, 457, 459-462.

Stramski, D., Boss, E., Bogucki, D., Voss, K.J., 2004. The role of seawater constituents in light backscattering in the ocean. *Progress in Oceanography*, 61, 27-56.

Stramski, D., Kiefer, D.A., 1991. Light scattering by microorganisms in the open ocean. *Progress in Oceanography*, 28, 343-383.

Stramski, D., Reynolds, R.A., Kaczmarek, S., Uitz, J., Zheng, G., 2015. Correction of pathlength amplification in the filter-pad technique for measurements of particulate absorption coefficient in the visible spectral region. *Appl Opt*, 54, 6763-6782.

Straneo, F., Cenedese, C., 2015. The Dynamics of Greenland's Glacial Fjords and Their Role in Climate. *Ann Rev Mar Sci*, 7, 89-112.

Straneo, F., Curry, R.G., Sutherland, D.A., Hamilton, G.S., Cenedese, C., Våge, K., Stearns, L.A., 2011. Impact of fjord dynamics and glacial runoff on the circulation near Helheim Glacier. *Nature Geoscience*, 4, 322-327.

Syvitski, J., 1989. On the deposition of sediment within glacier-influenced fjords: oceanographic controls. *Marine Geology*, 85, 301-329.

Syvitski, J., Burrell, D., Skei, J., 1987. *Fjords: Processes and Products*: Springer-Verlag.

Tassan, S., 1994. Local algorithms using SeaWiFS data for the retrieval of phytoplankton, pigments, suspended sediment, and yellow substance in coastal waters. *Applied Optics*, 33, 2369-2378.

Thomas, D.N., 2011. Biogeochemistry of sea ice. *Encyclopedia of Snow, Ice and Glaciers* (pp. 98-102): Springer.

Vaughan, D., 2006. Recent Trends in Melting Conditions on the Antarctic Peninsula and Their Implications for Ice-sheet Mass Balance and Sea Level. *Arctic, Antarctic, and Alpine Research*, 38, 147-152.

Vaughan, D., Marshall, G.J., Connolley, W.M., Parkinson, C., Mulvaney, R., Hodgson, D.A., King, J.C., Pudsey, C.J., Turner, J., 2003. Recent rapid regional climate warming on the Antarctic Peninsula. *Climatic change*, 60, 243-274.

Vernet, M., Martinson, D., Iannuzzi, R., Stammerjohn, S., Kozlowski, W., Sines, K., Smith, R., Garibotti, I., 2008a. Control of primary production by sea ice dynamics west of the Antarctic Peninsula. *Deep-Sea Research Part Ii-Topical Studies in Oceanography*, 55, 2068-2085.

Vernet, M., Martinson, D., Iannuzzi, R., Stammerjohn, S., Kozlowski, W., Sines, K., Smith, R., Garibotti, I., 2008b. Primary production within the sea-ice zone west of the Antarctic Peninsula: I—Sea ice, summer mixed layer, and irradiance. *Deep Sea Research Part II: Topical Studies in Oceanography*, 55, 2068-2085.

Węsławski, J.M., Kendall, M.A., Włodarska-Kowalczuk, M., Iken, K., Kędra, M., Legezynska, J., Sejr, M.K., 2010. Climate change effects on Arctic fjord and coastal macrobenthic diversity—observations and predictions. *Marine Biodiversity*, 41, 71-85.

Williams, C., Boies, C., Domack, E., 1989. Characteristics of glacial systems along the Graham Land Coast and Palmer Archipelago, Antarctic Peninsula. *Antarct. J. US*, 116-117.

Zhang, X., Hu, L., He, M.-X., 2009. Scattering by pure seawater: Effect of salinity. *Optics Express*, 17, 5698.

Chapter 3. Environmental Drivers of Phytoplankton Taxonomic Composition in an Antarctic Fjord

3.1. Abstract

The impact of ice-ocean interaction on the Southern Ocean is expected to intensify in the future. However, its influence on phytoplankton community composition remains an open question. The Antarctic Peninsula fjords offer an ideal system to understand the effect of ice-ocean forcing on phytoplankton community, providing an extreme in the spatial gradient from the glacio-marine boundary to the Western Antarctic Peninsula (WAP) continental shelf. During two cruises conducted in December 2015 and April 2016 in Andvord Bay, we found that glacial meltwater input altered surface salinity, promoting shallow mixed layers, and enriched surface waters in dissolved iron and nitrate. The three major groups of phytoplankton fueled by glacial input were: cryptophytes, diatoms, and a group of unidentified small flagellates. Prasinophytes and dinoflagellates were also present, in lower concentrations. In December, cryptophytes dominated the phytoplankton community and were correlated with relatively warmer temperatures in the surface layer; in addition, contrary to our hypothesis, no diatom bloom was observed in the fjord in spite of dissolved iron concentration >1 nM. By April, after the growth season, the overall phytoplankton abundance had decreased by an order of magnitude. Phytoplankton, in particular diatoms, were then limited by daytime length despite abundant macro-nutrient and iron concentrations. Mixed flagellates emerged as the dominant group during April due to the decline of other major taxa. Deep-learning algorithms for predicting the abundance of each major phytoplankton group captured the effects of these environmental factors on the phytoplankton community. Our results show that the fjord has relatively high phytoplankton biomass combined with high macro- and trace nutrient concentrations when compared to the broader WAP region. Based on this study, we confirm that flagellates can be the dominant taxon in Antarctic nearshore waters and we propose that iron concentration alone is insufficient to predict diatom growth.

Furthermore, marine terminating glaciers in the WAP can enrich surface waters with nitrate even if the main fjord circulation is not driven by glacier meltwater discharge.

3.2. Introduction

Glacial meltwater in the Western Antarctic Peninsula (WAP) has been found to impact phytoplankton abundance both over the shelf and within fjords (Annett et al., 2015) (Dierssen et al., 2002a) (Pan et al., 2019). Glacial meltwater can extend over 100 km offshore over the WAP shelf, and the meltwater plume has been found to impact phytoplankton by altering water column stratification and nearshore turbidity (Dierssen et al., 2002a). Glaciated fjords in the WAP are the source of this glacial meltwater, and phytoplankton abundance in these fjords have been found to positively correlate with meltwater fraction (Pan et al., 2019). The correlation is likely due to replenishment of macro- and micro-nutrients via meltwater processes (Cape et al., 2019b). For instance, glacially modified ocean waters can deliver macro-nutrients (such as nitrate, phosphate, and silicic acid) to a fjord's surface via upwelling along the glacial-marine interface; this process can also entrain dissolved micro-nutrients (i.e. dissolved iron) from depth (Annett et al., 2015) (Cape et al., 2019b) (Höfer et al., 2019). In addition, sub-glacial and sub-marine melting can also release iron into a fjord's water column directly (Hawkings et al., 2014) (Raiswell et al., 2006). These meltwater-driven nutrient replenishment mechanisms in the WAP fjords are also consistent with those found in Greenland. The presence of glaciers in contact with the ocean can be crucial to phytoplankton growth in fjords. For example, in western Greenland, Meire et al. found significantly higher primary production in Godthbsfjord (which has marine-terminating glaciers) when compared to Young Sound (which has land-terminating glaciers) (Cape et al., 2019a) (Meire et al., 2017).

The presence of glacial meltwater can benefit phytoplankton growth through enhanced water column stratification (Dierssen et al., 2002a) (Höfer et al., 2019) (Schloss et al., 2012). A stabilized water column and shallow mixed layer depth, creating favorable light conditions, are important for phytoplankton growth (Mitchell et al., 1991) (Venables et al., 2013). A shallow mixed

layer depth can impact the depth of light penetration into the water column, which in turn limits atmospheric heat input; this leads to warmer sea surface temperature (SST) having profound implications for biogeochemistry and local ecosystems (Dierssen et al., 2002b) (Prézelin et al., 2000) (Schloss et al., 2012) (Vernet et al., 2008). The shoaling of mixed layer depth in the southern WAP has been found to enhance phytoplankton carbon fixation rates, particularly south of Anvers Island (Schofield et al., 2018). However, prolonged water column stratification in coastal WAP can impact vertical mixing and ultimately limit phytoplankton growth over time due to nutrient depletion (Rozema et al., 2017).

Changes in the environment due to meltwater input do not uniformly affect all phytoplankton taxonomic groups. In the WAP, an increase in meltwater input is expected to increase cryptophyte abundance over diatoms which impacts carbon cycling and food web structure (Moline et al., 2004). While iron-enriched glacial meltwater can enhance diatom productivity (Buck et al., 2010), cryptophytes can also thrive in meltwater plumes (Mendes et al., 2013) (Rozema et al., 2017). Cryptophyte abundance over the WAP shelf was found to be loosely dictated by a gradual gradient of salinity from the coast towards open ocean, with highest concentrations at mid-shelf (Garibotti et al., 2005). In the Bransfield Strait, diatom dominance was associated with a deeper upper mixed layer, warmer SST, and higher salinity; while cryptophytes were associated with a shallower upper mixed layer, colder SST, and lower salinity (Mendes et al., 2013). In contrast, cryptophyte abundance in the Gerlache Strait was associated with relatively shallow mixed-layer and warmer temperatures; diatoms and haptophytes in this region were found to associate with deeper mixed layer and colder seawater temperature (Mendes et al., 2018). In summary, all taxonomic groups are found in shallow mixed layers, however, it is unclear what the optimal temperature is for sustaining cryptophytes or diatoms as they bloom in both cold and warm surface waters. These studies indicate that phytoplankton communities in the WAP respond to their ambient environment differently and a more comprehensive study is necessary to elucidate these relationships.

Understanding the influence of environmental conditions on phytoplankton taxonomic composition is critical to our ability to predict fjord ecological dynamics, effecting biogeochemical cycling. It is necessary to quantify and predict the relationship between common Antarctic phytoplankton groups and their ambient environment. In this study, we aim to understand the phytoplankton community composition in an Antarctic fjord, Andvord Bay, and how different environmental variables drive the abundance of each taxonomic group. We hypothesized that 1) diatom is the dominant phytoplankton group in Andvord Bay within both sampling periods due to high iron concentrations, light availability, and shallow mixed layer depth, 2) glacial meltwater enriches the fjord with macro-and trace nutrients which support phytoplankton growth, and 3) cryptophyte abundance is associated with low salinity and high water column temperature.

3.3. Material and Methods

3.3.1. Study Area & Field Program

Sampling and data presented in this study were primarily collected in Andvord Bay, a fjord system in the WAP that is adjacent to Anvers Island and connected to Gerlache Strait (Figure 3.1). Andvord Bay is located on the WAP's Danco Coast and is significantly glaciated; therefore, it is a distinct glacial ice drainage system (Williams et al., 1989). The bay is historically free of sea ice during the summer months (Domack & Williams, 1990). However, physical forcing, such as wind and currents, can temporarily cover the inner fjord with brash ice and icebergs. The geometry of Andvord Bay follows a typical fjord-type embayment. It is approximately 20 km in length and has two inner basins (Inner Basin West at ~64.8918 ^{o}S, 62.5973 ^{o}W, and Inner Basin East at ~64.8731 ^{o}S, 62.4476 ^{o}W). There are several partial and full sills throughout this fjord which contribute to variability in its bathymetry. At the head of the fjord (at ~64.8959 ^{o}S, 62.5397 ^{o}W), there are five glaciers in direct contact with oceanic water; Grubb Glacier and Bagshawe Glacier drain into Inner Basin West, while Arago Glacier, Moser Glacier, and Rudolph Glaicer drain into Inner Basin East. The distance from these glaciers is calculated as the shortest displacement from a single glacial boundary line that encompasses all five glaciers in both inner basins. Ice-

modified water masses are in contact with Gerlache Strait water at the mouth of the fjord situated at ~64.7697 ^{o}S, 62.7717 ^{o}W, approximately 20 km away from the glaciers.

The field program in Andvord Bay was conducted onboard R/V Gould (LMG1510) and RV/IB Palmer (NBP1603) within the FjordEco Program. Sampling on LMG1510 occurred between November 27th – December 20th, 2015, and then between April 4th—April 26th, 2016 on NBP1603, which coincided with late Austral spring and fall, respectively. Daily station sampling and various meridional and zonal transects were conducted in Andvord Bay and Gerlache Strait. At each daily station and during transects, water samples and temperature-salinity-depth data were collected using a Conductivity-Temperature-Depth (CTD) rosette sampler with twenty-four 10-L bottles (Seabird SBE, Sea-Bird Electronics Inc., USA). Mixed layer depth is derived based on water column density. It is determined by the depth of maximum change in the density of the water column, where the pycnocline begins and the mixed layer ends. A detailed description and methods for this calculation has been explained in a concurrent study (Christensen, 2017). Photosynthetically active radiation (PAR) was measured on top of the CTD rosette with a QSP-200L4S PAR radiometer (Biospherical Instruments Inc., USA). Euphotic layer depth was calculated as 1% of surface PAR. Glacial meltwater fraction measurement was calculated based on oxygen isotopic ratio and then interpolated to salinity profiles (Jenkins, 1999) (Jenkins & Jacobs, 2008). A detailed description of FjordEco phytoplankton ecology sampling program has been described previously (Pan et al., 2019).

3.3.2. High Performance Liquid Chromatography

High Performance Liquid Chromatography (HPLC) samples were collected as part of the FjordEco cruises during both December 2015 and April 2016. HPLC is used to obtain information on phytoplankton taxa through pigment analysis. HPLC measurements were collected on board by filtering seawater samples through Whatman GF/Fs under low vacuum, and the samples were immediately frozen at -80°C. The HPLC extraction, pigment sampling and analyses were

conducted at Scripps Institution of Oceanography, University of California San Diego. Each filter was ultrasonicated while held in a 20°C benchtop cooler in a dimly lit room for 10 s. The samples were then extracted in 3 ml of 90% HPLC-grade acetone solution and stored at -20°C for 24 hours. Before injection, the samples were pre-filtered through a 0.45 mm Whatman nylon Puradisk filter. HPLC grade mobile phase eluents followed an established method (Kozlowski et al., 2011) which was based on previous methods (Zapata et al., 2000).

3.3.3. CHEMical TAXonomy (CHEMTAX)

Phytoplankton community composition was determined by using the CHEMical TAXonomy (CHEMTAX) software (Mackey et al., 1996), a program that uses factor analysis and a steepest descent algorithm to determine the best fit to the data with a given input matrix of pigment ratios. Using an iterative process for a given input matrix, the software optimizes the pigment ratios for each group and applies the final ratio to the total chl-a in each sample to determine the proportion of chl-a concentration attributed to each phytoplankton group in the community. For this study, the Microsoft Excel based CHEMTAX 1.95 with ChemtaxHelper V7.1 was used.

Quality of results from HPLC pigment-derived community composition using CHEMTAX is obtained by giving special attention to two aspects in the analysis: 1) the input data quality and 2) the initial input of pigment ratios (Table B. 1). Input data in this project is obtained from a robust dataset that was collected according to a consistent protocol and has been quality-controlled. For initial pigment ratios, we used those developed by established methods (Kozlowski et al., 2011) (Wright et al., 2010) which optimized the ratios for the Southern Ocean (Table B. 1); these ratios compare well with the Southern Ocean average. Furthermore, the inter-annual variability in abundance and relative proportion of each taxon group can be expected to change, but taxon diversity and primary groups' presence are consistent in the WAP region (Garibotti et al., 2003b). Moreover, because CHEMTAX is known to be sensitive to the values in the initial ratio matrix, data was binned by light as described by Kozlowski *et al.* (Kozlowski et al., 2011). First, following

the recommendation of established methods (Latasa, 2007), six sets of ten CHEMTAX runs each were made on the dataset, with the first runs using initial ratio found in Table B. 1 and up to a 75% random error added to the initial ratio values. Each subsequent run applied the output ratio of the previous run as its initial ratio, and the output calculated from the tenth runs were considered final. Kozlowski et al. found this method produced consistent results that graphically converged and were ecologically sound in the context of WAP phytoplankton diversity (Garibotti et al., 2003b) (Garibotti et al., 2003a). Furthermore, the CHEMTAX results were independently verified with microscopy cell count (Figure B. 1). Phytoplankton community data in this study are presented as both absolute pigment concentration in unit of µg/l as well as relative abundance. Relative abundance is calculated as each discrete sample's taxon-specific chl-a normalized by that sample's total chl-a concentration.

Here, the terms "community composition" and "taxonomic composition" refer to the phytoplankton community structure characterized by the five taxonomic groups detected by HPLC/CHEMTAX analyses. We used term "taxa" or "taxonomic group" defined as "a taxonomic group of any rank, such as a species, family, or class" (Oxford Online Dictionary, 2020) referring to taxonomic class in this context. Prior studies using CHEMTAX referred to this classification as both "community composition/structure" (Everitt et al., 1990) (Wright et al., 2010) and "taxonomic composition" (Lewitus et al., 2005).

3.3.4. Macro- & Trace Nutrients

Macronutrient samples were collected in acid-washed polypropylene tubes that were rinsed three times with sample seawater before collection. All samples were unfiltered, kept refrigerated in the dark, and were analyzed within 12 hours of collection. Dissolved ortho-phosphate, nitrite, nitrate plus nitrite (N+N), ammonium, and silicic acid were measured using a Lachat QuikChem 8000 flow injection analysis system (Hach Instruments) using modified standard wet-chemistry methods (Gordon et al., 1993). Nitrate concentration was derived by subtracting nitrite from the N+N value. Nitrate anomaly was calculated based on comparison

between each discrete sample in the fjord and that in the Gerlache Strait within the same isopycnal layer. The Gerlache Strait reference values are specific to December 2015 and April 2016 respectively. A more detailed description of the macro-nutrient sampling and analyses from this study can be found in analysis by (Ekern, 2017).

All samples for dissolved iron were collected with trace metal clean 10 L GO Flo bottles (General Oceanics) deployed from an Amsteel line and triggered with custom Teflon messengers. Samples were filtered through 0.2 µm Acropak 200 capsule filters (VWR International) into acid-washed (trace metal grade nitric and hydrochloric acid, Fisher Scientific) low-density polyethylene bottles (Nalgene) under HEPA filtered air in a trace metal clean shipboard bubble. Samples were acidified to between pH 1.7 and 1.8 using HCl (optima grade). Dissolved iron in the resulting samples was oxidized to iron(III) for 1 h with 10 mM Q-H2O2, buffered in-line with ammonium acetate to pH ~3.5 and selectively pre-concentrated on a chelating column. Dissolved iron was eluted from the column using 0.14 M HCl (optima grade) and measured by chemiluminescence using flow-injection analysis (FIA). The methods used were similarly described by King and Barbeau (King & Barbeau, 2007) (King & Barbeau, 2011) and adapted from Lohan et al. (Lohan et al., 2006).

3.3.5. Daylight Length

Daylight length was calculated as a function of year-date and latitude (Forsythe et al., 1995).

$$\mathrm{D} = 24 - \left(\frac{24}{\pi}\right) * \mathrm{acos}\left(\frac{\sin\left(\frac{0.8333\ \pi}{180}\right) + \sin\left(\frac{\mathrm{L} *\ \pi}{180}\right) * \sin(\mathrm{P})}{\cos\left(\frac{\mathrm{L} *\ \pi}{180}\right) * \cos(\mathrm{P})}\right) \quad (1)$$

where D is the daylight length in units of hours, L is latitude in degrees, and P is a constant for each year-date where J is the day of the year (year-date):

$$P = \text{asin}\,[0.39795 * \cos(0.2163108 + 2 * \text{a}\tan\{0.9671396 * \tan[0.00860(J - 186)]\})] \quad (2)$$

3.3.6 Predictive Modeling

The impact of environmental factors and their influence on an individual taxonomic abundance were analyzed and predicted through machine learning techniques. The modeling and analysis were conducted with the Scikit Learn and H2O packages (3.20.0.8, H2O.ai. Repository at github.com/h2oai/h2o-3) in a Python 3 environment. We used the H2O's AutoML feature to automate a machine learning workflow, which includes automatic training and tuning of many deep-learning models within a user-specified time limit. Stacked ensembles were automatically trained on collections of individual models to produce highly predictive ensemble models. We used 80% of the data randomly selected from the dataset to train these machine learning algorithms (training data) and then used the remaining 20% to test the trained models (test data). The model performances were then ranked in the AutoML Leaderboard. Finally, the algorithm with the highest prediction power, based on root mean square error (RMSE) and coefficient of determination (R^2), was selected as the model for predicting a specific taxonomic abundance based on environmental factors. RMSE and R^2 values were generated based on the validation of model-predicted values by the test data (randomly selected 20% of the total dataset). Water column temperature, salinity, mixed layer depth, meltwater fraction, PAR, euphotic layer, nitrate, phosphate, silicic acid, and bathymetry were the input variables to each model. Dissolved iron concentration was not included in the input due to its limited data availability which would greatly restrict the size of the input datasets. The model output was used to understand how these environmental conditions influence each group's abundance. This was done by ranking the percentage of variance in each phytoplankton group explained by each environmental variable. Further analysis was conducted by examining the partial dependence plots which depict the response of modeled phytoplankton abundance to changes in the value of environmental factors.

3.4. Results

3.4.1. Spatial and Temporal Distributions

Using the CHEMTAX software, we were able to detect the presence of five major phytoplankton taxonomic groups in Andvord Bay: cryptophytes, diatoms, unidentified small photoflagellates, prasinophytes, and pigmented dinoflagellates. Between December 2015 and April 2016, there was an overall decline in chl-a concentrations of all five phytoplankton taxonomic groups. During December 2015, most cryptophytes were found in the inner basins (Figure 3.2a) while most diatoms were found at the fjord's mouth and in the outer basins (Figure 3.2b). Unidentified small phytoflagellates of various taxa ("mixed flagellates" hereafter) were found to be most abundant in inner basin (Figure 3.2c). Prasinophytes were more evenly distributed throughout the entire fjord with aggregates in the middle basin and outer basin (Figure 3.2d, Table 3.1). During April 2016, cryptophytes became more evenly distributed throughout the fjord, but their maximum chl-a values remained in the inner basins (Figure 3.2f). Diatoms became more abundant within the fjord, and their maximum value was found over a sill (Figure 3.2b, Table 3.1). Mixed flagellates also became more evenly distributed in the fjord when compared to December 2015 (Figure 3.2c). Prasinophytes appeared to decline both in its chl-a concentration and spatial extent (Figure 3.2d, Table 3.1). Pigmented dinoflagellates were the least significant group during both December and April. Their chl-a concentrations are found to be several orders of magnitude lower than those of other taxonomic groups (Figure 3.2e, 3.2j, Table 3.1). However, CHEMTAX detection of phytoplankton groups is based on chl-a content, and it cannot identify heterotrophic and non-pigmented dinoflagellates (Mascioni et al., 2019), hence the discrepancies between CHEMTAX classification and microscopy verification for this group (Figure B. 1).

When taxon-specific chl-a concentration is summed over each sampling period, cryptophytes dominated the phytoplankton community during December 2015 (67.7%, Figure 3.3a), while diatoms and mixed flagellates had similar relative abundances during this period (12.9% and 14.2% respectively). However, during April 2016, mixed flagellates became the majority of the community (38.3%, Figure 3.3a); while the relative abundance of cryptophytes

decreased in comparison to December of the previous year. The relative abundance of cryptophytes is similar to that of mixed flagellates during April (30.5%, Figure 3.3b). The relative abundance of diatoms experienced a moderate increase between the two time periods (Figure 3.3a, 3.3b). Cryptophyte chl-a absolute concentration was also found to correlate with cryptophyte relative abundance (R^2 = 0.64, p-value < 0.0001, n = 187, Figure 3.3c). This correlation between taxon-specific chl-a and relative abundance is also found among diatoms (R^2 = 0.59, p-value < 0.0001, n = 169, Figure 3.3d). However, the correlation is not statistically significant for mixed flagellates (n = 192, Figure 3.3e).

Overall water column temperature declined from December 2015 to April 2016. Salinity also decreased between the two months largely due to fresh glacial meltwater input (Table 3.2; (Pan et al., 2019)). While the range of meltwater fraction remained similar during both time periods, there was more meltwater overall in Andvord Bay during April than in December. More PAR was available during December than April based on light measurements, in addition to overall longer daylengths in December. The light availability between the two months is also reflected in the shallower mean euphotic depth during April in contrast to that of December. Macro-nutrient (nitrate, phosphate, silicic acid) concentrations were relatively high during both time periods, and there was not a significant change from December to April. Highest nutrient concentrations were found within Andvord Bay, mostly in the inner basins or in their proximity (Table 3.2; (Ekern, 2017)).

3.4.2. Predictions by Machine Learning Algorithms

The FjordEco dataset was ingested through the H2O package in a Python environment to train machine learning algorithms. A collection of models from the H2O library was trained and the model with the highest prediction power (based on RMSE and R^2 from test data) was selected from the model leader board. Cryptophyte chl-a concentration was best predicted by a gradient boosting model (RMSE = 0.006, R^2 = 0.97). Diatom, mixed flagellate, and prasinophyte chl-a concentrations were best predicted by H2O deep learning models, their prediction powers are at

RMSE = 0.009, R^2 = 0.89 for diatoms, RMSE = 0.021, R^2 = 0.91 for mixed flagellates, and RMSE = 0.006, R^2 = 0.90 for prasinophytes.

The model output produced a variable importance ranking for each target (phytoplankton taxonomic chl-a). The ten environmental variables were ranked based on percentage of variance within each model explained only by the input variables. The most important variable for cryptophyte chl-a concentration was temperature (explaining 48.38% of the variance) followed by meltwater fraction (11.56%). These first two variables already account for > 50% of the variance in the model (Figure 3.4a). The most important variable for diatoms was nitrate (15.34%), however it requires the first five variables to explain >50% of the model variance (nitrate 15.34%, euphotic depth 11.35%, silicic acid 10.83%, PAR 10.73%, and temperature 10.41%) (Figure 3.4b). Similar to cryptophytes, the most important variable for mixed flagellates was temperature, and four variables are required to explain over 50% of the variance (temperature 17.01%, euphotic depth 12.11%, PAR 12.01%, and nitrate 10.54%) (Figure 3.4c). Similar to diatoms, nitrate was the most important to prasinophytes and the first five variables were required to account for over 50% of the model variance (nitrate 12.99%, silicic acid 11.18%, salinity 10.88%, euphotic depth 10.64%, and phosphate 10.42%) (Figure 3.4d). For the chl-a concentrations of diatoms, mixed flagellates, and prasinophytes, it requires nearly all environmental variables to explain >90% of the model variance, while cryptophyte chl-a concentration only requires the first six variables to account for >90% of the variance (temperature 48.35%, meltwater fraction 11.56%, euphotic depth 11.27%, nitrate 7.86%, salinity 6%, and phosphate 5.13%) (Figure 3.4).

The H2O package generated partial dependence plots for the trained model of each phytoplankton taxonomic group. The partial dependence plots depict the model's resulting taxon-specific chl-a concentrations in response to changes in each environmental variable. Mean responses of taxon-specific chl-a vary by orders of magnitude in response to each environmental variable (Figure 3.5). Notably, cryptophyte chl-a increases significantly at -0.381 ^{o}C, which is similar to mixed flagellate chl-a increasing at -0.393 ^{o}C (Figure 3.5a). Crytophyte chl-a is elevated

between 33.78 and 33.91 PSU, while diatoms and mixed flagellates remain relatively the same in the range of salinities in the fjord. Prasinophyte chl-a exhibits an overall decrease as salinity increases (Figure 3.5b). Cryptophyte chl-a peaks between 15.47m and 17.16 m mixed layer depths while diatom chl-a and prasinophyte chl-a remain relatively unresponsive to changes in mixed layer depth. Mixed flagellate chl-a also exhibits an overall decrease with increasing mixed layer depth over the entire range of values (Figure 3.5c). Cryptophyte chl-a responds to meltwater fraction when it reaches a concentration of 1.31% in the water column. Diatom chl-a plateaus around 1.39% meltwater and mixed flagellate chl-a exhibit a decline after 1.68% meltwater concentration is reached. Meanwhile, prasinophyte chl-a exhibits an overall increase throughout the entire range of meltwater fraction (Figure 3.5d). Cryptophyte and diatom chl-a increase with underwater PAR until it reaches 121 µmol quanta m^{-2} s^{-1}, while mixed flagellate and prasinophyte chl-a gradually decrease with increasing PAR availability over the same range (Figure 3.5e). As euphotic depth deepens, cryptophyte chl-a exhibits a rapid decreasing trend while the decline of mixed flagellate chl-a is more gradual; diatom chl-a shows a similarly rapid decline as cryptophytes' (Figure 3.5f). Nitrate concentration appears to benefit diatoms the most and their chl-a show an overall increase with increasing nitrate availability, while cryptophyte and mixed flagellate chl-a rapidly decrease after the nitrate reaches ~ 25.87 µM (Figure 3.5g). All three major phytoplankton groups appear to increase with decreasing phosphate concentration, with the exception of a rapid increase in cryptophyte chl-a when phosphate concentration reaches 0.509 uM before the chl-a abruptly drops off (Figure 3.5h). Diatom chl-a increases with silicic acid concentration until it reaches 87.44 uM and then the chl-a begins to decrease. Cryptophyte and mixed flagellate chl-a remain relatively the same and then begin to increase when silicic acid reaches ~87.40 uM where diatom chl-a begins to decrease (Figure 3.5i). Bathymetry appears to have very little effect on diatom and prasinophyte chl-a, but deeper water columns appear to favor cryptophytes; there is also a gradual increase in mixed flagellate chl-a with deeper bathymetry (Figure 3.5j).

3.4.3. Impact of Temperature, Salinity and Nutrients on Phytoplankton Community

As the deep learning models indicate, temperature can account for nearly half of the variance in the cryptophyte model (Figure 3.4). When taxon-specific chl-a concentration is compared to temperature, most discrete samples where cryptophytes dominated coincided with relatively higher temperatures (Figure 3.6a). Cryptophyte abundance increased substantially with temperatures above approximately -0.5 ^{o}C (Figure 3.6b), as captured in the model (Figure 3.4a and Figure 3.5a). Diatoms occupied the same range of temperatures as cryptophytes. Mixed flagellates appear to occupy different temperature ranges than cryptophytes, where their dominance was found in relatively colder temperatures (Figure 3.6a).

In contrast to what we observed with temperature, all three major phytoplankton groups occupied the same salinity range (Figure 3.6a). The deep learning models indicate that cryptophytes correlated with a narrow range of salinity between 33.78 and 33.91 PSU (Figure 3.5b). Diatoms were more dominant at higher salinities while mixed flagellates and prasinophytes were more dominant at lower salinities (Figure 3.5b).

Within the fjord, total chl-a concentrations were correlated with meltwater fraction during both time periods (R^2 = 0.32, p-value < 0.0001, n = 121 for December, and R^2 = 0.49, p-value < 0.0001, n = 97 for April; Figure 3.7b). Low nitrate concentrations were associated with high meltwater and high chl-a concentrations; in this way, nitrate concentration was negatively correlated with meltwater fraction for both December 2015 (R^2 = 0.37 p-value < 0.0001, n = 120) and April 2016 (R^2 = 0.76, p-value < 0.0001, n = 96) (Figure 3.7a). To illustrate that Andvord Bay is enriched in nitrate, we compared waters in the fjord with that of the Gerlache Strait along the same isopycnals. By accounting for phytoplankton growth, we can estimate the remaining nitrate due to physical processes. The fjord water column in December showed negative nitrate anomalies, indicating nitrate drawdown in the water column. In contrast, fjord waters in April had positive anomalies, i.e. the waters were enriched in nitrate relative to outside waters (Figure 3.7c) – hence the difference approximates nitrate enrichment in the fjord. Although not included in the

deep learning models, we present dissolved iron concentrations to better understand the impact of nutrients on phytoplankton. In Andvord Bay, dissolved iron concentration was inversely correlated with meltwater fraction during December (R^2 = 0.48, p-value < 0.0001, n = 32) when iron concentrations were lower, but showed no correlation during April (n = 17) when iron concentration are relatively higher (Forsch et al., 2018).

In Andvord Bay, water column nitrate plays a more significant role in phytoplankton ecology than other macro-nutrient availability as identified by the deep learning models' output – nitrate was consistently ranked higher than both phosphate and silicic acid (Figure 3.4). To confirm these findings, we examined these macro-nutrient concentrations in more detail. Surface water column nitrate and phosphate concentrations (between 0 and 35 m) are significantly correlated, however this correlation is much weaker with silicic acid (Ekern, 2017). The importance of nitrate at the surface is demonstrated when it is compared to corresponding water column nitrate-to-silicic-acid ratios. The correlation between nitrate and the ratio is much higher than that between silicic acid and the ratio (Ekern, 2017). The importance of nitrate to phytoplankton is further illustrated when surface nitrate concentrations and nitrate:silicic acid ratios are compared to the major phytoplankton group chl-a concentrations – the impact of the ratio is nearly identical to that of nitrate (Figure B. 2a is identical to B. 2d, B. 2b to B. 2e, and B. 2c to B. 2f). Hence, nitrate is a more important macro-nutrient to phytoplankton communities in Andvord Bay confirming the findings by the deep learning models (Figure 3.4). Furthermore, we did not find significant correlation between silicic acid and phytoplankton chl-a concentration of major groups (p-values > 0.05, not shown in figures), thus silicic acid alone cannot explain diatom abundance in Andvord Bay during growth season (Figure B. 2).

In December, high chl-a concentrations in all taxonomic groups coincided with low dissolved iron concentrations, although dissolved iron concentration was never <1 nM (Figure 3.8). In April, lower concentrations in all groups were associated with higher iron concentrations compared to December. A moderate inverse relationship was found between cryptophyte, diatom,

and mixed-flagellate chl-a and dissolved iron concentrations (Figure 3.8). These relationships present two clusters of data points where chl-a concentrations increase when dissolved iron concentrations are between ~2 and 3 nM. There is a second cluster that is associated with low chl-a but high dissolved iron concentration generally > 3 nM. These relationships indicate a non-linear relationship between phytoplankton abundance and dissolved iron concentration. Hence, phytoplankton in Andvord Bay are likely co-limited by trace nutrient availability and other environmental factors.

3.4.4. Day Length and Phytoplankton Community

April coincides with Austral fall season; hence daylight hour decreases rapidly over time throughout this period. We observed a daylight loss of approximately 2 hours over the 20-day cruise in April. Total chlorophyll decreased over time as day length gradually became shorter (R^2 = 0.10, p-value < 0.0001, n = 178; Figure 3.9a). Over the same time period, cryptophyte relative abundance showed a moderate decrease (R^2 = 0.06, p-value < 0.05, n = 69; Figure 3.9b), while that of diatom decreased significantly (R^2 = 0.20, p-value < 0.0001, n = 69; Figure 3.9c). Over the same time period, mixed flagellate relative abundance increased significantly (R^2 = 0.38, p-value < 0.0001, n = 69; Figure 3.9d).

3.5. Discussion

Both glacial and sea ice meltwater can alter water column salinity and nutrient concentrations(Annett et al., 2015) (Halbach et al., 2019). Sea ice meltwater has been found to contain iron and thus can impact phytoplankton growth not only through increased water column stability but also by nutrient enrichment (Sedwick & DiTullio, 1997). However, fractional sea ice melt contribution in WAP fjords has been found to be relatively small (e.g. < 0.05% in Barilari Bay (Cape et al., 2019b)). During the two cruises conducted in December 2015 and April 2016 in Andvord Bay, the water lens of low salinity and low temperature observed along the glacio-marine interface, was identified as a mixture of glacial ice and deep water from Gerlache Strait suggesting this is glacial meltwater (Pan et al., 2019). Therefore, nutrient enrichment associated with

meltwater within the fjord is attributed to glacial input rather than sea ice (Figure 3.7c) with important implications for phytoplankton ecology (Henley et al., 2018).

In order to understand how glacial meltwater impacts phytoplankton in nearshore waters of Antarctica, we utilized deep-learning models as a novel method to study the impact of environmental variables on phytoplankton communities and guide additional analyses. Deep-learning algorithms demand higher correlation based on a training dataset, which can result in overfitting and do not perform well when they are applied to other datasets (Thessen, 2016). We have taken the approach to randomly group our dataset and used 80% of the data to train each model and tested the model on the remaining 20% (Figure 3.4, Figure 3.5). When a model is overfit, the prediction error is much lower on the training data than the test data; we did not find such scenario with our deep-learning algorithms (see section 3.2). The reported correlation coefficients (R^2) between the predicted and measured values were relatively high, and they were based on applying each trained model to the test datasets (see section 3.2).

This study focuses on understanding how abiotic environmental factors impact phytoplankton ecology in Andvord Bay. However, during both December 2015 and April 2016, we observed krill populations (*Euphausia superba*) and therefore recognize the potential importance of grazing pressure in our study site. Previous studies have attributed the high megafauna presence in WAP fjords to this abundant krill population and high primary production (Grange & Smith, 2013) (Smith et al., 2006), highlighting the important of krill to fjord's food web (Walsh et al., 2001). However, in this study, we focus on the abiotic factors and their impact on phytoplankton community composition, as future changes in the WAP have a first-order effect on environmental factors directly influencing phytoplankton.

3.4.1. Spatial and temporal variations in phytoplankton community composition

For our analysis, we primarily focus on cryptophytes, diatoms, and mixed flagellates, because they were the dominant groups in Andvord Bay (Figure 3.3). Initially, we expected to find a persistent diatom dominance in Andvord Bay, earlier identified as a major phytoplankton group

over the WAP and within fjords that has a strong influence on nutrient cycling and food web dynamics (Garibotti et al., 2003a) (Höfer et al., 2019) (Schloss et al., 2014). However, during our study period, we did not find such persistent diatom dominance in Andvord Bay. Rather, in December 2015, the fjord was dominated by cryptophytes (Figure 3.3a), while mixed flagellates and cryptophytes exhibited co-dominance in April 2016 (Figure 3.3b). There was also a distinct spatial distribution of each phytoplankton group identified in this study (Figure 3.2). Most cryptophytes and mixed flagellates were found within Andvord Bay, primarily aggregating in the inner basins (Figure 3.2a, c), while diatoms were found at the mouth of the fjord and in Gerlache Strait (Figure 3.2b). The high chl-a concentration near the fjord's mouth is likely due to accumulation along a front feature (Lundesgaard et al., 2019b). Concurrent physical oceanography studies in Andvord Bay, utilizing an idealized model simulation, found that katabatic wind events can create eddies within the fjord ~10 days after a wind event (Lundesgaard et al., 2019a). The positions of these eddies are similar to the high cryptophyte-, mixed-flagellate- and prasinophyte-chl-a concentrations found in the middle basin approximately 5 to 10 km from the glaciers (Figure 3.2a, c, d). The spatial pattern remained for cryptophytes and mixed flagellates during April 2016. In contrast, diatoms shifted from the front at the fjord's mouth to within the fjord during this period (Figure 3.2g); this is attributed to more optimal nutrient conditions within the fjord (Table 3.2). Mixed flagellates also appear to be more evenly distributed throughout the fjord in April as they began to exhibit their community dominance throughout the entire study area (Figure 3.2h).

The community dominance of mixed flagellate in April is exhibited primarily through an increase in relative abundance between the two study periods (Figure 3.3a, b); however, this increase was not due to mixed flagellate increase in absolute concentration (Figure 3.3e), but rather, due to the decline of other major groups over time (Figure 3.3a,b). This suggests a standing stock of mixed flagellates was always present in Andvord Bay that persisted regardless of seasonal succession of other phytoplankton groups with a decrease in concentration by a factor

of 3, from 0.130 to 0.045 µg/l chl-a (Figure 3.2c, h, and Table 3.1), compared to more than an order of magnitude decline in cryptophytes and diatoms (Figure 3.2a, b, f, g, and Table 3.1). Some mixed flagellates and cryptophytes are known to survive austral winter in Antarctica (Laybourn-Parry et al., 2005) (McKnight et al., 2000). This is attributed to their abilities to decrease respiration of their stored carbohydrate at low temperatures in the dark as demonstrated by studies under laboratory setting (Morgan & Kalff, 1975).

The seasonal succession of phytoplankton communities in Andvord Bay did not closely follow the classic model in the WAP of an early diatom bloom in relation to sea ice melt in the spring (Garibotti et al., 2003b) (Kim et al., 2016) as observed elsewhere in Antarctica (Deppeler & Davidson, 2017) (Petrou et al., 2016). In contrast, an abundant cryptophyte population was present during late spring (Figure 3.2a, Figure 3.3a). When coupling our observations with data gathered by a benthic camera system situated in Andvord Bay's middle basin over the entire growth season, it appeared that a massive diatom bloom occurred in January, likely an order of magnitude greater than levels of phytoplankton biomass observed in December. This bloom was observed as a rapid sedimentation event to the seafloor between mid-January and early February 2016, creating a 3-cm layer of marine snow with a dark green coloration, characteristic of a diatom bloom (Smith et al., 2018) (Ziegler et al., 2019). The summer diatom bloom was likely followed by a prasinophyte bloom during early March 2016 (Mascioni et al., 2019). By late March/early April, sediment accumulation rates had slowed down coinciding with the mixed flagellate and cryptophyte dominated surface phytoplankton community in Andvord Bay, with one order of magnitude decreased levels of biomass compared to December (Figure 3.2, Figure 3.3). Thus, the seasonal succession at Andvord Bay follows the general pattern of Antarctic phytoplankton albeit with an absence of a diatom bloom at the beginning of the season and an enriched cryptophyte biomass before and after the January diatom bloom.

Overall, total chl-a concentrations in December are one order of magnitude higher than that in April (Figure 3.7b). In Andvord Bay, cryptophyte chl-a varied between 0.0 and 3.1 µg/l

during December and it occupied over 67.7% of the phytoplankton community, while diatom chl-a varied between 0.0 and 0.6 µg/l and occupied ~13% of the community during the same time period (Figure 3.3, Table 3.1). In April, diatom chl-a was nearly 16% of the total chl-a while cryptophyte declined to 30.3%. In comparison, in the coastal region south of Anvers Island, the most dominant phytoplankton group was diatoms, and cryptophytes were the second most dominant (Henley et al., 2019) (Schofield et al., 2017). The monthly averaged taxon-associated chl-a values between November and February near Palmer Station indicate that cryptophyte chl-a varied between 0 and 0.3 ug/l and mixed flagellate chl-a varied between 0 and 0.2 µg/l. Neither ever exceeded diatom chl-a concentrations which varied between 0.4 and 0.8 µg/l between the four-month period (Schofield et al., 2017). In this way, diatom's chl-a reached 65% of the community total chl-a and cryptophyte's occupied 16% during years with anomalously high total chl-a values, and their relative abundance shifted during years with low total chl-a values where diatoms occupied 52% and cryptophytes occupied 27% (Schofield et al., 2017). Therefore, the spring phytoplankton community from Andvord Bay is enriched in cryptophytes in comparison with more open ocean locations.

3.4.2. Phytoplankton response to temperature

The dominance of cryptophytes during December 2015 in Andvord Bay indicate that they were strongly influenced by water column temperature (Figure 3.4a, Figure 3.6). We found elevated cryptophyte chl-a concentrations when temperature was above -0.5 ^{o}C (Figure 3.6b). This is similar to findings from previous studies in the WAP. Cryptophyte relative abundance increased sharply after air temperature reached above ~0^{o}C (Moline et al., 2004). Later studies in the Gerlache Strait suggested that ocean temperature can increase cryptophyte abundance, and the warming coincided with strong surface stratification and shallow mixed layer depth. In this case, higher cryptophyte concentrations were found after SST exceeded 1^{o}C (Mendes et al., 2018). In contrast, cryptophyte blooms in the Bransfield and off Palmer Station correlate with colder temperatures (Mendes et al., 2013) (Schofield et al., 2017). Differences in response to

temperature could be attributed to interspecific variability between the fjord and other coastal environments as recent studies suggest (Mascioni et al., 2019).

Temperature seems to define ecological niches for different phytoplankton taxa, where the abundant cryptophyte species in WAP fjords occupy a higher temperature niche and their dominance is only present when water column temperature is ≥ -0.5 ^{o}C (Figure 3.6b) while mixed flagellates appear to dominate the community at lower temperatures (Figure 3.6a). These results indicate that below approximately -0.5 ^{o}C is the realized ecological niche in temperature for mixed flagellates in spring/summer, while their fundamental niche can occupy the entire temperature range if competition is absent (De Wit & Bouvier, 2006) (Fenchel & Finlay, 2004). This is illustrated by their continuous presence in the fjord (Figure 3.2c, Figure 3.2h), and their community contribution is only revealed after declines in other groups (Figure 3.3a, Figure 3.3b, Figure 3.3e). In contrast, both the fundamental niche and realized niche for cryptophytes are in relatively warmer temperatures (Figure 3.6). This is demonstrated by the separation of the taxonomic groups by temperature and salinity ranges as well as an increase of cryptophyte chl-a concentration after certain temperature threshold is reached (Figure 3.6). These ecological conditions allowed cryptophytes in Andvord Bay to thrive during December 2015, and then allowed mixed flagellate to become the dominant taxon after the growth season in April 2016.

The effect of water column temperature on cryptophyte abundance was also captured by the deep learning model (Figure 3.4, Figure 3.5). The model predicts an increase in mean response of cryptophyte chl-a concentration after temperature reaches above -0.5 ^{o}C (Figure 3.5a). The relative importance ranking of different environmental variables for each phytoplankton taxon illustrates that temperature alone can explain nearly 50% of the model's variance for cryptophyte abundance (Figure 3.4a); however, no such variable with a disproportionate relative importance is present in other taxon models (Figure 3.4b, c, d). This indicates that changes in temperature alone can substantially influence the cryptophyte model output; while in the other three models, multiple environmental variables need to change simultaneously to induce a similar

change in model output. This means a temperature-driven environment could support cryptophyte dominance over other taxa, and this is what was likely observed during December 2015 prior to the peak growth season in January. While the observed optimal temperature range for cryptophyte in Andvord Bay is slightly different from that of previous study in the Gerlache Strait (Mendes et al., 2018), but within in the range found on the WAP shelf (Schofield et al., 2017) (Moline et al., 2004), the results from this study confirm the influence of relatively higher temperature on cryptophyte abundance.

3.4.3 Phytoplankton response to salinity

Glacial meltwater in isolation has a salinity of approximately 0 PSU (Jenkins, 1999) (Jenkins & Jacobs, 2008). Hence mixing glacial meltwater discharge with oceanic water masses can lower the overall water column salinity in a fjord, especially at the surface (Beaird et al., 2015) (Straneo et al., 2011). In terms of total phytoplankton abundance, the results from Andvord Bay (Figure 3.7b) are similar to those found over the WAP shelf where high chl-a persistently appeared in a relatively fresh surface layer (Dierssen et al., 2002a). However, the effect of salinity on particular taxonomic groups can offer further information (Figure 3.5b). Under laboratory settings, the impact of lower salinity on phytoplankton has also been studied. Experiments with phytoplankton from Potter Cove (a fjord-like embayment on King George Island) found that salinity can significantly impact phytoplankton growth and community structure (Hernando et al., 2015). Low salinity was found to inhibit instantaneous phytoplankton growth rate, carbon biomass accumulation, and reduced chl-a concentrations. These changes also coincided with a gradual replacement of big centric diatoms by small pennate diatoms. This indicates that phytoplankton response to low salinity is species-specific (Hernando et al., 2015). A lower diatom biomass induced by decreased salinity is in agreement with our observations of small diatoms being more abundant in April than in December, a time of higher meltwater (2.1% and 1.5% respectively) (Mascioni et al., 2019) (Pan et al., 2019).

Cryptophytes in the WAP have previously been found in relatively lower salinity waters (≤ ~33.6 PSU) (Moline et al., 2004). Similarly, off Anvers Island, cryptophyte populations were typically found between 32.5 and 33.75 PSU (Schofield et al., 2017). The salinity range for cryptophytes in Andvord Bay was from 33.5 to 34.4 PSU (Figure 3.6a). Results from the deep learning model indicate that salinity changes do not have a linear effect on cryptophyte abundance, rather cryptophytes appeared to thrive in an optimal salinity range (Figure 3.5b). Thus, as more meltwater may be released into the WAP (Meredith et al., 2010), we cannot predict cryptophyte abundance will continuously increase as meltwater discharge increases. These interpretations agree with observations in the WAP shelf waters where cryptophytes were not consistently found in low salinity waters, but rather they exhibited spatial patchiness (Garibotti et al., 2003a). This highlights that low salinity is necessary but not sufficient to explain cryptophyte bloom, which was likely based on a combined effect of multiple environmental factors.

3.4.4. Phytoplankton response to nutrients

The mean surface (≤35 m) nitrate concentrations in Andvord Bay were 28.55 μM in December and 25.10 μM in April. The minimum nitrate concentration detected in the fjord throughout our entire study period was 20.18 uM at the surface (Table 3.2). These nitrate values are higher than those found in other WAP embayments. In the surface of Ryder Bay (15 m), monthly mean values for five growth seasons was ~9.2 μM in late summer and ~20 μM in winter. It typically ranged from 0.13 to 8.2 μM as a summer minima and 15 to 34 μM in winter (Annett et al., 2015) (Henley et al., 2018). Interestingly, Andvord Bay values are comparable to subsurface concentrations at two regions over the WAP shelf that have been identified to have unique environmental conditions (Bowman et al., 2018). One such region, with a mean nitrate value of 29.81 μM, was widely distributed across the shelf and mostly observed in the middle to lower surface ocean (~30 m depth). Another region, with a mean nitrate value of 27.60 μM, concentrated deeper in the surface ocean (~60 m depth) and in the upper northwestern region of the WAP (Bowman et al., 2018). These comparisons indicate that the surface nitrate concentrations during

our study period were similar to the nitrate concentrations found in relatively deeper waters. Nitrate enrichment in Andvord Bay is most noticeable in April. While there was an observed decline of absolute nitrate concentrations relative to December due to drawdown during the previous growth season (Figure 3.7a), we observed the highest nitrate anomalies in April in Andvord Bay when compared to nitrate concentrations of outside waters (Figure 3.7c). This indicates the fjord is enriched with nitrate, as proposed for Barilari Bay (Cape et al., 2019b).

The contrast between the nitrate anomalies in December and April further suggests that the fjord is enriched in nitrate (Figure 3.7c). The difference in nitrate anomalies occurred between a time of high phytoplankton concentration during December and lower concentration during April (Figure 3.7b). This difference is attributed to nitrate uptake during December and lower uptake during April, hence the accumulated "ambient" nitrate concentration within the fjord when phytoplankton were mostly absent. The difference between the two monthly mean anomalies is ~3.0 μM. To account for this difference in nitrate anomalies, we note that this change within Andvord Bay is comparable to other observations in the Southern Ocean. For instance, the phytoplankton at the initiation of the European Iron Fertilization Experiment (EIFEX) resembles the April abundance in Andvord Bay. The water column nitrate pool decreased by ~ 3.4 μM over a period of 21 days after the stimulated phytoplankton growth (Assmy et al., 2013). This decline in nitrate concentration during EIFEX is similar to the difference in nitrate anomaly in our study site, which supports an increase of one order of magnitude in chl-a. This is similar to the chl-a concentration difference between April and December (Figure 3.7).

Both concurrent in-situ observations and idealized modeling studies using the Regional Ocean Model System (ROMS) have suggested that one pathway to replenish the surface with deep nutrient-rich water is through sporadic katabatic wind events (Ekern, 2017) (Lundesgaard et al., 2019a). One katabatic wind event during our cruise occurred from December 10th to12th 2015 and it drove substantial surface water out of Andvord Bay which was replenished in part via upwelling at the glacier front (Lundesgaard et al., 2019a). While the upwelled water after a wind

event was eventually countered by some downwelling, there was likely a net residual of upwelled nutrient-rich water at the surface (Lundesgaard et al., 2019b). For example, we observed nitrate enrichment during the December wind event (Ekern, 2017). The downwelled nutrient-rich water can then subduct to just below the surface layer (~60 m) which would allow entrainment back to the surface with any deepening of the mixed layer depth (Lundesgaard, 2018). While the rate of vertical nitrate fluxes through the pycnocline in Andvord Bay are unknown, rates of ~ 0.18 ± 0.17 mmol NO_3 m^{-2} d^{-1} with a maximum of 0.56 mmol NO_3 m^{-2} d^{-1} were observed during summer in Marguerite Bay (Henley et al., 2018). Similarly, the mean summer time vertical nitrate flux over the WAP shelf between 1998 and 2007 was about 1.36 ± 1.79 mmol NO_3 m^{-2} d^{-1} (Pedulli et al., 2014). Andvord Bay likely falls within this range: assuming a rate of 0.56 mmol NO_3 m^{-2} d^{-1}, we can expect an input of ~50 mmol NO_3 between the two study periods. This nitrate input from depth would enrich an average mixed layer of 15.7 m with an accumulation of ~3.2 µM nitrate, in the same order of magnitude as the nitrate anomaly difference between the two cruises (Figure 3.7c). Furthermore, the deep learning model identified nitrate as the best predictor of diatoms in Andvord Bay (Figure 3.4b) but nitrate was relatively abundant during both time periods as pointed out earlier. We interpreted this result as either nitrate can directly impact diatoms or nitrate is a proxy for other variables such as dissolved iron – both of which are associated with upwelling which is known to promote Antarctic diatom growth (Smith et al., 2007) (Timmermans et al., 2001) (Boyle, 1998). As neither vertical flux nor dissolved iron were part of the deep learning model, nitrate becomes a proxy for these processes.

While dissolved iron concentrations were not included in the deep learning models due to its limited sample size, concurrent dissolved iron concentrations are available for our study (Forsch et al., 2018). The mean surface dissolved iron concentration in Andvord Bay was >1nM in December and generally >3 nM in April (Figure 3.8). In April, the lack of correlation between dissolved iron concentration and meltwater fraction may be due to a saturation of dissolved iron concentrations in Andvord Bay; this also coincides with low phytoplankton abundance, so it is

also attributed to less phytoplankton uptake (Figure 3.7b). Dissolved iron concentration can reach as high as 8 nM in WAP coastal waters, and tends to decline towards shelf waters with < 0.1 nM iron over the mid-/outer WAP shelf (Annett et al., 2017). WAP fjords have been found to have relatively high dissolved iron concentrations. For instance, in Ryder Bay, dissolved iron concentrations were up to 9.5 nM (Annett et al., 2015). Similarly, in Barilari Bay, the estimated dissolved iron concentration was up to ~6.0 nM (Cape et al., 2019b).

Despite the relatively high concentrations of nitrate and dissolved iron in Andvord Bay, diatoms did not exhibit dominance over the community composition during either sampling period (Figure 3.3). The influence of iron on phytoplankton growth has often been considered in the context of the Southern Ocean because it is a high-nutrient low-chlorophyll region (HNLC), and multiple iron fertilization experiments in this region have demonstrated that iron addition can alleviate iron limitation (Blain et al., 2007) (Boyd et al., 2000). An overall abundance of dissolved iron (> 1nM) was expected to lead to an increase in taxon-specific chl-a concentrations, particularly diatoms. However, no diatom bloom was observed, but the inverse correlations found in all three major phytoplankton groups with dissolved iron, indicate uptake by phytoplankton is a major process for dissolved iron dynamics in surface waters (Figure 3.8). The presence of excess dissolved iron >1 nM suggest other factors beyond dissolved iron are crucial to support diatom growth in fjords. Therefore, despite high absolute concentrations of dissolved iron, we propose it was an insufficient factor to sustain phytoplankton growth, particularly diatoms.

3.4.5. Phytoplankton response to light

In addition to the influence of nutrients in the Southern Ocean, previous analyses have found light availability to be a co-limiting factor for phytoplankton growth (Mitchell et al., 1991). The deep-learning model indicates that light may be an especially important factor for diatom growth as it ranks the euphotic zone depth and PAR as two environmental variables explaining a significant portion of the variance in this model (Figure 3.4b). In our study, we ultimately chose daylight length over PAR as a factor to assess the influence of light on phytoplankton community

(Figure 3.9a). This is because instantaneous PAR measurements on a CTD do not represent an integrated view of the light conditions that the phytoplankton are experiencing. Persisting cloudy sky can dissipate shortly before or occur after a CTD deployment which significantly alters the correlation between PAR and parameters describing phytoplankton growth. Moreover, the research vessel needs to clear a patch of ocean to deploy the CTD instruments. This vessel maneuver can also change the underwater light field due to the removal of brash ice coverage on the surface. However, these factors do not affect the daylight length measurement and so it can allow a more integrated view of the impact of light on phytoplankton (Figure 3.9).

It is well known that light availability is a critical factor in determining phytoplankton growth in the Southern Ocean (Van Oijen et al., 2004) (Sunda & Huntsman, 1997) (Mitchell et al., 1991). The impact of light has been observed both in the open ocean (Boyd et al., 2001) and in coastal waters (Vernet et al., 2012); in particular, decreasing daylength has been found to impact total phytoplankton abundance over the WAP shelf, similar to the light conditions we observed during April in Andvord Bay. Phytoplankton sensitivity to photoinhibition has also been studied in other Antarctic coastal regions, such as the Amundsen Sea; while photoinhibition did not control the relative abundances of *Phaeocystis antarctica* and diatoms, and hence it was not a competitive advantage to either group, light limitation indeed altered each group's absolute concentrations (Alderkamp et al., 2013) similar to the decline in phytoplankton abundance with decreasing light observed elsewhere in Antarctica. The effect of light has likely contributed to the diatom decline in April 2016 as daylight length was substantially reduced over our study period (Figure 3.9c). The decline of diatoms was accompanied by an increase in the relative abundance of mixed flagellates due to the survival of their "standing stock" (Figure 3.3b, Figure 3.9d). Light availability may not entirely explain the decline in phytoplankton community abundance and changes in its composition during April. Other factors, such as grazing, can coincide with reduced daylight length and also contribute to the decrease in phytoplankton abundance (Smetacek et al., 2004).

Nevertheless, daylight length is a distinguishing factor during this time period as polar night would gradually set in after April.

3.4.6 The role of glacial meltwater on phytoplankton

The physical oceanography of Arctic and Greenland fjords reveal that meltwater can be discharged into a fjord through subglacial melting (via the base of glaciers) and submarine melting (along the vertical glacio-marine interface) (Motyka et al., 2003) (Rignot et al., 2010). These meltwaters can reach the fjord's surface by meltwater-driven upwelling at the glacial front (Straneo & Cenedese, 2015); for example, the subglacial discharge plume found in Saqqarliup Fjord in central western Greenland was ~20m in diameter at surface near the glaciers and was visible aerially due to glacial sediments (Mankoff et al., 2016). This upwelling mechanism can drive the overall fjord's circulation (Straneo et al., 2011). While glacial meltwater was present in Andvord Bay (Pan et al., 2019), meltwater discharge was found to be a very weak process (Lundesgaard et al., 2019b), and not sufficient to drive the overall fjord's circulation as in SE Greenland (Straneo et al., 2011) (Straneo & Cenedese, 2015).

However, idealized modeling based on field observations in Andvord Bay indicate that there is likely a pathway for deep meltwater to reach the euphotic layer and promote phytoplankton growth (Figure 3.7b). Such pathway is by surfacing of buoyant meltwater plumes along the glacial terminus at the head of the fjord (Lundesgaard, 2018). In spite of the weakness of meltwater production in Andvord Bay, nutrient enrichments, the surface stratification, higher temperatures, and phytoplankton abundance are enhanced by its presence.

Total chl-a concentrations are associated with higher meltwater fraction and follow a significant positive correlation (Figure 3.7b, Figure 3.10) while nitrate concentrations in spring time follow a significant inverse correlation with meltwater fraction (Figure 3.7a, Figure 3.10). This indicates a drawdown of nitrate by phytoplankton in glacially modified waters. The nutrient enrichment in Andvord Bay is partially a result of glacial meltwater input due to surfacing of buoyant plumes. Iron can also be brought into the euphotic layer via meltwater-driven upwelling

(Annett et al., 2015) (Cape et al., 2019b) and iron enrichment can be expected by any of the processes enriching nitrate at the surface. In addition to enrichment from deep water, iron input can come directly from the meltwater itself. Previous studies have found that iron nanoparticles, both in single particle and aggregate forms, are common in glacial meltwater around the world (Hawkings et al. 2014) (Raiswell et al., 2006). The presence of a sub-surface sediment plume close to the glacier front suggests this additional iron source is present in Andvord Bay (Forsch et al., 2018) (Pan et al., 2019). The effects of iron fertilization by glacial ice have also been shown near free-drifting icebergs in the NW Weddell Sea where dissolved iron concentrations in excess of 1-2 nM, with upward velocity of meltwater, facilitated diatom growth (Vernet et al., 2011); these calved icebergs contained 4 – 600 nM of iron content and have been identified as an iron resource in the Weddell Sea (Lin et al., 2011). Therefore, we speculate that the glacial front is an iron source for phytoplankton in Andvord Bay and likely over the WAP shelf, as glacial meltwater was found to extend several kilometers over the WAP shelf during summer (Dierssen et al., 2002a). The effects of these mechanisms resulted in a lower dissolved iron concentration in December relative to that in April, the latter is a time of expected lower iron uptake due to reduced phytoplankton abundance (Figures 3.7, 3.8, 3.10).

Surface freshening due to glacial meltwater entrainment can lead to increased stratification and stable water columns (Höfer et al., 2019) (Meredith et al., 2008) (Meredith et al., 2010) (Schloss et al., 2012), with shallow mixed layers favoring surface heating that alters phytoplankton community composition (Mendes et al., 2018). It is considered that a mixed layer depth <20 m promotes blooms in this region (Mitchell & Holm-Hansen, 1991). The mean mixed layer depth in Andvord Bay was 14.8 m during December and 16.7 m during April (Table 3.2). We found mixed layer depth ranked lower than most environmental variables in all deep-learning models (Figure 3.4), which indicates that mixed layer depth within Andvord Bay is not an important environmental variable to differentiate abundance of phytoplankton taxa. This is due to the overall shallow mixed layer depths and their low variability within the fjord (Table 3.2).

After katabatic wind events deepen the fjord's mixed layer, idealized models indicate that a sluggish circulation is re-established with the formation of a cyclonic eddy in the middle of the fjord, about 6-10 km away from the glacier front, extending to 100 m depth (Lundesgaard et al., 2019a). This feature, closely coinciding with the cryptophyte bloom (Figure 3.2a), is expected to concentrate phytoplankton cells as well as diminish any water or nutrient exchange. The reduced exchange retained meltwater and facilitated warming of surface waters (Figure 3.4a, Figure 3.6b). This eddy feature coincided with relatively higher surface potential temperature, higher meltwater fraction, and higher total chl-a concentration within the fjord (Pan et al., 2019).

Although it is known that glacial meltwater can alter underwater light field in Andvord Bay, the changes in the light field were negligible to influence phytoplankton growth (Figure 3.4) (Pan et al., 2019). In many Arctic and Greenland fjords where strong meltwater discharge can drive overall circulation in the fjord (Straneo & Cenedese, 2015), turbidity associated can limit light for phytoplankton growth. For example, in Kongsfjorden of Svalbard, subglacial discharge with fine sediments was found to limit light availability for phytoplankton; this was contrasted by bedrock with coarser sediments or locations with lower discharge rates, which were associated with more favorable light conditions that facilitated phytoplankton growth (Halbach et al., 2019). A similar trend has begun to occur in the northern WAP, particularly in relatively shallow embayments. In Potter Cover, there was an increase in total suspended particulate mass between 1991 and 2009 as the glacier retreated inland; this was especially prominent in the inner cove (Schloss et al., 2012). These results suggest that, in the future, if glacier fronts retreat away from the ocean, meltwater could contribute to light limitation of phytoplankton in shallow coastal areas. This process will complicate predictions on how the phytoplankton community will respond to meltwater-based nutrient enrichment that this study describes.

While the dataset in our study represents a snapshot of Andvord Bay, we speculate climate variabilities might have also impacted community composition and abundance. The Southern Annular Mode (SAM) is based on the zonal pressure difference between the latitudes

of 40°S and 65°S, hence SAM index measures the atmospheric masses between the middle and high latitudes of the Southern Hemisphere. Positive values of the SAM index (+SAM) correspond with stronger-than-average westerlies over the mid-high latitudes (50°S – 70°S), weaker westerlies in the mid-latitudes (30°S – 50°S) (Marshall, 2003) and shift the Antarctic Circumpolar Current (ACC) towards the Antarctic continent (Talley, 2011) (Thompson et al., 2011). These process affects the timing of sea-ice retreat and subsequent advance and retreat (Stammerjohn et al., 2008b) which in turn impacts phytoplankton communities and productivity (Vernet et al., 2008). Additionally, the winds associated with SAM can cause upwelling of warm circumpolar deep water (CDW) along the shelf break (Spence et al., 2014) which is linked to basal melt of ice shelves observed in eastern and western Antarctica and in southern WAP fjords (Cape et al., 2019b) (Greene et al., 2017) . SAM is also connected to other climate variabilities such as ENSO events (Pezza et al., 2012) (Fogt & Bromwich, 2006) – strong sea ice and atmospheric responses were found when +SAM coincided with La Niña and -SAM with El Niño (Stammerjohn et al., 2008a) and these climate processes led to variabilities in phytoplankton size structure in the WAP continental shelf (Montes-Hugo et al., 2008). +SAM was present during December 2015 (British Antarctic Survey, retrieved from http://www.nerc-bas.ac.uk/icd/gjma/sam.html) and coincided with the absence of the spring diatom bloom in Andvord Bay (Figure 3.2a). However, due to the temporal limitation of our data, this linkage among phytoplankton community, glacial meltwater discharge, and climate variabilities in fjords remains inconclusive. In the future, cost-effective long-term monitoring of Antarctic glacial fjords will provide more definitive answers to resolve this uncertainty (Cusick et al., 2020).

3.6. Conclusions

We conducted an ecological study during December 2015 and April 2016 in Andvord Bay to understand the phytoplankton taxonomic composition and the impact of multiple environmental variables on this distribution. Our results show that the fjord has high phytoplankton biomass combined with high macro- and trace nutrient concentrations. Contrary to our first hypothesis,

cryptophytes dominated the phytoplankton community in December and their abundance was positively correlated with higher temperatures (Figure 3.10). Diatom abundance was supported by shallow mixed layers; however, we did not find diatom blooms within Andvord Bay associated with high dissolved iron concentrations. Cryptophytes, the dominant taxon in December, were limited by temperatures less than ~ 0^{o}C, meltwater fraction less than ~1.31%, and euphotic layer deeper than ~35 m. In April, towards the end the growth season, both nitrate and dissolved iron concentrations remained high, but the overall phytoplankton abundance decreased by one order of magnitude. We attribute this to a decline in light availability which led to a decrease in both cryptophytes and diatoms. Mixed flagellates appeared to maintain a standing stock during the entire study period, and their relative abundance increased during April as the absolute concentrations of other phytoplankton groups declined. Over the course of the entire study period, total phytoplankton abundance in Andvord Bay showed a positive correlation with glacial meltwater indicating that changes in environmental factors due to the input of this meltwater led to favorable conditions for phytoplankton growth. Surface nitrate concentration can be replenished by episodic katabatic wind events and the resulting upwelling as identified by concurrent studies; additionally, surface enrichment can also occur via diffusion of nitrate-rich subsurface waters into the euphotic layer. While surface dissolved iron can be enriched via the same delivery mechanisms as for nitrate, it can also be directly released into the fjord via glacial meltwater discharge and buoyant plumes along the glacial-marine interface. Glacial meltwater can also induce stratification as the mixed layer is relatively shallow in Andvord Bay. These observations indicate that marine terminating glaciers can enrich surface nutrients and influence phytoplankton community even in fjords where the main circulation is not driven by meltwater discharge. As the WAP environment continues to change in the future, glacial meltwater contribution to the water column will also change and alter the phytoplankton taxonomic composition. This has an important implication for higher trophic levels and adds significant uncertainties to the prediction of regional ecosystem dynamics and biogeochemical cycles.

3.7. Acknowledgements

The authors would like to thank all participating principle investigators and their affiliates during the NSF FjordEco project, Dr. Craig Smith (University of Hawai'i at Manoa), Dr. Mark Merrifield (University of Hawai'i at Manoa), Dr. Brian Powell (University of Hawai'i at Manoa), Dr. Martin Truffer (University of Alaska at Fairbanks), and Dr. Peter Winsor (World Wildlife Fund Arctic). Our sampling efforts also received crucial help from Diana Gutierrez, Angela Klemmedson, and Dr. Lars Thoresen. Invaluable discussions and comments on the manuscript from Dr. Øyvind Lundesgaard (Norwegian Polar Institute), Allison Cusick (Scripps Institution of Oceanography, UCSD), Dr. Rick A. Reynolds (Marine Physical Laboratory, Scripps Institution of Oceanography, UCSD), and anonymous reviewers are acknowledged. The authors would also like to thank the captain and crew of R/V Lawrence M. Gould and RVIB Nathaniel B. Palmer and United States Antarctic Program contractors. This project was supported with funding from the National Science Foundation award PLR -1443705 to Maria Vernet.

Chapter 3, in full, is a manuscript of the material as it appears in Pan, B.J., Vernet, M., Manck, L., Forsch, K., Ekern, L., Mascioni, M., Barbeau, K, Almandoz, G., and Orona, A.J. (2020) Environmental Drivers of Phytoplankton Taxonomic Composition in an Antarctic Fjord. *Progress in Oceanography* 183: 102295. The dissertation author was the primary investigator and first author of this paper.

3.8. Figures and Tables

Table 3.1. The chlorophyll-a concentrations of phytoplankton taxonomic groups in Andvord Bay during December 2015 and April 2016.

December 2015		Depth (m)	Distance from Glaciers (km)	April 2016		Depth (m)	Distance from Glaciers (km)
	Cryptophyte (µg/l)				**Cryptophyte (µg/l)**		
Mean	0.645			Mean	0.034		
Minimum	0.000	14.0	0.3	Minimum	0.003	1.3	1.3
Maximum	3.106	4.5	2.4	Maximum	0.088	6.0	2.6
	Diatom (µg/l)				**Diatom (µg/l)**		
Mean	0.116			Mean	0.008		
Minimum	0.000	1.6	6.2	Minimum	0.000	34.0	4.8
Maximum	0.554	4.0	9.0	Maximum	0.028	9.0	4.8
	Mixed Flagellate (µg/l)				**Mixed Flagellate (µg/l)**		
Mean	0.130			Mean	0.045		
Minimum	0.001	14.0	11.1	Minimum	0.002	34.0	4.8
Maximum	0.422	1.5	2.4	Maximum	0.088	21.0	20.9
	Prasinophyte (µg/l)				**Prasinophyte (µg/l)**		
Mean	0.043			Mean	0.015		
Minimum	0.003	14.0	11.1	Minimum	0.004	34.0	4.8
Maximum	0.137	4.5	20.9	Maximum	0.042	1.2	3.4
	Dinoflagellate (µg/l)				**Dinoflagellate (µg/l)**		
Mean	0.003			Mean	0.002		
Minimum	0.000	10.5	2.4	Minimum	0.000	35.0	1.3
Maximum	0.013	4.5	20.9	Maximum	0.006	4.0	20.9

Table 3.2. Water column physical, hydrographic, and nutrient properties in Andvord Bay during December 2015 and April 2016.

December 2015		Depth (m)	Distance from Glaciers (km)	April 2016		Depth (m)	Distance from Glaciers (km)
	Temperature (Deg C)				**Temperature (Deg C)**		
Mean	−0.54			Mean	−0.35		
Minimum	−1.26	644.0	33.2	Minimum	−1.22	1.0	2.6
Maximum	0.67	150.0	31.8	Maximum	0.23	75.0	25.0
	Salinity (PSU)				**Salinity (PSU)**		
Mean	34.34			Mean	34.09		
Minimum	33.47	1.8	10.9	Minimum	33.49	1.0	2.2
Maximum	34.56	644.0	33.2	Maximum	34.54	683.0	33.1
	Mixed Layer Depth (m)				**Mixed Layer Depth (m)**		
Mean	14.8			Mean	16.7		
Minimum	2.0		11.0	Minimum	1.0		8.7
Maximum	62.0		10.6	Maximum	43.0		33.4
	Meltwater Fraction				**Meltwater Fraction**		
Mean	0.010			Mean	0.011		
Minimum	0.007	644.0	33.2	Minimum	0.001	683.0	33.1
Maximum	0.024	1.8	10.9	Maximum	0.024	1.0	2.2
	PAR (μmol quanta m^2 s^1)				**PAR (μmol quanta m^2 s^1)**		
Mean	30.64			Mean	9.96		
Minimum	0.00	319.0	1.7	Minimum	0.00	357.0	14.9
Maximum	2580.00	0.5	1.7	Maximum	1540.00	0.6	2.9
	Euphotic Depth (m)				**Euphotic Depth (m)**		
Mean	37.7			Mean	19.7		
Minimum	4.0		7.6	Minimum	1.0		33.1
Maximum	117.2		10.6	Maximum	47.0		33.2
	Nitrate (μM)				**Nitrate (μM)**		
Mean	30.858			Mean	28.956		
Minimum	20.177	1.8	10.9	Minimum	21.918	1.2	14.6
Maximum	34.061	120.0	2.5	Maximum	34.101	325.0	2.8
	Phosphate (μM)				**Phosphate (μM)**		
Mean	2.194			Mean	2.151		
Minimum	1.612	1.8	10.9	Minimum	0.679	25.0	8.7
Maximum	2.435	540.0	2.4	Maximum	2.505	375.0	1.9
	Silicic Acid (μM)				**Silicic Acid (μM)**		
Mean	88.851			Mean	88.306		
Minimum	81.345	404.0	23.3	Minimum	79.970	20.0	17.5
Maximum	94.945	150.0	31.8	Maximum	95.997	180.0	5.0

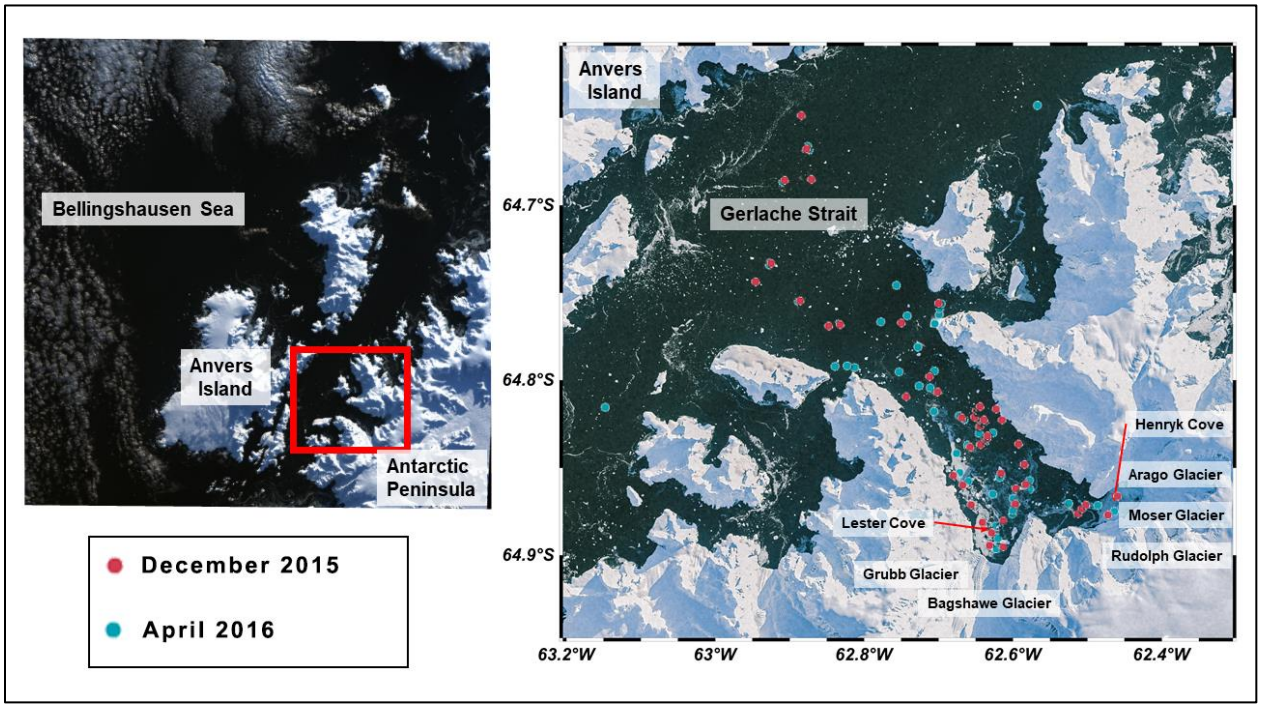

Figure 3.1. Map of the study region, Andvord Bay located on the Western Antarctic Peninsula. The distance from these glaciers in this study is calculated as the shortest displacement from a single glacial boundary line that encompasses all five glaciers in both inner basins. Satellite imagery retrieved from NASA/USGS Landsat 8 Scene ID LC82191052016109LGN00.

Figure 3.2. The cross-section plots of phytoplankton taxonomic groups in Andvord Bay. The figures depict the spatial distribution of individual taxonomic group's chlorophyll-a concentrations. The groups represented are (a & f) cryptophyte, (b & g) diatom, (c & h) mixed flagellate, (d & i) prasinophyte, and (e & j) pigmented dinoflagellate. The chl-a values are depicted as a function of their distance relative to the main glaciers situated in Andvord Bay. The differentiation between bottom topography is due to the slight differences in transect and sampling locations between the two study periods. Left panels: December 2015; right panels: April 2016. The data is not presented on the same scale; scales for each community during both time periods have been adjusted to present community's spatial distribution. Due to the large difference in chl-a concentration among the phytoplankton groups as well as between the two time periods, chl-a concentration scales have been adjusted in each panel to illustrate the spatial distribution of different phytoplankton taxa.

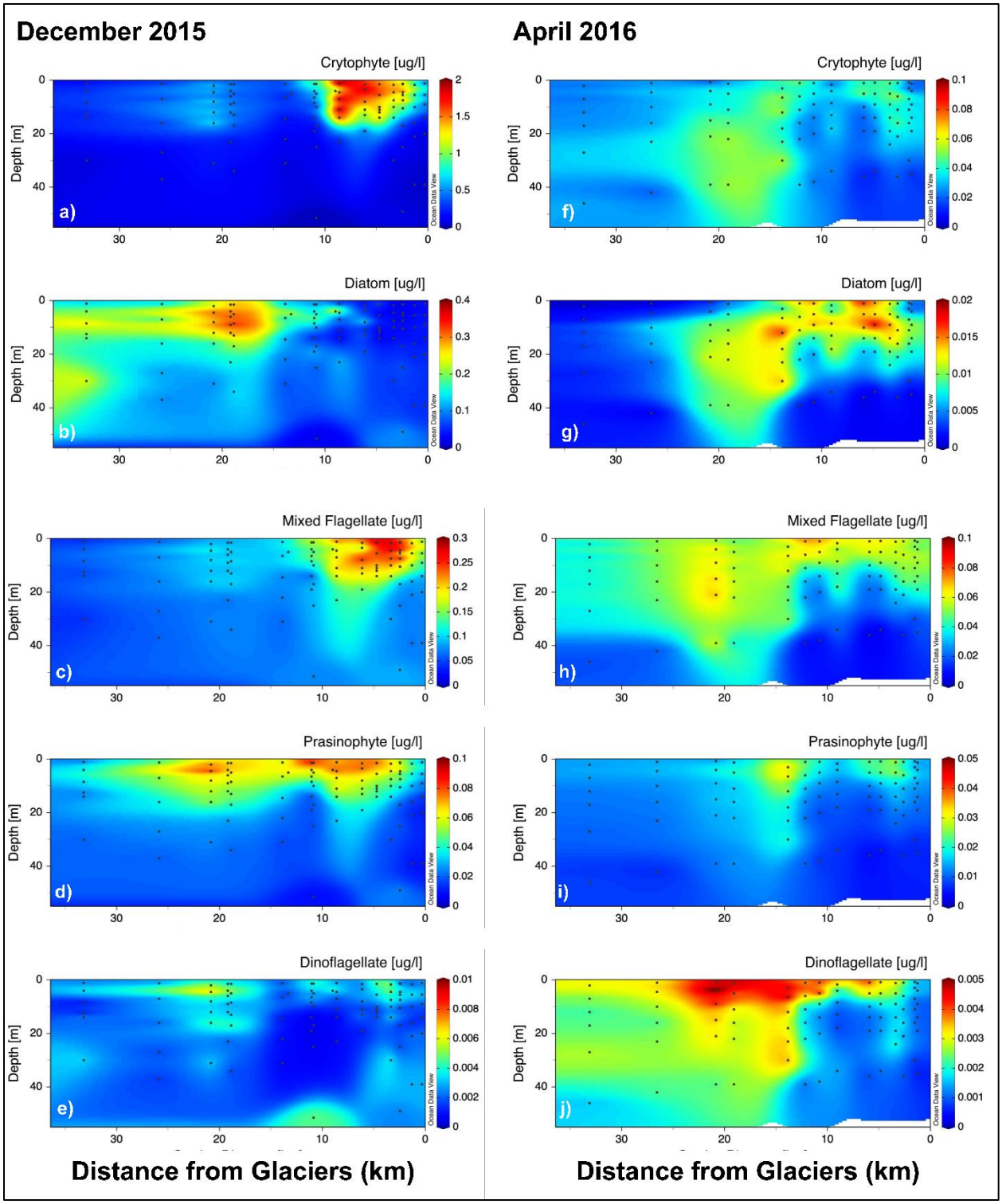
December 2015
April 2016
Crytophyte [ug/l]
Diatom [ug/l]
Mixed Flagellate [ug/l]
Prasinophyte [ug/l]
Dinoflagellate [ug/l]
Depth [m]
Distance from Glaciers (km)
a)
b)
c)
d)
e)
f)
g)
h)
i)
j)

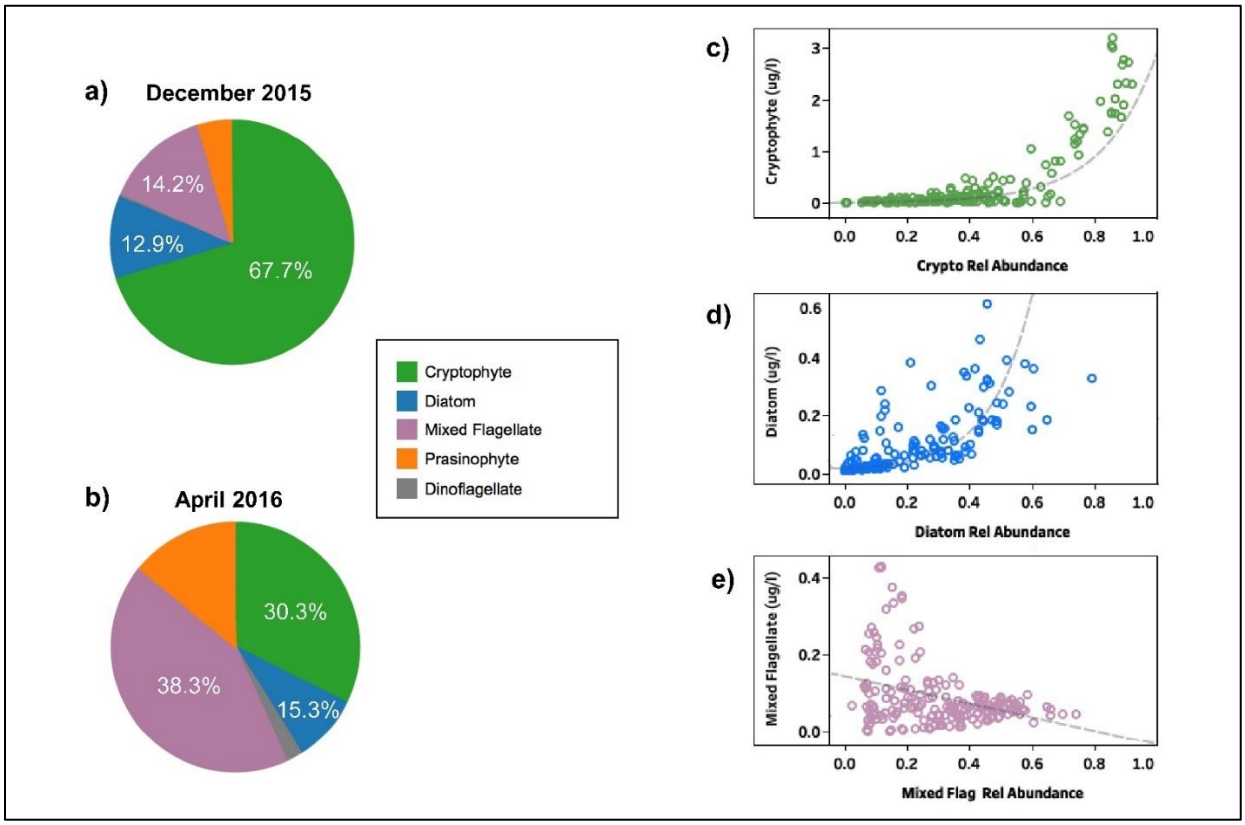

Figure 3.3. Phytoplankton community chl-a concentrations and their relative abundance. (a, b) The absolute chl-a concentration of each taxonomic group is summed and normalized to total chl-a concentration for each sampling period (upper: December 2015, lower: April 2016). (c, d, e) Correlation graphs between absolute chl-a concentration and relative abundance of the three major phytoplankton taxonomic groups in discrete samples.

Figure 3.4. The ranking of environmental variables based on machine learning models to predict chl-a concentration of each phytoplankton group. The bar graph represents the percentage of variance in the model that is explained by each environmental variable; the text over each bar presents the cumulative percentage of explained variance.

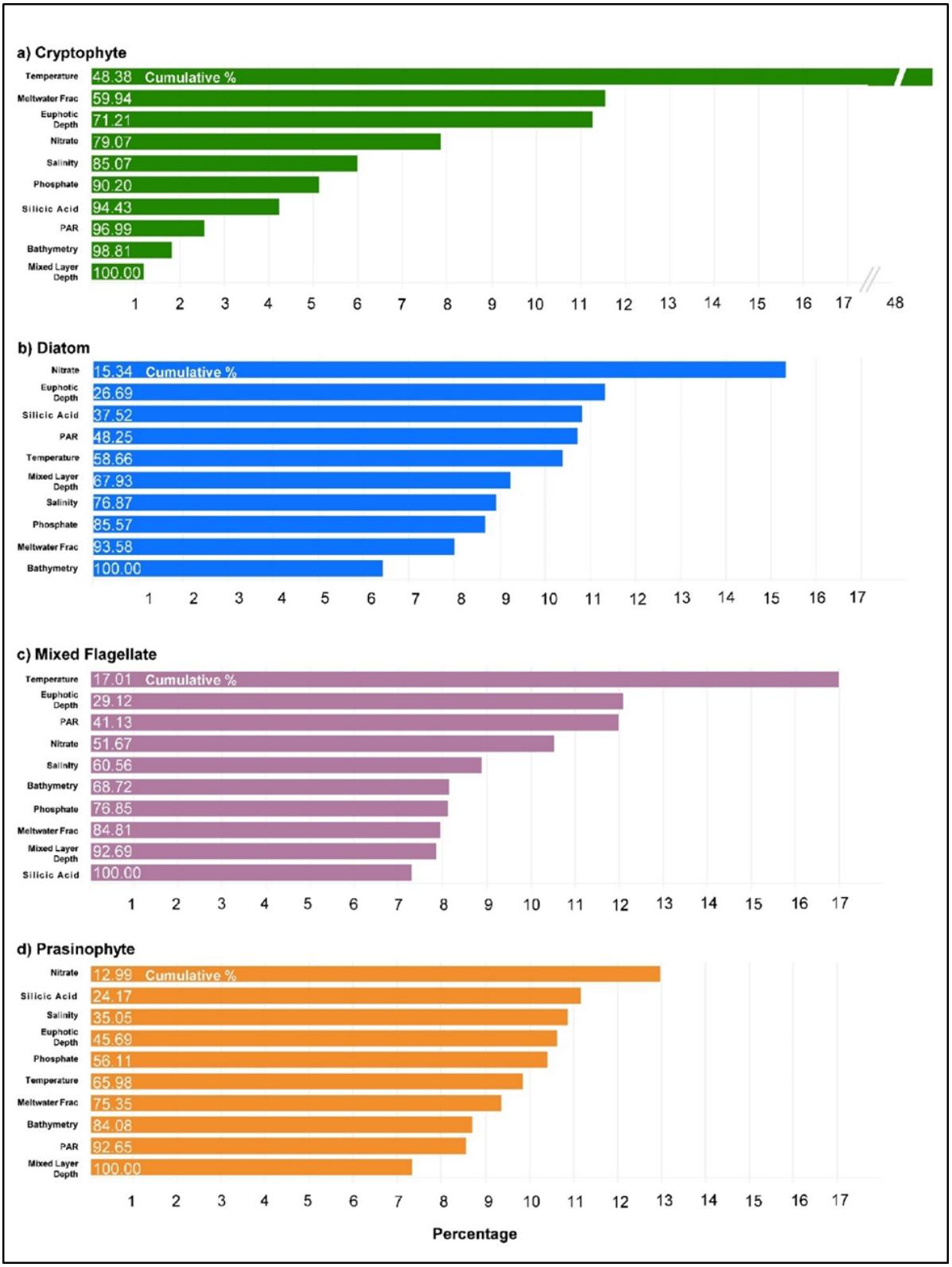
a) Cryptophyte
Temperature 48.38 Cumulative %
Meltwater Frac 59.94
Euphotic Depth 71.21
Nitrate 79.07
Salinity 85.07
Phosphate 90.20
Silicic Acid 94.43
PAR 96.99
Bathymetry 98.81
Mixed Layer Depth 100.00
1 2 3 4 5 6 7 8 9 10 11 12 13 14 15 16 17 48
b) Diatom
Nitrate 15.34 Cumulative %
Euphotic Depth 26.69
Silicic Acid 37.52
PAR 48.25
Temperature 58.66
Mixed Layer Depth 67.93
Salinity 76.87
Phosphate 85.57
Meltwater Frac 93.58
Bathymetry 100.00
1 2 3 4 5 6 7 8 9 10 11 12 13 14 15 16 17
c) Mixed Flagellate
Temperature 17.01 Cumulative %
Euphotic Depth 29.12
PAR 41.13
Nitrate 51.67
Salinity 60.56
Bathymetry 68.72
Phosphate 76.85
Meltwater Frac 84.81
Mixed Layer Depth 92.69
Silicic Acid 100.00
1 2 3 4 5 6 7 8 9 10 11 12 13 14 15 16 17
d) Prasinophyte
Nitrate 12.99 Cumulative %
Silicic Acid 24.17
Salinity 35.05
Euphotic Depth 45.69
Phosphate 56.11
Temperature 65.98
Meltwater Frac 75.35
Bathymetry 84.08
PAR 92.65
Mixed Layer Depth 100.00
1 2 3 4 5 6 7 8 9 10 11 12 13 14 15 16 17
Percentage

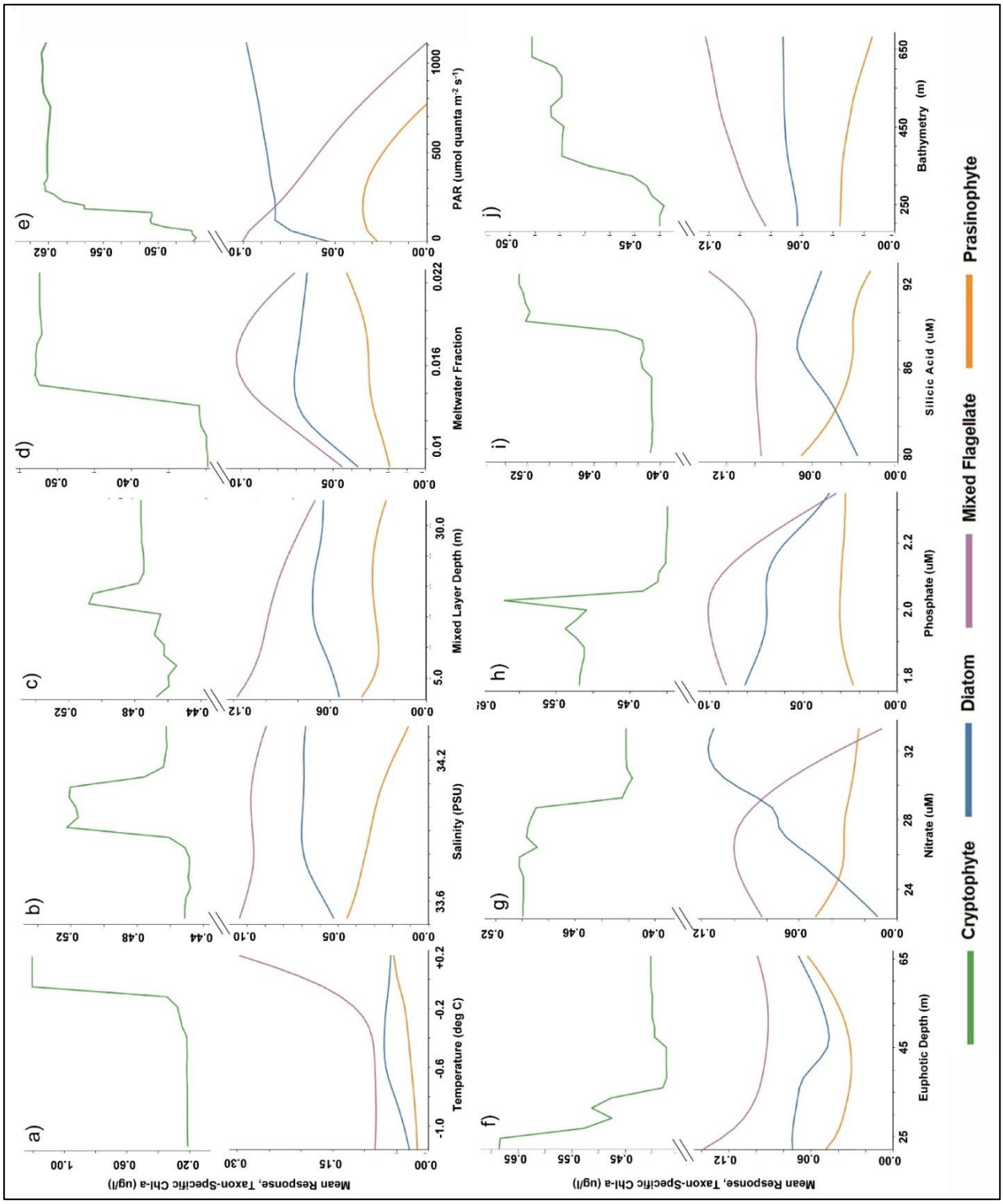

Figure 3.5. Partial dependence plots depicting machine learning models' mean response expressed in targeted taxonomic chl-a. The y-axes represent the models' mean responses in phytoplankton taxon-specific chl-a to changes in values of the environmental variables on x-axes: (a) temperature, (b) salinity, (c) mixed layer depth, (d) meltwater fraction, (e) PAR, (f) euphotic depth, (g) nitrate, (h) phosphate, (i) silicic acid, and (j) bathymetry.

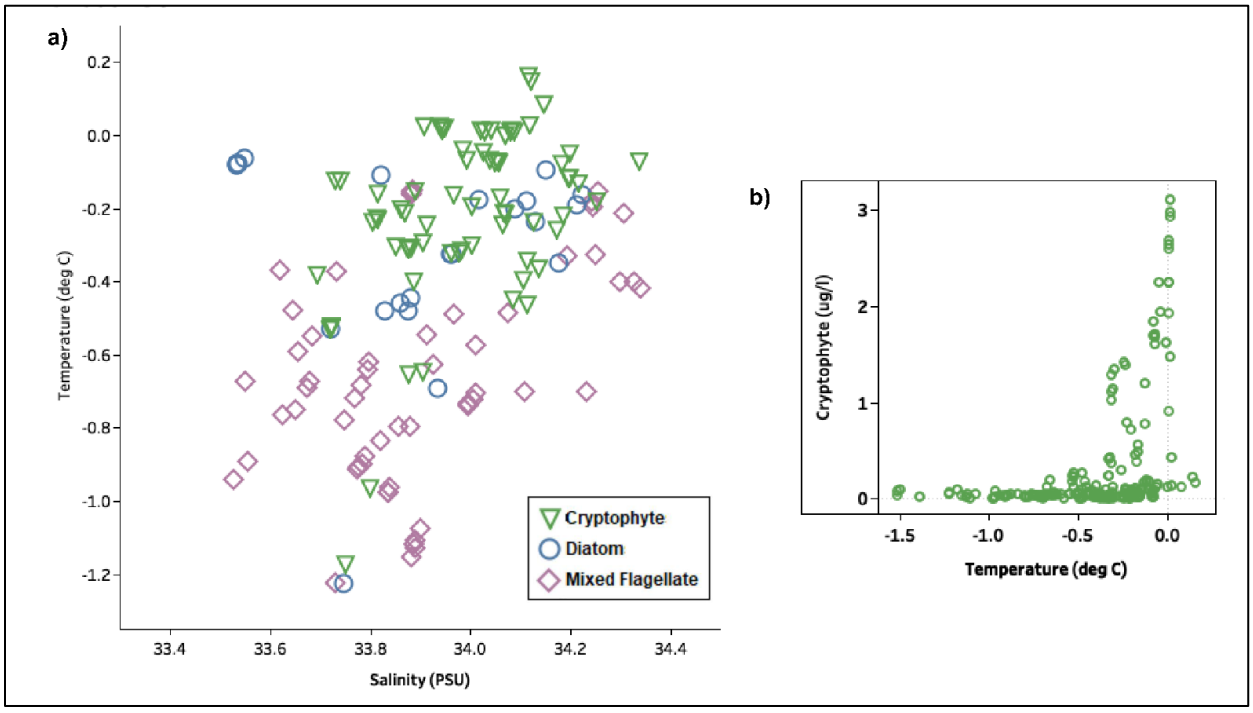

Figure 3.6. Major phytoplankton taxa abundance in a temperature-salinity diagram. (a) The three dominant taxonomic groups, cryptophyte, diatom, and mixed flagellate, are compared to their concurrent temperature and salinity values. Classification of discrete sample points indicate a ≥ 40% contribution to the total phytoplankton chl-a concentration by either cryptophytes, diatoms, or mixed flagellates. (b) Cryptophyte chl-a concentrations compared to their concurrent temperature values.

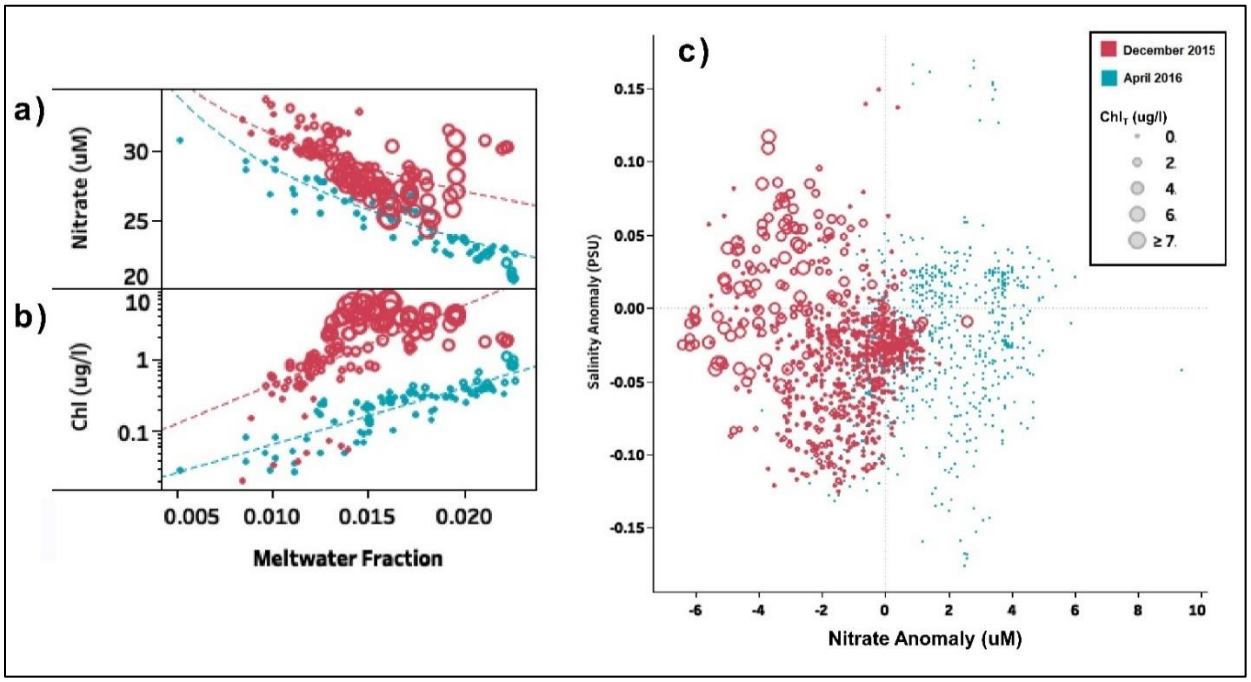

Figure 3.7. Nitrate concentrations and their relationships with meltwater and total chl-a concentration. (a) Nitrate concentration, and (b) total chl-a concentration vs. meltwater fraction with chl-a concentration expressed on a log-scale. c) Salinity anomaly vs. nitrate anomaly. The colors of data points represent December 2015 and April 2016 respectively; the size of circle represents total chl-a concentration of each discrete sample.

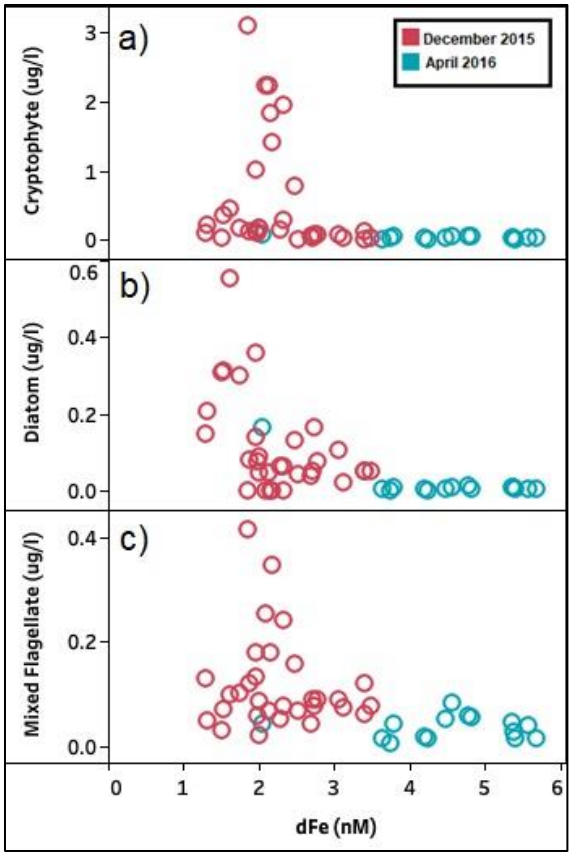

Figure 3.8. Relationship between taxon-specific chl-a and dissolved iron. (a) cryptophyte chl-a and dissolved iron, (b) diatom chl-a and dissolved iron, and (c) mixed-flagellate chl-a and dissolved iron. Color of data points indicate December 2015 and April 2016 respectively.

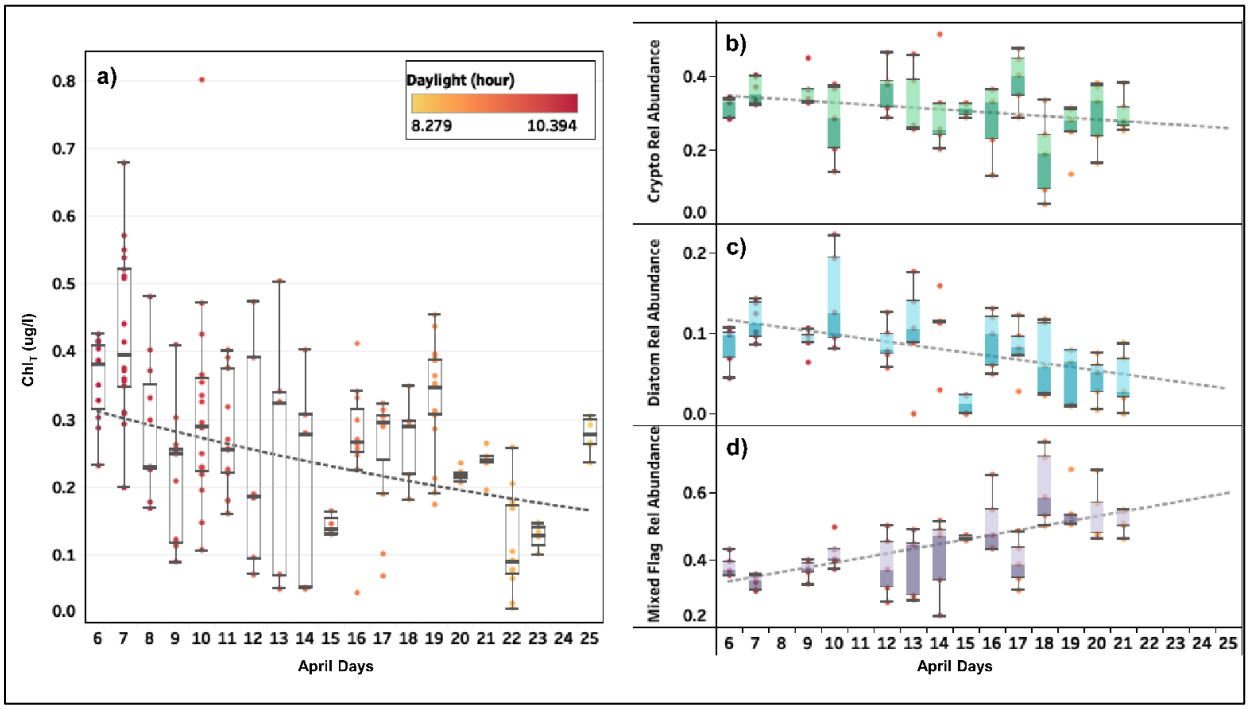

Figure 3.9. The impact of daylight hour on phytoplankton community during April 2016. (a) Total chl-a concentration vs. April days as a box whisker plot; each box represents the range of total chl-a values obtained during that day. The relative abundance of (b) cryptophyte, (c) diatom, and d) mixed flagellate vs. April days. These values represent the conditions of the top 35m within the fjord during April 2016.

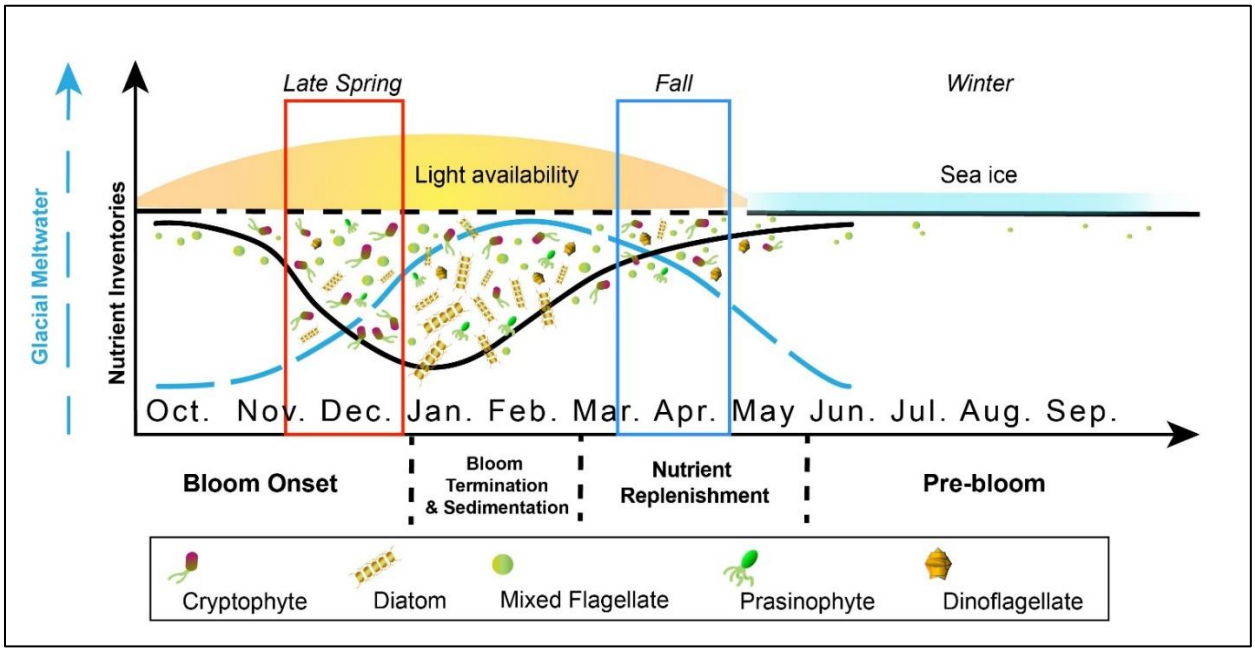

Figure 3.10. Conceptual diagram illustrating bloom phenology of the five major phytoplankton taxonomic groups in Andvord Bay during the 2015—2016 season. Main groups described are: cryptophyte, diatom, mixed flagellate, prasinophyte, and pigmented dinoflagellate. “Bloom onset” occurs during springtime and has high abundance of cryptophytes leading up to the major diatom bloom during summer. “Bloom termination & sedimentation” begins mid-summer according to benthic camera observations and the high quantity of sinking marine snow likely resulted from diatom blooms at the surface (Ziegler et al., 2019) (Smith et al., 2018). “Nutrient replenishment” by glacial meltwater occurs in fall when phytoplankton abundance of all groups declines, followed by “pre-bloom” conditions during winter with high abundance of nutrients and low concentration of phytoplankton. Mixed Flagellates likely maintains a standing stock throughout winter (Figures 3.3, 3.9). Please note that microscopy studies in Andvord Bay have found relatively high abundance of non-pigmented heterotrophic/mixotrophic dinoflagellate present in the fall, hence the discrepancy between HPLC/CHEMTAX-derived and microscopy-based dinoflagellate concentrations (Mascioni et al., 2019; Figure B. 1). In this study, HPLC/CHEMTAX method detected low abundance of pigmented dinoflagellate during both December and April (Figure 3.2, 3.3).

3.9. Appendix

Table B. 1. Pigment:Chl-a ratios used in CHEMTAX analysis of pigment data. Initial ratios before analysis, and optimized ratios as the averaged final ratios for each light bin after analysis. Numbers represent the amount of the given pigment predicted to be present for each unit of chl-a. Abbreviations: Chl, chlorophyll; Peri, peridinin; Fuco, fucoxanthin; Neo, neoxanthin; Pras, prasinoxanthin; 19'-hex, 19'-hexanoyloxyfucoxanthin; Allox, alloxanthin. Pigment ratio data source: cryptophytes, diatoms, mixed flagellates: (Kozlowski et al., 2011), mixed flagellates and prasinophytes: (Wright et al., 2010)**.**

Initial	Chl C3	Chlide-a	Chl C2	Peri	But-fuco	Fuco	Neox	Pras	Hex-fuco	Dino	Allo	Diat	Zea	Lut	Chl-b
Cryptophyte	0.0000	0.0000	0.1740	0.0000	0.0000	0.0000	0.0000	0.0000	0.0000	0.0000	0.2280	0.0000	0.0000	0.0000	0.0000
Diatom	0.0000	0.0000	0.1830	0.0000	0.0000	0.7450	0.0000	0.0000	0.0000	0.0000	0.0000	0.0000	0.0000	0.0000	0.0000
Mixed Flagellate	0.0000	0.0000	0.1260	0.0000	0.1220	0.2900	0.0000	0.0000	0.3150	0.0000	0.0000	0.0000	0.0000	0.0000	0.0000
Prasinophyte	0.0000	0.0000	0.0000	0.0000	0.0000	0.0000	0.0300	0.0970	0.0000	0.0000	0.0000	0.0000	0.0000	0.0060	0.6200
Dinoflagellate	0.0000	0.0000	0.0000	1.0600	0.0000	0.0000	0.0000	0.0000	0.0000	0.0000	0.0000	0.0000	0.0000	0.0000	0.0000
1–5%	Chl C3	Chlide-a	Chl C2	Peri	But-fuco	Fuco	Neox	Pras	Hex-fuco	Dino	Allo	Diat	Zea	Lut	Chl-b
Cryptophyte	0.0000	0.0000	0.0760	0.0000	0.0000	0.0000	0.0000	0.0000	0.0000	0.0000	0.1907	0.0000	0.0000	0.0000	0.0000
Diatom	0.0000	0.0000	0.1487	0.0000	0.0000	0.8910	0.0000	0.0000	0.0000	0.0000	0.0000	0.0000	0.0000	0.0000	0.0000
Mixed Flagellate	0.0000	0.0000	0.0826	0.0000	0.1431	0.3193	0.0000	0.0000	0.2308	0.0000	0.0000	0.0000	0.0000	0.0000	0.0000
Prasinophyte	0.0000	0.0000	0.0000	0.0000	0.0000	0.0000	0.0215	0.0937	0.0000	0.0000	0.0000	0.0000	0.0000	0.0095	0.8233
Dinoflagellate	0.0000	0.0000	0.0000	1.1881	0.0000	0.0000	0.0000	0.0000	0.0000	0.0000	0.0000	0.0000	0.0000	0.0000	0.0000
10–25%	Chl C3	Chlide-a	Chl C2	Peri	But-fuco	Fuco	Neox	Pras	Hex-fuco	Dino	Allo	Diat	Zea	Lut	Chl-b
Cryptophyte	0.0000	0.0000	0.1012	0.0000	0.0000	0.0000	0.0000	0.0000	0.0000	0.0000	0.2458	0.0000	0.0000	0.0000	0.0000
Diatom	0.0000	0.0000	0.1834	0.0000	0.0000	0.7568	0.0000	0.0000	0.0000	0.0000	0.0000	0.0000	0.0000	0.0000	0.0000
Mixed Flagellate	0.0000	0.0000	0.0752	0.0000	0.1381	0.2852	0.0000	0.0000	0.2455	0.0000	0.0000	0.0000	0.0000	0.0000	0.0000
Prasinophyte	0.0000	0.0000	0.0000	0.0000	0.0000	0.0000	0.0218	0.0738	0.0000	0.0000	0.0000	0.0000	0.0000	0.0099	0.6882
Dinoflagellate	0.0000	0.0000	0.0000	1.4135	0.0000	0.0000	0.0000	0.0000	0.0000	0.0000	0.0000	0.0000	0.0000	0.0000	0.0000
50–100%	Chl C3	Chlide-a	Chl C2	Peri	But-fuco	Fuco	Neox	Pras	Hex-fuco	Dino	Allo	Diat	Zea	Lut	Chl-b
Cryptophyte	0.0000	0.0000	0.1209	0.0000	0.0000	0.0000	0.0000	0.0000	0.0000	0.0000	0.3059	0.0000	0.0000	0.0000	0.0000
Diatom	0.0000	0.0000	0.2149	0.0000	0.0000	0.9668	0.0000	0.0000	0.0000	0.0000	0.0000	0.0000	0.0000	0.0000	0.0000
Mixed Flagellate	0.0000	0.0000	0.1330	0.0000	0.1443	0.3874	0.0000	0.0000	0.2712	0.0000	0.0000	0.0000	0.0000	0.0000	0.0000
Prasinophyte	0.0000	0.0000	0.0000	0.0000	0.0000	0.0000	0.0198	0.0650	0.0000	0.0000	0.0000	0.0000	0.0000	0.0074	0.5528
Dinoflagellate	0.0000	0.0000	0.0000	1.0410	0.0000	0.0000	0.0000	0.0000	0.0000	0.0000	0.0000	0.0000	0.0000	0.0000	0.0000

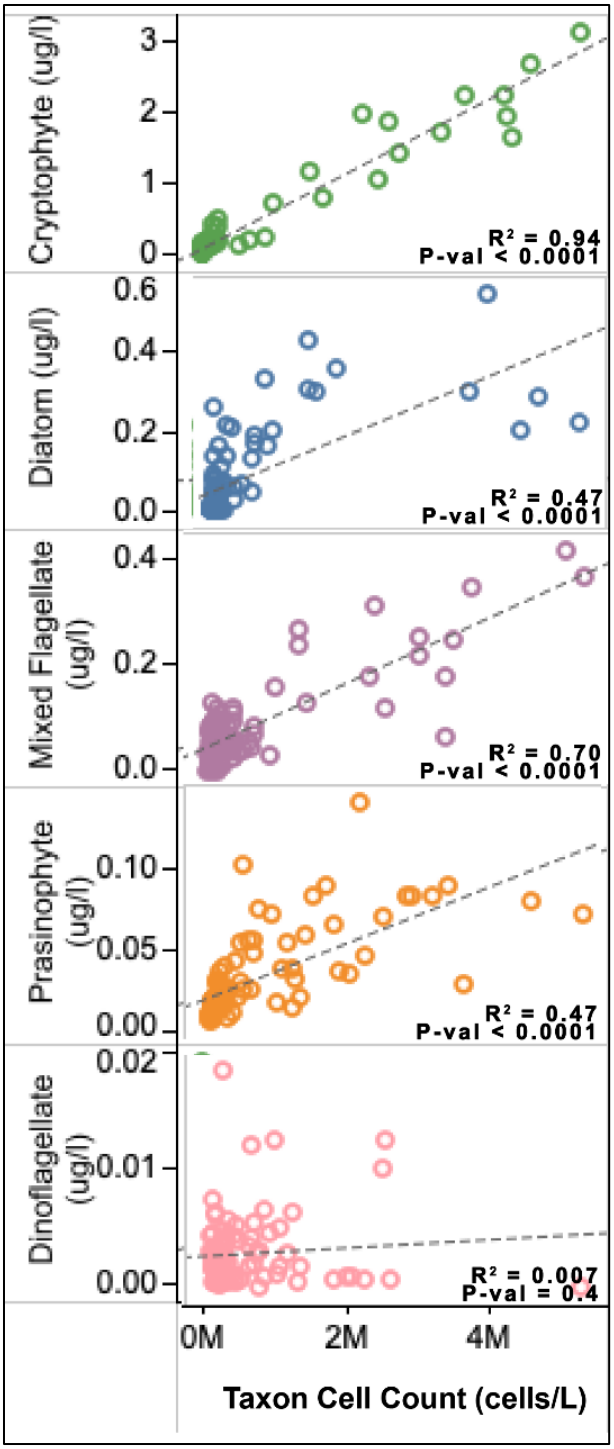

Figure B. 1. CHEMTAX vs. microscopy comparisons. Scatter plots of the microscopic calculations of carbon and cell count attributed to each phytoplankton taxon group (M. Mascioni, National University of La Plata) and CHEMTAX calculations of percentage of total chl-a attributed to each phytoplankton group.

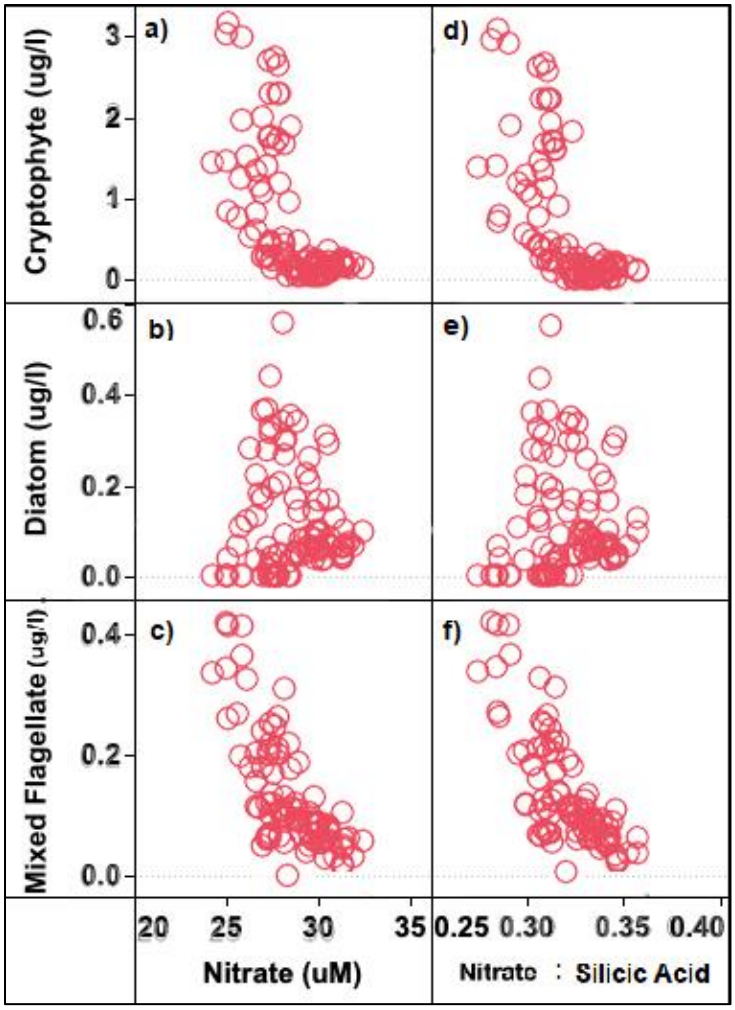

Figure B. 2. Surface (0 – 35 m) water column nitrate concentration in comparison to (a) cryptophyte chl-a concentration (n = 87), (b) diatom chl-a concentration (n = 87), and (c) mixed flagellate chl-a concentration (n = 87). Surface water column nitrate to silicic acid concentration in comparison to (d) cryptophyte chl-a concentration (n = 87), (e) diatom chl-a concentration (n = 87), and (f) mixed flagellate chl-a concentration (n = 87). All data points are from December 2015 –a more productive period in Andvord Bay during our study.

3.10. References

Alderkamp, A.-C., Mills, M.M., van Dijken, G.L., Arrigo, K.R., 2013. Photoacclimation and non-photochemical quenching under in situ irradiance in natural phytoplankton assemblages from the Amundsen Sea, Antarctica. *Marine Ecology Progress Series*, 475, 15-34.

Annett, A.L., Fitzsimmons, J.N., Séguret, M.J., Lagerström, M., Meredith, M.P., Schofield, O., Sherrell, R.M., 2017. Controls on dissolved and particulate iron distributions in surface waters of the Western Antarctic Peninsula shelf. *Marine Chemistry*, 196, 81-97.

Annett, A.L., Skiba, M., Henley, S.F., Venables, H.J., Meredith, M.P., Statham, P.J., Ganeshram, R.S., 2015. Comparative roles of upwelling and glacial iron sources in Ryder Bay, coastal western Antarctic Peninsula. *Marine Chemistry*, 176, 21-33.

Assmy, P., Smetacek, V., Montresor, M., Klaas, C., Henjes, J., Strass, V.H., Arrieta, J.M., Bathmann, U., Berg, G.M., Breitbarth, E., 2013. Thick-shelled, grazer-protected diatoms decouple ocean carbon and silicon cycles in the iron-limited Antarctic Circumpolar Current. *Proceedings of the National Academy of Sciences*, 110, 20633-20638.

Beaird, N., Straneo, F., Jenkins, W., 2015. Spreading of Greenland meltwaters in the ocean revealed by noble gases. *Geophysical Research Letters*, 42, 7705-7713.

Blain, S., Quéguiner, B., Armand, L., Belviso, S., Bombled, B., Bopp, L., Bowie, A., Brunet, C., Brussaard, C., Carlotti, F., 2007. Effect of natural iron fertilization on carbon sequestration in the Southern Ocean. *Nature*, 446, 1070.

Bowman, J.S., Kavanaugh, M.T., Doney, S.C., Ducklow, H.W., 2018. Recurrent seascape units identify key ecological processes along the western Antarctic Peninsula. *Global Change Biology*, 24, 3065-3078.

Boyd, P.W., Crossley, A., DiTullio, G., Griffiths, F., Hutchins, D., Queguiner, B., Sedwick, P.N., Trull, T., 2001. Control of phytoplankton growth by iron supply and irradiance in the subantarctic Southern Ocean: Experimental results from the SAZ Project. *Journal of Geophysical Research: Oceans*, 106, 31573-31583.

Boyd, P.W., Watson, A.J., Law, C.S., Abraham, E.R., Trull, T., Murdoch, R., Bakker, D.C., Bowie, A.R., Buesseler, K., Chang, H., 2000. A mesoscale phytoplankton bloom in the polar Southern Ocean stimulated by iron fertilization. *Nature*, 407, 695.

Boyle, E., 1998. Pumping iron makes thinner diatoms. *Nature*, 393, 733-734.

Buck, K.N., Selph, K.E., Barbeau, K.A., 2010. Iron-binding ligand production and copper speciation in an incubation experiment of Antarctic Peninsula shelf waters from the Bransfield Strait, Southern Ocean. *Marine Chemistry*, 122, 148-159.

Cape, M.R., Straneo, F., Beaird, N., Bundy, R.M., Charette, M.A., 2019a. Nutrient release to oceans from buoyancy-driven upwelling at Greenland tidewater glaciers. *Nature Geoscience*, 12, 34.

Cape, M.R., Vernet, M., Pettit, E.C., Wellner, J.S., Truffer, M., Akie, G., Domack, E., Leventer, A., Smith, C.R., Huber, B.A., 2019b. Circumpolar Deep Water impacts glacial meltwater export and coastal biogeochemical cycling along the west Antarctic Peninsula. *Frontiers in Marine Science*, 6, 144.

Christensen, K., 2017. The Upper Layer Structure and Variability of an Antarctic Glacio-Marine Fjord: Andvord Bay, Western Antarctic Peninsula. *Bachelor of Science Thesis*, University of Hawai'i at Mānoa.

Cusick, A.M., Gilmore, R., Mascioni, M., Almandoz, G.O., Vernet, M., 2020. Polar Tourism as an Effective Research Tool: Citizen Science in the Western Antarctic Peninsula. *Oceanography*.

De Wit, R., Bouvier, T., 2006. 'Everything is everywhere, but, the environment selects'; what did Baas Becking and Beijerinck really say? *Environmental Microbiology*, 8, 755-758.

Deppeler, S.L., Davidson, A.T., 2017. Southern Ocean phytoplankton in a changing climate. *Frontiers in Marine Science*, 4, 40.

Dierssen, H.M., Smith, R.C., Vernet, M., 2002a. Glacial meltwater dynamics in coastal waters west of the Antarctic peninsula. *Proceedings of the National Academy of Sciences*, 99, 1790-1795.

Dierssen, H.M., Smith, R.C., Vernet, M., 2002b. Glacial meltwater dynamics in coastal waters west of the Antarctic peninsula. *Proc Natl Acad Sci U S A*, 99, 1790-1795.

Domack, E., Williams, C., 1990. Fine structure and suspended sediment transport in three Antarctic fjords. *Contributions to Antarctic Research I*, 50, 71-89.

Ekern, L., 2017. Assessing Primary Production via nutrient deficits in Andvord Bay, Antarctica 2015-2016. *Scripps Institution of Oceanography*, Vol. Master's University of California, San Diego.

Everitt, D., Wright, S., Volkman, J., Thomas, D., Lindstrom, E., 1990. Phytoplankton community compositions in the western equatorial Pacific determined from chlorophyll and carotenoid pigment distributions. *Deep Sea Research Part A. Oceanographic Research Papers*, 37, 975-997.

Fenchel, T., Finlay, B.J., 2004. The ubiquity of small species: patterns of local and global diversity. *Bioscience*, 54, 777-784.

Fogt, R.L., Bromwich, D.H., 2006. Decadal variability of the ENSO teleconnection to the high-latitude South Pacific governed by coupling with the southern annular mode. *Journal of Climate*, 19, 979-997.

Forsch, K., Manck, L., Ekern, L., Pan, B.J., Vernet, M., Barbeau, K., 2018. Links Between Sources of Iron and Organic Iron-binding Ligands to the Supply of Cryospheric Iron to Coastal West Antarctic Peninsula. *Ocean Sciences Meeting*. Portland, Oregon.

Forsythe, W.C., Rykiel Jr, E.J., Stahl, R.S., Wu, H.-i., Schoolfield, R.M., 1995. A model comparison for daylength as a function of latitude and day of year. *Ecological Modelling*, 80, 87-95.

Garibotti, I.A., Vernet, M., Ferrario, M.E., 2005. Annually recurrent phytoplanktonic assemblages during summer in the seasonal ice zone west of the Antarctic Peninsula (Southern Ocean). *Deep Sea Research Part I: Oceanographic Research Papers*, 52, 1823-1841.

Garibotti, I.A., Vernet, M., Ferrario, M.E., Smith, R.C., Ross, R.M., Quetin, L.B., 2003a. Phytoplankton spatial distribution patterns along the western Antarctic Peninsula (Southern Ocean). *Marine Ecology Progress Series*, 261, 21-39.

Garibotti, I.A., Vernet, M., Kozlowski, W.A., Ferrario, M.E., 2003b. Composition and biomass of phytoplankton assemblages in coastal Antarctic waters: a comparison of chemotaxonomic and microscopic analyses. *Marine Ecology Progress Series*, 247, 27-42.

Gordon, L.I., Jennings Jr, J.C., Ross, A.A., Krest, J.M., 1993. A suggested protocol for continuous flow automated analysis of seawater nutrients (phosphate, nitrate, nitrite and silicic acid) in the WOCE Hydrographic Program and the Joint Global Ocean Fluxes Study. *WOCE Operations Manual, Part*, 3, 91-91.

Grange, L.J., Smith, C.R., 2013. Megafaunal communities in rapidly warming fjords along the West Antarctic Peninsula: hotspots of abundance and beta diversity. *Plos One*, 8, e77917.

Greene, C.A., Blankenship, D.D., Gwyther, D.E., Silvano, A., van Wijk, E., 2017. Wind causes Totten Ice Shelf melt and acceleration. *Science Advances*, 3, e1701681.

Halbach, L., Assmy, P., Vihtakari, M., Hop, H., Duarte, P., Wold, A., Kauko, H.M., Kristiansen, S., Everett, A., Myhre, P.I., 2019. Tidewater glaciers and bedrock characteristics control the phytoplankton growth environment in an Arctic fjord. *Frontiers in Marine Science*, 6, 254.

Hawkings, J.R., Wadham, J.L., Tranter, M., Raiswell, R., Benning, L.G., Statham, P.J., Tedstone, A., Nienow, P., Lee, K., Telling, J., 2014. Ice sheets as a significant source of highly reactive nanoparticulate iron to the oceans. *Nature Communications*, 5, 3929.

Henley, S.F., Schofield, O.M., Hendry, K.R., Schloss, I.R., Steinberg, D.K., Moffat, C., Peck, L.S., Costa, D.P., Bakker, D.C., Hughes, C., 2019. Variability and change in the west Antarctic Peninsula marine system: research priorities and opportunities. *Progress in Oceanography*.

Henley, S.F., Tuerena, R.E., Annett, A.L., Fallick, A.E., Meredith, M.P., Venables, H.J., Clarke, A., Ganeshram, R.S., 2018. Macronutrient supply, uptake and recycling in the coastal ocean of the west Antarctic Peninsula. *Deep Sea Research Part II: Topical Studies in Oceanography*, 139, 58-76.

Hernando, M., Schloss, I., Malanga, G., Almandoz, G., Ferreyra, G., Aguiar, M., Puntarulo, S., 2015. Effects of salinity changes on coastal Antarctic phytoplankton physiology and assemblage composition. *Journal of Experimental Marine Biology and Ecology*, 466, 110-119.

Höfer, J., Giesecke, R., Hopwood, M.J., Carrera, V., Alarcón, E., González, H.E., 2019. The role of water column stability and wind mixing in the production/export dynamics of two bays in the Western Antarctic Peninsula. *Progress in Oceanography*.

Jenkins, A., 1999. The Impact of Melting Ice on Ocean Waters. *Journal of Physical Oceanography*, 29, 2370-2381.

Jenkins, A., Jacobs, S., 2008. Circulation and melting beneath George VI Ice Shelf, Antarctica. *Journal of Geophysical Research*, 113.

Kim, H., Doney, S.C., Iannuzzi, R.A., Meredith, M.P., Martinson, D.G., Ducklow, H.W., 2016. Climate forcing for dynamics of dissolved inorganic nutrients at Palmer Station, Antarctica: an interdecadal (1993–2013) analysis. *Journal of Geophysical Research: Biogeosciences*, 121, 2369-2389.

King, A.L., Barbeau, K., 2007. Evidence for phytoplankton iron limitation in the southern California Current System. *Marine Ecology Progress Series*, 342, 91-103.

King, A.L., Barbeau, K.A., 2011. Dissolved iron and macronutrient distributions in the southern California Current System. *Journal of Geophysical Research: Oceans*, 116.

Kozlowski, W.A., Deutschman, D., Garibotti, I., Trees, C., Vernet, M., 2011. An evaluation of the application of CHEMTAX to Antarctic coastal pigment data. *Deep Sea Research Part I: Oceanographic Research Papers*, 58, 350-364.

Latasa, M., 2007. Improving estimations of phytoplankton class abundances using CHEMTAX. *Marine Ecology Progress Series*, 329, 13-21.

Laybourn-Parry, J., Marshall, W.A., Marchant, H.J., 2005. Flagellate nutritional versatility as a key to survival in two contrasting Antarctic saline lakes. *Freshwater Biology*, 50, 830-838.

Lewitus, A.J., White, D.L., Tymowski, R.G., Geesey, M.E., Hymel, S.N., Noble, P.A., 2005. Adapting the CHEMTAX method for assessing phytoplankton taxonomic composition in southeastern US estuaries. *Estuaries*, 28, 160-172.

Lin, H., Rauschenberg, S., Hexel, C.R., Shaw, T.J., Twining, B.S., 2011. Free-drifting icebergs as sources of iron to the Weddell Sea. *Deep Sea Research Part II: Topical Studies in Oceanography*, 58, 1392-1406.

Lohan, M.C., Aguilar-Islas, A.M., Bruland, K.W., 2006. Direct determination of iron in acidified (pH 1.7) seawater samples by flow injection analysis with catalytic spectrophotometric detection: Application and intercomparison. *Limnology and Oceanography: Methods*, 4, 164-171.

Lundesgaard, Ø., 2018. Physical Processes in a Western Antarctic Peninsula Fjord. University of Hawai'i at Manoa.

Lundesgaard, Ø., Powell, B., Merrifield, M., Hahn-Woernle, L., Winsor, P., 2019a. Response of an Antarctic Peninsula fjord to summer katabatic wind events. *Journal of Physical Oceanography*, 49, 1485-1502.

Lundesgaard, Ø., Winsor, P., Truffer, M., Merrifield, M., Powell, B., Statscewich, H., Eidam, E., Smith, C., 2019b. Hydrography and energetics of a cold subpolar fjord: Andvord Bay, western Antarctic Peninsula. *Progress in Oceanography*, In review.

Mackey, M., Mackey, D., Higgins, H., Wright, S., 1996. CHEMTAX-a program for estimating class abundances from chemical markers: application to HPLC measurements of phytoplankton. *Marine Ecology Progress Series*, 144, 265-283.

Mankoff, K.D., Straneo, F., Cenedese, C., Das, S.B., Richards, C.G., Singh, H., 2016. Structure and dynamics of a subglacial discharge plume in a Greenlandic fjord. *Journal of Geophysical Research: Oceans*, 121, 8670-8688.

Marshall, G.J., 2003. Trends in the Southern Annular Mode from observations and reanalyses. *Journal of Climate*, 16, 4134-4143.

Mascioni, M., Almandoz, G.O., Cefarelli, A.O., Cusick, A., Ferrario, M.E., Vernet, M., 2019. Phytoplankton composition and bloom formation in unexplored nearshore waters of the western Antarctic Peninsula. *Polar Biology*, In review.

McKnight, D.M., Howes, B., Taylor, C., Goehringer, d.D., 2000. Phytoplankton dynamics in a stably stratified Antarctic lake during winter darkness. *Journal of Phycology*, 36, 852-861.

Meire, L., Mortensen, J., Meire, P., Juul-Pedersen, T., Sejr, M.K., Rysgaard, S., Nygaard, R., Huybrechts, P., Meysman, F.J., 2017. Marine-terminating glaciers sustain high productivity in Greenland fjords. *Global Change Biology*, 23, 5344-5357.

Mendes, C.R.B., Tavano, V.M., Dotto, T.S., Kerr, R., De Souza, M.S., Garcia, C.A.E., Secchi, E.R., 2018. New insights on the dominance of cryptophytes in Antarctic coastal waters: a case study in Gerlache Strait. *Deep Sea Research Part II: Topical Studies in Oceanography*, 149, 161-170.

Mendes, C.R.B., Tavano, V.M., Leal, M.C., de Souza, M.S., Brotas, V., Garcia, C.A.E., 2013. Shifts in the dominance between diatoms and cryptophytes during three late summers in the Bransfield Strait (Antarctic Peninsula). *Polar Biology*, 36, 537-547.

Meredith, M., Brandon, M.A., Wallace, M.I., Clarke, A., Leng, M.J., Renfrew, I.A., van Lipzig, N.P.M., King, J.C., 2008. Variability in the freshwater balance of northern Marguerite Bay, Antarctic Peninsula: Results from δ18O. *Deep Sea Research Part II: Topical Studies in Oceanography*, 55, 309-322.

Meredith, M., Wallace, M.I., Stammerjohn, S.E., Renfrew, I.A., Clarke, A., Venables, H.J., Shoosmith, D.R., Souster, T., Leng, M.J., 2010. Changes in the freshwater composition of the upper ocean west of the Antarctic Peninsula during the first decade of the 21st century. *Progress in Oceanography*, 87, 127-143.

Mitchell, B.G., Brody, E.A., Holm-Hansen, O., McClain, C., Bishop, J., 1991. Light limitation of phytoplankton biomass and macronutrient utilization in the Southern Ocean. *Limnology and Oceanography*, 36, 1662-1677.

Mitchell, B.G., Holm-Hansen, O., 1991. Maximum Antarctic phytoplankton crop in relation to mixing depth: Observations and modeling. *Deep Sea Res*, 38, 981-1008.

Moline, M.A., Claustre, H., Frazer, T.K., Schofield, O., Vernet, M., 2004. Alteration of the food web along the Antarctic Peninsula in response to a regional warming trend. *Global Change Biology*, 10, 1973-1980.

Montes-Hugo, M., Vernet, M., Martinson, D., Smith, R., Iannuzzi, R., 2008. Variability on phytoplankton size structure in the western Antarctic Peninsula (1997–2006). *Deep Sea Research Part II: Topical Studies in Oceanography*, 55, 2106-2117.

Morgan, K., Kalff, J., 1975. The winter dark survival of an algal flagellate—Cryptomonas erosa (Skuja) With 5 figures and 1 table in the text. *Internationale Vereinigung für theoretische und angewandte Limnologie: Verhandlungen*, 19, 2734-2740.

Motyka, R.J., Hunter, L., Echelmeyer, K.A., Connor, C., 2003. Submarine melting at the terminus of a temperate tidewater glacier, LeConte Glacier, Alaska, U.S.A. *Annals of Glaciology*, 36, 57-65.

Oxford Online Dictionary, 2020. Taxon. Retrieved from https://en.oxforddictionaries.com/definition/taxon.

Pan, B.J., Vernet, M., Reynolds, R.A., Mitchell, B.G., 2019. The optical and biological properties of glacial meltwater in an Antarctic fjord. *Plos One*, 14, e0211107.

Pedulli, M., Bisagni, J.J., Ducklow, H.W., Beardsley, R., Pilskaln, C., 2014. Estimates of potential new production (PNP) for the waters off the western Antarctic Peninsula (WAP) region. *Continental Shelf Research*, 84, 54-69.

Petrou, K., Kranz, S.A., Trimborn, S., Hassler, C.S., Ameijeiras, S.B., Sackett, O., Ralph, P.J., Davidson, A.T., 2016. Southern Ocean phytoplankton physiology in a changing climate. *Journal of Plant Physiology*, 203, 135-150.

Pezza, A.B., Rashid, H.A., Simmonds, I., 2012. Climate links and recent extremes in Antarctic sea ice, high-latitude cyclones, Southern Annular Mode and ENSO. *Climate Dynamics*, 38, 57-73.

Prézelin, B.B., Hofmann, E.E., Mengelt, C., Klinck, J.M., 2000. The linkage between Upper Circumpolar Deep Water (UCDW) and phytoplankton assemblages on the west Antarctic Peninsula continental shelf. *Journal of Marine Research*, 58, 165-202.

Raiswell, R., Tranter, M., Benning, L.G., Siegert, M., De'ath, R., Huybrechts, P., Payne, T., 2006. Contributions from glacially derived sediment to the global iron (oxyhydr)oxide cycle: Implications for iron delivery to the oceans. *Geochimica Et Cosmochimica Acta*, 70, 2765-2780.

Rignot, E., Koppes, M., Velicogna, I., 2010. Rapid submarine melting of the calving faces of West Greenland glaciers. *Nature Geoscience*, 3, 187.

Rozema, P., Venables, H., Poll, W., Clarke, A., Meredith, M., Buma, A., 2017. Interannual variability in phytoplankton biomass and species composition in northern Marguerite Bay (West Antarctic Peninsula) is governed by both winter sea ice cover and summer stratification. *Limnology and Oceanography*, 62, 235-252.

Schloss, I.R., Abele, D., Moreau, S., Demers, S., Bers, A.V., González, O., Ferreyra, G.A., 2012. Response of phytoplankton dynamics to 19-year (1991–2009) climate trends in Potter Cove (Antarctica). *Journal of Marine Systems*, 92, 53-66.

Schloss, I.R., Wasilowska, A., Dumont, D., Almandoz, G.O., Hernando, M.P., Michaud-Tremblay, C.-A., Saravia, L., Rzepecki, M., Monien, P., Monien, D., 2014. On the phytoplankton bloom in coastal waters of southern King George Island (Antarctica) in January 2010: An exceptional feature? *Limnology and Oceanography*, 59, 195-210.

Schofield, O., Brown, M., Kohut, J., Nardelli, S., Saba, G., Waite, N., Ducklow, H., 2018. Changes in the upper ocean mixed layer and phytoplankton productivity along the West Antarctic Peninsula. *Philosophical Transactions of the Royal Society A: Mathematical, Physical and Engineering Sciences*, 376, 20170173.

Schofield, O., Saba, G., Coleman, K., Carvalho, F., Couto, N., Ducklow, H., Finkel, Z., Irwin, A., Kahl, A., Miles, T., 2017. Decadal variability in coastal phytoplankton community composition in a changing West Antarctic Peninsula. *Deep Sea Research Part I: Oceanographic Research Papers*, 124, 42-54.

Sedwick, P.N., DiTullio, G.R., 1997. Regulation of algal blooms in Antarctic shelf waters by the release of iron from melting sea ice. *Geophysical Research Letters*, 24, 2515-2518.

Smetacek, V., Assmy, P., Henjes, J., 2004. The role of grazing in structuring Southern Ocean pelagic ecosystems and biogeochemical cycles. *Antarctic Science*, 16, 541-558.

Smith, C.R., Mincks, S., DeMaster, D.J., 2006. A synthesis of bentho-pelagic coupling on the Antarctic shelf: food banks, ecosystem inertia and global climate change. *Deep Sea Research Part II: Topical Studies in Oceanography*, 53, 875-894.

Smith, C.R., Sweetman, A.K., Nunnally, C.C., Lewis, M., Vernet, M., Ekern, L., Ziegler, A., 2018. Benthic Ecosystem Studies in a Rapidly Warming Antarctic Fjord Reveal High Export Flux and Benthic Abundance Very Near Tidewater Glaciers, Indicating High Sensitivity to Climate Warming. *Ocean Sciences Meeting*. Portland, Oregon: American Geophysical Union.

Smith, K.L., Robison, B.H., Helly, J.J., Kaufmann, R.S., Ruhl, H.A., Shaw, T.J., Twining, B.S., Vernet, M., 2007. Free-drifting icebergs: hot spots of chemical and biological enrichment in the Weddell Sea. *Science*, 317, 478-482.

Spence, P., Griffies, S.M., England, M.H., Hogg, A.M., Saenko, O.A., Jourdain, N.C., 2014. Rapid subsurface warming and circulation changes of Antarctic coastal waters by poleward shifting winds. *Geophysical Research Letters*, 41, 4601-4610.

Stammerjohn, S., Martinson, D., Smith, R., Yuan, X., Rind, D., 2008a. Trends in Antarctic annual sea ice retreat and advance and their relation to El Niño–Southern Oscillation and Southern Annular Mode variability. *Journal of Geophysical Research: Oceans*, 113.

Stammerjohn, S.E., Martinson, D.G., Smith, R.C., Iannuzzi, R.A., 2008b. Sea ice in the western Antarctic Peninsula region: Spatio-temporal variability from ecological and climate change perspectives. *Deep Sea Research Part II: Topical Studies in Oceanography*, 55, 2041-2058.

Straneo, F., Cenedese, C., 2015. The Dynamics of Greenland's Glacial Fjords and Their Role in Climate. *Ann Rev Mar Sci*, 7, 89-112.

Straneo, F., Curry, R.G., Sutherland, D.A., Hamilton, G.S., Cenedese, C., Våge, K., Stearns, L.A., 2011. Impact of fjord dynamics and glacial runoff on the circulation near Helheim Glacier. *Nature Geoscience*, 4, 322-327.

Sunda, W.G., Huntsman, S.A., 1997. Interrelated influence of iron, light and cell size on marine phytoplankton growth. *Nature*, 390, 389.

Talley, L.D., 2011. *Descriptive physical oceanography: an introduction*: Academic press.

Thessen, A., 2016. Adoption of machine learning techniques in ecology and earth science. *One Ecosystem*, 1, e8621.

Thompson, D.W., Solomon, S., Kushner, P.J., England, M.H., Grise, K.M., Karoly, D.J., 2011. Signatures of the Antarctic ozone hole in Southern Hemisphere surface climate change. *Nature Geoscience*, 4, 741.

Timmermans, K.R., Gerringa, L.J., De Baar, H.J., Van Der Wagt, B., Veldhuis, M.J., De Jong, J.T., Croot, P.L., Boye, M., 2001. Growth rates of large and small Southern Ocean diatoms in relation to availability o iron in natural seawater. *Limnology and Oceanography*, 46, 260-266.

Van Oijen, T., Van Leeuwe, M., Granum, E., Weissing, F., Bellerby, R., Gieskes, W., De Baar, H., 2004. Light rather than iron controls photosynthate production and allocation in Southern Ocean phytoplankton populations during austral autumn. *Journal of Plankton Research*, 26, 885-900.

Venables, H.J., Clarke, A., Meredith, M.P., 2013. Wintertime controls on summer stratification and productivity at the western Antarctic Peninsula. *Limnology and Oceanography*, 58, 1035-1047.

Vernet, M., Kozlowski, W.A., Yarmey, L.R., Lowe, A.T., Ross, R.M., Quetin, L.B., Fritsen, C.H., 2012. Primary production throughout austral fall, during a time of decreasing daylength in the western Antarctic Peninsula. *Marine Ecology Progress Series*, 452, 45-61.

Vernet, M., Martinson, D., Iannuzzi, R., Stammerjohn, S., Kozlowski, W., Sines, K., Smith, R., Garibotti, I., 2008. Primary production within the sea-ice zone west of the Antarctic Peninsula: I—Sea ice, summer mixed layer, and irradiance. *Deep Sea Research Part II: Topical Studies in Oceanography*, 55, 2068-2085.

Vernet, M., Sines, K., Chakos, D., Cefarelli, A., Ekern, L., 2011. Impacts on phytoplankton dynamics by free-drifting icebergs in the NW Weddell Sea. *Deep Sea Research Part II: Topical Studies in Oceanography*, 58, 1422-1435.

Walsh, J.J., Dieterle, D.A., Lenes, J., 2001. A numerical analysis of carbon dynamics of the Southern Ocean phytoplankton community: the roles of light and grazing in effecting both sequestration of atmospheric CO2 and food availability to larval krill. *Deep Sea Research Part I: Oceanographic Research Papers*, 48, 1-48.

Williams, C., Boies, C., Domack, E., 1989. Characteristics of glacial systems along the Graham Land Coast and Palmer Archipelago, Antarctic Peninsula. *Antarctic Journal*, 116-117.

Wright, S.W., van den Enden, R.L., Pearce, I., Davidson, A.T., Scott, F.J., Westwood, K.J., 2010. Phytoplankton community structure and stocks in the Southern Ocean (30–80 E) determined by CHEMTAX analysis of HPLC pigment signatures. *Deep Sea Research Part II: Topical Studies in Oceanography*, 57, 758-778.

Zapata, M., Rodríguez, F., Garrido, J.L., 2000. Separation of chlorophylls and carotenoids from marine phytoplankton: a new HPLC method using a reversed phase C8 column and pyridine-containing mobile phases. *Marine Ecology Progress Series*, 195, 29-45.

Ziegler, A., Cape, M.R., Lundesgaard, Ø., Smith, C.R., 2019. Intense deposition and rapid processing of seafloor phytodetritus in a glaciomarine fjord, Andvord Bay (Antarctica). *Progress in Oceanography*, In Prep.

Chapter 4. Environmental Drivers Modulate Phytoplankton Community Seasonal Succession in the Western Antarctic Peninsula

4.1. Abstract

Phytoplankton community is an important part of the ecosystem in the Western Antarctic Peninsula. Ambient environmental conditions have been suggested as the main driver for controlling phytoplankton abundance and community composition. These environmental conditions are expected to change in the future as the impact of ice-ocean interaction in this region intensifies. More studies with extensive spatial and temporal data are needed to comprehensively examine the environment's influences on the phytoplankton community. In this study, we leverage a multi-decadal dataset collected in the Western Antarctic Peninsula as part of the Palmer Long-Term Ecological Research Program. The program conducts research cruises in this region during every January from 1991 to the present-day. We use both standard statistical methods as well as an Automatic Machine Learning (AutoML) technique to better understand how environmental conditions impact the phytoplankton ecology. AutoML is an ideal approach to analyzing large ecological datasets, because it removes any preconceived notion about the ecosystem, and AutoML can autonomously train and test on multiple machine learning models that are difficult to implement individually. We found that the phytoplankton community in this region is mainly comprised of two major groups – diatoms and cryptophytes. During bloom condition, diatom dominates the community which has high total chlorophyll-a concentration and low community diversity. However, when there is relatively lower sea ice presence prior to the growing season, cryptophyte becomes the dominant group with lower total chlorophyll-a concentration but higher community diversity. After years with extremely low sea ice presence, dinoflagellates and mixed flagellates became the dominant groups with record-low total chlorophyll-a concentration and high community diversity. The observed changes in phytoplankton abundance and community composition are a result of seasonal succession modulated by both sea ice and alterations in the water column. Sea ice conditions prior to the growing season determine the initial stage of

community succession. Later in the growing season, water column properties play a more important role to facilitate the succession process. Therefore, phytoplankton community dominance and changes in composition can be explained as a process of seasonal succession influenced by both sea ice and water column properties over time. Combining these environmental drivers with the traits of major phytoplankton groups, we suggest that diatoms are more adaptive to high nutrient conditions as a result of initial sea ice melting earlier in the growing season. After these diatoms sink out of the euphotic layer, cryptophye blooms follow as they benefit from the shallow mixed layer with high irradiance, as well as from the high bacterial abundance and dissolved organic carbon as a result of the preceding diatom bloom.

4.2. Introduction

The Western Antarctic Peninsula (WAP) is a biologically productive habitat that hosts a variety of megafauna (Grange & Smith, 2013), including whales (Friedlaender et al., 2006), seals (Hückstädt et al., 2012), and penguins (Chapman et al., 2011). It is also an important commercial fishery (Forcada et al., 2012) (Casaux et al., 2003). This region's high productivity is largely driven by the phytoplankton community as primary producers (Ducklow et al., 2007). The phytoplankton community in the WAP is predominately comprised of diatoms (Kozlowski et al., 2011) (Garibotti et al., 2003a). Diatom is a preferred diet for *Euphausia Superba* (Antarctic krill) (Haberman et al., 2003) which is a vital food source for upper trophic levels (Ducklow et al., 2007). Therefore, changes in phytoplankton community composition can have significant impacts on the broader WAP ecosystem (Ducklow et al., 2013) .

The WAP is experiencing a rapid environmental change (Vaughan et al., 2003) and changes in phytoplankton abundance and/or composition may be expected (Montes-Hugo et al., 2008) (Petrou et al., 2016). Mean air temperature in the WAP has increased significantly (1–2 ˚C) over the last 50 years (Steig et al., 2009). This increase in temperature has profound consequences on sea ice, ice shelves, and glacial melting (Dierssen et al., 2002) (Smith & Stammerjohn, 2001). This change had already triggered the collapse of Larsen ice shelf A and B

east of the Peninsula (Cape et al., 2014). The environmental change in the WAP can also impact phytoplankton community composition. For instance, a decline in salinity is expected to increase cryptophyte abundance over diatoms which impacts carbon cycling and food web structure (Moline et al., 2004). Currently, mid-summer phytoplankton blooms in the WAP are often dominated by diatoms and cryptophytes; while mixed flagellates and *Phaeocystis spp.* can also become abundant (Kozlowski et al., 2011). Spring diatom blooms are usually absent in ice-free regions of the outer WAP shelf (Prézelin et al., 2000). In the Bransfield Strait, diatoms dominated water columns with a deeper upper mixed layer, warmer (sea surface temperature) SST, and higher salinity; while cryptophytes were found in a shallower upper mixed layer, colder SST, and lower salinity (Mendes et al., 2013). In contrast, most cryptophytes in the Gerlache Strait were found in relatively shallow mixed-layer and warmer temperatures, while diatoms and haptophytes were found in deeper mixed layer and colder seawater temperature (Mendes et al., 2018a). These contrasting results reveal multiple non-linear responses from different phytoplankton taxonomic groups to their ambient environment.

Other studies have suggested that these non-linear relationships can result from seasonal phytoplankton community succession (Garibotti et al., 2003a) (Arrigo et al., 2008) (Kang et al., 2001) (Wright et al., 2010) (Garibotti et al., 2003b). For instance, Garibotti *et al.* found significantly different phytoplankton assemblages dominating the WAP community over 3 austral summers (Garibotti et al., 2005). Although most water column properties were similar over this period, different sea ice retreat dates and changes in nitrate concentrations led to a shift in phytoplankton community composition. They attributed the changes in composition to a community succession driven by sea ice (Garibotti et al., 2005). Given the importance of the phytoplankton community in the WAP, a more comprehensive study with extended spatial and temporal data coverage is needed; through such study, we can test this hypothesis and elucidate how the ambient environment impact community succession and alter phytoplankton abundance and community composition. In this study, we aim to understand how environmental variables in the WAP can

impact different phytoplankton taxonomic groups' abundance and the overall community composition. We will also examine how changes in the WAP environment can determine the state of phytoplankton community succession. We hypothesize that the averaged sea ice conditions from previous year determine spring diatom blooms due to sea ice seeding and its nutrient supply, thus low sea ice presence leads to low diatom abundance and potentially more cyptophytes in the spring. Later in the summer, phytoplankton abundance and community composition are determined by water column properties such as temperature and salinity, facilitated by glacial meltwater which provide stratification and macro-nutrients – therefore, we hypothesize that the presence and absence of phytoplankton groups in the WAP are determined by their community seasonal succession modulated by the ambient environment.

4.3. Methods

4.3.1. Study Site

The WAP region covers a variety of zones from glacial coastlines to the continental shelf and the shelf break in the west (Fig. 4.1a). The WAP shelf is within the Antarctic Sea Ice Zone and seasonal and interannual variation in sea ice properties have a strong influence on the WAP and its ecosystem (Stammerjohn et al., 2008b). The Palmer Long-Term Ecological Research program (LTER) has an extensive public dataset which includes environmental and phytoplankton variables pertaining to the environmental conditions and local ecosystems in this region. This program covers both coastal zones, continental shelf, and the shelf break (for every January from 1991 to present). Datasets were retrieved from Palmer LTER Datazoo (www.pal.lternet.edu/data). Multiple datasets from 1995 to 2016 were merged including the conductivity-temperature-depth (CTD) dataset, the high-performance liquid chromatography (HPLC) pigment dataset, the dissolved inorganic nutrient dataset, and sea ice datasets. For detailed sampling and data processing procedures, please see *Smith et al.* (Smith et al., 1995) for CTD, Kozlowski et al. (Kozlowski et al., 2011) for HPLC, Prezelin *et al.* (Prezelin et al., 1992) for nutrients, and Stammerjohn *et al.* (Stammerjohn et al., 2008b) for sea ice properties. Sea ice variables used in

this study include averaged monthly sea ice extent and area, prior-year averaged annual sea ice extent and area, prior-year sea ice retreat date, advance date, and overall duration.

4.3.2. Data Processing

The study site covers a broad continental shelf and coastal zone of the WAP, with about 450m in depth excluding canyons (Fig. 4.1). Similar to the three zones defined by Martinson *et al.*, the WAP was assigned into three zones in our study – coast, shelf, and slope. Data in this study were selected for each zone based on their bathymetry, locations relative to the coastline, and hydrographic properties (Fig. 4.1) (Martinson et al., 2008). Bathymetry data in this study were retrieved from NOAA's ETOPO1 Global Relief Model, which has a spatial resolution of 1/60 degree.

The combined Palmer LTER dataset went through a quality control process. First, each CTD cast and the associated water column data were manually inspected. Each measured variable presented in this study was also compared to its mean of the entire study period, the annual mean, and the mean within the CTD cast; values that were beyond ±2 standard deviations were inspected, and no significant anomalies were detected. The key variables presented in this study (Table 1, Table 2, Table 3) are absent in some years. When one or more of the key variables were absent, the sample was omitted from our analysis. The following years were omitted entirely due to the lack of one or more key variables: 1997, 1998, 2002, 2007, 2010, 2012, and 2017 resulting in a 16-year time series.

Water column inorganic nitrate+nitrite concentrations were further evaluated. This is because distinct clusters of nitrate+nitrite values were found at depths during some years. Typically, the deep ocean lacks phytoplankton growth and it is replete with macro-nutrients due to the circumpolar deep water and interaction with the sea floor (Smith et al., 1995). However, in some CTD profiles, clusters of low nitrate+nitrite values were found below 27.5 kg/m^3 in potential density; these clusters of low concentrations are typically < 35 μM. We believe these low nitrate + nitrite values at depths are likely erroneous (pers. comm. M. Vernet, Scripps Institution of

Oceanography, M. Bender, Princeton University). Samples from each year were inspected. CTD profiles associated with these low nitrate+nitrite values at depth were omitted from this study.

Mixed layer depth was calculated based on an established method for the WAP region (Carvalho et al., 2017). For each CTD profile, surface mixed layer depth is estimated by finding the depth of the maximum water column buoyancy frequency. This method is focused on the water column vertical structure. A quality index filter is also applied to identify CTD profiles without significant stratification. For more details, please see Carvalho et al. (2017).

4.3.3. Chemical TAXonomy (CHEMTAX)

Phytoplankton taxonomic chlorophyll-a (chl-a) concentrations were determined by using the CHEMical TAXonomy (CHEMTAX) software (Mackey et al., 1996). CHEMTAX uses factor analysis and a steepest descent algorithm to determine the best fit to the data with a given input matrix of pigment ratios. Using an iterative process for a given input matrix, the software optimizes the pigment ratios for each group and applies the final ratio to the total chl-a in each sample to determine the proportion of chl-a concentration attributed to each phytoplankton group in the community. For this study, the Microsoft Excel based CHEMTAX 1.95 with ChemtaxHelper V7.1 was used. Quality of results from HPLC pigment-derived community composition using CHEMTAX is obtained by giving special attention to two aspects in the analysis: (1) the input data quality and (2) the initial input of pigment ratios (Table C1). Input data in this project is obtained from Palmer LTER datazoo, which had already been quality-controlled. For initial pigment ratios, we used those developed by established methods (Kozlowski et al., 2011) (Wright et al., 2010) which optimized the ratios for the Southern Ocean (Table C1), and they compare well with the Southern Ocean average. Furthermore, the interannual variability in abundance and relative proportion of each taxon group can be expected to change, but taxon diversity and primary groups' presence are consistent in the WAP region (Garibotti et al., 2003b). The method in this study followed the recommendation of established methods (Latasa, 2007), six sets of ten CHEMTAX runs each were made on the dataset each time, with the first runs using initial ratio

found in Table C1 and up to a 75% random error added to the initial ratio values. Each subsequent run applied the output ratio of the previous run as its initial ratio, and the output calculated from the tenth runs were considered final. Kozlowski *et al.* found this method produced consistent results that graphically converged and were ecologically sound in the context of WAP phytoplankton diversity (Garibotti et al., 2003a) (Garibotti et al., 2003b). In this study, we used CHEMTAX to partition total chl-a concentration into six groups: diatom, cryptophyte, mixed flagellate (which are small flagellates that were unidentifiable by microscopy), dinoflagellate, haptophyte *Phaeocystis spp.*, and prasinophyte.

4.3.4. Derived Phytoplankton Variables

Phytoplankton community data in this study are presented as both absolute chl-a concentration in units of µg/l and relative abundance. Relative abundance was calculated as each discrete sample's taxon-specific chl-a normalized by that sample's total chl-a concentration and it was expressed as a percentage (%).

Community dominance was calculated based on chl-a concentrations associated with different phytoplankton taxonomic groups. In each discrete sample, the six phytoplankton groups' chl-a concentrations were ranked from the lowest to the highest, then a slope was fitted through the six data points. Hence, large slope values indicate community dominance by fewer groups, and small slope values indicate the total chl-a concentration is more evenly distributed among the six groups.

Community diversity was also assessed in this study. We used the Shannon Index (H_s) (Shannon, 1948) (Spellerberg & Fedor, 2003) which was calculated as the following, where $Chla_i$ is the chl-a concentration associated with each taxonomic group and $Chla_{total}$ is the total chl-a concentration of each discrete sample:

$$H_s = -\sum_{1}^{i} \left(\frac{Chla_i}{Chla_{total}}\right)\left(\ln\left(\frac{Chla_i}{Chla_{total}}\right)\right) \quad (1)$$

4.3.6. Daylight Length

Daylight length, or the hours between sunrise and sunset, was calculated as a function of year-date and latitude (Forsythe et al., 1995):

$$D = 24 - \left(\frac{24}{\pi}\right) * \operatorname{acos}\left(\frac{\sin\left(\frac{0.8333\,\pi}{180}\right) + \sin\left(\frac{L * \pi}{180}\right) * \sin(P)}{\cos\left(\frac{L * \pi}{180}\right) * \cos(P)}\right) \quad (2)$$

where D is the daylight length in units of hours, L is latitude in degrees, and P is a constant for each year-date where J is the day of the year (year-date):

$$P = \operatorname{asin}\left[0.39795 * \cos(0.2163108 + 2 * \operatorname{atan}\{0.9671396 * \tan[0.00860(J - 186)]\})\right] \quad (3)$$

4.3.7. Predictive Modeling

The impact of environmental factors on individual phytoplankton groups predicted and analyzed through machine learning techniques. This method has been applied to understand phytoplankton ecology in Andvord Bay (an WAP fjord) (Pan et al., 2020). Similarly, we choose the automated machine learning (AutoML) method for this study. AutoML is a process of automating the process of applying machine learning. AutoML covers the complete pipeline from raw dataset to deployable machine learning model. AutoML has been proposed as an artificial-intelligence-based solution to applied machine learning problems (Thornton et al., 2013) – problems such as the ones we are tackling in this study. This highly automated process allows non-experts to make use of machine learning models and techniques (Hutter et al., 2014).

The modeling and analysis were conducted with the Scikit Learn and H2O packages (3.20.0.8, H2O.ai. Repository at github.com/h2oai/h2o-3) in a Python 3 environment. We used the H2O's AutoML feature to automate a machine learning workflow, which includes automatic training and tuning of many deep-learning models within a user-specified time limit. The AutoML is an ideal method for analyzing large ecological datasets because it removes any preconceived

notion about the ecosystem. AutoML can also test and train multiple complex machine learning models that are difficult to implement individually. We used 80% of the data randomly selected from the dataset to train these machine learning algorithms (training data) and then used the remaining 20% to test the trained models (test data). The model performances were then ranked in the AutoML Leaderboard. Finally, the algorithm with the highest prediction power, based on root mean square error (RMSE) and coefficient of determination (R^2), was selected as the model for predicting a specific taxonomic abundance based on environmental factors. RMSE and R^2 values were generated based on the validation of model-predicted values by the test data (randomly selected 20% of the total dataset). Water column temperature, salinity, mixed layer depth, daylight length, nitrate+nitrite, phosphate, silicic acid, bathymetry, and seven sea ice variables were the input variables to each model; this is with the exception of the mixed flagellate model which excluded the sea ice variables. The model output was used to understand how these environmental conditions influence each group's abundance. This was done by ranking the percentage of variance in each phytoplankton group explained by each environmental variable within the model. Further analysis was conducted by examining the partial dependence plots which depict the response of modeled phytoplankton abundance to changes in the value of environmental factors.

4.4. Results

4.4.1. Overview of Physical, Chemical and Phytoplankton Properties of the WAP Region

The WAP region between 64^{o}S and 68^{o}S demonstrated distinct physical and biological properties in space and over time. We observed unique environmental and phytoplankton properties associated with each of the three zones over the sampling area, the coast, shelf, and slope (Fig. 4.1). Overall, the coastal and shelf zones are shallower than the slope. The coastal zone has relatively colder temperature and lower salinity within its mixed layers (Table 1). A relatively deeper mixed layer is also found over the slope in comparison to the coast and shelf.

Nitrate and phosphate concentrations gradually declined from the slope to the coast, while silicic acid concentration increased (Table 1).

The environmental properties facilitated phytoplankton growth and their community composition. Within the top 10 m of the water column, high phytoplankton biomass, as indicated by chl-a concentration, is predominantly associated with the coastal zone, and it decreases towards the slope (Fig. 4.2a). High chl-a concentrations are also associated with community dominance with the highest observed community dominance in the coastal zone (Fig. 4.2b). The high chl-a concentrations and strong community dominance in the coastal zone also results in lower diversity, indicated by the Shannon Index, with diversity increased towards the slope (Fig. 2c). The high chl-a concentrations were mostly due to diatoms (Fig. 4.3); the diatom-driven high chl-a concentrations led to strong community dominance and low diversity (Fig. 4.3a, 4.3b, 4.3d, 4.3e). The other major phytoplankton group is cryptophyte; however, they contributed less to the overall chl-a concentration when compared to diatoms (Fig. 4.3c). Overall, diatoms and cryptophytes are the two major phytoplankton groups by average chl-a concentrations in all three zones and over time; while mixed flagellate, *Phaeocystis*, dinoflagellate, and prasinophyte are minor groups (Fig. 4.3, Table 4.2). Overall, the community composition remains consistent in most years with some interannual variability within each group (Table 4.2).

4.4.2. Environmental Drivers of Phytoplankton Blooms in WAP

We used autoML-generated models and their output to investigate how environmental variables relate to different phytoplankton groups, both dominant as well as minor groups, and how they influence the overall community composition. Within the major phytoplankton groups, the diatom model, with a R^2 value of 0.89 on test data, suggests that diatoms are most strongly related by the macronutrients nitrate + nitrite and phosphate concentrations (Fig. 4.4a) and these two variables account for 40.86% of the variance. Daylight hour is the third most important variable accounting for 11.37% of the variance, followed by salinity accounting for 8.75%, and temperature accounting for 5.34% (Fig. 4.4a). Together, these four variables account for 66.32% of the

variance within the diatom model. The other major phytoplankton group, the cryptophytes, has a test model with an R^2 of 0.68. The daylight length is the most important variable accounting for 18.51% of the variance in the model (Fig. 4.4b). Daylight length is followed by salinity which accounts for 13.14% of the variance, temperature for 12.08%, and bathymetry for 10.86% (Fig. 4.4b). Together, these four variables account for >50% of the variance within the cryptophyte model.

In the minor phytoplankton groups, mixed flagellate is generally the most abundant (Table 2). Their model has a R^2 value of 0.64 on test data. The model suggests silicic acid concentration is the most important variable which accounts for 17.48% of the variance. It is followed by daylight length which accounts for 15.69% of the model variance, phosphate concentration for 12.79%, and mixed layer depth for 12.72%. These first four variables account for 58.68% of the model's variance (Fig. 4.4c). The *Phaeocystis* model, with a R^2 value of 0.71 on test data, suggests daylight length is the most important variable (Fig. 4.4d), accounting for 15.69% of the model's variance. This is followed by salinity (13.46%), temperature (11.80%), and annual sea ice extent (10.77%). These four variables account for 51.72% of the variance within the *Phaeocystis* model (Fig. 4.4d). The dinoflagellate model has a R^2 value of 0.53 on test data and suggests daylight length is also the most important variable for this group (accounting for 13.27% of the model's variance), similar to other minor phytoplankton groups. This is followed by annual sea ice advance date (accounts for 10.36%), salinity (accounts for 9.27%), temperature (accounts for 9.08%), bathymetry (7.38%), and nitrate + nitrite concentration (6.58%) (Fig. 4.4e). These five variables account for 42.67% of the variance in dinoflagellate distribution, taking nearly all environmental variables to explain over 90% of the variance within the model. The prasinophyte model has a R^2 value of 0.67 on test data (Fig. 4.4f) and similar to the dinoflagellate model, no one variable dominates within the model. The most important variable for prasinophyte is bathymetry accounting for 11% of the total variance (Fig. 4.4f).

Each model also generates partial dependence plots, illustrating the model's prediction of each group's chl-a concentration within the range of each environmental variable (Fig. 4.5, Fig. 4.6). There are some notable features in the major phytoplankton groups. For diatoms, their chl-a concentration appears to increase below 1 ^{o}C, while cryptophyte is associated with higher temperature between 1.8 ^{o}C and 2.4 ^{o}C (Fig. 4.5a). Both diatom and cryptophyte chl-a increases rapidly with a decrease in salinity at around 34 PSU, but diatom chl-a concentration continues to increase until salinity drops below ~32.8 PSU, while cryptophyte chl-a concentration stops to increase when salinity declines below ~33.2 PSU (Fig. 4.5b). A deep mixed layer depth, deeper than 52.6 m, appears to favor diatoms (Fig. 4.5c). Diatom chl-a concentration shows a bimodal distribution with respect to daylight length, being relatively higher when daylight length is at its maximum and minimum, while cryptophyte chl-a concentration is at its highest at maximum daylight length and gradually decreases with a decrease in daylight hours (Fig. 4.5d). Both nitrate + nitrite and phosphate concentrations appear to influence diatom in similar ways, where diatom chl-a concentration rapidly elevates when nitrate + nitrite concentration is < ~26.98 uM and when phosphate concentration is < ~ 2.12 uM (Fig 4.5e, 4.5f). Nitrate + nitrite concentration also appears to influence cryptophyte chl-a concentration, but the changes in chl-a is more attenuated in comparison to these nutrients' effect on diatoms; cryptophyte chl-a gradually increases after nitrate + nitrite concentration < 24.73 uM (Fig. 4.5e). Silicic acid concentration is related to an increase in diatom chl-a when concentration is > 81.2 uM (Fig. 4.5f); it also elevates cryptophyte chl-a concentration when the concentration is > 54.5 uM (Fig. 4.5g). Diatom chl-a concentration appears to decrease rapidly between shallow bathymetry and down to areas with seafloor at ~448 m and remains relatively steady for areas deeper than 448 m (Fig. 4.5h).

The environmental variables also influence minor phytoplankton groups (Fig. C1), but the changes in their chl-a concentrations are orders of magnitude less in comparison to the major groups (i.e. diatom and cryptophyte) (Fig. 4.5). Notably, both *Phaeocystis* and mixed flagellate abundance increase with lower salinity (Fig. C1b). These two groups also exhibit similar

relationships to macro-nutrients similar to the response of diatoms. Minor groups increase with a decrease in nitrate + nitrite concentration (except dinoflagellates); particularly, mixed flagellate increase rapidly below 13.49 uM and *Phaeocystis* increase below ~26.98 uM (Fig. C1e). Meanwhile, dinoflagellate abundance rapidly increases when temperature is above ~2.66 ^{o}C (Fig. C1a), salinity is above ~33.72 PSU (Fig. C1b). Dinoflagellate is also more abundant when daylight length is longer than 21.8 hours corresponding to early January of each year (Fig. C1d). Other minor groups also show elevated abundance earlier in the season, but their increases are less than that of dinoflagellate (Fig. C1d).

These relationships between the environment variables and phytoplankton community composition and abundance are often non-linear and exhibit strong variabilities within the range of values observed in the WAP (Fig. 4.5 and Fig. 4.6). Although the two major phytoplankton groups, diatom and cryptophyte, appear to occupy similar ranges of temperature and salinity, further analysis reveals that higher diatom chl-a concentrations are associated with lower salinity, while higher cryptophyte chl-a concentrations are associated with higher temperature (Fig. 4.7). All flagellates, including the minor phytoplankton groups, mixed flagellate, *Phaeocystis*, dinoflagellate, and prasinophyte, are more dominant at higher salinities (Fig. 4.7), which are related also to lower community dominance, higher diversity, and lower total chl-a concentration encountered towards the slope (Fig. 4.1, Fig. 4.3).

Sea ice variables were part of the input to these autoML-generated models (with the exception of the mixed flagellate model; the absence of sea ice variables in this model resulted in higher R^2 on test data), so they can predict phytoplankton groups' responses based on changes in monthly and prior-year sea-ice properties (Fig. 4.6). Sea ice conditions appear to disproportionately impact major phytoplankton group distribution, in particular diatoms. Monthly sea ice area between 22,545 km^2 and 48,049 km^2 appear to support maximum diatom chl-a concentration, while monthly sea ice area above this range supports higher diatom chl-a concentration than those below this range (Fig. 4.6b). Prior year annual sea ice properties also

appear to impact diatom strongly. Diatom chl-a concentration elevates rapidly when prior year sea ice area is over 100,951 km^2 (Fig. 4.6c). Higher diatom chl-a concentrations are also associated with prior year earlier sea ice advance date (Fig. 4.6d), later retreat date (Fig. 4.6e), which result in longer sea ice duration (Fig. 4.6f). In contrast, late sea ice advance date in the prior year leads to an increase in cryptophyte concentration (Fig. 4.6d).

Similar to the other environmental variables, sea ice properties also influence minor phytoplankton groups, but the changes in these groups' chl-a concentrations are general < 0.2 ug/l (Fig. C2) and so they are orders of magnitude lower than the changes exhibited by the major groups (Fig. 4.6). However, smaller sea ice extent and shorter sea ice duration appear to favor dinoflagellates and prasinophytes (Fig. C2c, C2g). Dinoflagellate abundance increases rapidly when prior-year annual sea ice extent is below 108,335 km^2 (Fig. C2c), advance date is later than Julian day 161 (Fig. C2e), and sea ice duration is less than 204 days (Fig. C2g). In comparison, *Phaeocystis* showed very little change due to sea ice area or extent, but their abundance increases when the prior-year sea ice advance date is earlier than Julian date 170 (Fig. C2e), and the overall duration is over 232 days (Fig. C2g). Prasinophyte abundance appears to increase with a decrease in sea ice extent, similar to the response of dinoflagellate; however, their abundance increases rapid with low sea ice area (Fig. C2d) and early sea ice retreat (Fig. C2f).

Light conditions in the WAP in relation to phytoplankton are summarized by daylight length (Fig. 4.8). This variable reveals two different environmental factors and their influence on the phytoplankton community. One is the overall light condition at the time of sampling; the other is to serve as a temporal proxy to assess community variability over time (Fig. 4.8). The latter effect has likely contributed to the autoML-generated model output, hence the models indicate daylight length is an important variable to describe phytoplankton distribution in the WAP, especially to minor groups (Fig. 4.4). However, daylight length can also indicate the timing of sampling extending from 5 January to 9 February (Julian day 5 to 40, Fig. 4.8). The correlation between

daylight hours and Julian dates indicates that daylight hour reflects both the overall light condition and each sample collection.

To further understand the effect of daylight hours on phytoplankton composition, three variables of the dominant group's chl-a in the coastal zone was divided into 2 periods, from 1-20 January and 21 January to 9 February. Annual average phytoplankton biomass, as chl-a, and diatom and cryptophyte relative abundance are largely unrelated to annual average temperature and salinity values during the first 20 days of the year (Julian date 0 to 20); the correlation between these environmental and phytoplankton variables are not statistically significant (Fig 4.9b, 4.9c, 4.9d, 4.9e). However, after 20 days, annual average temperature and salinity exhibit stronger and statistically significant correlations with diatom and cryptophyte relative abundance (Fig. 9i, 9j, 9k, 9l). The correlations between the environmental variables and averaged total chl-a concentration also improve after 20 days (Fig. 4.9a, 4.9b, 4.9g, 4.9h). Major nutrients in the euphoric layer also exhibit similar patterns over time (Fig. 4.10). For an example, during the first 20 days of each year, there is a weak correlation between averaged annual nitrate + nitrite, phosphate concentrations when they are compared to diatom relative abundance (Fig. 4.10a, 4.10b). In contrast, R^2 values are higher and these correlations are statically significant after 21 days (Fig. 4.10c, 4.10d).

4.4.4. Phytoplankton and Water Column Interannual Variabilities in the Context of Sea Ice Dynamics

When phytoplankton variables within the mixed layer are examined as averaged annual properties, they follow the overall patterns exhibited within discrete samples (Fig. 4.3) – where high total chl-a concentration is a result of the variability in abundance of the two major phytoplankton groups, diatom and cryptophyte. Annual chl-a concentration average peaks in 1996, 2006, 2011, 2014 and 2016, with a maximum of 5.06 µg/l in 1996 (Fig. 4.11a). These high chl-a years correspond to years with high diatom relative abundance, where diatom accounts for over 60% of the total chl-a concentration (Fig. 4.11b). In contrast, cryptophytes generally become abundant when diatom relative abundance is low, such as in 2000, 2005, and 2013 accounting

for over 60% of total chl-a concentration (Fig. 4.11b). In this way, interannual variability in phytoplankton abundance and community composition is an alternation of diatom vs cryptophyte blooms (Fig. 4.11b) with highest overall biomass during diatom blooms (Fig. 4.11a; Fig. 4.3). The abundance of diatoms leads to higher community dominance and lower diversity (Fig. 4.11a, 4.11b, 11d). In contrast, years with lower total chl-a concentrations show higher relative abundance of minor phytoplankton groups, which lead to lower community dominance and higher diversity (Fig. 4.11a, 4.11c, 4.11d).

Average water column properties also show interannual variability Fig 4.11 e—j). Years with higher chl-a concentrations and higher diatom relative abundance in 1996, 2006, 2011, 2014 and 2016, had relatively lower salinity with a minimum of 32.97 PSU in 2014 and a local minimum of 33.29 PSU in 2006 (Fig. 4.11f). In addition, shallower mixed layer depths were observed during these years (Fig. 4.11g); between 2013 and 2016, mixed layer depths are generally between 26 m and 32 m. High diatom years also corresponds to low nitrate + nitrite and phosphate concentrations (Fig. 4.11h, Fig. 4.11i), for instance, a minimum of 13.73 μM of nitrate + nitrite and 0.85 μM of phosphate concentrations were found in 2014. In comparison, years with higher cryptophyte relative abundance in 2000, 2005, and 2013, had relatively higher macro-nutrient concentrations, > 20 μM of nitrate + nitrite and > 1.4 μM of phosphate concentrations (Fig. 4.11h, 4.11i, 4.11j), with temperatures and salinities around the interannual average (Fig. 4.11e, 4.11f, Table 2).

While water column properties can influence phytoplankton community during the growing season, sea ice has a strong influence on the overall annual community composition and summer chl-a abundance (Fig. 4.11). Prior to the high-diatom years, there were larger sea ice areas exceeding 94,000 km^2 over the WAP shelf (except 2011). Maximum annual sea ice area occurred in 2005 (Fig. 4.11k) corresponds to maximum diatom relative abundance in 2006 (Fig. 4.11b). The large sea ice areas are also related to early sea ice advance and late retreat, resulting in longer sea ice duration (Fig. 4.11k, 4.11l, 4.11m, 4.11n). For instance, prior to years with high

diatom abundance, sea ice generally advanced prior to Julian day 160, retreated after Julian day 350, resulting in sea ice duration > 210 days. These high sea-ice years also correspond to low salinity, shallow mixed layer, and relatively low macro-nutrient concentrations (Fig. 4.11g, 4.11h, 4.11i, 4.11j). In contrast, prior to high-cryptophyte years, sea ice advanced at a relatively later date after Julian day 160, but retreated at a date around the interannual average (Fig. 4.11l, 4.11m, Table 2). Relatively higher nutrients concentrations and salinity were also found in these years (Fig. 4.11f, 4.11h, 4.11i, 4.11j).

Several anomalous years are also observed in this timeseries, where neither diatoms or cryptophytes dominate. The lowest averaged total chl-a over the entire study period is found in 2009 (Fig. 4.11a), accompanied by one of the lowest relative abundance of diatom and cryptophyte, and highest relative abundance of mixed flagellate and, notably, dinoflagellate (Fig. 4.11c). These values also coincide with low value in community dominance and high in diversity (Fig. 4.11d). Year 2004 show high diversity coincided with high cryptophyte relative abundance with lower and similar diatom and *Phaeocystis* relative abundance (Fig. 4.11d). The anomalous year of 2009 had a salinity maximum at 33.92 PSU, deep mixed layer depth maximum at 74.54 m, and higher macro-nutrient concentrations particularly nitrate + nitrite reaching a maximum of 25.25 μM (Fig. 4.11h, 4.11i, 4.11j). Most notably, 2009 followed the lowest annual sea ice area average in the entire study period at 43,571 km^2 (Fig. 4.11k). During the prior year, sea ice had one of the latest advance date (Julian day 175, Fig. 4.11l) and the earliest retreat date (Julian day 296, Fig. 4.11m), resulted in the shortest sea ice duration in the entire study period (121 days, Fig. 4.11n).

4.5. Discussion

4.5.1. Phytoplankton Community Dominated by Diatoms & Cryptophytes

The dominance of diatoms and cryptophytes in the WAP was expected, as demonstrated by previous studies (Garibotti et al., 2005) (Pan et al., 2020) (Schofield et al., 2017). Diatoms and cryptophytes dominate the phytoplankton community over the WAP (Fig. 4.2, Fig. 4.3, Fig. 4.11b)

(Schofield et al., 2017) (Garibotti et al., 2005). This leads to low community diversity (Fig. 4.2c). Phytoplankton blooms of these monoculture-like communities have also been observed beyond the WAP. For instance, over the entire Southern Ocean, spring blooms are mainly comprised of diatoms which represent the bulk of the region's primary production (Alvain et al., 2008) (Arrigo et al., 2008). The marine ecosystem over the WAP is different in comparison to most terrestrial ecosystems, where vegetation biodiversity is often positively correlated with primary productivity (Liang et al., 2016). In the WAP marine environment, diatom community is the main primary producer even when diatoms are less numerous in comparison to other communities. For instance, studies in Andvord Bay during spring found that a cryptophyte-dominant community (Pan et al., 2020); however, diatoms dominate primary productivity despite their low abundance (Mascioni et al., 2020).

The high abundance of diatoms, and secondarily, cryptophytes are found in the coastal zone. They care characterized by low salinity, high temperature, and high macro-nutrient concentrations (Fig. 4.5b, 4.5e, 4.5f). This is likely attributed to the coast zone's proximity to the ice-ocean interface and freshwater input from glacial and sea ice melting. Glacial meltwater and various inshore meltwater upwelling mechanisms are known to lower water column salinity as they deliver fresh meltwater to the water column (Dierssen et al., 2002) (Pan et al., 2019). Additionally, glacial meltwater can deliver nutrients for phytoplankton growth (Pan et al., 2020). Melting of sea ice can also release fresh buoyant, iron enriched meltwater that support phytoplankton growth, and the iron enrichment is mostly due to previous winter accumulation of aerosol input (Constable et al., 2014) (Lannuzel et al., 2008). Vertical flux of macro-nutrients from depths, particularly nitrate, can sustain phytoplankton growth in the WAP (Pedulli et al., 2014). These nutrient supply mechanisms coupled with both glacial and sea ice meltwater are prominent features associated the coast and shallow shelf zones (Dierssen et al., 2002) (Stammerjohn & Smith, 1995) and so they are expected to have an important impact on this region's phytoplankton growth. The response of the Auto-ML models (particularly the diatom and cryptophyte models)

also confirms the influence ice-ocean interaction. The models show phytoplankton abundance responds to bathymetry and other meltwater-moderated environmental variables, such as salinity and nutrients (Fig. 4.5). In the case of nutrients, all phytoplankton groups, especially diatom, show rapid increases as they deplete macro-nutrients. This inverse relationship between nitrate + nitrite/phosphate concentrations and chl-a concentration are attributed to phytoplankton nutrient drawdown. This relationship has observed elsewhere in the WAP, especially in the fjord environment during growing season (Ekern, 2017) (Pan et al., 2020).

A notable difference in phytoplankton response to macro-nutrients is diatom's response to changes in silicic acid concentration (Fig. 4.5g). Diatom is a main source of silicic acid uptake in the Southern Ocean (Boyd & Law, 2001), thus, it is expected a strong response of diatoms to silicic acid (Mendes et al., 2013). However, we saw that diatom chl-a concentration's response to silicic acid concentration deviated from those of nitrate + nitrite and phosphate (Fig. 4.5g). As silicic acid decreases, a moderate increase in diatom chl-a concentration suggests nutrient drawdown – similar to their response to nitrate + nitrite and phosphate; but the sharp increase in diatom chl-a when silicic acid concentration is high is unexpected, and likely suggests the presence of a different assemblage of diatoms responding to high silicic acid concentrations (Fig. 4.5g). A shift in diatom assemblage has been observed elsewhere in the Southern Ocean, particularly during iron addition experiments (EIFEX) (Assmy et al., 2013). There was an observed increase in *Chaetoceros dichaeta* after iron addition, followed by a shift to *Fragilariopsis kerguelensis* towards the end of the experiment as iron concentration depleted (Assmy et al., 2013). This shift in diatom assemblage corresponded with an increase of biogenic silica concentration in the water column (Cavagna et al., 2011). Assmy et al. concluded that the behavior of these two assemblages of diatoms indicate two distinct life cycle strategies – the *Chaetoceros* assemblage accumulates biomass during favorable growth conditions that are iron-replete, followed by its mass mortality and rapid population decline. The growth of the first diatom assemblage creates iron-limited conditions in the water column, but its demise does not lead to

silica export. These processes lead to iron-limited but silicic-acid-rich conditions, which gives rise to the *Fragilariopsis* assemblage which leverages the abundant silicic acid to build frustules and eventually result in silica export and burial (Assmy et al., 2013). This change in water column silica is similar to the response captured by the diatom model in our study (Fig. 4.5g). In this study, silicic acid concentration in the mixed layer is relatively higher later on during the growing season, therefore the bimodal response of diatoms to silicic acid concentration is also reflected in its response to daylight hours (Fig. 4.5d) – where an increase in diatom abundance is observed at the beginning and the end of the growing season (Fig. 4.5d, Fig. 4.8) suggesting two diatom assemblages. This difference in assemblages within the diatom group has also been captured by other studies. Garibotti et al. found two distinct diatom assemblages in the WAP – one is associated with sea ice edge and appears at the beginning of the growing season, another associated with open ocean and appears later (Garibotti et al., 2005). Similarly, Mascioni et al. found diatom biomass in Andvord Bay and Gerlache Strait was dominated by microplanktonic diatoms, *Odontella weissflogii* (Mascioni et al., 2020). However, there was also a variety of diatom species existing concurrently; for instance, diatom blooms were mostly dominated by large centric diatoms instead of *Odontella weissflogii (Mascioni et al., 2019)*. The coastal and shallow shelf zones in the WAP receive dissolved iron from glacial and sea ice meltwater discharge (Annett et al., 2017) (Pan et al., 2020), and this meltwater-driven natural iron fertilization likely facilitates a transition between two diatom assemblages similar to that observed during the EIFEX experiment (Assmy et al., 2013), which is also reflected in changes in water column silicic acid and the timing of the bloom.

In addition to the water column environment, sea ice is also important to phytoplankton abundance and community composition in the WAP, particularly for diatoms (Ducklow et al., 2013) (Schofield et al., 2017) (Smith et al., 1995). The timing of sea ice retreat and duration during the previous year have been found to impact diatom abundance in highly stratified waters in the Southern Ocean and over the WAP shelf (Arrigo et al., 2008) (Garibotti et al., 2003a). Over the

entire Antarctic coastline, low salinity surface waters persist for about two weeks after sea ice retreat from a given region; this is then followed by wind-driven advection and mixing which weakens surface stratification and phytoplankton abundance rapidly declines (Arrigo et al., 2008). This is confirmed by our AutoML-generated models where diatom concentration increases with larger sea ice extent and area, coupled with early advance, late retreat, resulting in longer duration (Fig. 4.6). Moreover, these models also found monthly sea ice variables to be impactful (Fig. 4.6), but not the most important variables for influencing phytoplankton abundance (Fig. 4.4) – this illustrates the compound influence of sea ice, which include surface stratification, creating favorable light condition through the meltwater lens, and nutrient addition. However, these factors often have an impact on phytoplankton over time and the community does not have immediate responses. These results indicate the integrated effect of sea ice over time is more important to phytoplankton than its immediate impact.

When sea ice variables are examined on an interannual scale (Fig. 4.11), rather than on a seasonal basis (Fig. 4.6), their impact on phytoplankton community composition is more clearly illustrated. High annual sea ice presence (larger total area, early advance, late retreat, and longer duration from prior year) resulted in higher relative abundance of major phytoplankton groups, especially diatoms, suggesting seeding from sea ice. This is consistent with the results from other studies in the WAP, where a distinct diatom assemblage was found to be associated with the sea ice edge (Garibotti et al., 2005). Past mesocosm experiments with sea ice from Terra Nova Bay of the Ross Sea also found sea ice micro-algae was dominated by diatoms (Mangoni et al., 2009). Later in their experiment, high growth capacity was observed in *Fragilariopsis cylindrus* and *Chaetoceros spp.* in the water column, even though these diatom species did not make up the majority of the diatom assemblage within the sea ice. In particular, *Fragilariopsis cylindrus* showed high growth rates under both high and low light and nutrient conditions. From these results, Mangoni *et al.* suggested that *Fragilariopsis spp.* and *Chaetoceros spp.* are important in seeding blooms when sea ice break up and melt (Mangoni et al., 2009). In other parts of the Southern

Ocean, a majority of these sea-ice-seeded diatom blooms in the marginal ice zone often rapidly sediment from the euphotic layer (Wright et al., 2010) (Wright & van den Enden, 2000). Coupling the influence of interannual sea ice dynamics with results with the insights from the EIFEX iron addition experiment (Assmy et al., 2013) (Cavagna et al., 2011), we suggest that initial diatom blooms observed are sea ice edge blooms, presumably influenced by sea ice seeding. Their success in the coastal zone is influenced first by sea ice meltwater and then glacial meltwater (as meltwater changes salinity and macro-nutrient concentrations in the water column, particularly at the surface) (Annett et al., 2017) (Forsch et al., 2018) (Pan et al., 2020). Later, the changes in diatom chl-a concentration over the season is attributed to changes in the diatom assemblage. This shift in diatom community alters silicic acid concentration in the water column (Fig. 4.5g), and it was captured in predicted diatom responses to daylight hour (as a proxy for timing) and silicic acid concentration (Fig. 4.5d, Fig. 4.5g).

There is a clear alternation of the major phytoplankton groups, years of diatom dominance and years of cryptophyte dominance. When phytoplankton community composition is examined as annual averages over the entire sampling period (Fig. 4.11), there is a clear dichotomy within the major phytoplankton group -- between diatoms and cryptophytes (Fig. 4.11b). Averaged diatom relative abundance is high during years with high total chl-a concentration, while cryptophyte relative abundance dominated the community in years with relatively low total chl-a concentrations. This alternation has been observed in other areas of the WAP – for instance, near Averse Island, high diatom relative abundance was found to associate with years with high chl-a anomalies, while higher cryptophyte relative abundance was related to low chl-a anomalies (Schofield et al., 2017). Diatoms and cryptophyte also appear to occupy unique environmental niches (Fig. 4.5, Fig. 4.7). For example, high cryptophyte relative abundance appears to associate with temperatures above 0^{o}C while diatoms occupy a wider temperature range encompassing both high and low temperatures (Fig. 4.7). This is similar to other studies over the WAP and in a nearby fjord, where cryptophytes were found in relatively warm temperatures (Mendes et al.,

2018a) (Moline et al., 2004) (Pan et al., 2020), while diatoms were more adaptive to a wider range of temperatures (Schofield et al., 2017). Some of these studies over the WAP also found cryptophytes to be associated with lower salinity (Moline et al., 2004) (Schofield et al., 2017). These results confirm our observed dichotomy between diatoms and cryptophytes within the major phytoplankton group. In summary, if the WAP environment continues to shift to warmer temperatures (Vaughan et al., 2003) (Vaughan & Doake, 1996) due to the ongoing regional warming, in addition to lower salinity due to more glacial and sea ice meltwater input (Cook et al., 2005) (Meredith et al., 2017) (Vaughan et al., 2003), then these new environmental conditions will make cryptophyte and other flagellate dominance more common in the WAP phytoplankton community (van Leeuwe et al., 2020).

4.5.2. Minor Groups & Low Chl-a Conditions: Mixed Flagellate, Dinoflagellate, *Phaeocystis*, Prasinophyte

Annual averages of sea ice properties illustrate the integrated effect of sea ice on phytoplankton abundance and community composition (Fig. 4.11). Since sea ice area is generally at its annual minimal during summer (or they completely disappear in most of the WAP in summer), their impact is particularly crucial for setting the overall condition for most of the growing season. For instance, 2008 had the lowest sea ice presence in entire study period (Fig. 4.11k, 4.11l, 4.11m, 4.11n), and this resulted in the highest averaged dinoflagellate and mixed flagellate relative abundance (Fig. 4.11c). Over the entire study period, the minimal sea ice total area, latest advance date, earliest retreat date, and the resulting shortest sea ice duration observed in 2008 have likely set the conditions that are favorable for dinoflagellates during the growing season in 2009 (Fig. 4.11, Table 3). This impact of sea ice on community composition has also be observed in the Northern Antarctic Peninsula, where dinoflagellates (dominated by Gymnodinium *spp.*) were found in locations with low sea ice meltwater (Mendes et al., 2018b). Their study sites were far away from the coast so there was also likely no influence of glacial meltwater. These results suggest the nutrient supply and stratification established by both glacial meltwater (Pan et al.,

2020) and sea ice meltwater (Lannuzel et al., 2007) input are crucial for the dominance of major phytoplankton groups (especially for diatoms) (Annett et al., 2010) (Vernet et al., 2008). In contrast, the lack of glacial and sea ice presence induces favorable conditions for minor groups, especially dinoflagellates (Mendes et al., 2018b) (Fig. 11).

The presence of sea ice, particularly late retreat and longer duration have also been found to be associated with shallower summer mixed layer over the WAP, which led to high chl-a concentrations dominated by diatoms (Vernet et al., 2008) (Fig. 4.2, 4.3, 4.11). The lack of water column stability as a result of the low sea ice presence in 2008, has likely led to the deepest mixed layer depth in 2009 (Fig. 4.11, Table 4.2, Table 4.3). This is another potential favorable condition for dinoflagellates. For instance, in the Baltic Sea, Klais *et al.* hypothesized that the dinoflagellate abundance is likely due to deep mixing and resuspension of dinoflagellate cysts (dinocysts) (Kremp, 2001), which led to a clear dominance of dinoflagellates during spring blooms in the central Baltic Proper that was free of sea ice (Klais et al., 2011). These resuspended dinocysts have likely been accumulated over multiple years as benthic cyst beds. The accumulated cysts are biologically viable, as shown by growth experiments with sediment cores from Koljö Fjord, where extracted dinocysts that were dormant for 87 (±12) years were able to germinate and grow (Ribeiro et al., 2011). In addition to removing the competition of diatoms and cryptophytes, the absence of sea ice also created deeper mixing (Vernet et al., 2008) and potentially facilitated dinocyst resuspension (Klais et al., 2011), hence these combined conditions likely compounded dinoflagellates' success in 2009 (Fig. 4.11c).

Mixed Flagellates is another group with an increase in averaged relative abundance during 2009 (Fig. 4.11c). This is likely due to mixed flagellates maintaining a standing stock throughout the entire year and only becoming a dominant group when the other groups are reduced. In Andvord Bay (a WAP fjord), the relative abundance of mixed flagellates increased over time when major groups (diatoms and cryptophytes) and total chl-a concentrations declined, suggesting a standing stock of mixed flagellates (Pan et al., 2020). Other studies have also pointed out that the

Southern Ocean phytoplankton community is dominated by diatoms, haptophytes, and dinoflagellates, but they are superimposed upon a background of pico- and nanophytoplankton (Wolf et al., 2013) (Wright et al., 2010). As the background standing stock, these small cryptophytes and flagellates are known to survive austral winter in Antarctica (Laybourn-Parry et al., 2005) (McKnight et al., 2000). This is attributed to their abilities to decrease respiration of their stored carbohydrate at low temperatures in the dark as demonstrated by studies under laboratory setting (Morgan & Kalff, 1975).

Phaeocystis spp. was a minor group that was fewer in both absolute concentration and relative abundance throughout the entire study period (Fig. 4.11). Other studies in the Southern Ocean found that *Phaeocystis antarctica* have a rapid photoacclimation capacity and are consistently growing in water columns with deep mixed layers; their photosynthesis is maximized when they are exposed to sunlight at the surface of the mixed layer, and then any photoinhibition incurred due to high light exposure is repaired at depth (Kropuenske et al., 2010) (Kropuenske et al., 2009). This is confirmed by the output from the AutoML model, where *Phaeocystis spp.* abundance is higher in deeper mixed layers (Fig. C1c). When *P. antarctica* is compared to diatoms (such as *Fragilariopsis cylindrus*) in the Southern Ocean, the photo-acclimation properties of *P. antarctica* allowed this group to quickly adapt to changes in irradiance, but they are slower to induce nonphotochemical quenching (Kropuenske et al., 2009) (Miller et al., 1991). Therefore, the uniform growth conditions of shallow mixed layers and sea ice presence favor diatoms; particularly in the coast zone over the WAP. Meanwhile, deeper mixed layers and open ocean conditions are more suitable for *Phaeocystis spp.* (Kropuenske et al., 2010) (Schoemann et al., 2005). These factors explain why *Phaeocystis spp.* were not abundant over the WAP, especially in the coastal zone.

Prasinophyte is also a minor phytoplankton group, and like *Phaeocystis spp.*, they did not reach high concentration or high relative abundance during the entire study period (Fig. 4.11). Both field and laboratory studies from the Arctic, where prasinophytes are more abundant in

comparison to the WAP, have demonstrated that they are more suitable to surviving in open ocean conditions (Jin et al., 2017) (Liefer et al., 2018). In comparison to diatoms, culture experiments found that prasinophytes (*Micromonas spp.*) from the Arctic showed little change in their photosynthetic pigments and structures to nitrogen stress (Liefer et al., 2018). This was also observed in the field where the Alaska Coastal Water had low nutrients and low phytoplankton biomass, and this region was dominated by pico- and nano-phytoplankton comprised of prasinophytes and other small flagellates (Jin et al., 2017). Similarly, in the WAP, prasinophytes are present in the slope and shelf zones, which are also associated with low nitrate + nitrite and phosphate concentrations (Fig. C1e, C1f). Particularly, during the summer of 1997, the highest prasinophyte abundance was found in zones with low nitrate + nitrite concentrations (Garibotti et al., 2003a). In the past, a massive prasinophyte bloom was observed north of the Antarctic peninsula during the growing season of 1989—1990 (Bird & Karl, 1991) (Vernet et al., 1991). Coincidentally, low sea ice areas were observed throughout 1989 (Stammerjohn et al., 2008b). These results suggest annual sea ice dynamics can set the environmental conditions in the following year, and in turn, significantly alter phytoplankton community composition during their growing season (Fig. 4.11).

4.5.3. Phytoplankton Community Succession over the WAP

Among the environmental variables in this study, daylight length is the environmental variable ranked in the top three as influencing community composition and abundance (Fig. 4.5d, Fig. C1d). First, daylight length is a direct assessment of the photosynthetically active radiation (PAR) over each day. We chose daylight length over PAR as a variable to assess the influence of light on phytoplankton community, because instantaneous PAR measurements at each station collected with a sensor on the CTD rosette do not represent an integrated view of the light conditions that the phytoplankton are experiencing. Cloud conditions can change shortly before or after a CTD deployment which significantly alters the correlation between PAR and phytoplankton variables. In addition, the research vessel is required to maneuver and clear a

patch of ocean to deploy the CTD instrument; this often changes the underwater light field due to the removal of brash ice coverage on the surface. Therefore, daylight length measurement can allow a more integrated view of the impact of light on phytoplankton as chosen when modeling daily primary production (Fig. 4.5d, Fig. C1d) (Behrenfeld & Falkowski, 1997) (Dierssen & Smith, 2000). Secondly, daylight length is also related to the timing of sampling since daylength changes as the season progresses and it is calculated based on latitude, between 64.5^{o} S and 68.5^{o} S (Fig. 4.1), and Julian year-day (see methods, Fig. 4.8). This means the daylight length is also an assessment of how different phytoplankton groups change over time between the beginning of January to mid-February (Fig. 4.4, 4.5). Given the abundance of each phytoplankton group varies over the entire range of daylength, these results suggest the influence of seasonal community succession on phytoplankton abundance and community composition (Fig. 4.5d, Fig. C1d, Fig. 4.8).

In the Southern Ocean coastal and shelf waters, phytoplankton blooms are predominantly composed of netplankton (cells > 20um), diatoms, haptophytes, and dinoflagellates, with a relatively constant and lower abundance of pico- and nanophytoplankton, the latter dominating in the winter (Wolf et al., 2013) (Wright et al., 2010). Generally, prior to the growing season, sea ice hosts a diverse population of active micro-algae dominated by diatoms (Kattner et al., 2004) (Petrou et al., 2010) (Stoecker et al., 2000). The retreat of sea ice seeds the surface ocean and initiates the phytoplankton succession process with a bloom of diatoms (Alvain et al., 2008) (Arrigo et al., 2008) (Garibotti et al., 2005). At this stage, sea ice meltwater induces stratification (Vernet et al., 2008) and supplies nutrients to the water column; these sea-ice edge blooms become abundant in the springtime, at the time of maximum sea ice retreat. (Lannuzel et al., 2008) (Lannuzel et al., 2007). Diatom blooms cause significant macro-nutrients and iron drawdown (Boyd, 2002), which leads to blooms of flagellates like *Phaeocystis antarctica* that can better adapt to low micro-nutrient conditions than diatoms (Kropuenske et al., 2010) (Miller et al., 1991). Since *Phaeocystis antarctica* is not heavily grazed due to its gelatinous nature (Dennett et

al., 2001), it becomes the dominant group especially in areas with deep mixing and iron-depleted water columns (Wright et al., 2010). Following the senescence of *Phaeocystis spp.* blooms, the total chl-a concentration continues to decline, and the succeeding community becomes more diverse comprised of autotrophic nanoflagellates, such as cryptophytes, dinoflagellates, prasinophytes, chlorophytes, chrysophytes and some diatoms but not abundant; this final stage of the community succession has been documented towards the end of growing season in late summer and early fall across the Southern Ocean (Kang et al., 2001) (Mills et al., 2012) (Peeken, 1997) (Wright et al., 2010). An emerging pattern from these observations is that diatoms appear to dominate the community earlier in the growing season, and flagellated phytoplankton groups are more abundant later in the season.

This pattern of phytoplankton community succession in the WAP has been documented sporadically in the past and attributed to changes in environmental conditions. In the WAP shelf waters, previous studies have also demonstrated community succession events, with the difference that the haptophyte, *Phaeocystis antarctica*, is less abundant and usually not found in its colonial form, with cryptophytes as the second most abundant group (Fig. 4.3, Fig. 4.11b) (Garibotti et al., 2005) (Kozlowski et al., 2011). For instance, both diatom and cryptophyte assemblages were observed during summers of 1996, 1997 and 1999. However, diatoms were more abundant throughout 1996, while cryptophytes were more abundant with extended spatial distribution in 1997 and 1999 (Garibotti et al., 2005). Similarly, in nearshore waters of Anvers Island, cryptophyte blooms in January followed early spring diatom blooms (Moline et al., 1996) and silicic acid drawdown (Kim et al., 2016). Southern Ocean cryptophytes are considered as competitors to diatoms for nutrients and light, so low diatom abundance can result in cryptophyte blooms (Walsh et al., 2001). Community succession was also observed in WAP fjords (Andvord Bay), however, at this location, the process began with abundant cryptophytes in late spring, followed by a massive bloom of diatoms during summer (Pan et al., 2020). In comparison, the spring cryptophyte bloom observed over the WAP shelf in 2015 followed a relatively lower sea ice

in the WAP comparing to 2014 and 2016 (Fig. 4.11k – 4.11n). These observations confirm that prior-year sea ice conditions and the presence of diatom groups would modulate cryptophyte abundance at the beginning of the growing season.

The pattern and sequence of community succession in the WAP coastal/shelf zones are likely due to the abundant re-supply of macro-nutrients and dissolved iron from glacial meltwater (Dierssen et al., 2002) (Pan et al., 2019) and sea ice meltwater (Lannuzel et al., 2008) (Mendes et al., 2018b) (Vernet et al., 2008). Meltwater content is generally higher in the coastal zone than the open ocean, and so it provides water column nutrients and stability which favor the major phytoplankton groups (Mendes et al., 2018a) (Mendes et al., 2013). This pattern of macro-nutrients is also common across the broader Southern Ocean; for instance, nitrate generally declines northwards in the open ocean from ~25 to ~20 μmol^{-1} (Deppeler & Davidson, 2017). Henley et al. have demonstrated that nutrient supply, uptake and cycling are important to high primary productivity over the WAP continental shelf (Henley et al., 2018b). During the growthing season, nutrient drawdown by the phytoplankton drives a net seasonal nitrate uptake of 1.83 mol m^{-2} yr^{-1}, equivalent to net carbon uptake of 146 g m^{-2} yr^{-1} – this high primary production is mainly supported by deep nitrate supply and results in diatom domination (Henley et al., 2018b). The strong nutrient drawdown in the uppermost surface ocean has the potential to cause short-term nitrogen limitation in the water column before it is re-supplied or re-generated (Henley et al., 2018a) (Luria et al., 2017). Interannual variability of surface nutrient inventory in the water column and utilization by phytoplankton correspond to prior-year sea ice conditions, upper ocean mixing during winter, glacial meltwater supply and sea ice melt process (Henley et al., 2018a) (Henley et al., 2018b) (Ruiz-Halpern et al., 2014) (Carrillo et al., 2004) (Prézelin et al., 2000). These nutrient processes contribute to the annual pattern of community succession (Fig. 4.11, 4.12).

We propose that the presence of melting sea ice determines community composition at the beginning of the growing season (Fig. 12), and then water column properties become more impactful to determining species abundance and composition later in the season (Fig. 4.9, 4.10,

4.11), as initially proposed by Garibotti et al. (2003b). Sea ice likely sets the overall condition for the phytoplankton community in late winter. At the beginning of the growing season, sea ice meltwater stabilizes the water column, contributes additional nutrients and seeds diatom blooms (Fig. 4.11). However, as the growing season evolves, changes in the water column properties might play a more important role in determining community composition: increasing temperature, decreasing stratification as the meltwater lens is mixed and deepened by winds, and decline in macro-nutrients by phytoplankton drawdown. This is illustrated by comparing the first 20 days of sampling to the rest of the sampling period, where temperature, salinity, and macro-nutrient concentrations are better correlated with diatom and cryptophyte abundance after 21 January (Fig. 4.9, Fig. 4.10). Other studies in the WAP have shown sea ice meltwater reaches its annual maximum generally between January and February, and it is often followed by the annual maximum of glacial meltwater concentration (Meredith et al., 2013). The occurrence of high glacial meltwater content later on in the season has also been recorded in WAP inshore waters (such as Andvord Bay and Marguerite Bay), where glacial meltwater fraction in the water column remains relatively high between late February and April (Cape et al., 2019) (Pan et al., 2019) (Meredith et al., 2008) and its presence in the WAP shelf waters is attributed to iron enrichment (Annett et al., 2017). These findings indicate that nutrient concentrations over the WAP shelf are influenced by meltwater of sea ice and glaciers, and the magnitude and timing of these meltwater processes play a critical role in determining phytoplankton community succession.

Furthermore, climate variabilities on a broader scale has been found to influence sea ice in the WAP (Stammerjohn et al., 2008b). The Southern Annular Mode (SAM) is based on the zonal pressure difference between the latitudes of 40^{o}S and 65^{o}S (Marshall, 2003). Positive SAM index (+SAM) corresponds with stronger-than-average westerlies over the mid-high latitudes (50°S – 70°S), weaker westerlies in the mid-latitudes (30°S – 50°S) (Marshall, 2003) and shift the Antarctic Circumpolar Current (ACC) towards the Antarctic continent (Talley, 2011) (Thompson et al., 2011). Strong sea ice and atmospheric responses were found when +SAM coincided with

La Niña and -SAM with El Niño (Stammerjohn et al., 2008a). In areas around the Antarctic Peninsula, this high SAM+ leads to stronger northerly winds, which causes the Peninsula to become warmer and lower sea ice concentration (Stammerjohn et al., 2008b). This process also leads to southward sea ice motion and suppresses sea ice meltwater input which allow more frequent occurrences of high glacial meltwater concentration near shore (Meredith et al., 2017). These processes have been found to alter phytoplankton size structure in the WAP (Montes-Hugo et al., 2008). These observations of climate variability impacts on sea ice concentration and the resulting phytoplankton community composition imply the WAP phytoplankton community succession is also likely susceptible to broader scale climate processes.

The transition from early-season diatom bloom to a community dominated by cryptophytes can be explained by phytoplankton environmental and physiological traits in response to changes in water column conditions. These traits allow diatoms to bloom at the beginning of the growing season and rapidly dominate the WAP phytoplankton community. Diatoms can take advantage of the melting of sea ice in early growing season which opens up surface ocean for light availability (Carvalho et al., 2020) (Joy-Warren et al., 2019). In particular, diatoms are known to favor high nutrient environments, rich in iron and nitrate (Deppeler & Davidson, 2017) (Schofield et al., 2017) (Petrou et al., 2016) (Litchman & Klausmeier, 2008). When diatoms enter the water column due to sea ice seeding (Riaux-Gobin et al., 2011) macro- and trace nutrients are high after winter replenishment due to deep convection and supply from sea ice meltwater (Meredith et al., 2013) (Lannuzel et al., 2008) (Gleitz et al., 1995) (Fig. 4.11). Diatoms can rapidly take up dissolved iron in the water column (Petrou et al., 2014) (Strzepek et al., 2011) (Boyd et al., 2000) and has a lower N:P uptake ratio of 11.9 in comparison to the average phytoplankton Redfield Ratio (Arrigo et al., 2002) indicating diatoms would not completely exhaust nitrate in the water column in spite of their rapid nutrient uptake. They are also characterized by high growth rates competing successfully under the high nutrient conditions of early spring (Smetacek, 1999) as they reproduce both sexually and asexually and cellularly divide more rapidly than other groups

(Armbrust, 2009) (Armbrust et al., 2004). We expect these early-season diatoms in the WAP to exhibit a boom-and-bust life cycle similar to those observed during the early stage of the EIFEX iron-enrichment experiment where *Fragilariopsis kerguelensis* reached concentrations of 1 g C m^{-2} (from < 0.5 g C m^{-2} before the experiment); this increase occurred over ~24 days (Assmy et al., 2013) (Smetacek et al., 2012). These early bloom diatoms are known to produce resting spores that eventually sink out of the euphotic zone (Rembauville et al., 2018) (Armbrust, 2009) (Ferrario et al., 1998) (Karentz & Smayda, 1984).

To set the stage for the cryptophyte bloom that follows, the diatoms that first dominate early-season bloom have a high C:Chl-a ratio (Mascioni et al., 2020) (Huysman et al., 2010) (Winder & Cloern, 2010). We expect their carbon excretion leads to high dissolved organic carbon (DOC) concentration in the water column, as known for the Arctic (Vernet et al., 1998) and Antarctic (Aslam et al., 2018), as well as under laboratory settings (Yan et al., 2020). After exhausting vital nutrients for rapid growth, the diatoms begin to sink out of the surface (Pan et al., 2020) (Ziegler et al., 2019) and their senescence alleviates ecological competition for the rest of the phytoplankton community. Typically, cryptophytes have a slower growth rate than diatoms (Mascioni et al., 2020); this has been measured in freshwater systems where cryptophyte growth rate maximum is ~1.2 d^{-1}, while diatoms can reach up to 1.8 d^{-1} (Edwards et al., 2012). However, cryptophytes are mixotrophic and can leverage conditions associated with high DOC (van Leeuwe et al., 2020) (Franzè et al., 2018) (Stoecker & Lavrentyev, 2018). Cryptophytes are also known for bacterivory (Roberts & Laybourn-Parry, 1999), whereby ingestion of bacteria provides cells with nutrients. For example, in two lakes at the McMurdo Dry Valleys, cryptophytes' bacterium ingestion rates varied between 0.2 and 3.6 bacteria $cell^{-1}$ h^{-1} (Roberts & Laybourn-Parry, 1999). Bacteria abundance and production in Southern Ocean waters are highest after a diatom bloom (Landa et al., 2018), thus both high DOC and bacterial production can act as food sources for cryptophytes, independent of other factors present. However, cryptophytes have also been found to adapt to lower dissolved iron conditions, as expected after diatoms have consumed dissolved

iron (Vernet et al., 2020) (Pan et al., 2020). In addition, light availability in the middle of the austral summer is higher in comparison to earlier in the growing season (Fig. 4.8). Cryptophytes with more variety of photosynthetic and photo-protective pigments are found to absorb light more effectively under a wide range of light conditions (Brody et al., 1992) (Gieskes & Kraay, 1983). The presence of freshwater at the surface induces stratification and a “meltwater lens” (Dierssen et al., 2002). Since cryptophytes also have physiological traits to adapt to a high light environment, they can take advantage of these environmental conditions and dominate the phytoplankton community after the initial diatom bloom (Fig. 4.12).

In summary, the phytoplankton community composition in the WAP follows a clear succession pattern (Fig. 4.5, Fig. C1, Fig. 4.12), where community succession starts with diatoms seeded from sea ice that supports rapid growth creating blooms of diatom assemblages. This is followed by cryptophytes that sometimes also bloom. In nearshore waters, a second summer diatom bloom can occur in January, as seen in Andvord Bay, near Anverse Island, and in other WAP fjords (Fig. 4.12a) (Pan et al., 2020) (van Leeuwe et al., 2020). In some cases, before the final stage in late summer, a new assemblage of diatoms can be found (Fig. 4.5d). This assemblage of diatoms is often associated with ice-free conditions (Garibotti et al., 2005) and features highly silicified diatom frustules, such as the transition to *Fragilariopsis spp.* observed during EIFEX (Assmy et al., 2013). The succession ends with a transition to minor phytoplankton flagellate groups as total chl-a concentration declines and winter sets in (Pan et al., 2020). However, if sea ice presence is low prior to the growing season (especially when multiple factors are compounded, such as late sea ice advance and early sea ice retreat, resulting in shorter duration and smaller total area), then the entire succession process begins at an advanced stage, where the early sea-ice edge bloom is not present, and an assemblage of cryptophytes can dominate (Pan et al., 2020) (Garibotti et al., 2005). In more extreme cases, such as the sea ice minimum in 2008 observed in our study, the succession in 2008-2009 growing season begins early (presumably without diatoms), and in January, we already observe the final stage of the

seasonal succession with minor phytoplankton groups. Alternatively, these minor phytoplankton groups persist throughout the entire growing season resulting in low total chl-a concentration (Fig. 4.11a, 4.11c, Fig. 4.12b).

4.6. Acknowledgements

Chapter 4 is currently being prepared for publication as: Pan, B.J., Vernet, M., Barton, A.D. and Orona, A.J. Environmental Drivers Modulate Phytoplankton Community Seasonal Succession in the Western Antarctic Peninsula. The dissertation author was the primary investigator and first author of this paper.

Data from the Palmer LTER data repository were supported by Office of Polar Programs, NSF Grants OPP-9011927, OPP-9632763 and OPP-0217282. Data used in this study were retrieved from the PAL LTER DataZoo (oceaninformatics.ucsd.edu/datazoo). The authors of this manuscript would also like to acknowledge the United States Antarctic Program (USAP), its research vessel captains, crews and contractors who participated in previous Palmer LTER campaigns, as well as past and present PIs of the Palmer LTER Program.

4.7. Figures and Tables

Table 4.1. Water column physical, hydrographic, and nutrient properties in the Western Antarctic Peninsula between 1995 and 2016.

		Year																	
regions		1995	1996	1999	2000	2001	2003	2004	2005	2006	2007	2008	2009	2011	2013	2014	2015	2016	Total Avg.
coast	Temperature (C)	0.35	0.00	0.56	0.34	1.83	0.72	1.22	-0.39	0.14	1.50	1.09	0.93	1.08	0.98	0.09	-0.62	-0.83	**0.53**
	Salinity (PSU)	33.24	33.08	33.52	33.30	33.59	33.47	33.49	32.94	32.93	33.22	33.51	33.74	33.40	33.51	32.96	33.02	33.16	**33.30**
	Mixed Layer Depth (m)	47.47	35.37	47.69	33.55	39.92	49.46	42.28	21.62	27.06	24.69	24.48	53.52	29.74	24.14	37.72	28.35	31.10	**35.19**
	Nitrate + Nitrite (uM)	22.80	15.69	17.05	20.94	15.44	21.80	18.86	19.85	17.69	9.82	16.27	23.41	9.26	21.06	9.94	16.14	21.64	**17.51**
	Phosphate (uM)	1.07	1.22	1.35	1.46	1.03	1.37	1.23	1.49	1.20	1.10	1.43	1.40	0.53	1.39	0.54	1.18	1.40	**1.20**
	Silicic Acid (uM)	80.64	69.81	53.87	73.46	56.54	74.23	67.45	72.44	66.82	69.20	68.64	68.00	48.95	60.98	37.11	49.88	64.99	**63.71**
shelf	Temperature (C)	0.33	1.08	0.71	0.78	1.40	0.97	0.88	0.74	0.91	1.35	1.16	0.51	0.70	0.90	-0.73	-0.06	-1.01	**0.62**
	Salinity (PSU)	33.56	33.57	33.78	33.64	33.77	33.69	33.67	33.56	33.30	33.69	33.90	33.98	33.87	33.46	32.95	33.31	33.20	**33.58**
	Mixed Layer Depth (m)	58.84	39.31	71.77	44.00	45.46	47.45	58.62	34.30	27.79	53.20	53.72	76.49	74.17	29.45	17.32	30.97	27.80	**46.51**
	Nitrate + Nitrite (uM)	23.74	20.26	20.54	22.69	20.36	23.22	20.81	21.68	20.20	16.62	20.01	26.47	20.48	21.40	18.52	19.31	23.35	**21.16**
	Phosphate (uM)	1.29	1.56	1.46	1.54	1.27	1.47	1.31	1.72	1.30	1.44	1.58	1.61	1.14	1.39	1.27	1.38	1.55	**1.43**
	Silicic Acid (uM)	70.16	65.36	48.04	71.05	57.87	65.11	58.98	71.25	65.76	70.97	60.86	63.58	49.73	54.19	43.12	48.49	60.67	**60.31**
slope	Temperature (C)	0.71	1.28	0.94	1.08	1.25	1.14	0.85	0.81	1.82	1.62	0.57	0.48	0.45	0.23	-0.36	0.80	-0.53	**0.77**
	Salinity (PSU)	33.62	33.75	33.85	33.86	33.77	33.68	33.58	33.83	33.68	33.83	33.90	34.01	33.87	33.42	33.04	33.66	33.10	**33.67**
	Mixed Layer Depth (m)	61.92	55.18	58.61	58.11	46.73	40.84	40.99	62.96	33.66	45.82	58.52	89.00	72.09	30.69	25.08	31.26	25.74	**49.25**
	Nitrate + Nitrite (uM)	24.76	23.05	19.34	23.98	22.01	24.97	21.77	25.56	20.37	18.51	21.89	25.50	23.15	24.63	24.23	24.55	23.62	**23.05**
	Phosphate (uM)	1.27	1.68	1.42	1.58	1.35	1.48	1.31	1.86	1.41	1.40	1.65	1.51	1.25	1.52	1.63	1.69	1.59	**1.51**
	Silicic Acid (uM)	49.59	55.23	33.37	50.04	37.73	43.34	41.90	62.26	51.42	32.61	41.61	60.51	31.09	42.30	33.15	38.57	53.18	**44.58**

Table 4.2. The chlorophyll-a concentrations of phytoplankton taxonomic groups in the Western Antarctic Peninsula.

		Year																	
regions		1995	1996	1999	2000	2001	2003	2004	2005	2006	2007	2008	2009	2011	2013	2014	2015	2016	Total Avg.
coast	Avg. Total Chl	1.940	7.233	3.940	2.380	1.737	0.755	0.851	1.479	4.067	3.257	1.110	0.441	2.776	1.088	3.741	1.931	2.849	**2.446**
	Avg. Diatom	0.803	6.658	2.706	0.015	1.175	0.164	0.119	0.980	3.576	1.351	0.419	0.000	2.427	0.272	2.975	1.082	2.545	**1.604**
	Avg. Crypto	0.761	0.284	0.890	1.583	0.057	0.429	0.451	0.399	0.119	0.420	0.580	0.023	0.154	0.391	0.173	0.411	0.065	**0.423**
	Avg. Mixflag	0.288	0.083	0.159	0.544	0.465	0.087	0.177	0.054	0.113	0.382	0.045	0.169	0.062	0.161	0.108	0.077	0.034	**0.177**
	Avg. Phaeocys	0.016	0.057	0.104	0.000	0.021	0.053	0.074	0.025	0.065	0.091	0.056	0.011	0.036	0.184	0.293	0.213	0.058	**0.080**
	Avg. Dino	0.015	0.014	0.007	0.107	0.001	0.004	0.004	0.004	0.057	0.037	0.001	0.220	0.084	0.004	0.041	0.023	0.072	**0.041**
	Avg. Prasino	0.058	0.136	0.074	0.132	0.019	0.019	0.025	0.017	0.138	0.975	0.009	0.017	0.013	0.076	0.152	0.124	0.076	**0.121**
shelf	Avg. Total Chl	1.024	0.993	0.649	0.830	0.997	0.369	0.454	0.884	2.147	0.746	0.994	0.235	0.566	0.841	1.389	0.689	1.139	**0.879**
	Avg. Diatom	0.219	0.288	0.128	0.005	0.581	0.050	0.106	0.058	1.713	0.466	0.107	0.000	0.410	0.262	1.016	0.280	0.602	**0.370**
	Avg. Crypto	0.613	0.362	0.248	0.552	0.043	0.195	0.148	0.678	0.027	0.088	0.736	0.004	0.058	0.222	0.083	0.127	0.369	**0.268**
	Avg. Mixflag	0.148	0.191	0.164	0.190	0.247	0.053	0.077	0.081	0.190	0.129	0.077	0.083	0.057	0.153	0.089	0.110	0.069	**0.124**
	Avg. Phaeocys	0.020	0.071	0.091	0.000	0.079	0.061	0.084	0.048	0.131	0.040	0.055	0.006	0.019	0.152	0.088	0.093	0.038	**0.063**
	Avg. Dino	0.007	0.045	0.007	0.037	0.000	0.003	0.012	0.008	0.048	0.015	0.006	0.131	0.009	0.000	0.017	0.019	0.015	**0.022**
	Avg. Prasino	0.016	0.037	0.011	0.046	0.047	0.007	0.027	0.011	0.038	0.008	0.011	0.011	0.012	0.052	0.097	0.059	0.046	**0.032**
slope	Avg. Total Chl	0.374	0.407	0.220	0.407	0.183	0.126	0.226	0.336	0.712	0.300	0.164	0.165	0.205	0.273	0.279	0.262	0.589	**0.308**
	Avg. Diatom	0.106	0.160	0.115	0.003	0.090	0.049	0.055	0.059	0.456	0.110	0.064	0.001	0.138	0.054	0.078	0.090	0.161	**0.105**
	Avg. Crypto	0.154	0.032	0.011	0.271	0.007	0.013	0.052	0.170	0.029	0.020	0.007	0.001	0.005	0.040	0.030	0.024	0.224	**0.064**
	Avg. Mixflag	0.083	0.092	0.040	0.093	0.040	0.031	0.038	0.062	0.098	0.046	0.032	0.066	0.011	0.087	0.076	0.067	0.102	**0.063**
	Avg. Phaeocys	0.022	0.075	0.042	0.000	0.030	0.023	0.056	0.020	0.107	0.116	0.044	0.007	0.045	0.049	0.042	0.038	0.040	**0.045**
	Avg. Dino	0.004	0.034	0.005	0.018	0.000	0.004	0.007	0.020	0.016	0.006	0.010	0.082	0.003	0.001	0.007	0.009	0.012	**0.014**
	Avg. Prasino	0.005	0.014	0.008	0.023	0.016	0.007	0.018	0.005	0.007	0.002	0.008	0.007	0.003	0.041	0.046	0.035	0.050	**0.017**
Total Avg. by Year	Avg. Total Chl	**1.112**	**2.878**	**1.603**	**1.206**	**0.973**	**0.417**	**0.510**	**0.900**	**2.309**	**1.434**	**0.756**	**0.280**	**1.182**	**0.734**	**1.803**	**0.961**	**1.526**	**1.211**
	Avg. Diatom	**0.376**	**2.369**	**0.983**	**0.008**	**0.615**	**0.088**	**0.093**	**0.366**	**1.915**	**0.642**	**0.197**	**0.000**	**0.992**	**0.196**	**1.356**	**0.484**	**1.103**	**0.693**
	Avg. Crypto	**0.509**	**0.226**	**0.383**	**0.802**	**0.036**	**0.212**	**0.217**	**0.416**	**0.058**	**0.176**	**0.441**	**0.009**	**0.072**	**0.218**	**0.095**	**0.187**	**0.219**	**0.252**
	Avg. Mixflag	**0.173**	**0.122**	**0.121**	**0.275**	**0.251**	**0.057**	**0.097**	**0.065**	**0.134**	**0.186**	**0.051**	**0.106**	**0.043**	**0.134**	**0.091**	**0.085**	**0.068**	**0.121**
	Avg. Phaeocys	**0.019**	**0.067**	**0.079**	**0.000**	**0.043**	**0.046**	**0.071**	**0.031**	**0.101**	**0.082**	**0.052**	**0.008**	**0.034**	**0.129**	**0.141**	**0.115**	**0.045**	**0.062**
	Avg. Dino	**0.009**	**0.031**	**0.006**	**0.054**	**0.000**	**0.004**	**0.008**	**0.011**	**0.041**	**0.020**	**0.006**	**0.144**	**0.032**	**0.002**	**0.022**	**0.017**	**0.033**	**0.026**
	Avg. Prasino	**0.026**	**0.063**	**0.031**	**0.067**	**0.027**	**0.011**	**0.024**	**0.011**	**0.061**	**0.328**	**0.009**	**0.012**	**0.009**	**0.056**	**0.099**	**0.073**	**0.057**	**0.057**

Table 4.3. Sea ice properties in the Western Antarctic Peninsula.

Year	Monthly Sea Ice Extent (km^2)	Monthly Sea Ice Area (km^2)	Prior Year Annual Sea Ice Extent (km^2)	Prior Year Annual Sea Ice Area (km^2)	Prior Year Annual Sea Ice Advance Date	Prior Year Annual Sea Ice Retreat Date	Prior Year Annual Sea Ice Duration
1995	43,183	22,570	125,911	98,828	141	354	214
1996	61,853	40,138	121,593	94,837	139	353	215
1999	7,703	3,081	102,169	61,797	151	324	175
2000	53,141	29,914	99,988	75,104	175	345	171
2001	49,005	19,615	107,138	76,605	162	345	185
2003	34,323	20,889	137,179	105,090	121	352	233
2004	23,577	9,543	114,893	82,900	150	346	197
2005	115,319	82,055	118,564	99,009	156	377	223
2006	71,086	49,953	141,748	111,709	120	359	240
2007	17,963	8,416	114,776	81,388	145	328	184
2008	8,385	2,766	86,664	56,215	168	313	145
2009	11,733	5,182	71,209	43,571	175	296	121
2011	14,841	7,045	82,046	53,553	158	301	144
2013	34,741	12,485	115,212	83,302	155	354	200
2014	111,640	52,246	126,965	104,648	147	382	237
2015	39,095	24,067	128,271	92,193	149	357	209
2016	127,423	74,204	131,672	107,644	135	387	253
Total Avg.	**45,423**	**26,092**	**115,692**	**86,085**	**147**	**345**	**199**

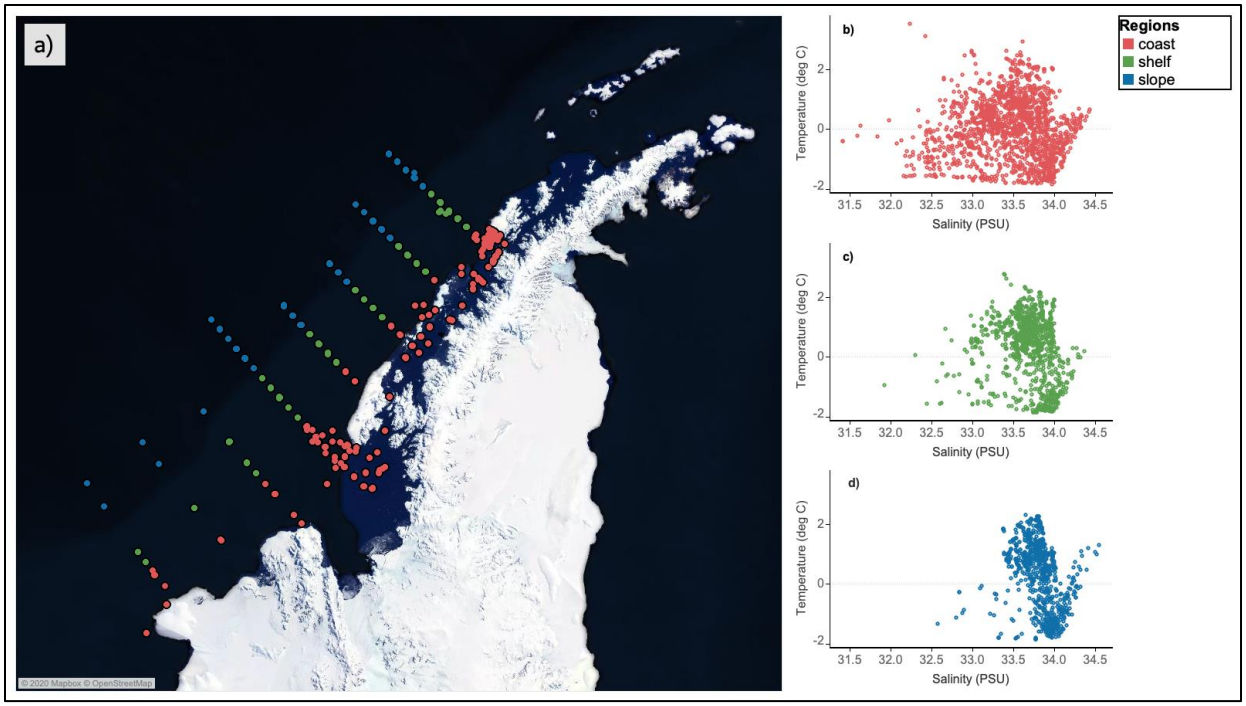

Figure 4.1. Map of the Western Antarctic Peninsula with sampling stations categorized by their geography. (a) The coastal region is associated with areas close to shore and shallow bathymetry (red). The shelf zone is the area directly over the western peninsula's shelf (green). The slope zone is off the shelf and generally associated with deeper bathymetry (blue). (b, c, d) Temperature-Salinity diagrams for each of the coastal, shelf and slope zones, respectively (see methods and Martinson et al. 2008 for more details on definition of the three zones). Satellite imagery retrieved from NASA/USGS Landsat.

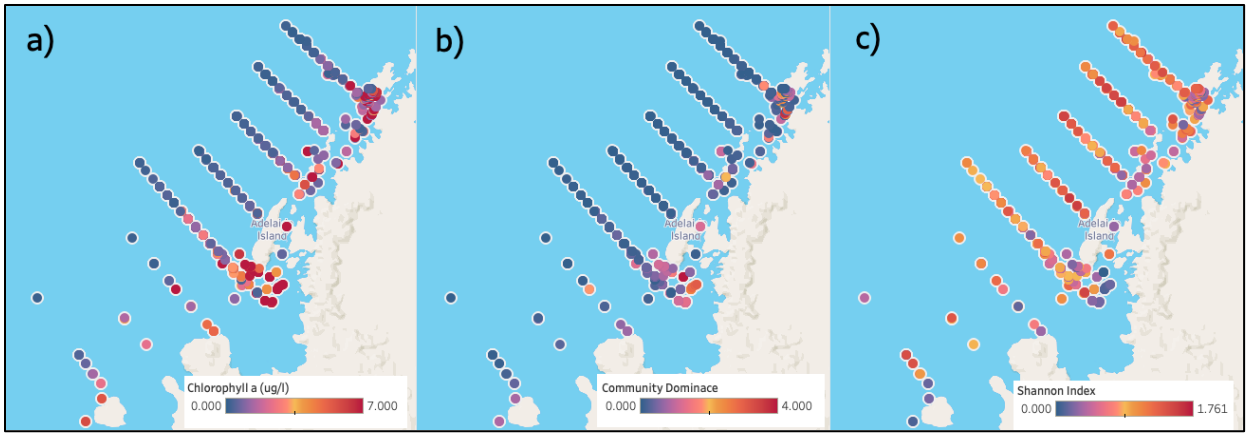

Figure 4.2. Surface samples collected annually over the entire study period from beginning of January to mid-February (1994-2016; < 10m depth). (a) Average phytoplankton total chlorophyll-a concentration, a proxy for total biomass. (b) Community dominance index where high values indicate higher relative abundance of fewer groups. (c) Shannon diversity index where high values indicate high community diversity.

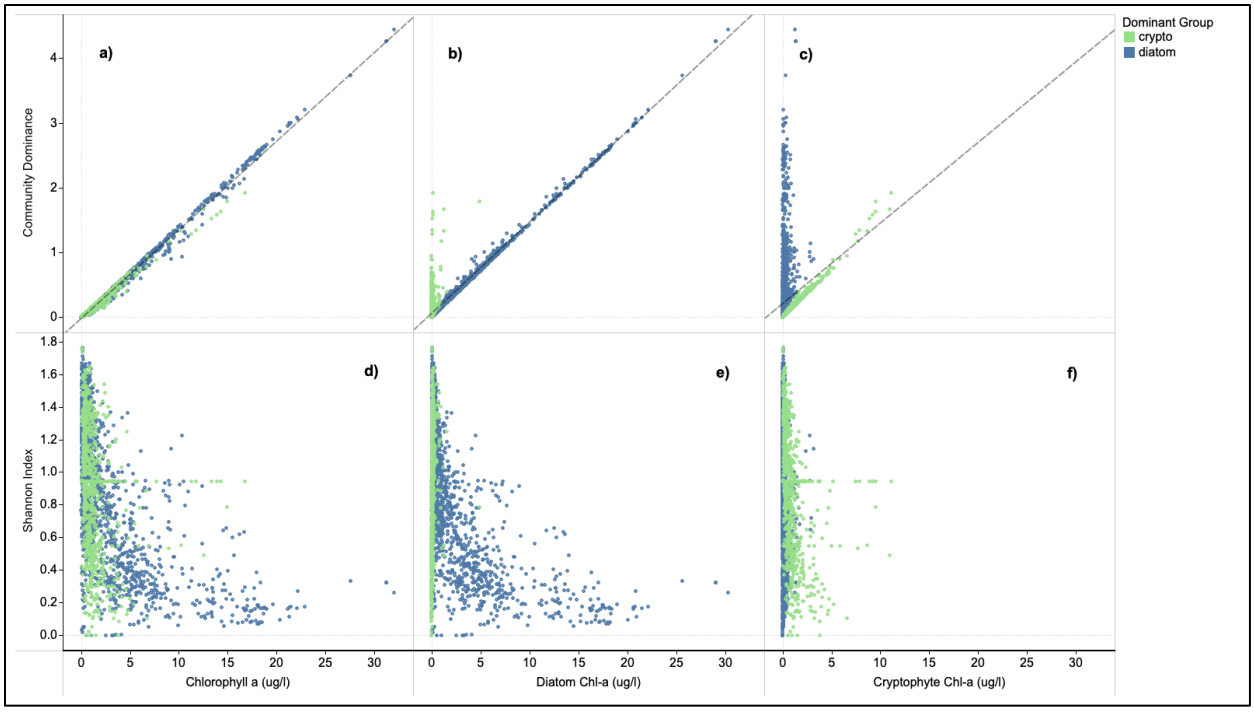

Figure 4.3. Phytoplankton biomass indicated by (a, d) total chlorophyll-a concentrations and the two major phytoplankton groups, (b, e) diatoms and (c, f) cryptophytes and their relationships with (a, b, c) community dominance and (d, e, f) the Shannon diversity index. The color of data points indicates the group with the highest relative abundance in each sample.

Figure 4.4. The ranking of environmental variables based on machine learning models to predict chlorophyll-a concentration of each of the six phytoplankton groups analyzed in this study: a) diatoms, b) cryptophytes, c) mixes flagellates, d) Phaeocystis spp., d) dinoflagellates and f) prasinophytes. Variable importance is illustrated by the bar graph, and it represents the percentage of variance in the model that is explained by each environmental variable (x-axis).

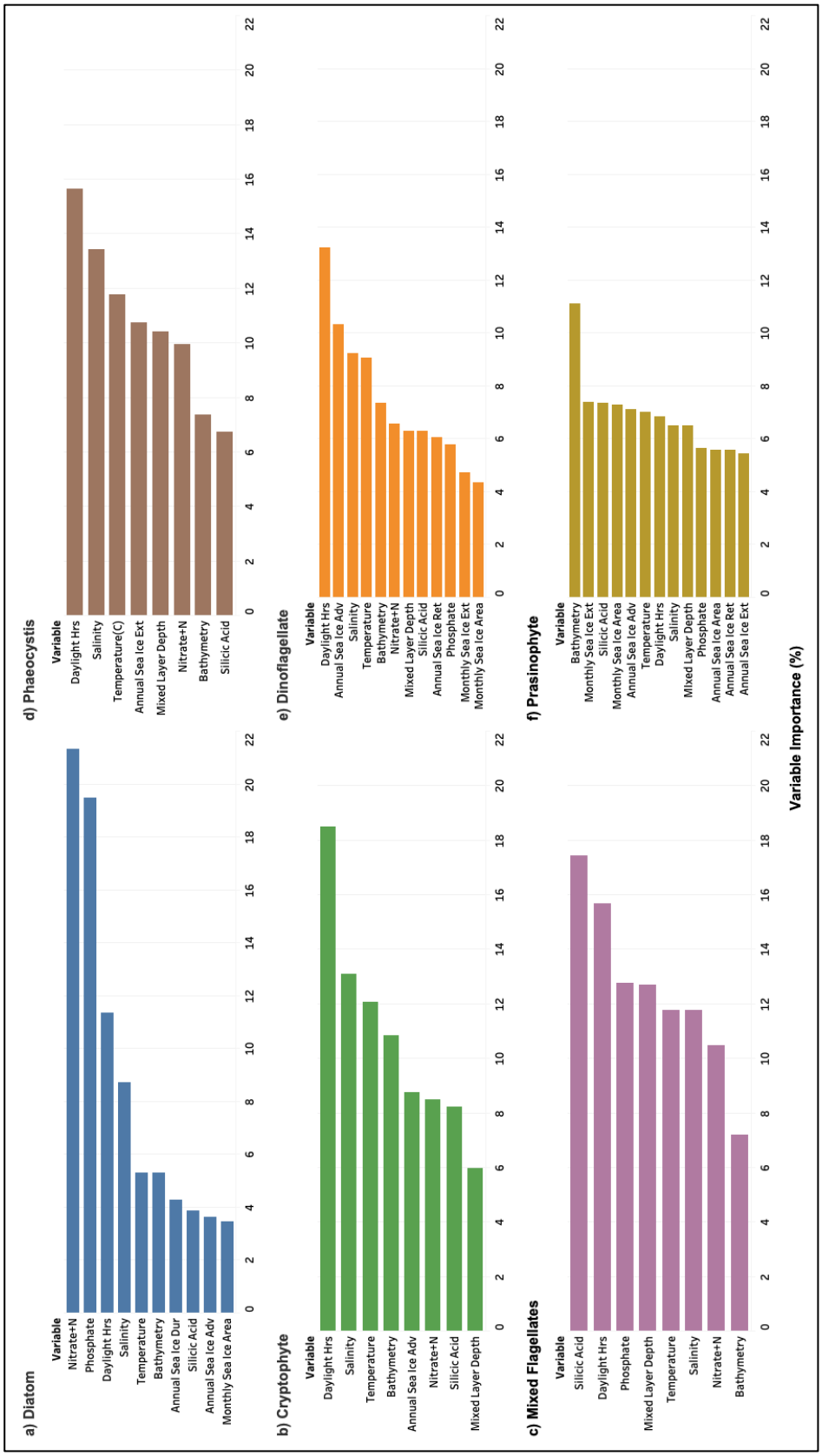
a) Diatom
Variable
Nitrate+N
Phosphate
Daylight Hrs
Salinity
Temperature
Bathymetry
Annual Sea Ice Dur
Silicic Acid
Annual Sea Ice Adv
Monthly Sea Ice Area
b) Cryptophyte
Variable
Daylight Hrs
Salinity
Temperature
Bathymetry
Annual Sea Ice Adv
Nitrate+N
Silicic Acid
Mixed Layer Depth
c) Mixed Flagellates
Variable
Silicic Acid
Daylight Hrs
Phosphate
Mixed Layer Depth
Temperature
Salinity
Nitrate+N
Bathymetry
d) Phaeocystis
Variable
Daylight Hrs
Salinity
Temperature(C)
Annual Sea Ice Ext
Mixed Layer Depth
Nitrate+N
Bathymetry
Silicic Acid
e) Dinoflagellate
Variable
Daylight Hrs
Annual Sea Ice Adv
Salinity
Temperature
Bathymetry
Nitrate+N
Mixed Layer Depth
Silicic Acid
Annual Sea Ice Ret
Phosphate
Monthly Sea Ice Ext
Monthly Sea Ice Area
f) Prasinophyte
Variable
Bathymetry
Monthly Sea Ice Ext
Silicic Acid
Monthly Sea Ice Area
Annual Sea Ice Adv
Temperature
Daylight Hrs
Salinity
Mixed Layer Depth
Phosphate
Annual Sea Ice Area
Annual Sea Ice Ret
Annual Sea Ice Ext
0 2 4 6 8 10 12 14 16 18 20 22
Variable Importance (%)

Figure 4.5. Partial dependence plots depicting machine learning models' mean response expressed in targeted taxonomic chlorophyll-a concentration; line colors represent different phytoplankton groups. The y-axes represent the models' mean responses in each group's chlorophyll-a concentration to changes in values of the environmental variables on x-axes: (a) temperature, (b) salinity, (c) mixed layer depth, (d) daylight hours, (e) nitrate + nitrite, (f) phosphate, (g) silicic acid, and (h) bathymetry. The daylight hours axis is reversed to reflect progression over time from mid- to late summer (see methods and Figure 4.8).

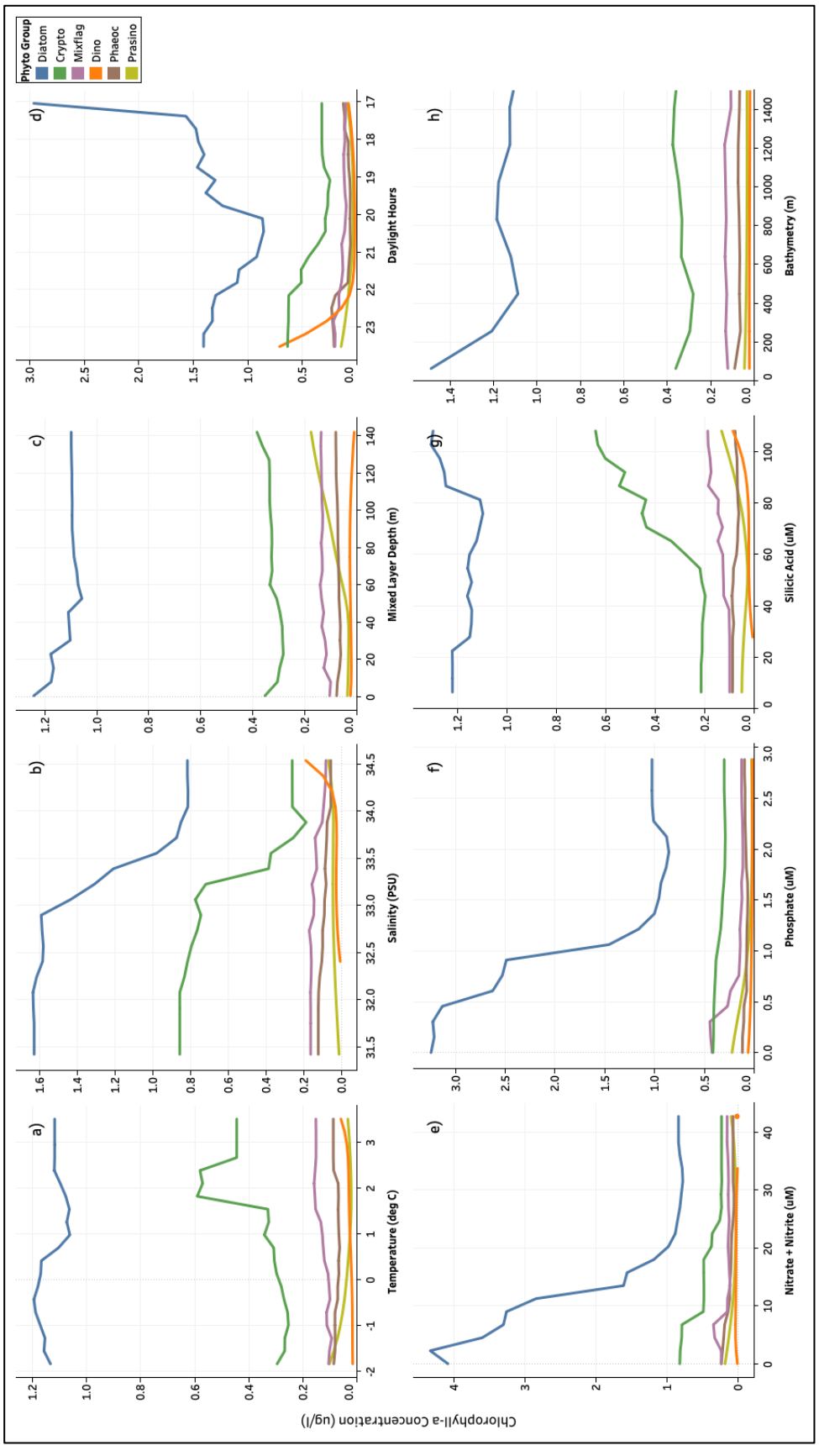
Phyto Group
Diatom
Crypto
Mixflag
Dino
Phaeoc
Prasino
Chlorophyll-a Concentration (ug/l)
a)
Temperature (deg C)
b)
Salinity (PSU)
c)
Mixed Layer Depth (m)
d)
Daylight Hours
e)
Nitrate + Nitrite (uM)
f)
Phosphate (uM)
g)
Silicic Acid (uM)
h)
Bathymetry (m)

Figure 4.6. Partial dependence plots depicting machine learning models' mean response expressed in targeted taxonomic chlorophyll-a concentration; line colors represent different phytoplankton groups. The y-axes represent the models' mean responses in each group's chlorophyll-a concentration to changes in sea ice variables on x-axes: (a) monthly sea ice extent, (b) monthly sea ice area, (c) annual sea ice extent, (d) annual sea ice area, (e) prior-year annual sea ice advance date, (f) prior-year annual sea ice retreat date, (g) prior-year sea ice duration.

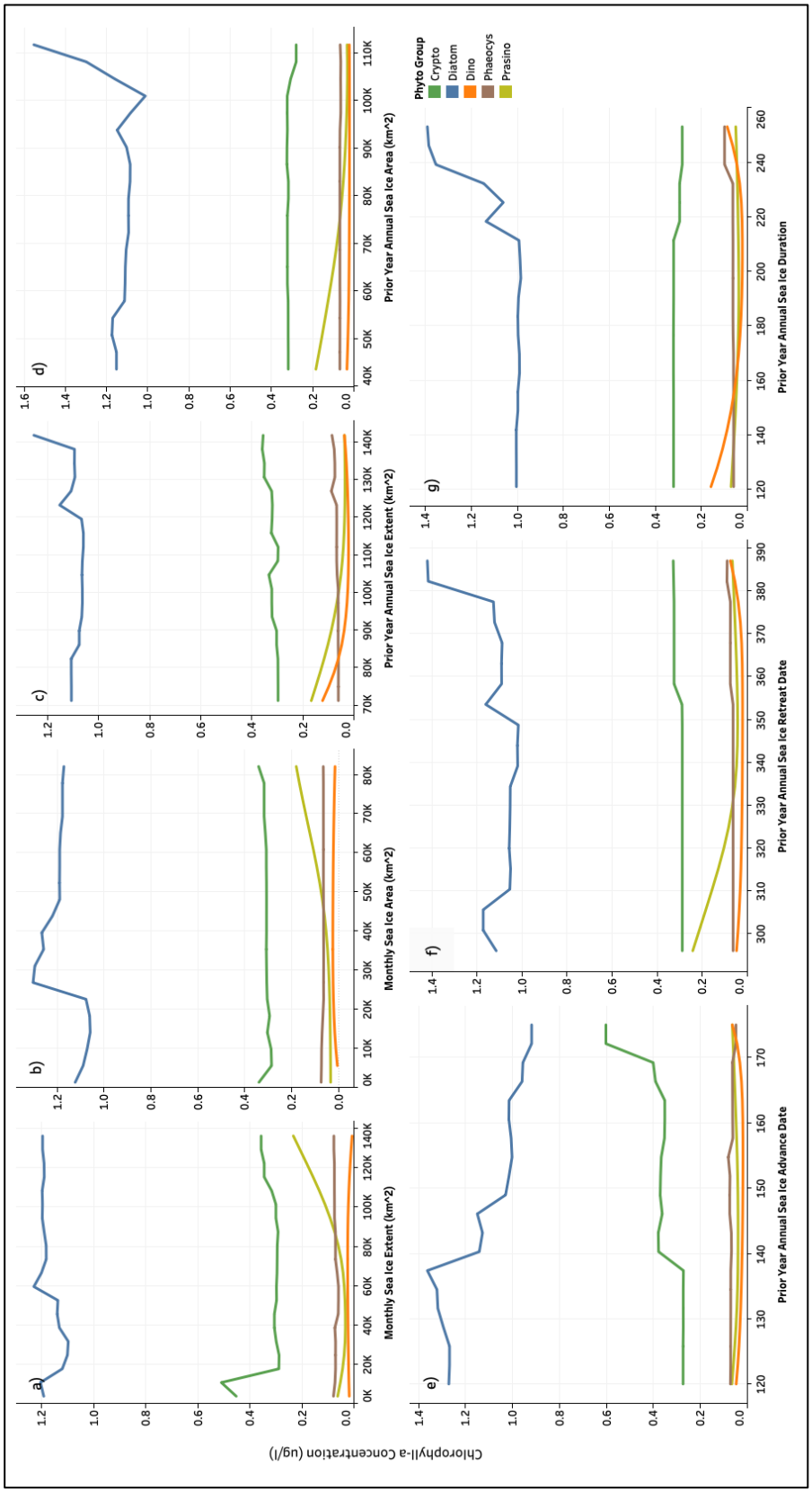
Chlorophyll-a Concentration (ug/l)
a)
b)
c)
d)
e)
f)
g)
Monthly Sea Ice Extent (km^2)
Monthly Sea Ice Area (km^2)
Prior Year Annual Sea Ice Extent (km^2)
Prior Year Annual Sea Ice Area (km^2)
Prior Year Annual Sea Ice Advance Date
Prior Year Annual Sea Ice Retreat Date
Prior Year Annual Sea Ice Duration
Phyto Group
Crypto
Diatom
Dino
Phaeocys
Prasino

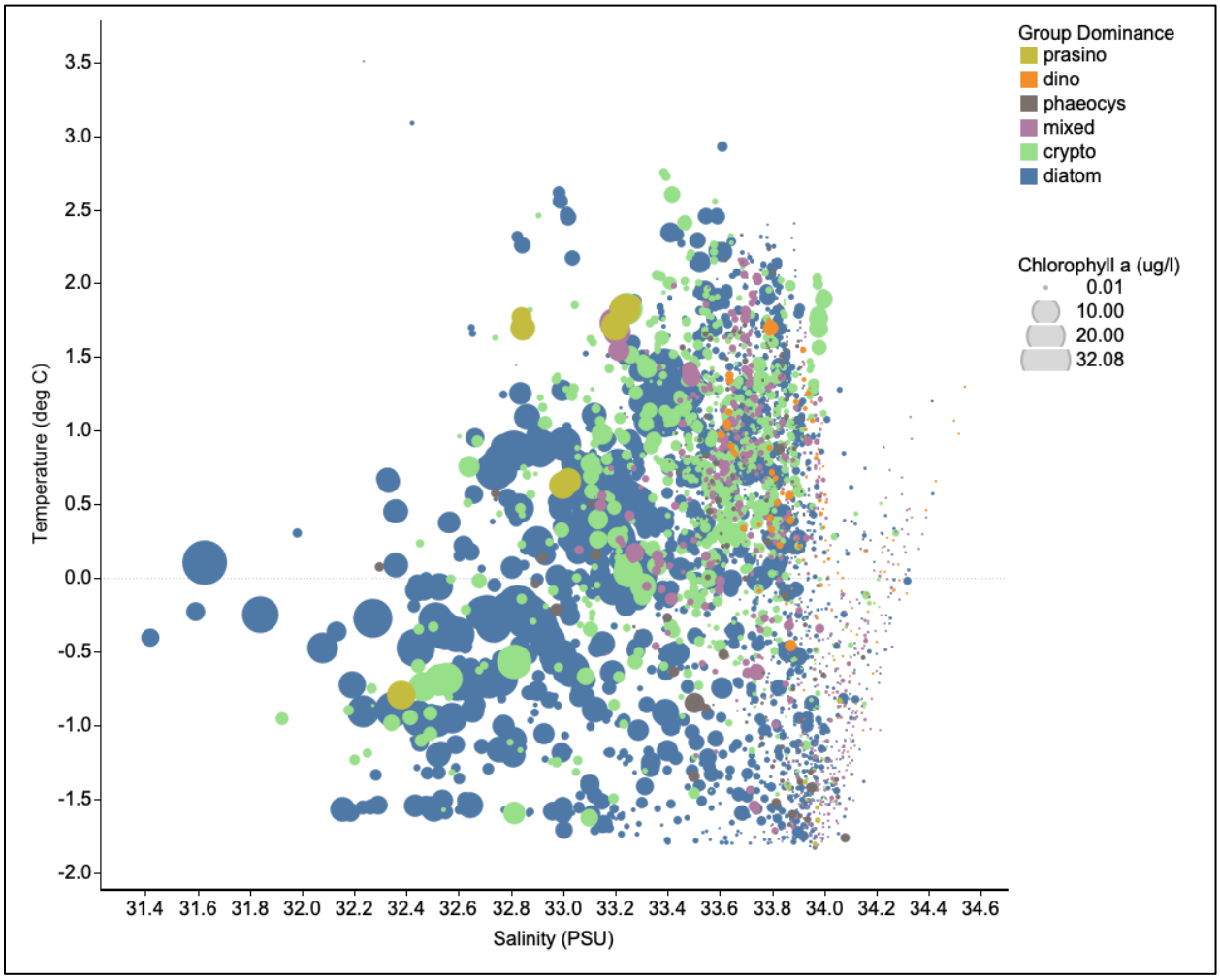

Figure 4.7. Phytoplankton taxa abundance in a temperature-salinity diagram. The color of data points indicates the group with the highest relative abundance in each sample.

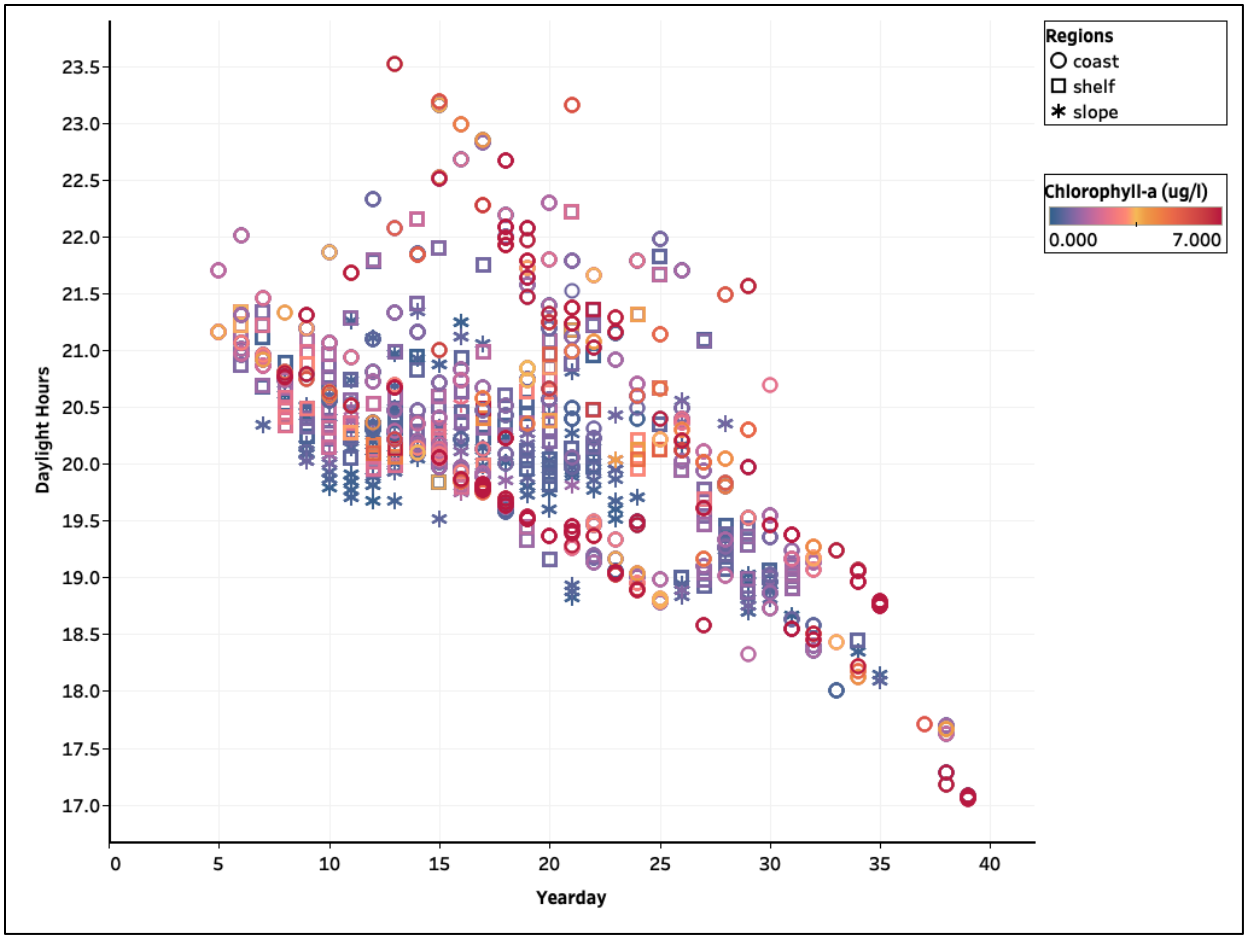

Figure 4.8. The correlation between daylight hours and Julian yearday, indicates that daylight hour reflects both the overall light condition and the timing of each sample collection.

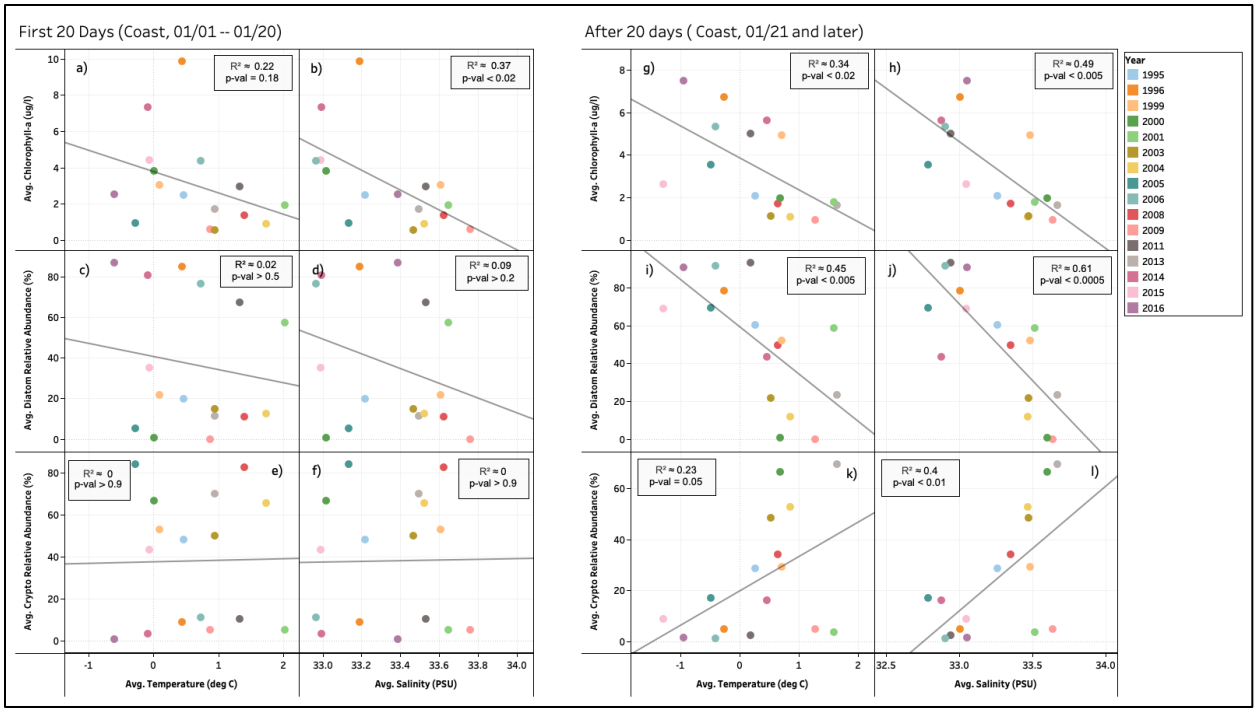

Figure 4.9. Comparison of phytoplankton and water column properties between two sampling periods of each year. Annual averages of total chlorophyll-a concentration, diatom and cryptophyte relative abundance, and their correlations with annual average temperature and salinity within the mixed layer in the coastal zone, (a--f) during the first 20 days of the year (1-20 January), and (g--l) after 20 days (after 21 January).

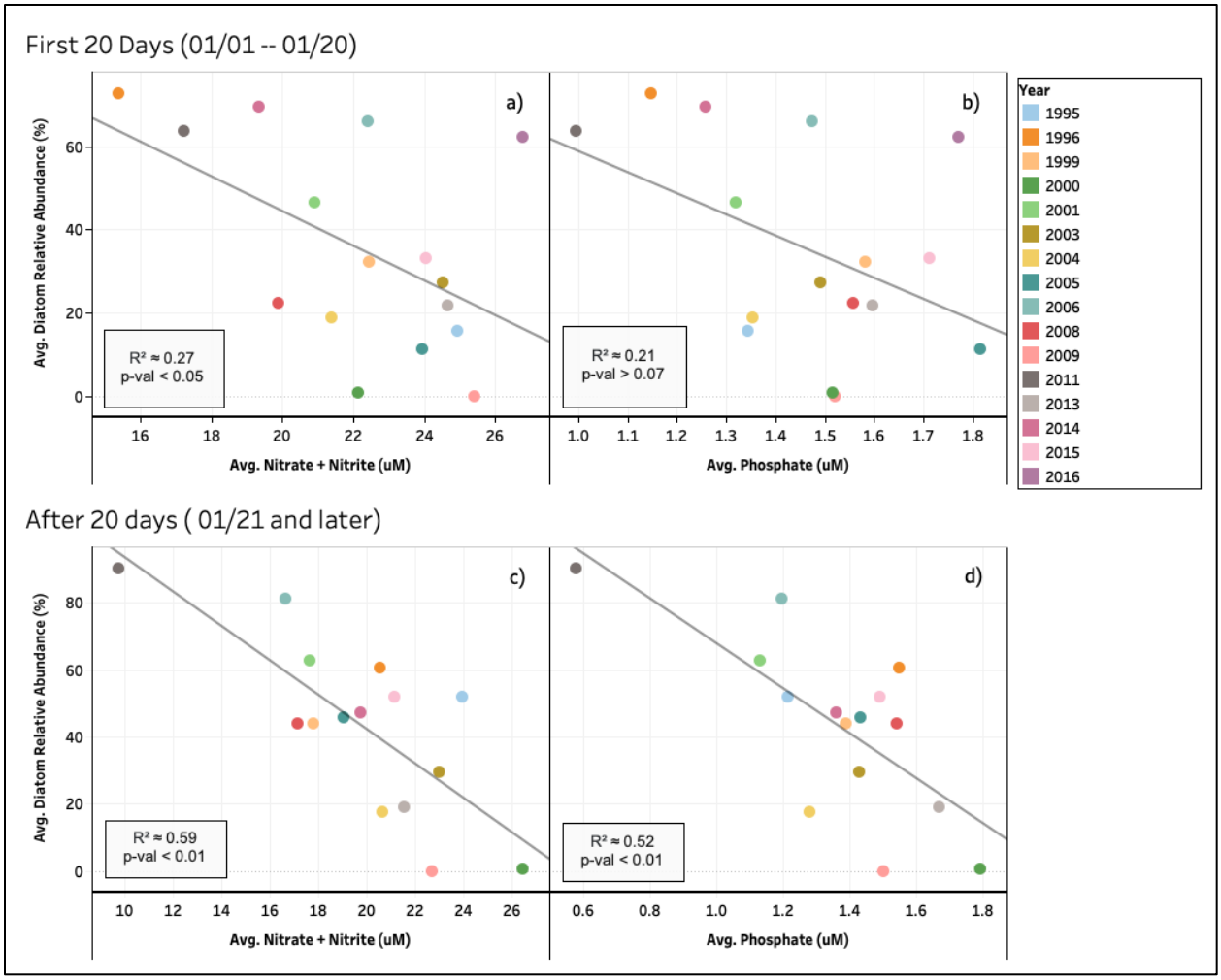

Figure 4.10. Comparison of phytoplankton and macro-nutrient concentrations between two sampling periods of each year. Annual averages of diatom, and cryptophyte relative abundance and their correlations with nitrate + nitrite and phosphate concentrations within the euphotic layer in the coastal zone, (a, b) during the first 20 days of the year (1—20 January), and (c, d) after 20 days (after 20 January).

Figure 4.11. Annual averages of properties associated with phytoplankton community and water column variables within the mixed layer, as well as prior-year sea ice conditions. The annual averages of these properties illustrate interannual variability and how they are related to one another. Panels a—d depict the phytoplankton community between 1994 and 2016: (a) total chlorophyll-a concentration, (b) relative abundance of major groups, diatom and cryptophyte, (c) relative abundance of minor groups, mixed flagellate, dinoflagellate, Phaeocystis, and prasinophyte. (d) community dominance and Shannon diversity index. Similarly, panels e—j depict the interannual variability of water column properties that are important to phytoplankton community. Panels k—n depict the averaged conditions of prior-year sea ice conditions in the WAP: (k) total area, (l) advance date and (m) retreat date in Julian days, and (n) sea ice duration (days between advance and retreat).

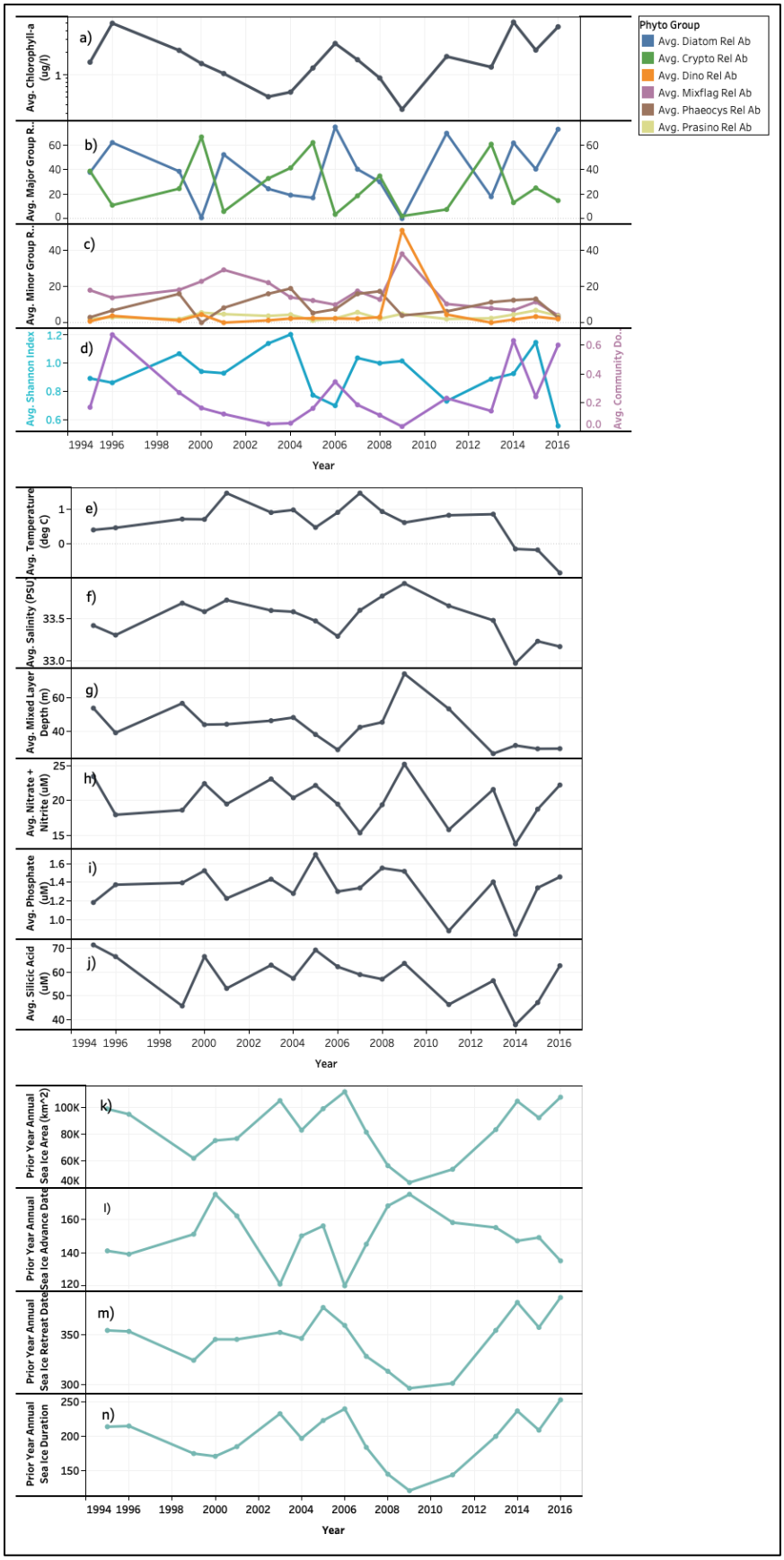
Phyto Group
Avg. Diatom Rel Ab
Avg. Crypto Rel Ab
Avg. Dino Rel Ab
Avg. Mixflag Rel Ab
Avg. Phaeocys Rel Ab
Avg. Prasino Rel Ab
a)
b)
c)
d)
e)
f)
g)
h)
i)
j)
k)
l)
m)
n)
Avg. Chlorophyll-a (ug/l)
Avg. Major Group R..
Avg. Minor Group R..
Avg. Shannon Index
Avg. Community Do..
Avg. Temperature (deg C)
Avg. Salinity (PSU)
Avg. Mixed Layer Depth (m)
Avg. Nitrate + Nitrite (uM)
Avg. Phosphate (uM)
Avg. Silicic Acid (uM)
Prior Year Annual Sea Ice Area (km^2)
Prior Year Annual Sea Ice Advance Date
Prior Year Annual Sea Ice Retreat Date
Prior Year Annual Sea Ice Duration
1994 1996 1998 2000 2002 2004 2006 2008 2010 2012 2014 2016
Year

Figure 4.12. Conceptual diagram illustrating bloom phenology of the phytoplankton taxonomic groups over the Western Antarctic Peninsula. Main groups described in this study are: diatom, cryptophyte, mixed flagellate, dinoflagellate, haptophyte *Phaeocystis spp.*, and prasinophyte. Diatom and cryptophyte are major groups associated with high chlorophyll-a concentrations, while the other taxa are minor groups associated with low chlorophyll-a concentrations (Figure 3). The color gradient represents total chlorophyll-a concentration, and it also illustrates the different stages of community succession. Panel a depicts the community succession under nominal sea ice conditions, and panel b depicts anomalously low sea ice conditions where the succession begins in an advanced stage and persists during the rest of the growing season. In addition to the results from this study, this diagram also adopted community succession information from Arrigo et al. (2008) and Petrou et al. (2016) which focus on the boarder Southern Ocean community succession. The transition between diatoms and cryptophytes due to prior-year sea ice condition have also been observed by Garibotti et al. (2005) in the Western Antarctic Peninsula. Similarly, Pan et al (2020) have observed cryptophyte community dominance in inshore waters with low sea ice presence and positive Southern Annular Mode conditions during December 2015. The transition between diatom assemblages have been observed during past iron fertilization experiment in the open ocean (Assmy et al., 2013), over the shelf (Garibotti et al., 2005), and in inshore waters of our study region (Mascioni et al., 2020) (Mascioni et al., 2019). In addition to our analyses, the impact of sea ice on phytoplankton abundance and community composition is also supported by previous studies (Garibotti et al., 2005) (Stammerjohn et al., 2008b) (Vernet et al., 2008). Overall, glacial meltwater fraction is higher than sea ice meltwater fraction in the water column; seasonal sea ice meltwater maximum is closely followed by the arrival of glacial meltwater (Meredith et al., 2017) (Meredith et al., 2013) (Meredith et al., 2008). Glacial meltwater accumulates in the water column and reaches its maximum later on; this timing appears to be consistent both inshore and over the self (Meredith et al., 2008) (Meredith et al., 2013) (Pan et al., 2019). During late fall and winter, small flagellates likely maintain a standing stock which persists until the next growing season (Pan et al., 2020).

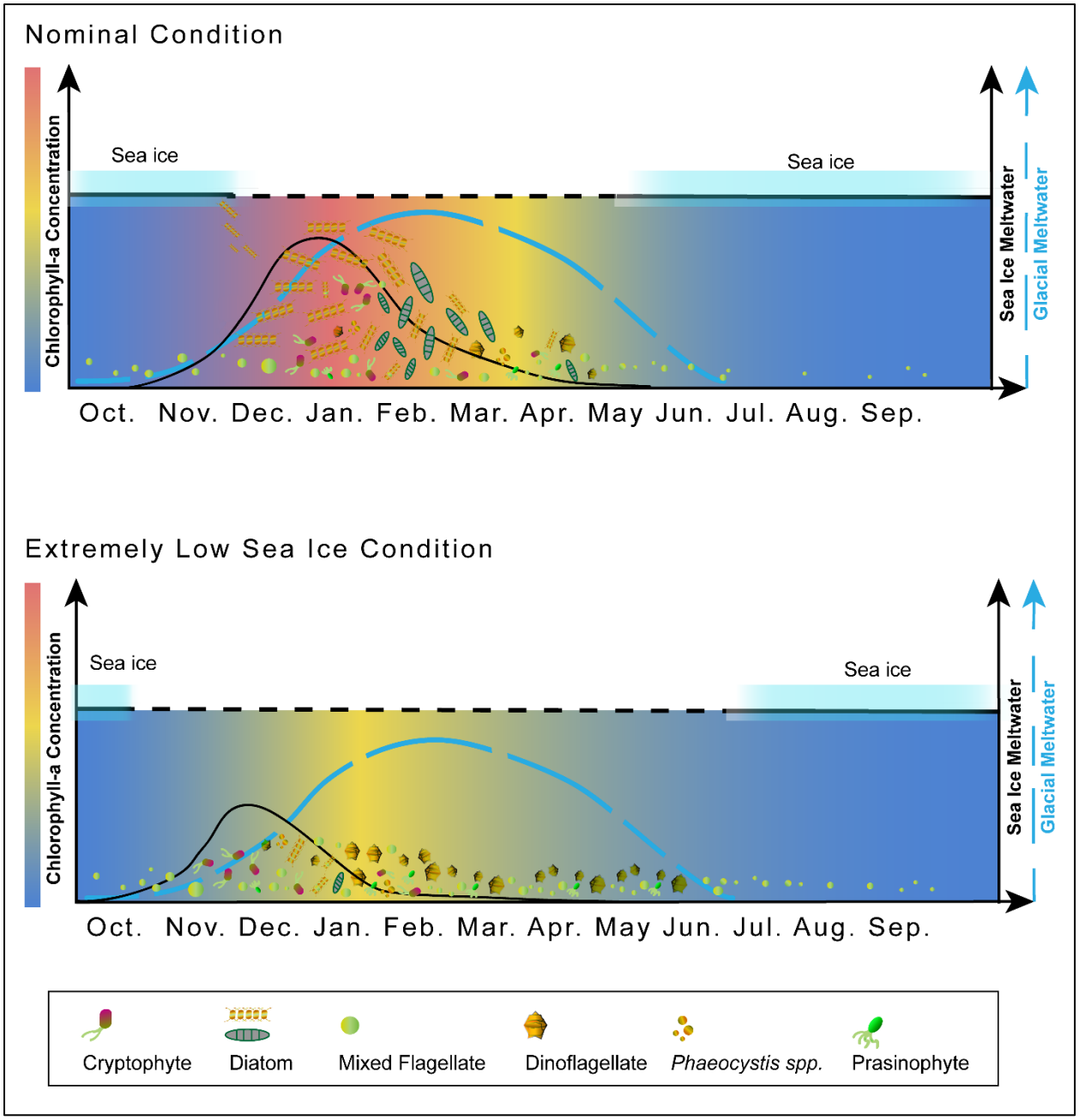
Nominal Condition
Chlorophyll-a Concentration
Sea ice
Sea ice
Sea Ice Meltwater
Glacial Meltwater
Oct. Nov. Dec. Jan. Feb. Mar. Apr. May Jun. Jul. Aug. Sep.
Extremely Low Sea Ice Condition
Chlorophyll-a Concentration
Sea ice
Sea ice
Sea Ice Meltwater
Glacial Meltwater
Oct. Nov. Dec. Jan. Feb. Mar. Apr. May Jun. Jul. Aug. Sep.
Cryptophyte
Diatom
Mixed Flagellate
Dinoflagellate
Phaeocystis spp.
Prasinophyte

4.8. Appendix

Table C1. Pigment:Chl-a initial ratios used in CHEMTAX analysis of pigment data. Numbers represent the amount of the given pigment predicted to be present for each unit of chl-a concentration (µg/l). Abbreviations: Chl_c2, chlorophyll-c2; Peri, peridinin; Fuco, fucoxanthin; But, 19'-butanoyloxyfucoxanthin; Hex, 19'-hexanoyloxyfucoxanthin; Allox, alloxanthin; Chlorophyll-b, Chl_b; Chlorophyll-a, Chl_a. Pigment ratio data source: diatoms, cryptophytes, mixed flagellates, dinoflagellates, *Phaeocystis spp.*, and prasinophytes (Kozlowski et al., 2011) (Wright et al., 2010)**.**

Class / Pigment	Chl_c2	Peri	Fuco	But	Hex	Allo	Chl_b	Chl_a
Prasinophyte	0	0	0	0	0	0	1	1
Cryptophyte	0.174	0	0	0	0	0.228	0	1
Mixed Flagellate	0.126	0	0.29	0.122	0.315	0	0	1
Diatom	0.183	0	0.745	0	0	0	0	1
Phaeocys spp.	0.144	0	0.011	0.08	1.111	0	0	1
Dinoflagellate	0	1.06	0	0	0	0	0	1

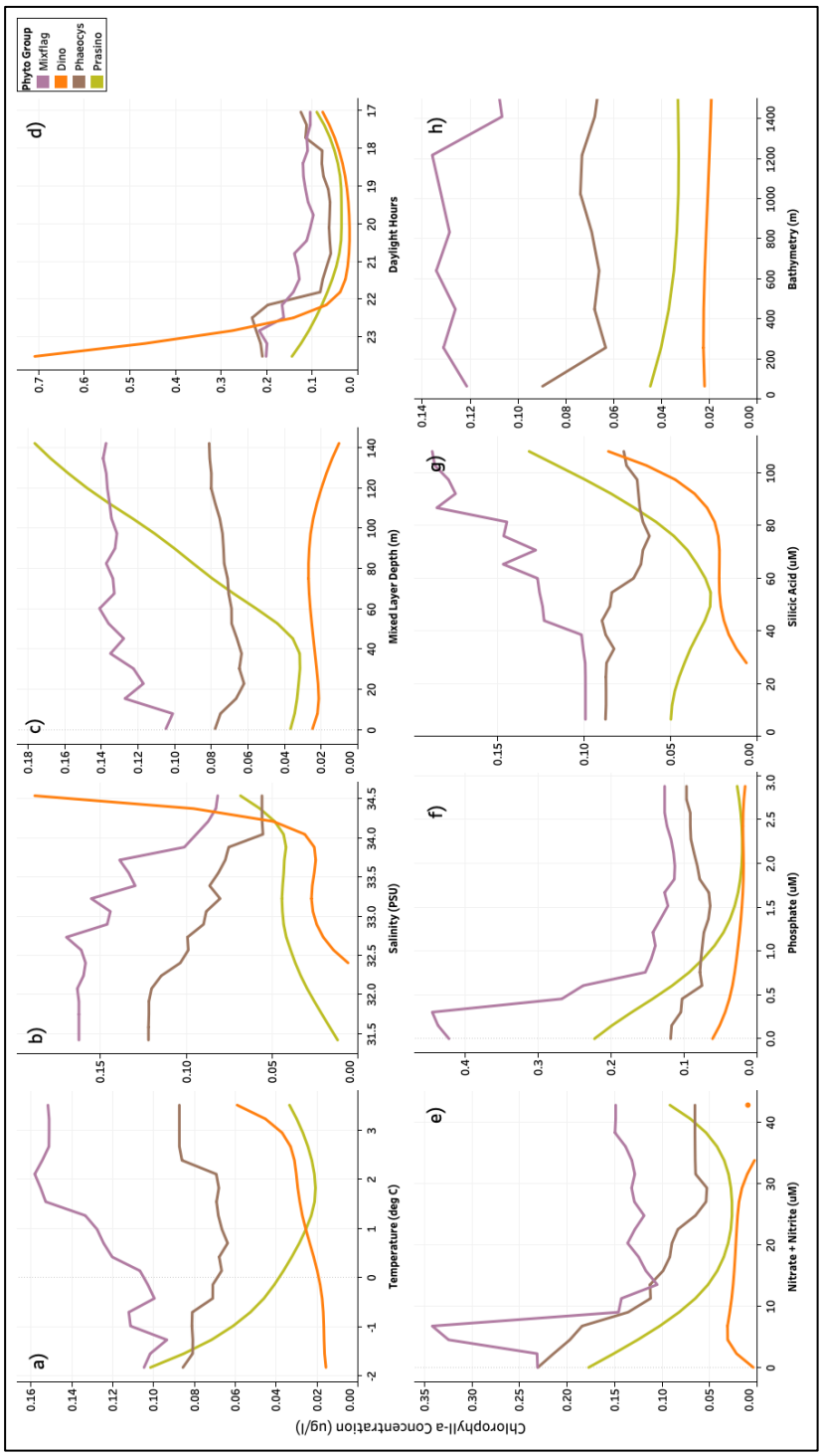

Figure C1. Partial dependence plots depicting machine learning models' mean response expressed in targeted taxonomic chlorophyll-a concentration (minor groups – mixed flagellates, dinoflagellate, *Phaeocystis spp.*, and prasinophytes); line colors represent different phytoplankton groups. The y-axes represent the models' mean responses in each group's chlorophyll-a concentration to changes in values of the environmental variables on x-axes. The daylight hours axis is reversed to reflect progression over time from mid- to late summer (see methods and Figure 4.8).

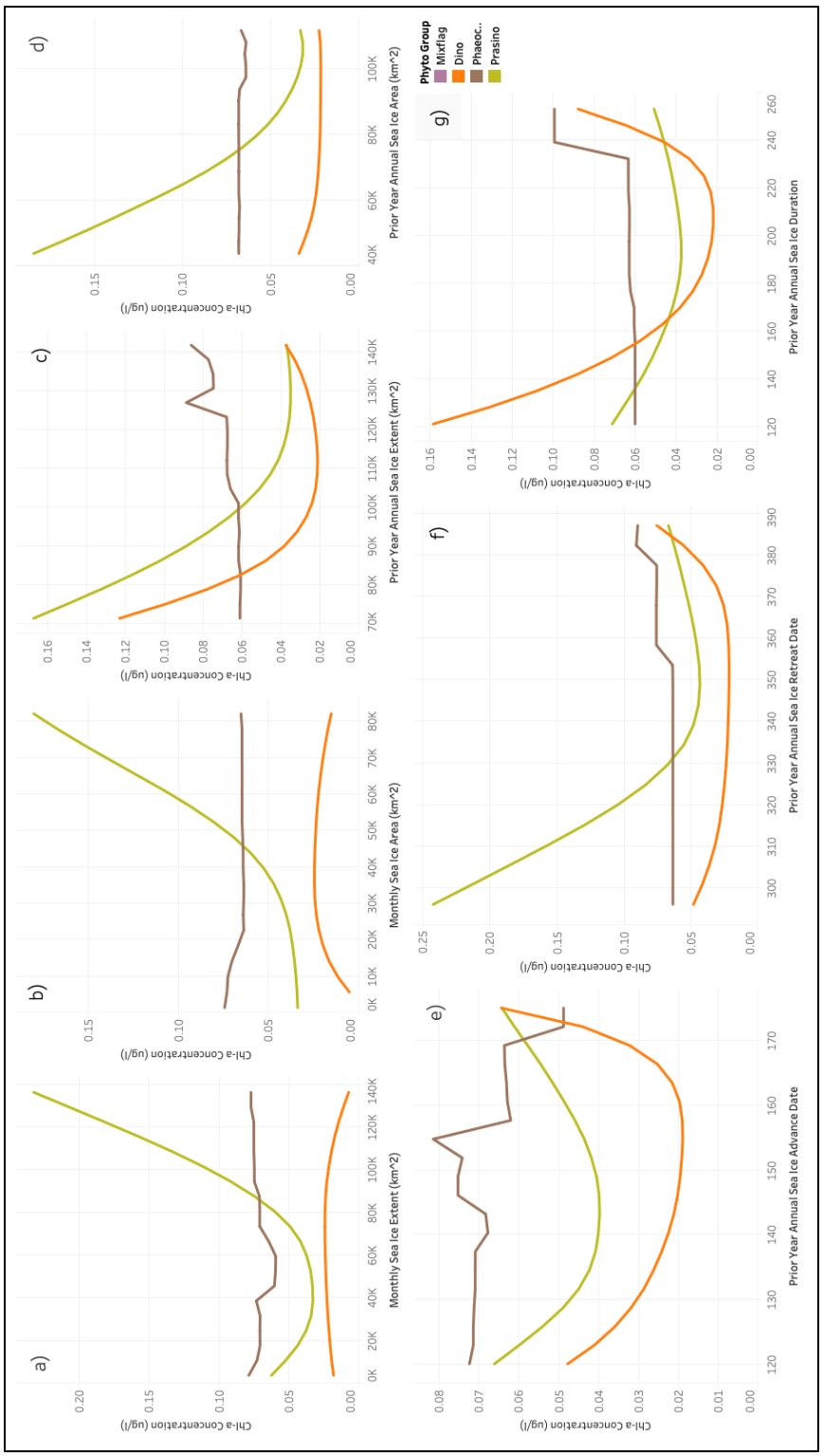

Figure C2. Partial dependence plots depicting machine learning models' mean response expressed in targeted taxonomic chlorophyll-a concentration (minor groups – mixed flagellates, dinoflagellate, *Phaeocystis spp.*, and prasinophytes); line colors represent different phytoplankton groups. The y-axes represent the models' mean responses in each group's chlorophyll-a concentration to changes in sea ice variables on x-axes.

4.9. References

Alvain, S., Moulin, C., Dandonneau, Y., Loisel, H., 2008. Seasonal distribution and succession of dominant phytoplankton groups in the global ocean: A satellite view. *Global Biogeochemical Cycles*, 22.

Annett, A.L., Carson, D.S., Crosta, X., Clarke, A., Ganeshram, R.S., 2010. Seasonal progression of diatom assemblages in surface waters of Ryder Bay, Antarctica. *Polar Biology*, 33, 13-29.

Annett, A.L., Fitzsimmons, J.N., Séguret, M.J., Lagerström, M., Meredith, M.P., Schofield, O., Sherrell, R.M., 2017. Controls on dissolved and particulate iron distributions in surface waters of the Western Antarctic Peninsula shelf. *Marine Chemistry*, 196, 81-97.

Armbrust, E.V., 2009. The life of diatoms in the world's oceans. *Nature*, 459, 185-192.

Armbrust, E.V., Berges, J.A., Bowler, C., Green, B.R., Martinez, D., Putnam, N.H., Zhou, S., Allen, A.E., Apt, K.E., Bechner, M., 2004. The genome of the diatom Thalassiosira pseudonana: ecology, evolution, and metabolism. *Science*, 306, 79-86.

Arrigo, K.R., Dunbar, R.B., Lizotte, M.P., Robinson, D., 2002. Taxon-specific differences in C/P and N/P drawdown for phytoplankton in the Ross Sea, Antarctica. *Geophysical Research Letters*, 29, 44-41-44-44.

Arrigo, K.R., van Dijken, G.L., Bushinsky, S., 2008. Primary production in the Southern Ocean, 1997–2006. *Journal of Geophysical Research: Oceans*, 113.

Aslam, S.N., Strauss, J., Thomas, D.N., Mock, T., Underwood, G.J., 2018. Identifying metabolic pathways for production of extracellular polymeric substances by the diatom Fragilariopsis cylindrus inhabiting sea ice. *The ISME journal*, 12, 1237-1251.

Assmy, P., Smetacek, V., Montresor, M., Klaas, C., Henjes, J., Strass, V.H., Arrieta, J.M., Bathmann, U., Berg, G.M., Breitbarth, E., 2013. Thick-shelled, grazer-protected diatoms decouple ocean carbon and silicon cycles in the iron-limited Antarctic Circumpolar Current. *Proceedings of the National Academy of Sciences*, 110, 20633-20638.

Behrenfeld, M.J., Falkowski, P.G., 1997. Photosynthetic rates derived from satellite-based chlorophyll concentration. *Limnology and Oceanography*, 42, 1-20.

Bird, D., Karl, D., 1991. Massive prasinophyte bloom in northern Gerlache Strait. *Antarct J US*, 26, 152-154.

Boyd, P., Law, C., 2001. The Southern Ocean iron release experiment (SOIREE)—introduction and summary. *Deep Sea Research Part II: Topical Studies in Oceanography*, 48, 2425-2438.

Boyd, P.W., 2002. Environmental factors controlling phytoplankton processes in the Southern Ocean1. *Journal of Phycology*, 38, 844-861.

Boyd, P.W., Watson, A.J., Law, C.S., Abraham, E.R., Trull, T., Murdoch, R., Bakker, D.C., Bowie, A.R., Buesseler, K., Chang, H., 2000. A mesoscale phytoplankton bloom in the polar Southern Ocean stimulated by iron fertilization. *Nature*, 407, 695-702.

Brody, E., Mitchell, B.G., Holm-Hansen, O., Vernet, M., 1992. Species-dependent variations of the absorption coefficient. *Antarctic Journal of the United States*, 27, 160.

Cape, M., Vernet, M., Kahru, M., Spreen, G., 2014. Polynya dynamics drive primary production in the Larsen A and B embayments following ice shelf collapse. *Journal of Geophysical Research: Oceans*, 119, 572-594.

Cape, M.R., Vernet, M., Pettit, E.C., Wellner, J.S., Truffer, M., Akie, G., Domack, E., Leventer, A., Smith, C.R., Huber, B.A., 2019. Circumpolar Deep Water impacts glacial meltwater export and coastal biogeochemical cycling along the west Antarctic Peninsula. *Frontiers in Marine Science*, 6, 144.

Carrillo, C.J., Smith, R.C., Karl, D.M., 2004. Processes regulating oxygen and carbon dioxide in surface waters west of the Antarctic Peninsula. *Marine Chemistry*, 84, 161-179.

Carvalho, F., Fitzsimmons, J.N., Couto, N., Waite, N., Gorbunov, M., Kohut, J., Oliver, M.J., Sherrell, R.M., Schofield, O., 2020. Testing the Canyon Hypothesis: Evaluating light and nutrient controls of phytoplankton growth in penguin foraging hotspots along the West Antarctic Peninsula. *Limnology and Oceanography*, 65, 455-470.

Carvalho, F., Kohut, J., Oliver, M.J., Schofield, O., 2017. Defining the ecologically relevant mixed-layer depth for Antarctica's coastal seas. *Geophysical Research Letters*, 44, 338-345.

Casaux, R., Barrera-Oro, E., Baroni, A., Ramón, A., 2003. Ecology of inshore notothenioid fish from the Danco Coast, Antarctic Peninsula. *Polar Biology*, 26, 157-165.

Cavagna, A.-J., Fripiat, F., Dehairs, F., Wolf-Gladrow, D., Cisewski, B., Savoye, N., André, L., Cardinal, D., 2011. Silicon uptake and supply during a Southern Ocean iron fertilization experiment (EIFEX) tracked by Si isotopes. *Limnology and Oceanography*, 56, 147-160.

Chapman, E.W., Hofmann, E.E., Patterson, D.L., Ribic, C.A., Fraser, W.R., 2011. Marine and terrestrial factors affecting Adélie penguin Pygoscelis adeliae chick growth and recruitment off the western Antarctic Peninsula. *Marine Ecology Progress Series*, 436, 273-289.

Constable, A.J., Melbourne-Thomas, J., Corney, S.P., Arrigo, K.R., Barbraud, C., Barnes, D.K., Bindoff, N.L., Boyd, P.W., Brandt, A., Costa, D.P., 2014. Climate change and Southern Ocean ecosystems I: how changes in physical habitats directly affect marine biota. *Global Change Biology*, 20, 3004-3025.

Cook, A., Fox, A., Vaughan, D., Ferrigno, J., 2005. Retreating glacier fronts on the Antarctic Peninsula over the past half-century. *Science*, 308, 541-544.

Dennett, M.R., Mathot, S., Caron, D.A., Smith Jr, W.O., Lonsdale, D.J., 2001. Abundance and distribution of phototrophic and heterotrophic nano-and microplankton in the southern Ross Sea. *Deep Sea Research Part II: Topical Studies in Oceanography*, 48, 4019-4037.

Deppeler, S.L., Davidson, A.T., 2017. Southern Ocean phytoplankton in a changing climate. *Frontiers in Marine Science*, 4, 40.

Dierssen, H.M., Smith, R.C., 2000. Bio-optical properties and remote sensing ocean color algorithms for Antarctic Peninsula waters. *Journal of Geophysical Research: Oceans*, 105, 26301-26312.

Dierssen, H.M., Smith, R.C., Vernet, M., 2002. Glacial meltwater dynamics in coastal waters west of the Antarctic peninsula. *Proceedings of the National Academy of Sciences*, 99, 1790-1795.

Ducklow, H.W., Baker, K., Martinson, D.G., Quetin, L.B., Ross, R.M., Smith, R.C., Stammerjohn, S.E., Vernet, M., Fraser, W., 2007. Marine pelagic ecosystems: the west Antarctic Peninsula. *Philosophical Transactions of the Royal Society B: Biological Sciences*, 362, 67-94.

Ducklow, H.W., Fraser, W.R., Meredith, M.P., Stammerjohn, S.E., Doney, S.C., Martinson, D.G., Sailley, S.F., Schofield, O.M., Steinberg, D.K., Venables, H.J., 2013. West Antarctic Peninsula: an ice-dependent coastal marine ecosystem in transition. *Oceanography*, 26, 190-203.

Edwards, K.F., Thomas, M.K., Klausmeier, C.A., Litchman, E., 2012. Allometric scaling and taxonomic variation in nutrient utilization traits and maximum growth rate of phytoplankton. *Limnology and Oceanography*, 57, 554-566.

Ekern, L., 2017. Assessing Primary Production via nutrient deficits in Andvord Bay, Antarctica 2015-2016. *Scripps Institution of Oceanography*, Vol. Master's University of California, San Diego.

Ferrario, M.E., Sar, E.A., Vernet, M., 1998. Chaetoceros resting spores in the Gerlache Strait, Antarctic Peninsula. *Polar Biology*, 19, 286-288.

Forcada, J., Trathan, P.N., Boveng, P.L., Boyd, I.L., Burns, J.M., Costa, D.P., Fedak, M., Rogers, T.L., Southwell, C.J., 2012. Responses of Antarctic pack-ice seals to environmental change and increasing krill fishing. *Biological Conservation*, 149, 40-50.

Forsch, K., Manck, L., Ekern, L., Pan, B.J., Vernet, M., Barbeau, K., 2018. Links Between Sources of Iron and Organic Iron-binding Ligands to the Supply of Cryospheric Iron to Coastal West Antarctic Peninsula. *Ocean Sciences Meeting*. Portland, Oregon.

Forsythe, W.C., Rykiel Jr, E.J., Stahl, R.S., Wu, H.-i., Schoolfield, R.M., 1995. A model comparison for daylength as a function of latitude and day of year. *Ecological Modelling*, 80, 87-95.

Franzè, G., Pierson, J.J., Stoecker, D.K., Lavrentyev, P.J., 2018. Diatom-produced allelochemicals trigger trophic cascades in the planktonic food web. *Limnology and Oceanography*, 63, 1093-1108.

Friedlaender, A.S., Halpin, P.N., Qian, S.S., Lawson, G.L., Wiebe, P.H., Thiele, D., Read, A.J., 2006. Whale distribution in relation to prey abundance and oceanographic processes in shelf waters of the Western Antarctic Peninsula. *Marine Ecology Progress Series*, 317, 297-310.

Garibotti, I.A., Vernet, M., Ferrario, M.E., 2005. Annually recurrent phytoplanktonic assemblages during summer in the seasonal ice zone west of the Antarctic Peninsula (Southern Ocean). *Deep Sea Research Part I: Oceanographic Research Papers*, 52, 1823-1841.

Garibotti, I.A., Vernet, M., Ferrario, M.E., Smith, R.C., Ross, R.M., Quetin, L.B., 2003a. Phytoplankton spatial distribution patterns along the western Antarctic Peninsula (Southern Ocean). *Marine Ecology Progress Series*, 261, 21-39.

Garibotti, I.A., Vernet, M., Kozlowski, W.A., Ferrario, M.E., 2003b. Composition and biomass of phytoplankton assemblages in coastal Antarctic waters: a comparison of chemotaxonomic and microscopic analyses. *Marine Ecology Progress Series*, 247, 27-42.

Gieskes, W., Kraay, G., 1983. Dominance of Cryptophyceae during the phytoplankton spring bloom in the central North Sea detected by HPLC analysis of pigments. *Marine Biology*, 75, 179-185.

Gleitz, M., vd Loeff, M.R., Thomas, D.N., Dieckmann, G.S., Millero, F.J., 1995. Comparison of summer and winter inorganic carbon, oxygen and nutrient concentrations in Antarctic sea ice brine. *Marine Chemistry*, 51, 81-91.

Grange, L.J., Smith, C.R., 2013. Megafaunal communities in rapidly warming fjords along the West Antarctic Peninsula: hotspots of abundance and beta diversity. *Plos One*, 8, e77917.

Haberman, K.L., Ross, R.M., Quetin, L.B., 2003. Diet of the Antarctic krill (Euphausia superba Dana): II. Selective grazing in mixed phytoplankton assemblages. *Journal of Experimental Marine Biology and Ecology*, 283, 97-113.

Henley, S.F., Jones, E.M., Venables, H.J., Meredith, M.P., Firing, Y.L., Dittrich, R., Heiser, S., Stefels, J., Dougans, J., 2018a. Macronutrient and carbon supply, uptake and cycling across the Antarctic Peninsula shelf during summer. *Philosophical Transactions of the Royal Society A: Mathematical, Physical and Engineering Sciences*, 376, 20170168.

Henley, S.F., Tuerena, R.E., Annett, A.L., Fallick, A.E., Meredith, M.P., Venables, H.J., Clarke, A., Ganeshram, R.S., 2018b. Macronutrient supply, uptake and recycling in the coastal ocean of the west Antarctic Peninsula. *Deep Sea Research Part II: Topical Studies in Oceanography*, 139, 58-76.

Hückstädt, L., Burns, J., Koch, P., McDonald, B., Crocker, D.E., Costa, D., 2012. Diet of a specialist in a changing environment: the crabeater seal along the western Antarctic Peninsula. *Marine Ecology Progress Series*, 455, 287-301.

Hutter, F., Caruana, R., Remi, B., Misha, B., Isabelle, G., Balazs, K., Hugo, L., 2014. What is AutoML? , *AutoML workshop @ ICML'14*.

Huysman, M.J., Martens, C., Vandepoele, K., Gillard, J., Rayko, E., Heijde, M., Bowler, C., Inzé, D., Van de Peer, Y., De Veylder, L., 2010. Genome-wide analysis of the diatom cell cycle unveils a novel type of cyclins involved in environmental signaling. *Genome biology*, 11, R17.

Jin, H., Zhuang, Y., Li, H., Chen, J., Gao, S., Ji, Z., Zhang, Y., 2017. Response of phytoplankton community to different water types in the western Arctic Ocean surface water based on pigment analysis in summer 2008. *Acta Oceanologica Sinica*, 36, 109-121.

Joy-Warren, H.L., van Dijken, G.L., Alderkamp, A.C., Leventer, A., Lewis, K.M., Selz, V., Lowry, K.E., van de Poll, W., Arrigo, K.R., 2019. Light is the primary driver of early season phytoplankton production along the western Antarctic Peninsula. *Journal of Geophysical Research: Oceans*, 124, 7375-7399.

Kang, S.-H., Kang, J.-S., Lee, S., Chung, K.H., Kim, D., Park, M.G., 2001. Antarctic phytoplankton assemblages in the marginal ice zone of the northwestern Weddell Sea. *Journal of Plankton Research*, 23, 333-352.

Karentz, D., Smayda, T.J., 1984. Temperature and seasonal occurrence patterns of 30 dominant phytoplankton species in Narragansett Bay over a 22-year period (1959–1980). *Mar. Ecol. Prog. Ser*, 18, 277-293.

Kattner, G., Thomas, D.N., Haas, C., Kennedy, H., Dieckmann, G.S., 2004. Surface ice and gap layers in Antarctic sea ice: highly productive habitats. *Marine Ecology Progress Series*, 277, 1-12.

Kim, H., Doney, S.C., Iannuzzi, R.A., Meredith, M.P., Martinson, D.G., Ducklow, H.W., 2016. Climate forcing for dynamics of dissolved inorganic nutrients at Palmer Station, Antarctica: an interdecadal (1993–2013) analysis. *Journal of Geophysical Research: Biogeosciences*, 121, 2369-2389.

Klais, R., Tamminen, T., Kremp, A., Spilling, K., Olli, K., 2011. Decadal-scale changes of dinoflagellates and diatoms in the anomalous Baltic Sea spring bloom. *Plos One*, 6.

Kozlowski, W.A., Deutschman, D., Garibotti, I., Trees, C., Vernet, M., 2011. An evaluation of the application of CHEMTAX to Antarctic coastal pigment data. *Deep Sea Research Part I: Oceanographic Research Papers*, 58, 350-364.

Kremp, A., 2001. Effects of cyst resuspension on germination and seeding of two bloom-forming dinoflagellates in the Baltic Sea. *Marine Ecology Progress Series*, 216, 57-66.

Kropuenske, L.R., Mills, M.M., Van Dijken, G.L., Alderkamp, A.C., Mine Berg, G., Robinson, D.H., Welschmeyer, N.A., Arrigo, K.R., 2010. Strategies And Rates Of Photoacclimation In Two Major Southern Ocean Phytoplankton Taxa: Phaeocystis Antarctica (Haptophyta) And Fragilariopsis Cylindrus (Bacillariophyceae) 1. *Journal of Phycology*, 46, 1138-1151.

Kropuenske, L.R., Mills, M.M., van Dijken, G.L., Bailey, S., Robinson, D.H., Welschmeyer, N.A., Arrigoa, K.R., 2009. Photophysiology in two major Southern Ocean phytoplankton taxa: photoprotection in Phaeocystis antarctica and Fragilariopsis cylindrus. *Limnology and Oceanography*, 54, 1176-1196.

Landa, M., Blain, S., Harmand, J., Monchy, S., Rapaport, A., Obernosterer, I., 2018. Major changes in the composition of a Southern Ocean bacterial community in response to diatom-derived dissolved organic matter. *Fems Microbiology Ecology*, 94, fiy034.

Lannuzel, D., Schoemann, V., De Jong, J., Chou, L., Delille, B., Becquevort, S., Tison, J.-L., 2008. Iron study during a time series in the western Weddell pack ice. *Marine Chemistry*, 108, 85-95.

Lannuzel, D., Schoemann, V., De Jong, J., Tison, J.-L., Chou, L., 2007. Distribution and biogeochemical behaviour of iron in the East Antarctic sea ice. *Marine Chemistry*, 106, 18-32.

Latasa, M., 2007. Improving estimations of phytoplankton class abundances using CHEMTAX. *Marine Ecology Progress Series*, 329, 13-21.

Laybourn-Parry, J., Marshall, W.A., Marchant, H.J., 2005. Flagellate nutritional versatility as a key to survival in two contrasting Antarctic saline lakes. *Freshwater Biology*, 50, 830-838.

Liang, J., Crowther, T.W., Picard, N., Wiser, S., Zhou, M., Alberti, G., Schulze, E.-D., McGuire, A.D., Bozzato, F., Pretzsch, H., 2016. Positive biodiversity-productivity relationship predominant in global forests. *Science*, 354, aaf8957.

Liefer, J.D., Garg, A., Campbell, D.A., Irwin, A.J., Finkel, Z.V., 2018. Nitrogen starvation induces distinct photosynthetic responses and recovery dynamics in diatoms and prasinophytes. *Plos One*, 13.

Litchman, E., Klausmeier, C.A., 2008. Trait-based community ecology of phytoplankton. *Annual review of ecology, evolution, and systematics*, 39, 615-639.

Luria, C.M., Amaral-Zettler, L.A., Ducklow, H.W., Repeta, D.J., Rhyne, A.L., Rich, J.J., 2017. Seasonal shifts in bacterial community responses to phytoplankton-derived dissolved organic matter in the Western Antarctic Peninsula. *Frontiers in Microbiology*, 8, 2117.

Mackey, M., Mackey, D., Higgins, H., Wright, S., 1996. CHEMTAX-a program for estimating class abundances from chemical markers: application to HPLC measurements of phytoplankton. *Marine Ecology Progress Series*, 144, 265-283.

Mangoni, O., Saggiomo, M., Modigh, M., Catalano, G., Zingone, A., Saggiomo, V., 2009. The role of platelet ice microalgae in seeding phytoplankton blooms in Terra Nova Bay (Ross Sea, Antarctica): a mesocosm experiment. *Polar Biology*, 32, 311-323.

Marshall, G.J., 2003. Trends in the Southern Annular Mode from observations and reanalyses. *Journal of Climate*, 16, 4134-4143.

Martinson, D.G., Stammerjohn, S.E., Iannuzzi, R.A., Smith, R.C., Vernet, M., 2008. Western Antarctic Peninsula physical oceanography and spatio–temporal variability. *Deep Sea Research Part II: Topical Studies in Oceanography*, 55, 1964-1987.

Mascioni, M., Almandoz, G.O., Cefarelli, A.O., Cusick, A., Ferrario, M.E., Vernet, M., 2019. Phytoplankton composition and bloom formation in unexplored nearshore waters of the western Antarctic Peninsula. *Polar Biology*, 42, 1859-1872.

Mascioni, M., Almandoz, G.O., Ekern, L., Pan, B.J., Vernet, M., 2020. Microplanktonic diatom assemblages dominated the primary production in an Antarctic fjord. *in prep.*

McKnight, D.M., Howes, B., Taylor, C., Goehringer, d.D., 2000. Phytoplankton dynamics in a stably stratified Antarctic lake during winter darkness. *Journal of Phycology*, 36, 852-861.

Mendes, C.R.B., Tavano, V.M., Dotto, T.S., Kerr, R., De Souza, M.S., Garcia, C.A.E., Secchi, E.R., 2018a. New insights on the dominance of cryptophytes in Antarctic coastal waters: a case study in Gerlache Strait. *Deep Sea Research Part II: Topical Studies in Oceanography*, 149, 161-170.

Mendes, C.R.B., Tavano, V.M., Kerr, R., Dotto, T.S., Maximiano, T., Secchi, E.R., 2018b. Impact of sea ice on the structure of phytoplankton communities in the northern Antarctic Peninsula. *Deep Sea Research Part II: Topical Studies in Oceanography*, 149, 111-123.

Mendes, C.R.B., Tavano, V.M., Leal, M.C., de Souza, M.S., Brotas, V., Garcia, C.A.E., 2013. Shifts in the dominance between diatoms and cryptophytes during three late summers in the Bransfield Strait (Antarctic Peninsula). *Polar Biology*, 36, 537-547.

Meredith, M.P., Brandon, M.A., Wallace, M.I., Clarke, A., Leng, M.J., Renfrew, I.A., van Lipzig, N.P.M., King, J.C., 2008. Variability in the freshwater balance of northern Marguerite Bay, Antarctic Peninsula: Results from δ18O. *Deep Sea Research Part II: Topical Studies in Oceanography*, 55, 309-322.

Meredith, M.P., Stammerjohn, S.E., Venables, H.J., Ducklow, H.W., Martinson, D.G., Iannuzzi, R.A., Leng, M.J., van Wessem, J.M., Reijmer, C.H., Barrand, N.E., 2017. Changing distributions of sea ice melt and meteoric water west of the Antarctic Peninsula. *Deep Sea Research Part II: Topical Studies in Oceanography*, 139, 40-57.

Meredith, M.P., Venables, H.J., Clarke, A., Ducklow, H.W., Erickson, M., Leng, M.J., Lenaerts, J.T., van den Broeke, M.R., 2013. The freshwater system west of the Antarctic Peninsula: spatial and temporal changes. *Journal of Climate*, 26, 1669-1684.

Miller, C.B., Frost, B.W., Wheeler, P.A., Landry, M.R., Welschmeyer, N., Powell, T.M., 1991. Ecological dynamics in the subarctic Pacific, a possibly iron-limited ecosystem. *Limnology and Oceanography*, 36, 1600-1615.

Mills, M.M., Alderkamp, A.-C., Thuróczy, C.-E., van Dijken, G.L., Laan, P., de Baar, H.J., Arrigo, K.R., 2012. Phytoplankton biomass and pigment responses to Fe amendments in the Pine Island and Amundsen polynyas. *Deep Sea Research Part II: Topical Studies in Oceanography*, 71, 61-76.

Moline, M.A., Claustre, H., Frazer, T.K., Schofield, O., Vernet, M., 2004. Alteration of the food web along the Antarctic Peninsula in response to a regional warming trend. *Global Change Biology*, 10, 1973-1980.

Moline, M.A., Prezelin, B.B., Schofield, O., Smith, R.C., 1996. Temporal dynamics of coastal Antarctic phytoplankton: Environmental driving forces and impact of 1991/92 summer diatom bloom on the nutrient regimes.

Montes-Hugo, M., Vernet, M., Martinson, D., Smith, R., Iannuzzi, R., 2008. Variability on phytoplankton size structure in the western Antarctic Peninsula (1997–2006). *Deep Sea Research Part II: Topical Studies in Oceanography*, 55, 2106-2117.

Morgan, K., Kalff, J., 1975. The winter dark survival of an algal flagellate—Cryptomonas erosa (Skuja) With 5 figures and 1 table in the text. *Internationale Vereinigung für theoretische und angewandte Limnologie: Verhandlungen*, 19, 2734-2740.

Pan, B.J., Vernet, M., Manck, L., Forsch, K., Ekern, L., Mascioni, M., Barbeau, K.A., Almandoz, G.O., Orona, A.J., 2020. Environmental drivers of phytoplankton taxonomic composition in an Antarctic fjord. *Progress in Oceanography*, 183, 102295.

Pan, B.J., Vernet, M., Reynolds, R.A., Mitchell, B.G., 2019. The optical and biological properties of glacial meltwater in an Antarctic fjord. *Plos One*, 14, e0211107.

Pedulli, M., Bisagni, J.J., Ducklow, H.W., Beardsley, R., Pilskaln, C., 2014. Estimates of potential new production (PNP) for the waters off the western Antarctic Peninsula (WAP) region. *Continental Shelf Research*, 84, 54-69.

Peeken, I., 1997. Photosynthetic pigment fingerprints as indicators of phytoplankton biomass and development in different water masses of the Southern Ocean during austral spring. *Deep Sea Research Part II: Topical Studies in Oceanography*, 44, 261-282.

Petrou, K., Hill, R., Brown, C.M., Campbell, D.A., Doblin, M.A., Ralph, P.J., 2010. Rapid photoprotection in sea-ice diatoms from the East Antarctic pack ice. *Limnology and Oceanography*, 55, 1400-1407.

Petrou, K., Kranz, S.A., Trimborn, S., Hassler, C.S., Ameijeiras, S.B., Sackett, O., Ralph, P.J., Davidson, A.T., 2016. Southern Ocean phytoplankton physiology in a changing climate. *Journal of Plant Physiology*, 203, 135-150.

Petrou, K., Trimborn, S., Rost, B., Ralph, P.J., Hassler, C.S., 2014. The impact of iron limitation on the physiology of the Antarctic diatom Chaetoceros simplex. *Marine Biology*, 161, 925-937.

Prézelin, B.B., Hofmann, E.E., Mengelt, C., Klinck, J.M., 2000. The linkage between Upper Circumpolar Deep Water (UCDW) and phytoplankton assemblages on the west Antarctic Peninsula continental shelf. *Journal of Marine Research*, 58, 165-202.

Prezelin, B.B., Moline, M.A., Seydel, K., Scheppe, K., 1992. Palmer LTER: Temporal variability in HPLC pigmentation and inorganic nutrient distribution in surface waters adjacent to Palmer Station, December 1991-February 1992. *Biological Sciences*, 125.

Rembauville, M., Blain, S., Manno, C., Tarling, G., Thompson, A., Wolff, G., Salter, I., 2018. The role of diatom resting spores in pelagic–benthic coupling in the Southern Ocean.

Riaux-Gobin, C., Poulin, M., Dieckmann, G., Labrune, C., Vétion, G., 2011. Spring phytoplankton onset after the ice break-up and sea-ice signature (Adélie Land, East Antarctica). *Polar Research*, 30, 5910.

Ribeiro, S., Berge, T., Lundholm, N., Andersen, T.J., Abrantes, F., Ellegaard, M., 2011. Phytoplankton growth after a century of dormancy illuminates past resilience to catastrophic darkness. *Nature Communications*, 2, 1-7.

Roberts, E.C., Laybourn-Parry, J., 1999. Mixotrophic cryptophytes and their predators in the Dry Valley lakes of Antarctica. *Freshwater Biology*, 41, 737-746.

Ruiz-Halpern, S., Calleja, M.L., Dachs, J., Vento, S.d., Pastor, M., Palmer, M., Agustí, S., Duarte, C.M., 2014. Ocean-atmosphere exchange of organic carbon and CO2 surrounding the Antarctic Peninsula.

Schoemann, V., Becquevort, S., Stefels, J., Rousseau, V., Lancelot, C., 2005. Phaeocystis blooms in the global ocean and their controlling mechanisms: a review. *Journal of Sea Research*, 53, 43-66.

Schofield, O., Saba, G., Coleman, K., Carvalho, F., Couto, N., Ducklow, H., Finkel, Z., Irwin, A., Kahl, A., Miles, T., 2017. Decadal variability in coastal phytoplankton community composition in a changing West Antarctic Peninsula. *Deep Sea Research Part I: Oceanographic Research Papers*, 124, 42-54.

Shannon, C.E., 1948. A mathematical theory of communication. *The Bell system technical journal*, 27, 379-423.

Smetacek, V., 1999. Diatoms and the ocean carbon cycle. *Protist*, 150, 25-32.

Smetacek, V., Klaas, C., Strass, V.H., Assmy, P., Montresor, M., Cisewski, B., Savoye, N., Webb, A., d'Ovidio, F., Arrieta, J.M., 2012. Deep carbon export from a Southern Ocean iron-fertilized diatom bloom. *Nature*, 487, 313-319.

Smith, R., Stammerjohn, S., 2001. Variations of surface air temperature and sea-ice extent in the western Antarctic Peninsula region. *Annals of Glaciology*, 33, 493-500.

Smith, R.C., Baker, K.S., Fraser, W.R., Hofmann, E.E., Karl, D.M., Klinck, J.M., Quetin, L.B., Prézelin, B.B., Ross, R.M., Trivelpiece, W.Z., 1995. The Palmer LTER: A long-term ecological research program at Palmer Station, Antarctica. *Oceanography*, 8, 77-86.

Spellerberg, I.F., Fedor, P.J., 2003. A tribute to Claude Shannon (1916–2001) and a plea for more rigorous use of species richness, species diversity and the 'Shannon–Wiener'Index. *Global ecology and biogeography*, 12, 177-179.

Stammerjohn, S., Martinson, D., Smith, R., Yuan, X., Rind, D., 2008a. Trends in Antarctic annual sea ice retreat and advance and their relation to El Niño–Southern Oscillation and Southern Annular Mode variability. *Journal of Geophysical Research: Oceans*, 113.

Stammerjohn, S.E., Martinson, D.G., Smith, R.C., Iannuzzi, R.A., 2008b. Sea ice in the western Antarctic Peninsula region: Spatio-temporal variability from ecological and climate change perspectives. *Deep Sea Research Part II: Topical Studies in Oceanography*, 55, 2041-2058.

Stammerjohn, S.E., Smith, R.C., 1995. Palmer LTER: Sea-ice coverage in the Long-Term Ecological. *Antarctic Journal of the United States*, 30, 255.

Steig, E.J., Schneider, D., Rutherford, S., Mann, M., Comiso, J., Shindell, D., 2009. Warming of the Antarctic ice-sheet surface since the 1957 International Geophysical Year. *Nature*, 457, 459-462.

Stoecker, D.K., Gustafson, D.E., Baier, C.T., Black, M.M., 2000. Primary production in the upper sea ice. *Aquatic Microbial Ecology*, 21, 275-287.

Stoecker, D.K., Lavrentyev, P.J., 2018. Mixotrophic plankton in the Polar Seas: a Pan-Arctic review. *Frontiers in Marine Science*, 5, 292.

Strzepek, R.F., Maldonado, M.T., Hunter, K.A., Frew, R.D., Boyd, P.W., 2011. Adaptive strategies by Southern Ocean phytoplankton to lessen iron limitation: Uptake of organically complexed iron and reduced cellular iron requirements. *Limnology and Oceanography*, 56, 1983-2002.

Talley, L.D., 2011. *Descriptive physical oceanography: an introduction*: Academic press.

Thompson, D.W., Solomon, S., Kushner, P.J., England, M.H., Grise, K.M., Karoly, D.J., 2011. Signatures of the Antarctic ozone hole in Southern Hemisphere surface climate change. *Nature Geoscience*, 4, 741.

Thornton, C., Hutter, F., Hoos, H.H., Leyton-Brown, K., 2013. Auto-WEKA: Combined selection and hyperparameter optimization of classification algorithms. *Proceedings of the 19th ACM SIGKDD international conference on Knowledge discovery and data mining* (pp. 847-855).

van Leeuwe, M.A., Webb, A.L., Venables, H.J., Visser, R.J., Meredith, M.P., Elzenga, J.T.M., Stefels, J., 2020. Annual patterns in phytoplankton phenology in Antarctic coastal waters explained by environmental drivers. *Limnology and Oceanography*.

Vaughan, D., Marshall, G.J., Connolley, W.M., Parkinson, C., Mulvaney, R., Hodgson, D.A., King, J.C., Pudsey, C.J., Turner, J., 2003. Recent rapid regional climate warming on the Antarctic Peninsula. *Climatic change*, 60, 243-274.

Vaughan, D.G., Doake, C., 1996. Recent atmospheric warming and retreat of ice shelves on the Antarctic Peninsula. *Nature*, 379, 328-331.

Vernet, M., Letelier, R., Karl, D.M., 1991. RACER: Phytoplankton growth rates in the northern Gerlache Strait during the spring bloom of 1989. *Antarctic Journal of the United States*, 26, 154.

Vernet, M., Martinson, D., Iannuzzi, R., Stammerjohn, S., Kozlowski, W., Sines, K., Smith, R., Garibotti, I., 2008. Primary production within the sea-ice zone west of the Antarctic Peninsula: I—Sea ice, summer mixed layer, and irradiance. *Deep Sea Research Part II: Topical Studies in Oceanography*, 55, 2068-2085.

Vernet, M., Matrai, P.A., Andreassen, I., 1998. Synthesis of particulate and extracellular carbon by phytoplankton at the marginal ice zone in the Barents Sea. *Journal of Geophysical Research: Oceans*, 103, 1023-1037.

Vernet, M., Pan, B.J., Forsch, K., Manck, L., Barbeau, K., 2020. The nitrate-to-dissolved-iron ratio in West Antarctica coastal waters *SCAR 2020*. Online.

Walsh, J.J., Dieterle, D.A., Lenes, J., 2001. A numerical analysis of carbon dynamics of the Southern Ocean phytoplankton community: the roles of light and grazing in effecting both sequestration of atmospheric CO2 and food availability to larval krill. *Deep Sea Research Part I: Oceanographic Research Papers*, 48, 1-48.

Winder, M., Cloern, J.E., 2010. The annual cycles of phytoplankton biomass. *Philosophical Transactions of the Royal Society B: Biological Sciences*, 365, 3215-3226.

Wolf, C., Frickenhaus, S., Kilias, E.S., Peeken, I., Metfies, K., 2013. Regional variability in eukaryotic protist communities in the Amundsen Sea. *Antarctic Science*, 25, 741-751.

Wright, S.W., van den Enden, R.L., 2000. Phytoplankton community structure and stocks in the East Antarctic marginal ice zone (BROKE survey, January–March 1996) determined by CHEMTAX analysis of HPLC pigment signatures. *Deep Sea Research Part II: Topical Studies in Oceanography*, 47, 2363-2400.

Wright, S.W., van den Enden, R.L., Pearce, I., Davidson, A.T., Scott, F.J., Westwood, K.J., 2010. Phytoplankton community structure and stocks in the Southern Ocean (30–80 E) determined by CHEMTAX analysis of HPLC pigment signatures. *Deep Sea Research Part II: Topical Studies in Oceanography*, 57, 758-778.

Yan, D., Yoshida, K., Nishioka, J., Ito, M., Toyota, T., Suzuki, K., 2020. Response to Sea Ice Melt Indicates High Seeding Potential of the Ice Diatom Thalassiosira to Spring Phytoplankton Blooms: A Laboratory Study on an Ice Algal Community From the Sea of Okhotsk. *Frontiers in Marine Science*, 7, 613.

Ziegler, A., Cape, M.R., Lundesgaard, Ø., Smith, C.R., 2019. Intense deposition and rapid processing of seafloor phytodetritus in a glaciomarine fjord, Andvord Bay (Antarctica). *Progress in Oceanography*, In Prep.

Chapter 5. Conclusions

In this dissertation, coastal Antarctic phytoplankton ecology was examined through field work, numerical models, data science, and machine learning studies. The results reveal the seasonal environmental variabilities of Antarctic nearshore waters and over the continental shelf, and how they impact phytoplankton abundance and community composition.

First, glacial meltwater presence was measured in Andvord Bay (a fjord in the WAP, Fig. 2.1) – a location found to be a source of meltwater. A clear seasonality of meltwater was observed (Fig. 2.7). The meltwater exhibited distinct optical characteristics, particularly as high values of particulate backscattering coefficient at 442 nm and beam attenuation coefficient at 660 nm (Fig. 2.4). These optical features are attributed to suspended iron nanoparticles entrained in glacial meltwater. Glacial meltwater was found to be an important environmental factor for phytoplankton, where higher meltwater fraction in the water column led to higher phytoplankton biomass (Fig. 2.10). These results confirm that surface freshening due to meltwater can aid phytoplankton growth (Dierssen et al., 2002), further validates that this positive impact from freshening-induced stratification can be caused by glacial meltwater in addition to sea ice melt (Mitchell & Holm-Hansen, 1991). Through this study, a novel optical algorithm is developed to detect in-situ meltwater fraction using its unique inherent and apparent optical properties. This technique can aid future ocean color algorithm development and serve as a proxy for remotely detecting and monitoring glacial meltwater at ocean surface (Chapter 2).

Then, the meltwater measurements were combined with others oceanographic variables to gain a more comprehensive understanding of how ice-ocean interaction impacts phytoplankton ecology in Andvord Bay. Chapter 3 illustrates that this WAP fjord is a model system with nearshore water properties representing an extreme in environmental gradients due to its proximity to multiple glacial termini. Andvord Bay is enriched in macro- and trace nutrients and it is a biologically productive region. There are three major phytoplankton groups found in the spring

and fall – cryptophyte, diatom, and mixed flagellate (Fig. 3.2). Unlike the phytoplankton community over the continental shelf and in the broader Southern Ocean, cryptophytes were the most abundant taxon during spring in Andvord Bay (Fig. 3.3). The phytoplankton growth was fueled by nitrate and iron replenishment (Fig. 3.7, Fig. 3.8). Glacial meltwater induces shallow mixed layers and creates favorable growing conditions; in addition, the resulting warmer surface layer is another favorable growing condition for cryptophytes (Fig. 3.5, Fig. 3.6). These results are important to our understanding of nearshore phytoplankton ecology. Chapter 3 also demonstrates that surface nitrate in Andvord Bay is replenished by vertical diffusion and upwelling driven by Katabatic wind events; deep nitrate content can also surface via buoyant meltwater plume along the ice-ocean interface. Surface dissolved iron is supplied by similar mechanisms as nitrate, and via sub-glacial and sub-marine melting of glaciers. These important mechanisms are shown to fuel phytoplankton growth in the very productive Andvord Bay. Moreover, this is one of the first studies to use deep learning models to understand phytoplankton ecology in the WAP. The method was deployed using Automatic Machine Learning, which allows non-experts of data science to train and test complex machine learning models and achieve accurate predictions without overfitting. This technique can also help generate new hypotheses for more in-depth investigations (Chapter 3).

Finally, the new insights and methods are applied to the WAP continental shelf in Chapter 4 to better understand a broader ecosystem. The analyses of a multi-decadal times series of the WAP indicate that the phytoplankton community is dominated by diatoms, with cryptophytes as the second most abundant group; particularly, diatoms dominate phytoplankton blooms. Nitrate + nitrite concentrations are found to fuel this diatom growth (Fig. 4.5), and it is likely replenished through sea ice melting and mixing by storms. Temporally, phytoplankton biomass is found to be first modulated by sea ice (or its absence), and then by water column properties after it is generally ice-free at surface (Fig. 4.9, Fig. 4.10). These results demonstrate that the impact of ambient environment on phytoplankton community is not deterministic; rather, it is reflected as changes in

the environment leading to a stage of seasonal phytoplankton succession (Fig. 4.12). For instance, following years with low sea ice, seasonal succession starts at a relatively more advanced stage in comparison to nominal conditions. Under this scenario, overall phytoplankton biomass is lower with cryptophytes dominating the community (Fig. 4.11). In extreme cases, such as the sea ice minimum in 2008, succession begins at an even later stage, resulting in a biomass minimum and dinoflagellates dominating the community in the following year (Fig. 4.11).

To understand how these results are connected and to gain a compressive perspective of phytoplankton ecology in the WAP, it is important to point out the distinctions between nearshore waters and the coastal ocean over the continental shelf presented in this dissertation. There have been multiple studies on the WAP continental shelf oceanography which demonstrate this region is dominated by three main water masses (Martinson et al., 2008). These water masses are generally labelled as coastal, shelf, and slope zones (Chapter 4). They are different from that of the broader Southern Ocean, particularly due to the warmer temperature and less saline conditions at the surface. In T-S diagrams, these properties are illustrated as a cluster of V-shaped data points over the slope that transform towards a U-shaped cluster as the waters are modified from shelf break towards the coast (Fig. 4.1). These characteristics are different from those of the WAP fjord. Andvord Bay exhibited a cluster of “upside-down U-shaped” data points in T-S diagrams (Fig. 2.10). Due to the presence of multiple glacial drainages in the fjord, this nearshore location experiences more significant impacts from ice-ocean interactions when compared to the WAP shelf – this causes the fjord to have relatively colder temperatures. I label these waters as nearshore, as they are distinctly different from the three water masses over the continental shelf. Surface salinity of the WAP coastal zone is relatively similar to the fjord’s surface in contrast to the WAP slope zone. This provides evidence that glacial meltwater can extend beyond nearshore waters and impact water column over the shelf (Fig. 2.7, Fig. 4.7).

Sea surface temperature (SST) monthly climatology data between 2003 and 2020 reveal the seasonal progression of nearshore waters in the WAP (Fig. 5.1). Water masses with SST

between -0.1 and 0.5 ^{o}C are observed close to the coast in January and February. Then, these water masses expand towards the shelf in March and dominate the entire region in April and May; this spatial pattern from April/May is also found in December, earlier in the growing season. A similar temperature range is found in Andvord Bay, presented in Chapter 2 and 3 (Fig. 2.10). These results suggest a connectivity between nearshore waters and coastal ocean over the WAP continental shelf, alluding to an export of glacial meltwater from fjords to the shelf over time. The export of glacial meltwater can lead to dissolved iron supply to the shelf as Annett et al. hypothesized – the distribution of dissolved iron over the WAP shelf is related to the presence of glacial meltwater (Annett et al., 2017). Their hypothesis is supported by Forsch et al. who found a gradient of dissolved iron in the surface ocean, where concentrations are high in Andvord Bay and diminish towards the continental shelf, about 40km offshore of the inland channels and fjords (Forsch et al., 2018). Nearshore glacial meltwater export is also associated with lower salinity – such as the “meltwater lens” being a persistent feature in coastal waters of the WAP shelf, especially during the growing season, where surface water masses with lower salinity extend from nearshore region to >100 km over the shelf (Martinson et al., 2008) (Dierssen et al., 2002). These observations highlight the impact of nearshore waters on the WAP continental shelf.

The distinctions between nearshore oceans and waters over the continental shelf lead to different phytoplankton community composition, where abundant cryptophytes were observed in Andvord Bay (Chapter 3) while diatom dominated bloom conditions over the shelf (Chapter 4). However, as our sampling did not coincide with the summer bloom attributed to diatoms in Andvord Bay (Ziegler et al., 2020), some of these distinctions between these two regions can be attributed to timing of sampling. As pointed out in Chapter 4, the difference in environmental conditions and the resulting phytoplankton community composition and abundance are not merely deterministic. Rather, it reflects seasonal community succession modulated by changes in the ambient environment. This process is more noticeable with time series such as that presented in Chapter 4 – where difference in prior-year sea ice coupled with changes in water column

properties can shift the stage of phytoplankton community succession sampled in the month of January. Particularly, lower sea ice presence prior to the growing season leads to more advanced stage of succession in comparison to nominal conditions where the initial stage is diatom assemblage by sea ice seeding (Fig. 4.12).

The timing of different stages of the phytoplankton community succession will change as the warming of the WAP continues to intensify. The waters over the continental shelf will transition to nearshore conditions (like those of the fjord). As a result, overall sea ice will be lower prior to the growing season, and glacial meltwater is expected to increase throughout the growing season but especially during summer. These conditions will cause more intense surface freshening which leads to stronger stratification and increase macro-nutrients and dissolved iron concentrations in the water column. As a result, future phytoplankton community over the continental shelf will be at a relatively more advanced stage of succession at the beginning of the growing season. This stage corresponds to cryptophyte abundance as observed in Andvord Bay in spring of 2015 (Chapter 3) and over the WAP continental shelf during summers of 2000, 2005, and 2013 (Chapter 4).

Currently, glacial meltwater discharge into the WAP is relatively weak in comparison to the Arctic. These meltwater plumes in the WAP have entrained nanoparticles and so they do not impede underwater light field and hinder phytoplankton growth. Overall, meltwater currently provides favorable conditions for phytoplankton community in the WAP (Chapter 3). However, in the future, a significant increase in glacial meltwater input is expected in the WAP, coupled with sea ice area continuing to decline further. Under such scenario, glacial meltwater will play a more crucial role in phytoplankton ecology potentially on par with sea ice. Under this scenario, glacial meltwater discharge is substantially higher than that of the current level. High level of meltwater input is commonly associated with sediment input (Hudson et al., 2014), especially after glaciers retreat inland and transition from marine-terminating to land-terminating (Henley et al., 2020) (Meire et al., 2017) (Schloss et al., 2012). This impact can already be seen in some Arctic and

Greenland fjords – where higher nutrient concentrations are near the glacial-marine terminus (Cape et al., 2019), but phytoplankton can only utilize these nutrients and grow downstream if the sediment load is high (Hopwood et al., 2020). This means, with sediment-laden glacial meltwater, phytoplankton community is negatively impacted near the source of meltwater, but they benefit from the resulting stratification and nutrient supply farther downstream where the meltwater is modified by water masses from the open ocean. This effect of sediments in meltwater is observed not only in the Arctic and Greenland, but also in limited cases in the WAP where the glacier has retreated inland leading to heavy sediment discharge (e.g. Potter Cove) (Monien et al., 2017) (Schloss et al., 2012). Furthermore, without modifying by oceanic water (via dilution to increase salinity), the decline in salinity due to glacial meltwater will also create hypoosmotic condition for phytoplankton cells which prevents biomass accumulation (Hernando et al., 2015). This means significant glacial meltwater in the future will cause phytoplankton productivity to decline in fjords but will increase phytoplankton growth farther downstream over the WAP continental shelf. The downstream effect of meltwater has already been observed in the Labrador Sea where the arrival of meltwater from Greenland Ice Sheet initiates phytoplankton blooms (Arrigo et al., 2017).

If the rapid warming trend continues in the WAP, productivity in fjords will experience a non-linear change due to increasing glacial meltwater – at first, productivity will increase due to surface stratification and increases in nitrate and dissolved iron concentration attributed to an increase in meltwater. As glaciers continue to retreat inland, productivity will decrease due to sediment plumes associated with glacial discharge. Phytoplankton community composition over the continental shelf will change substantially. The lower sea ice presence, warmer temperature, surface freshening and stronger stratification due to glacial meltwater, and additional nutrients will favor cryptophytes and hence shift the seasonal phytoplankton succession to a more advanced stage in January; the initial stage of diatom assemblage from sea ice seeding will be observed earlier in the season and in shorter durations. As a result, there will be relatively lower total chl-a concentrations during the growing season. Under a more extreme scenario where sea ice

declines significantly or completely disappear during winter coupled with substantial sediment-laden glacial meltwater discharge, phytoplankton community will be dominated by small flagellates (other than cryptophytes), such as dinoflagellates and prasinophytes observed in 2009 (Fig. 4.11, Chapter 4). This means late stage community succession will persist throughout the entire growing season and total chl-a concentration will be significantly lower. These extreme conditions are expected to cause the overall productivity of the WAP to decline significantly.

To further our understanding of how the changing environment of the WAP will impact the phytoplankton community and the broader ecosystem, we need to continue long-term sampling in both nearshore and over the continental shelf of this region. Particularly, additional sampling prior to and after growing seasons are important for understanding the progression of seasonal community succession. As the Antarctic environment continues to change in the future, phytoplankton abundance and community composition will experience more severe and erratic shifts, which will substantially impact the rest of the ecosystem. These changes add significant uncertainties to the prediction of ecosystem dynamics and biogeochemical cycles of this productive region.

5.1. Figures and Tables

Figure 5.1. Sea surface temperature monthly climatology of the Western Antarctic Peninsula from November to May, 2003 -- 2020. Level 3 data retrieved from NASA GSFC (oceancolor.gsfc.nasa.gov).

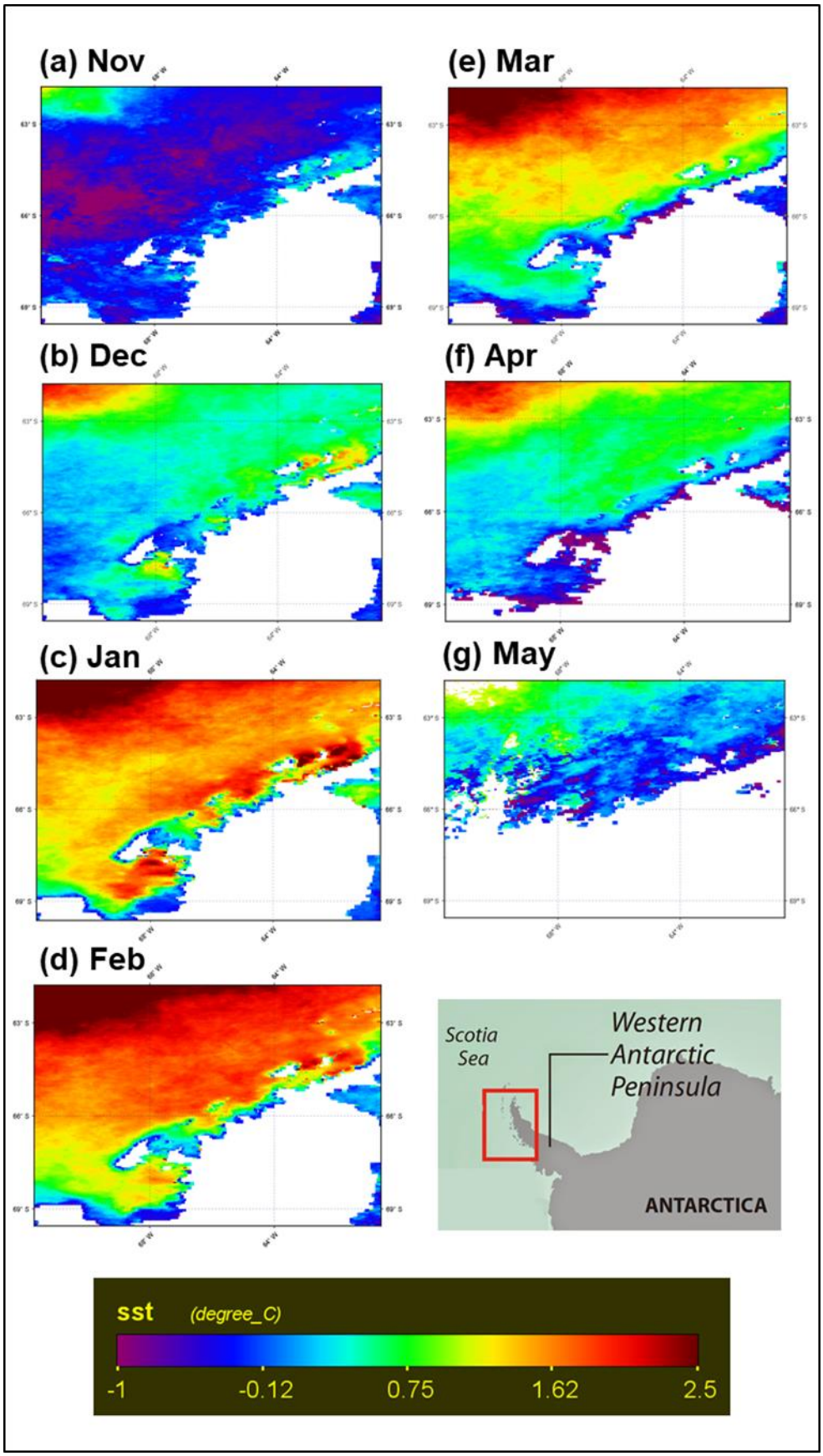
(a) Nov
(e) Mar
(b) Dec
(f) Apr
(c) Jan
(g) May
(d) Feb
Scotia Sea
Western Antarctic Peninsula
ANTARCTICA
sst (degree_C)
-1
-0.12
0.75
1.62
2.5

5.2. References

Annett, A.L., Fitzsimmons, J.N., Séguret, M.J., Lagerström, M., Meredith, M.P., Schofield, O., Sherrell, R.M., 2017. Controls on dissolved and particulate iron distributions in surface waters of the Western Antarctic Peninsula shelf. *Marine Chemistry*, 196, 81-97.

Arrigo, K.R., Dijken, G.L., Castelao, R.M., Luo, H., Rennermalm, Å.K., Tedesco, M., Mote, T.L., Oliver, H., Yager, P.L., 2017. Melting glaciers stimulate large summer phytoplankton blooms in southwest Greenland waters. *Geophysical Research Letters*.

Cape, M.R., Straneo, F., Beaird, N., Bundy, R.M., Charette, M.A., 2019. Nutrient release to oceans from buoyancy-driven upwelling at Greenland tidewater glaciers. *Nature Geoscience*, 12, 34.

Dierssen, H.M., Smith, R.C., Vernet, M., 2002. Glacial meltwater dynamics in coastal waters west of the Antarctic peninsula. *Proceedings of the National Academy of Sciences*, 99, 1790-1795.

Forsch, K., Manck, L., Ekern, L., Pan, B.J., Vernet, M., Barbeau, K., 2018. Links Between Sources of Iron and Organic Iron-binding Ligands to the Supply of Cryospheric Iron to Coastal West Antarctic Peninsula. *Ocean Sciences Meeting*. Portland, Oregon.

Henley, S.F., Cavan, E.L., Fawcett, S.E., Kerr, R., Monteiro, T., Sherrell, R.M., Bowie, A.R., Boyd, P.W., Barnes, D.K., Schloss, I.R., 2020. Changing biogeochemistry of the Southern Ocean and its ecosystem implications. *Frontiers in Marine Science*.

Hernando, M., Schloss, I., Malanga, G., Almandoz, G., Ferreyra, G., Aguiar, M., Puntarulo, S., 2015. Effects of salinity changes on coastal Antarctic phytoplankton physiology and assemblage composition. *Journal of Experimental Marine Biology and Ecology*, 466, 110-119.

Hopwood, M.J., Carroll, D., Dunse, T., Hodson, A., Holding, J.M., Iriarte, J.L., Ribeiro, S., Achterberg, E.P., Cantoni, C., Carlson, D.F., 2020. How does glacier discharge affect marine biogeochemistry and primary production in the Arctic? *The Cryosphere*, 14, 1347-1383.

Hudson, B., Overeem, I., McGrath, D., Syvitski, J., Mikkelsen, A., Hasholt, B., 2014. MODIS observed increase in duration and spatial extent of sediment plumes in Greenland fjords. *The Cryosphere*, 8, 1161-1176.

Martinson, D.G., Stammerjohn, S.E., Iannuzzi, R.A., Smith, R.C., Vernet, M., 2008. Western Antarctic Peninsula physical oceanography and spatio–temporal variability. *Deep Sea Research Part II: Topical Studies in Oceanography*, 55, 1964-1987.

Meire, L., Mortensen, J., Meire, P., Juul-Pedersen, T., Sejr, M.K., Rysgaard, S., Nygaard, R., Huybrechts, P., Meysman, F.J., 2017. Marine-terminating glaciers sustain high productivity in Greenland fjords. *Global Change Biology*, 23, 5344-5357.

Mitchell, B.G., Holm-Hansen, O., 1991. Observations of modeling of the Antartic phytoplankton crop in relation to mixing depth. *Deep Sea Research Part A. Oceanographic Research Papers*, 38, 981-1007.

Monien, D., Monien, P., Brünjes, R., Widmer, T., Kappenberg, A., Busso, A.A.S., Schnetger, B., Brumsack, H.-J., 2017. Meltwater as a source of potentially bioavailable iron to Antarctica waters. *Antarctic Science*, 29, 277.

Schloss, I.R., Abele, D., Moreau, S., Demers, S., Bers, A.V., González, O., Ferreyra, G.A., 2012. Response of phytoplankton dynamics to 19-year (1991–2009) climate trends in Potter Cove (Antarctica). *Journal of Marine Systems*, 92, 53-66.

Ziegler, A., Cape, M., Lundesgaard, Ø., Smith, C., 2020. Intense deposition and rapid processing of seafloor phytodetritus in a glaciomarine fjord, Andvord Bay (Antarctica). *Progress in Oceanography*, 102413.

Fin